December 2014
Research Report: UCPRC-RR-2014-04.2

Development and HVS Validation of Design Tables for Permeable Interlocking Concrete Pavement: Final Report

Authors:
H. Li, D. Jones, R. Wu, and J. Harvey

Concrete Masonry Association of California and Nevada. Grant Agreement UCPRC-PP-2011-01

PREPARED FOR:

Concrete Masonry Association of California and Nevada

PREPARED BY:

University of California
Pavement Research Center
UC Davis, UC Berkeley

DOCUMENT RETRIEVAL PAGE		**Research Report: UCPRC-RR-2014-04.2**
Title: Development and HVS Validation of Design Tables for Permeable Interlocking Concrete Pavement: Final Report		
Authors: H. Li, D. Jones, R. Wu, and J. Harvey		
Prepared for: Concrete Masonry Association of California and Nevada	**Work submitted:** December 2014	**Date:** December 2014
UC Davis Contract No: UCPRC-PP-2011-01	**Status:** Final	**Version No.:** 1.2*

Abstract:
This report details the research undertaken to develop revised design tables for permeable interlocking concrete pavement using a mechanistic-empirical design approach. The study included a literature review, field testing of existing projects and test sections, estimation of the effective stiffness of each layer in permeable interlocking concrete pavement structures, mechanistic analysis and structural design of a test track incorporating three different subbase thicknesses (low, medium, and higher risk), tests on the track with a Heavy Vehicle Simulator to collect performance data to validate the design approach using accelerated loading, refinement and calibration of the design procedure using the test track data, development of a spreadsheet based design tool, and development of revised design tables using the design tool. Key findings from the mechanistic analysis include:

- Higher shear stress/strength ratios at the top of the subgrade, which equate to a higher risk of rutting in the subgrade, require thicker subbase layers, as expected.
- An increase in the stiffness of the surface layer reduces the required subbase layer thickness to achieve the shear stress/strength ratio. However, the effect of the surface layer stiffness on overall pavement performance is not significant due to the relatively low thickness of the pavers (80 mm) and the reduced interlock between them compared to pavers with sand joints.
- For the same shear stress/strength ratio at the top of the subbase, an increase in the stiffness of the subbase layer reduces the required thickness of that subbase layer, especially when the subgrade has a low stiffness.
- For the same shear stress/strength ratio at the top of the subgrade, wet conditions require thicker subbase layers compared to the dry condition, confirming that wet conditions are the most critical condition for design.

The study also developed new example design tables that are based on either a specific number of target days with standing water in the subbase or on a range of days. The tables use a similar format to that currently used in the ICPI Permeable Interlocking Concrete Pavements guideline. The minimum design thicknesses required to prevent subgrade rutting that are proposed in the new tables do not differ significantly from those in the current ICPI guide, and are mostly less conservative. Designs for a specific set of project circumstances can be undertaken using the same *Excel*® spreadsheet-based design tool used to develop the tables in conjunction with the hydrological design procedures provided in the ICPI guide.

- **Note: Version 1.2 includes the corrected term "drained test" in the first paragraph of Section 7.2, and new sets of proposed example design tables in Chapter 9. The first set of tables has additional columns for days with water in the subbase. The second set has a range of days, instead of a single day value.*

Keywords:
Permeable interlocking concrete pavement, permeable pavement, mechanistic-empirical design, accelerated pavement testing.

Proposals for implementation:

Related documents:
UCPRC-TM-2013-03, UCPRC-TM-2013-09

Signatures:

H. Li **1st Author**	J. Harvey **Technical Review**	D. Jones **Principal Investigator**	D.R. Smith **For CMACN**

DISCLAIMER

The contents of this report reflect the views of the authors who are responsible for the facts and accuracy of the data presented herein. The contents do not necessarily reflect the official views or policies of the Concrete Masonry Association of California and Nevada (CMACN), the California Nevada Cement Association (CNCA), the Interlocking Concrete Pavement Institute Foundation for Education & Research (ICPIF) or the Interlocking Concrete Pavement Institute (ICPI). This report does not constitute a standard, specification, or regulation.

PROJECT OBJECTIVES/GOALS

The objective of this project was to produce thickness design tables for permeable interlocking concrete pavement (PICP) based on mechanistic analysis and partially validated with accelerated pavement testing (APT). The following tasks were completed to achieve this objective:

1. Perform a literature and field survey to identify critical responses, failure mechanisms, appropriate performance transfer functions, and modeling assumptions for mechanistic analysis of PICP under truck loading.
2. Measure pavement deflection in the field on several PICP locations to characterize effective stiffness of the different layers in the structure for use in modeling.
3. Perform mechanistic analyses of PICP to develop design tables following the approach documented in California Department of Transportation (Caltrans) Research Report CTSW-RR-09-249.04 for development of structural design tables for permeable/pervious/porous asphalt and concrete pavement.
4. Prepare a plan for validation with accelerated load testing based on the results of the mechanistic analysis.
5. Test responses and, if possible, failure of up to three PICP structures in dry and wet condition with a Heavy Vehicle Simulator (HVS).
6. Analyze the results of the HVS testing to revise/update the structural design tables where necessary.
7. Write a final report documenting the results of all tasks in the study and demonstrating the design tables.
8. Present findings to Caltrans Office of Concrete Pavements and Foundation Program and Office of Stormwater - Design staff in Sacramento, CA.

This report covers Tasks 1 through 7.

ACKNOWLEDGEMENTS

The University of California Pavement Research Center acknowledges the following individuals and organizations.

- Financial Support:
  - ICPI Foundation for Education and Research, Chantilly, Virginia
  - Concrete Masonry Association of California and Nevada, Citrus Heights, California
  - California Nevada Cement Association, Yorba Linda, California
- Material and Labor Donations:
  - Basalite Concrete Products, Dixon, California (donated concrete pavers)
  - Kessler Soils Engineering, Leesburg, Virginia (undertook lightweight deflectometer testing)
  - Tencate Mirafi, Pendergrass, Georgia (donated geotextile)
  - WeberMT, Bangor, Maine (loan of a CR-7 vibrator plate compactor with compaction indicator)
- Project Support:
  - David R. Smith, Technical Director, Interlocking Concrete Pavement Institute, Chantilly, Virgina
  - David K. Hein, PEng, Principal Engineer, Vice President, Applied Research Associates, Toronto, Ontario, Canada
  - Dr. T. Joseph Holland, Caltrans, Sacramento, California
  - California Pavers, Lodi, California (Test section construction)
  - The UCPRC Heavy Vehicle Simulator crew and UCPRC laboratory staff, Davis and Berkeley, California.

Blank page

EXECUTIVE SUMMARY

This report details the research undertaken to develop revised design tables for permeable interlocking concrete pavement using a mechanistic-empirical design approach. The study included a literature review, field testing of existing projects and test sections, estimation of the effective stiffness of each layer in permeable interlocking concrete pavement structures, mechanistic analysis and structural design of a test track incorporating three different subbase thicknesses (low, medium, and higher risk), tests on the track with a Heavy Vehicle Simulator to collect performance data to validate the design approach using accelerated loading, refinement and calibration of the design procedure using the test track data, development of a spreadsheet based design tool, and development of design tables using the design tool.

Rut development rate as a function of the shear stress to shear strength to ratios at the top of the subbase and the top of the subgrade was used as the basis for the design approach. This approach was selected based on a review of the literature, past research on permeable pavements by the authors, and the results of deflection testing on in-service permeable interlocking concrete pavements. The shear stress/strength ratio was originally developed for airfield pavements where the shear stresses from aircraft loads and tire pressures are high relative to the strengths of the subgrade materials. On permeable road pavements, subgrade materials are often uncompacted or only lightly compacted and wet or saturated for much of the service life, resulting in relatively low shear strengths compared with the high shear stresses from trucks. Deeper ruts are usually also tolerated on permeable pavements due to the absence of ponding on the surface during rainfall. The alternative approach of using a vertical strain criterion was considered inappropriate for permeable pavements, given that this is typically used where the shear stresses relative to the shear strains are relatively low, which typically results in low overall rutting.

Key observations from the study include:

- Infiltration of water into the subgrade is significantly reduced when the subgrade is compacted prior to placing the subbase. In this study, light compaction of the subgrade soil (~ 91 percent of laboratory determined modified Proctor maximum dry density) added very little to the structural performance of the pavement and would not have permitted reducing the design thickness of the subbase layer.
- There was a significant difference in rutting performance and rutting behavior between the wet and dry tests, as expected.
- A large proportion of the rutting on all three sections occurred as initial embedment in the first 2,000 to 5,000 load repetitions of the test and again after each of the load changes, indicating that much of the rutting in the base and subbase layers was attributed to bedding in, densification, and/or reorientation of the aggregate particles. This behavior is consistent with rutting behavior on interlocking concrete pavements with sand joints on dense-graded or stabilized bases as well as on other types of structures.

- During testing under dry conditions, limited permanent deformation (< 4 mm) was recorded in the bedding and base layers on all three subsections, and most occurred very early in the test. On the subsection with the 450 mm subbase, rutting occurred in both the subbase (10 mm rut) and subgrade (13 mm rut). On the 650 mm and 950 mm subbase subsections, rutting occurred mostly in the subbase. Total permanent deformation on the 450 mm, 650 mm, and 950 mm subbase subsections was 27 mm, 23 mm and 17 mm respectively, implying a generally linear trend of increasing permanent deformation with decreasing subbase thickness.
- During testing under wet conditions (i.e., water level maintained at the top of the subbase), rutting in the bedding and base layers was dependent on the thickness of the subbase (9 mm, 5 mm and 2 mm on the 450 mm, 650 mm, and 950 mm subbase subsections, respectively). Rutting occurred in both the subbase and the subgrade on all subsections, with rutting in the subbase consistent across all three sections (~ 25 mm). Rutting in the subgrade differed between sections relative to subbase thickness, with 15 mm, 6 mm, and 4 mm of rut recorded on the 450 mm, 650 mm, and 950 mm subbase subsections, respectively.
- Although only limited testing was undertaken under drained conditions (i.e., wet subgrade but no standing water in the subbase), rutting behavior appeared to show similar trends and behavior to the test under dry conditions.
- The thickness of the subbase influenced rut depth in the subgrade, as expected, but did not influence the rutting behavior in the subbase itself. Rutting in these layers is therefore governed by the aggregate properties and construction quality.
- Deflection during dry testing was dependent on subbase thickness and it increased with increasing load. Deflections were relatively high compared to more traditional pavements with dense graded layers. Deflection during wet testing was higher compared to that recorded during dry testing, with deflection on the 450 mm subbase subsection significantly higher compared to that recorded on the 650 mm and 950 mm subbase subsections, indicating a load-sensitive, weaker overall structure as a result of the wet subgrade.
- No distress was noted on any individual concrete pavers and no pavers were dislodged from the pavement during testing.
- The infiltration rate of water through the joints between the pavers reduced over the course of HVS testing; however, it was still considered to be rapid and effective.

Key findings from the mechanistic analysis include:

- The use of the shear stress to shear strength ratios at the top of the subbase and top of the subgrade as inputs for modelling the rut development rate at the top of these layers is considered to be an appropriate design approach for permeable interlocking concrete pavers (PICP).
- Higher shear stress/strength ratios at the top of the subgrade, which equate to a higher risk of rutting in the subgrade, require thicker subbase layers, as expected.
- An increase in the stiffness of the surface layer reduces the required subbase layer thickness to achieve the same shear stress/strength ratio. However, the effect of the surface layer stiffness on overall pavement performance is not significant due to the relatively small thickness of the pavers (80 mm) and the reduced interlock between them compared to pavers with sand joints.

- For the same shear stress/strength ratio at the top of the subbase, an increase in the stiffness of the subbase layer reduces the required thickness of that subbase layer, especially when the subgrade has a low stiffness.
- For the same shear stress/strength ratio at the top of the subgrade, wet conditions require thicker subbase layers compared to the dry condition, confirming that wet conditions are the most critical condition for design.

New example design tables, based on the number of days with standing water in the subbase (target days including 0, 10, 30, 50, 70, 90, 110, and 130 days and range of days including 0, <10, 10-29, 30-49, 50-69, 70-89, 90-109, and 110-130) have been developed. The tables use a similar format to that currently used in the ICPI Permeable Interlocking Concrete Pavements guideline. The design thicknesses proposed in the new tables do not differ significantly from those in the current ICPI table. Designs for a specific set of project circumstances can be undertaken by using the same *Excel*® spreadsheet-based design tool used to develop these tables in conjunction with the hydrological design procedures provided in the ICPI guide. The design tool output and corresponding values in the tables should be considered as best estimate designs since they were developed from the results of only two HVS tests. Designers should continue to use sound engineering judgment when designing permeable interlocking concrete pavements and can introduce additional conservatism/reliability by altering one or more of the design inputs, namely the material properties, number of days that the subbase will contain standing water, and/or traffic.

Blank page

TABLE OF CONTENTS

LIST OF TABLES

LIST OF FIGURES

SI* (MODERN METRIC) CONVERSION FACTORS

APPROXIMATE CONVERSIONS TO SI UNITS

Symbol	When You Know	Multiply By	To Find	Symbol
		LENGTH		
in	inches	25.4	Millimeters	mm
ft	feet	0.305	Meters	m
yd	yards	0.914	Meters	m
mi	miles	1.61	Kilometers	Km
		AREA		
in^2	square inches	645.2	Square millimeters	mm^2
ft^2	square feet	0.093	Square meters	m^2
yd^2	square yard	0.836	Square meters	m^2
ac	acres	0.405	Hectares	ha
mi^2	square miles	2.59	Square kilometers	km^2
		VOLUME		
fl oz	fluid ounces	29.57	Milliliters	mL
gal	gallons	3.785	Liters	L
ft^3	cubic feet	0.028	cubic meters	m^3
yd^3	cubic yards	0.765	cubic meters	m^3
		NOTE: volumes greater than 1000 L shall be shown in m^3		
		MASS		
oz	ounces	28.35	Grams	g
lb	pounds	0.454	Kilograms	kg
T	short tons (2000 lb)	0.907	megagrams (or "metric ton")	Mg (or "t")
		TEMPERATURE (exact degrees)		
°F	Fahrenheit	5 (F-32)/9 or (F-32)/1.8	Celsius	°C
		ILLUMINATION		
fc	foot-candles	10.76	Lux	lx
fl	foot-Lamberts	3.426	$candela/m^2$	cd/m^2
		FORCE and PRESSURE or STRESS		
lbf	poundforce	4.45	Newtons	N
lbf/in^2	poundforce per square inch	6.89	Kilopascals	kPa

APPROXIMATE CONVERSIONS FROM SI UNITS

Symbol	When You Know	Multiply By	To Find	Symbol
		LENGTH		
mm	millimeters	0.039	Inches	in
m	meters	3.28	Feet	ft
m	meters	1.09	Yards	yd
km	kilometers	0.621	Miles	mi
		AREA		
mm^2	square millimeters	0.0016	square inches	in^2
m^2	square meters	10.764	square feet	ft^2
m^2	square meters	1.195	square yards	yd^2
ha	Hectares	2.47	Acres	ac
km^2	square kilometers	0.386	square miles	mi^2
		VOLUME		
mL	Milliliters	0.034	fluid ounces	fl oz
L	liters	0.264	Gallons	gal
m^3	cubic meters	35.314	cubic feet	ft^3
m^3	cubic meters	1.307	cubic yards	yd^3
		MASS		
g	grams	0.035	Ounces	oz
kg	kilograms	2.202	Pounds	lb
Mg (or "t")	megagrams (or "metric ton")	1.103	short tons (2000 lb)	T
		TEMPERATURE (exact degrees)		
°C	Celsius	1.8C+32	Fahrenheit	°F
		ILLUMINATION		
lx	lux	0.0929	foot-candles	fc
cd/m^2	$candela/m^2$	0.2919	foot-Lamberts	fl
		FORCE and PRESSURE or STRESS		
N	newtons	0.225	Poundforce	lbf
kPa	kilopascals	0.145	poundforce per square inch	lbf/in^2

*SI is the symbol for the International System of Units. Appropriate rounding should be made to comply with Section 4 of ASTM E380 (Revised March 2003)

Blank page

1. INTRODUCTION

1.1 Project Scope

This project was coordinated through the Interlocking Concrete Pavement Institute (ICPI) and the Concrete Masonry Association of California and Nevada with additional support from the California Nevada Cement Association. The objective of this project was to produce thickness design tables for permeable interlocking concrete pavement (PICP) based on mechanistic analysis and partially validated with accelerated pavement testing (APT).

1.2 Background to the Study

Although permeable pavements are becoming increasingly common across the United States, they are mostly used in parking lots, basic access streets, recreation areas, and landscaped areas, all of which carry very light, slow moving traffic. Only limited research has been undertaken on the mechanistic design and long-term performance monitoring of permeable pavements carrying higher traffic volumes and heavier loads, and the work that has been done has focused primarily on pavements with open-graded asphalt or portland cement concrete surfacings. Very little research has been undertaken on the use of permeable concrete paver surfaces on these more heavily trafficked pavements.

1.3 Study Objective

The objective of this project was to produce design tables for permeable interlocking concrete pavement (PICP) based on mechanistic analysis and partially validated with accelerated pavement testing (APT). The tasks to complete this objective include the following:

1. Perform a literature and field survey to identify critical responses, failure mechanisms, appropriate performance transfer functions, and modeling assumptions for mechanistic analysis of PICP under truck loading (*completed in May 2013, UCPRC Technical Memorandum, TM-2013-03 [1]*).
2. Measure pavement deflection in the field on several PICP locations to characterize effective stiffness of the different layers in the structure for use in modeling (*completed in July 2013, UCPRC Technical Memorandum, TM-2013-09 [2]*).
3. Perform mechanistic analyses of PICP to develop design tables following the approach documented in California Department of Transportation (Caltrans) Research Report CTSW-RR-09-249.04 for development of structural design tables for permeable/pervious/porous asphalt and concrete pavement (*completed in November 2013, UCPRC Technical Memorandum, TM-2013-09 [2]*).
4. Prepare a plan for validation with accelerated load testing based on the results of the mechanistic analysis (*completed in November 2013, UCPRC Technical Memorandum, TM-2013-09 [2]*).

5. Test responses and, if possible, failure of up to three PICP structures in dry and wet condition with a Heavy Vehicle Simulator (HVS) (*this report*).
6. Analyze the results of the HVS testing to revise/update the structural design tables where necessary (*this report*).
7. Write a final report documenting the results of all tasks in the study and demonstrating the design tables (*this report*).
8. Present findings to Caltrans Office of Concrete Pavements and Foundation Program and Office of Stormwater - Design staff in Sacramento, CA.

This report covers Tasks 1 through 7.

1.4 Report Layout

This report covers the research detailed in the tasks listed in Section 1.3 and required to meet the project objective. Chapters in the report include the following:

- Chapter 1 provides the background and introduction to the report.
- Chapter 2 summarizes the findings from the literature review completed earlier in the study. The complete literature review is included as an appendix (Appendix A).
- Chapter 3 summarizes the findings from pavement deflection testing on three existing permeable interlocking concrete pavement projects and details how the findings were used to design the test track for accelerated pavement testing. The complete report on deflection testing is included as an appendix (Appendix B).
- Chapter 4 summarizes the test track location and design.
- Chapter 5 provides an overview of the test track construction.
- Chapter 6 details the test track layout, instrumentation, test criteria, and loading summary.
- Chapter 7 presents a summary of the Heavy Vehicle Simulator test data.
- Chapter 8 details the data analysis and development of mechanistic design criteria for permeable interlocking concrete pavements.
- Chapter 9 presents example design tables.
- Chapter 10 provides a summary of the research and lists key observations and findings.
- Appendix A contains the complete literature review completed earlier in the study.
- Appendix B contains the complete deflection testing report completed earlier in the study.

1.5 Introduction to Accelerated Pavement Testing

Accelerated pavement testing (APT) is defined as "*the controlled application of a prototype wheel loading, at or above the appropriate legal load limit to a prototype or actual, layered, structural pavement system to determine pavement response and performance under a controlled, accelerated accumulation of damage in a compressed time period*" *(3)*. APT at the UCPRC is carried out with a Heavy Vehicle Simulator (HVS) (Figure 1.1 and Figure 1.2). The HVS applies half-axle wheel loads between 25 kN and 200 kN (5,625 lb and 45,000 lb). An aircraft wheel is required for loads greater than 100 kN (22,500 lb).

Loads can be applied in one or both directions, and in channelized mode or with wandering. Trafficking speeds can be varied between creep speed and 20 km/h (12 mph). Approximately 20,000 load repetitions can be applied in a 24-hour period. If required, the pavement temperature can be controlled between 10°C and 60°C (50°F and 140°F) inside an environmental chamber (Figure 1.3). A standard HVS test section is 8 m (26.3 ft) long and 1 m (3.3 ft) wide, but an extension beam can be added to increase the test section length to 15 m (49.2 ft) (Figure 1.4). The extended HVS with no environmental chamber was used for testing in this study.

Figure 1.1: Heavy Vehicle Simulator (HVS).

Figure 1.2: HVS test carriage.

Figure 1.3: HVS with environmental chamber.

Figure 1.4: Heavy Vehicle Simulator with extended beam.

1.6 Measurement Units

Metric units are always used by the UCPRC in mechanistic design, the design and layout of HVS test tracks, for laboratory, accelerated load testing, and field measurements, and for data storage. Where appropriate in this report, both U.S. customary and metric units are provided. In other cases where data is collected, analyzed, and discussed, only metric units are used. A conversion table is provided on page xv at the beginning of this report.

Blank page

2. LITERATURE REVIEW

A review of the recent literature on permeable interlocking concrete pavements was undertaken at the start of the study and a summary report prepared *(1)*. A copy of the complete report is included in Appendix A.

The literature review found that only a few organizations worldwide have undertaken detailed research on permeable interlocking concrete pavements, with many studies focusing on infiltration on low volume traffic roads, rather than structural design of roads carrying truck traffic. Limited published record was found on controlled load testing on permeable pavements in general and permeable interlocking concrete pavements in particular. No references were located with respect to accelerated testing as described in this report.

Laboratory studies have focused on resilient modulus of saturated and unsaturated materials. Well-graded materials with no fines (typical of that used under PICP) appeared to perform best under both conditions. Permeable pavements are generally designed for the worst case condition (i.e., a saturated soil subgrade and possibly a subbase/reservoir layer immersed in water). These conditions may (conservatively) require a reduction in resilient modulus as much as 50 percent of the dry material value. The use of cemented materials and geogrids in the base to compensate for this lower subgrade and aggregate base stiffness is gaining interest.

Failure mechanisms appear to be mostly rutting of the surface layer due to shearing in the bedding, base and/or subbase layers. Choice of paver thickness, paver shape, and paver laying pattern can limit this to a certain extent. However, optimizing the base and subbase material grading and thickness, material hardness, stabilization of the base and/or subbase materials with cement, asphalt, or a geogrid, quality of construction, and the use of geosynthetics to prevent contamination of the subbase are all design considerations with substantially greater influence on control of rutting and failure.

Mechanistic-empirical design has been considered in Australian and United Kingdom design procedures to some extent, with the work done in Australia appearing to be the most comprehensive. For unstabilized aggregates, these procedures typically use repetitive compressive strain at the top of the soil subgrade as the mechanistic response that is correlated with the rutting failure mechanism. Tension was generally not considered since these materials are not in tension. However, the measurement and understanding of stress distribution within and at the bottom of an open-graded base is not well documented or understood (compared to dense-graded materials), and this topic will likely require further research, modeling, and full-scale verification beyond what was determined within the scope of this project. Measuring stiffness

and stress distributions within the open-graded bedding/base/subbase from repeated loads was identified as a challenge, as was the need for undertaking research to enable the development of models/tools that can predict permeable pavement performance, including surface distresses, maintenance/rehabilitation remedies, and ultimate structural life.

3. DEFLECTION TESTING ON EXISTING PROJECTS

3.1 Introduction

Pavement surface deflection measurements are a primary method of evaluating the behavior of pavement structures when subjected to a load, and to characterize the stiffness of the pavement layers for use in mechanistic design. These measurements, which are non-destructive, are used to assess a pavement's structural condition, by taking most relevant factors into consideration, including traffic type and volume, pavement structural section, temperature, and moisture condition. Deflection measurements can be used in backcalculation procedures to determine pavement subgrade and structural layer stiffnesses, which are used as input to structural models to calculate stress, strains, and deformations that are correlated to distress mechanisms. Deflections can also be used directly in empirical design methods as an indicator to determine what level of traffic loading the pavement can withstand (i.e., design life or remaining life in terms of number of axle loads).

Deflection measurements are used by most departments of transportation as the basis for rehabilitation designs and often as a trigger for when rehabilitation or reconstruction is required.

All pavements bend under loading to some degree. Although this bending can normally not be distinguished with the naked eye (measurements are typically recorded in microns or mils) it has a significant effect on the integrity of the different layers over time. Repeated bending and then relaxation as the load moves onto and then off a point on a pavement is analogous to repeatedly bending a piece of wire back and forth – it eventually breaks. In pavements, the "damage" usually materializes as reorientation of the material particles, cracks and/or shearing, which leads to a reduction in stiffness over time, which in turn leads to moisture ingress, rutting, and other associated problems. Since moisture ingress and cracking are not relevant issues on permeable interlocking concrete pavements, this study focused on shearing and resulting rutting in the surface and underlying layers.

This chapter summarizes the results of a deflection study on three existing permeable interlocking concrete pavement projects in northern California *(2)* and backcalculation analysis of the test results. The full report is included in Appendix B, and it includes chapters covering a description of pavement deflection testing, the experiment plan for field deflection testing of existing PICP sections, results of the deflection testing, results of the mechanistic analysis, preliminary structural designs, and the test plan for thickness validation with accelerated pavement testing.

3.2 Deflection Testing

3.2.1 Deflection Measurement Method

Pavement deflection is most commonly measured with a falling weight deflectometer (FWD). However, this equipment is designed for continuous (monolithic) asphalt concrete and portland cement concrete pavements built on dense-graded aggregate bases, and was not considered appropriate for testing deflection on pavements constructed with interlocking concrete pavers (because of the segmented nature of the pavement surface), overlying open-graded aggregate bases. An FWD also applies an instantaneous dynamic load onto the pavement surface to simulate a truck wheel load passing over that point at a speed of about 60 km/h (40 mph). Deflection in the pavement is measured under this load. Open-graded aggregate bases used in permeable pavements, are usually more stress dependent than dense-graded bases, and can therefore have a bigger range of stiffness increase and relaxation as the wheel load passes over it. Backcalculating stiffnesses based on deflection measurements using an FWD may therefore provide incorrect results when analyzing PICP. A review of the literature on PICP *(1)* revealed that other researchers had experienced problems with accurately analyzing the stiffness of PICP from FWD deflection measurements.

Based on these concerns, a modified Benkelman beam (road surface deflectometer [RSD]) was instead used to measure deflection on the test sections. This device, which is standard equipment for measuring surface deflections on accelerated pavement tests at the UCPRC, measures the actual deflection between the dual wheels of a truck as it passes at slow speed over the instrument (see Figure 6.9 in Chapter 6). The RSD is not influenced by the segmental nature of the pavers (provided that the four reference points of the device are in contact with the paver surface and not on a joint) and is considered more appropriate for accommodating the stress dependent nature of the open-graded aggregate base. These deflection measurements were used to backcalculate the effective stiffnesses of individual pavement layers based on multilayer linear elastic theory. A comparison between the FWD and RSD was undertaken on a fully permeable pavement with a continuous open-graded asphalt surface to compare the backcalculated stiffnesses of the open-graded base using the two deflection methods. Testing was done under both dry and wet conditions on this section.

3.2.2 Test Section Locations

Three sites in northern California were selected for the deflection measurements, two in Davis and one in Sacramento. Construction records indicated that the pavement structures at the different sites consisted of an ASTM No. 57 aggregate base layer 300 mm to 400 mm (12 to 16 in.) thick, underneath an ASTM No. 8 aggregate bedding layer 25 mm to 50 mm (1 to 2 in.) thick (i.e., a very light traffic design per the ICPI Permeable Interlocking Concrete Pavement guide *[4]*). The surface pavers used at all three sites were

80 mm (3.2 in.) thick. Different laying patterns were used at each site. Actual pavement structures were not verified in the field with coring or test pits.

Since the testing on the existing PICP projects discussed above was all undertaken at the end of the dry season, only best case scenario measurements were obtained. Any pavement will exhibit high stiffnesses when all the materials are dry. However, these stiffnesses can drop significantly when the materials get wet, and consequently, most pavements are designed for wet conditions rather than dry (i.e., layers are thicker to prevent rutting in the subgrade), and considerable effort is placed into ensuring that water is effectively drained away from the road. Given that permeable pavements allow rain water to flow through the structure and into the subgrade, and that the subbase layers may actually be used to "store" water while it infiltrates into the subgrade, it is important to fully understand how the pavement will behave under these soaked conditions before thickness design tables can be prepared.

The three existing PICP sections that were assessed could not be flooded with water to assess moisture conditions, and time and resources did not allow for a second round of tests at the end of the rain season. As an alternative, deflection testing was undertaken on a permeable pavement structure with a porous asphalt concrete surface at the UCPRC test facility. This experiment is close to the site selected for construction of the test track for accelerated load testing of PICP. Deflection testing was done under both dry and wet conditions (water was allowed to flow through the surface until it overtopped to represent a worst case moisture condition). Deflection measurements were taken with both the RSD and the FWD and the results backcalculated to assess the difference in stiffnesses of the open-graded aggregate base and the subgrade under the two moisture conditions. This UCPRC test section was originally constructed as part of a larger experiment to measure the influence of permeable pavements on near surface temperature, albedo, and evaporation. Although not truly representative of typical PICP projects in terms of edge conditions, base/subbase thickness design and aggregate properties, it was considered suitable for comparing the change in uncompacted subgrade properties under an open-graded aggregate base/subbase when conditions changed from dry to wet.

3.3 Deflection Measurement Analysis

The primary component of deflection measurement analysis was the backcalculation of the stiffnesses of the different pavement layers at the different test sections. Backcalculation is a mechanistic evaluation of pavement surface deflection basins generated by pavement deflection testing devices. In the backcalculation process, measured surface deflections are matched, within some tolerable error, with a calculated surface deflection generated from an identical pavement structure using assumed layer stiffnesses (moduli). The assumed layer moduli in the calculated model are adjusted until they produce a

surface deflection basin that closely matches the measured one. The combination of assumed layer stiffnesses that results in this match is then assumed to be near the actual in situ moduli for the various pavement layers. The backcalculation process is usually iterative and normally done with computer software.

In this study, layer stiffness backcalculation using RSD data was conducted using a *Matlab* script (*KalmanBack*) developed by the UCPRC. *KalmanBack* uses *OpenPave (5)* for the deflection calculation and then uses a Kalman Filter as the search algorithm *(6)*. When matching surface deflections measured with the RSD, the deflection at the RSD anchoring feet was also accounted for.

3.4 Backcalculation of Stiffness for Davis and Sacramento Sections

The pavement structures were simplified into three layers for the backcalculation of stiffness: surface layer (paver), base layer (including bedding, base, and subbase aggregate layers), and subgrade (soil). The as-designed layer thicknesses were used for the backcalculation analysis. The effective stiffnesses of these three layers were optimized through minimizing the error between the calculated and the measured deflection basin curves based on multilayer linear elastic theory, which is commonly used as the basis for pavement design procedures.

3.4.1 Backcalculated Effective Stiffness of the Surface Layers

The main observations from the analysis of the effective stiffness of the surface layers under two different load levels and for two testing lines (centerline [CL] and wheelpath [WP]) include the following:

- There was a significant variation in surface effective stiffness among the three test sections, with very low stiffnesses measured at the Sacramento section, intermediate stiffnesses measured at one of the Davis sections, and higher stiffnesses measured at the other Davis site. Variation in stiffness was attributed to paver shape, paving laying pattern, degree of interlock between pavers, and confinement.
- Variations in surface effective stiffness were noted along the length of each test section on both the centerline and the wheelpath. This was attributed in part to construction variability and loosening of the paver interlock under traffic.
- The mean effective stiffness of the surface layer under the heavier load was generally slightly higher than that under the lighter load on all three sections. This was attributed to temporary confinement under the wheel load.
- Lower variation in effective stiffness was measured along the wheelpath compared to the centerline. This was attributed to the stronger and more uniform confining effect from the concrete curb and underlying edge walls close to the wheelpath.

3.4.2 Backcalculated Effective Stiffness of the Base Layers

The main observations from the analysis of the effective stiffness of the base layers for the two load levels and two testing paths at all three test sites include the following:

- The mean effective stiffnesses of the base layers calculated for the three sites were in the range of 20 MPa to 120 MPa (2.9 ksi to 17.4 ksi). However, average effective base layer stiffnesses were more consistent across the three sections compared to the surface stiffnesses. It should be noted that calculated stiffnesses will be influenced by and are sensitive to layer thickness and that design thicknesses were used in the analysis. These were not verified with on-site excavation. Consequently, actual layer stiffnesses could be lower or higher if the as-built thicknesses were thinner or thicker than the design.
- Effective stiffness along the wheelpath had lower variation compared to the centerline, which was again attributed to constraining effects of the curb and edge walls. The Sacramento test section had the highest variability.
- In most instances, the effective stiffness of the base layer was slightly higher under the heavier load, as expected. This was attributed to the higher confining stresses under the heavier load.

3.4.3 Backcalculated Effective Stiffness of the Subgrade

The main observations from the analysis of the effective stiffnesses of the subgrade under dry conditions for the three test sites include the following:

- The mean effective stiffnesses of the subgrade varied between 20 MPa and 100 MPa (2.9 ksi and 14.5 ksi) for the three test sites.
- The Sacramento section had the highest effective subgrade stiffness of the three sections, but also the highest variability. This was attributed to the likely alluvial (river gravel) nature of the subgrade material. The Davis sites had a similar range of subgrade stiffnesses consistent with silty-clay materials common in this area.
- Trends and variation along the two test paths were similar to those observed for the surface and base layers.
- The effect of the different load levels was less apparent on the subgrade stiffness compared to the effect it had on base and surface layer stiffnesses. This was attributed to the subgrade materials being of a less granular nature than the base materials and therefore less susceptible to confining stress.

3.4.4 Effective Stiffness Analysis

The distributed backcalculated effective stiffnesses of the surface layers, base layers, and subgrades at the three test sites were analyzed using empirical cumulative distribution functions (CDF). The median effective stiffnesses (50^{th} percentile) for the surface and base layers and the subgrade were approximately 400 MPa, 40 MPa, and 40 MPa (58 ksi, 5.8 ksi, and 5.8 ksi), respectively. Given that subgrade conditions at the Davis sites were likely different to the Sacramento site, the exercise was repeated for the two Davis sites only. Effective stiffness values changed to approximately 500 MPa, 35 MPa and 35 MPa (73 ksi, 5.1 ksi, and 5.1 ksi), respectively.

The results indicate that the effective stiffnesses at the 50th percentile of the surface layers at the Davis sites were higher than that at the Sacramento site, which was again attributed to paver type, laying pattern, and degree of paver interlock. The effective stiffnesses at 50 percent CDF of the base layers and subgrades at the Davis sites were slightly lower than that of the Sacramento site, which was attributed to different base aggregate sources and the likelihood that the Sacramento site had an alluvial aggregate subgrade, compared to the silty-clay subgrades common in the Davis area. These effective stiffnesses are comparable to the results obtained during earlier laboratory testing *(7)* and results cited in the literature *(1)*.

3.5 Backcalculation of Stiffness for UCPRC Section

3.5.1 Backcalculated Effective Stiffness from RSD Measurements

Observations from the results of the backcalculated effective stiffness from RSD measurements on the porous asphalt section include the following:

- There was no significant difference between the stiffnesses measured under the two different wheel loads.
- The stiffnesses of the base layer across the test section were relatively uniform, but relatively low compared to the results from the Davis and Sacramento test sections described above. This was attributed to the small size of the UCPRC test section (lack of confinement), relatively thin base layers, different base aggregates, very light compaction of the base materials during construction, the absence of any subgrade compaction, and the absence of any trafficking on the sections after construction.
- Stiffnesses under soaked conditions were lower than those measured under dry conditions, as expected.

3.5.2 Backcalculated Effective Stiffness from FWD Measurements

FWD-determined base and subgrade stiffnesses were comparable, but higher than those determined from RSD measurements, especially for the subgrade. This was attributed in part to the different loading nature of the two test methods (i.e., the RSD load is measured between the dual wheels of a truck travelling at creep speed, the FWD load is dynamic).

3.6 DCP Tests on the UCPRC Sections

Dynamic cone penetrometer (DCP) tests were used to empirically characterize the thickness and strength of the base layer and subgrade after completion of the deflection testing on the UCPRC section to obtain a different measure of strength and stiffness for comparison purposes. The strength characteristics of the base and subgrade materials were estimated from the DCP measurements. The slightly higher subgrade

strengths on the test section compared to the adjacent area was attributed to the confinement provided by the pavement structure. The results were consistent with silty clay subgrade materials in the Davis area.

Blank page

4. TEST TRACK LOCATION AND DESIGN

4.1 Test Track Location

The PICP experiment was located on a specially constructed test track adjacent to the Outer West Track at the University of California Pavement Research Center facility in Davis, California. An aerial view of the site is shown in Figure 4.1. Prior to construction of the Center, the area was used for agriculture (primarily alfalfa cultivation) and consequently the soil was relatively undisturbed in terms of compaction. A view of the test track site prior to construction is shown in Figure 4.2

Figure 4.1: Aerial view of the UCPRC research facility.

Figure 4.2: View of the test track site prior to construction.

4.2 Test Track Design

The test track design is discussed in detail in the interim report prepared after completion of pavement deflection testing and mechanistic analysis *(2)*. The full report is included in Appendix B.

The design was derived from a sensitivity analysis that considered a range of mechanistic values from worst-case to best-case scenarios. Selection of the input values was based on previous work by the authors, work by others on the topic identified during literature reviews, and the results of the deflection testing study.

4.2.1 Design Criteria

The most likely failure mode of permeable interlocking concrete pavements is permanent deformation in the base, subbase, and/or subgrade layers, which will manifest as rutting and/or paver displacement on the surface. The design criteria for the test track were therefore focused on this type of distress.

4.2.2 Design Variables

Shear stress/strength ratio (SSR or τ_f / τ_{max}) was used as the main design variable in this study. The basis for the use of shear stress to shear strength ratio for design comes from work done at the University of Illinois, primarily under Prof. Marshall Thompson and carried out by Prof. Erol Tutumleur *(8,9)*. It is based on decades of laboratory testing for permanent deformation, followed by field validation. The concept was primarily developed for use in airfields where the shear stresses from aircraft loads and tire pressures are high relative to the strengths of the subgrade materials. It was selected for use on this permeable pavement project because of the low shear strengths of saturated, uncompacted or poorly compacted subgrades (which are common conditions in permeable pavements) where the ratio between shear stresses and strengths can also be high given highway loads and tire pressures.

The alternative approach considered was the use of a vertical strain criterion, which is typically used where the shear stresses relative to shear strains are relatively low, which results in relatively low overall rutting. In this approach, vertical strains are typically calculated from pavement deflection measured over the full pavement structure. Strains in the localized areas at the top of the base layer and subgrade cannot be directly measured unless a strain gauge has been specifically installed in that position. Consequently, the damage and stiffness is calculated from measured deflections and then the strain is calculated from the calibrated damage and stiffness model. Vertical strain based approaches are difficult to calibrate when high shear stress to strength ratios occur in high water content environments, which in turn lead to large ruts. This has been learned from UCPRC experience on other projects that investigated pavement

performance under soaked conditions and consequently the vertical strain approach was not considered appropriate for designing permeable pavements.

Shear stress data has not been directly measured for ANY materials in the field because there is currently no instrument that can effectively measure shear stresses under a wheel load in a pavement structure. In the laboratory, shear stresses for all materials are calculated based on assumptions about the material and mechanics. Only limited shear strength data is available from shear and resilient modulus laboratory tests on open-graded granular bases and subbases. Similarly, there is very little laboratory or field data to support a strain based rutting model for open graded granular bases. Given these limitations, the stress/strength ratio concept was considered the most logical approach to accommodate the high stress to strength ratios, and higher allowable ruts that are part of designing permeable pavements.

Shear Stress/Strength Ratio

Shear stress/strength ratio is defined as the ratio between the applied shear stress (τ_f) and the material shear strength (τ_{max} [$\tau_{max} = c + \sigma_f \tan\phi$ in a triaxial strength test, where c is the cohesion of the material]) on the failure plane at a specific applied normal and confining stress state *(8)*. The normal and shear stresses (σ_f and τ_{max}) acting on a failure plane (oriented at an angle of $45° + \phi/2$, where ϕ is the internal friction angle of the material) can be calculated according to the Mohr-Coulomb failure theory for specific confining (σ_3) and deviator (σ_d) stresses applied to a laboratory specimen during triaxial testing.

Materials with lower shear stress/strength ratios are less likely to fail due to shear (i.e., rutting and permanent deformation) than materials with higher shear stress/strength ratios. Research studies *(10,11)* have shown that materials subjected to shear stress/strength ratios higher than 0.7 are likely to accumulate high permanent deformation and present a higher rutting risk, leading to rapid shear failure in the pavement. Materials with shear stress/strength ratios between 0.3 and 0.7 represent a medium risk with a steady but reasonable rate of rutting, while those with shear stress/strength ratios less than about 0.3 are expected to have little or no rutting after an initial small "bedding-in" rut. Based on these findings, the following three shear stress ratio design variable categories aligned to the level of rutting risk were defined for permeable interlocking concrete pavements *(1,9)*:

- SSR < 0.3, low risk of rutting;
- 0.3 ≤ SSR ≤ 0.7, medium risk of rutting;
- SSR > 0.7, high risk of rutting.

The equations used to calculate the SSR corresponding to the stress state applied during triaxial testing or other conditions are listed below:

$$Shear\ Stress/Strength\ Ratio\ (SSR) = \frac{\tau_f}{\tau_{max}} \quad \textbf{(4.1)}$$

$$\tau_f = \frac{\sigma_1 - \sigma_3}{2} cos\phi = \frac{\sigma_d}{2} cos\phi \quad \textbf{(4.2)}$$

$$T_{max} = c + \sigma_f tan\phi \quad \textbf{(4.3)}$$

$$\sigma_f = \frac{\sigma_1 + \sigma_3}{2} - \frac{\sigma_1 - \sigma_3}{2} sin\phi = \frac{\sigma_d + 2\sigma_3}{2} - \frac{\sigma_d}{2} sin\phi \quad \textbf{(4.4)}$$

Where: τ_{max} is applied shear stress acting on the failure plane oriented at an angle of 45° + ϕ/2;
σ_f is applied normal stress acting on the failure plane oriented at an angle of 45° + ϕ/2;
τ_f is the shear strength of the material under a certain stress state;
σ_1 and σ_3 are the major and minor principal stresses, respectively;
σ_d is the deviator stress, $\sigma_d = \sigma_1 - \sigma_3$;
c is the cohesion of the material;
ϕ is the internal friction angle of the material (ϕ = 0 for stress-independent materials).

Critical Responses

In mechanistic analyses, the major and minor principal stresses (σ_1 and σ_3) on top of the base and subgrade layers are the critical responses required for calculating the shear stress/strength ratio for designing permeable interlocking concrete pavements. These stresses can be calculated using multilayer linear elastic theory. The *OpenPave* software program *(5)* was used for these analyses.

4.2.3 Input Parameters for Mechanistic Modeling and Structural Analysis

The input parameters used in the mechanistic modelling and structural analysis are summarized in Table 4.1 and discussed in the following sections. Where appropriate, worst case conditions were assumed (i.e., soaked subgrade, maximum legal axle load, etc.).

Pavement Structure

A standard permeable interlocking concrete pavement structure with the following layers was used in the mechanistic analysis:

- Surface (interlocking concrete paver, 80 mm thick)
- Bedding layer (ASTM #8 aggregate, 50 mm thick)
- Base layer (ASTM #57 aggregate, 100 mm thick)
- Subbase layer (ASTM #2 aggregate, with varying thickness)
- Subgrade soil

The bedding and base layers provide intermediate levelling layers between the coarse subbase aggregate and the concrete pavers. Rather than applying marginally different shear strengths to each layer, all of the aggregate layers (bedding, base, and subbase) were integrated into one nominal aggregate base (AB) layer and assumed to have similar strength properties (a range of strength properties was used). Nine different thicknesses of this nominal aggregate base (AB) layer, ranging from 300 mm to 1,500 mm (12 in. to 59 in.), were used in the mechanistic analysis.

Table 4.1: Summary of Input Factorials for Rutting Performance Modeling of PICP

Variable	Surface		Base			Subgrade		Axle Type	Axle Load (kN)	Stress Location
	Thickness (mm)	Stiffness (MPa)	Thickness (mm)	Stiffness (MPa)	c, ϕ (kPa, °)	Stiffness (MPa)	c, ϕ (kPa, °)			
Label	h1	E1	h2	E2	c, ϕ	E3	c, ϕ	AT	AL	SL
Value	80	200 500 1,000 2,000	300 450 600 750 900 1,050 1,200 1,350 1,500	60 90 120 180	0, 45	20 50 100 150	0 and 10, 20 0 and 15, 25 0 and 20, 30 0 and 25, 35	Dual Single	89	UW[1] BW[2]
Factorial Levels	1	4	9	4	1	4	2	1	1	2
Total Calculations	2,304									

[1] UW = under wheel [2] BW=between wheel

Materials Properties

The material properties used in the mechanistic analysis included stiffness and Poisson's ratio for each layer in the pavement structure, and cohesion and internal friction angle of the composite base aggregate and subgrade soil materials. These properties were selected from the deflection testing analyses (discussed in Chapter 3) and from the results of other studies documented in the literature. No laboratory testing to measure actual material properties was undertaken in this study.

Four different stiffnesses were selected for each layer (surface, base and subgrade) based on the backcalculated effective stiffnesses from the deflection testing analyses discussed in Chapter 3:

- Surface (pavers): 200, 500, 1,000, and 2,000 MPa
- Base (combined bedding, base, and subbase layers): 60, 90, 120, and 180 MPa
- Subgrade: 20, 50, 100, and 150 MPa

The Poisson's ratio for each layer was assumed to be 0.35 based on measurements documented in other studies *(10,12)*.

The cohesion and internal friction angle (c, ϕ) of the aggregate base material was assumed to be 0 kPa and 45° respectively, based on a review of the literature *(10,12)*. For the subgrade material, both non-zero ($\phi \neq 0$) and zero ($\phi = 0$) internal friction angles were used in the analysis for all stiffness levels to simulate drained and soaked, undrained soil conditions, respectively. Based on a review of the literature *(13-17)*, the subgrade cohesion and internal friction angles (c, ϕ) were set at the following levels for each of the four subgrade stiffnesses:

- 20 MPa: 10 kPa and 20° and 0°
- 50 MPa: 15 kPa and 25° and 0°
- 100 MPa: 20 kPa and 30° and 0°
- 150 MPa: 25 kPa and 35° and 0°

Traffic Load

A single rear axle with dual wheels was used in the analysis. The axle load was set at 89 kN (20,000 lb) and the tire pressure was set at 700 kPa (101 psi), which is the tire pressure used in accelerated load tests. The distance between the two tire centers was set at 340 mm (13.4 in.). The stress under the wheel and the stress between the wheels were both calculated to identify the most critical stress.

4.2.4 Mechanistic Analysis Results

Combined Base and Subbase Layer

The results of the mechanistic analysis for the different base layer (combined bedding, base, and subbase layers) stiffness values and thicknesses include the major and minor principal stresses, normal stress at the

failure plane, shear strength at the selected stress state, shear stress at the failure plane, and the shear stress/strength ratio at the failure plane at the top of the combined base layer. The results are detailed in the full report in Appendix B and indicate that, according to the multilayer linear elastic design theory, an increase in the thickness of the combined base and subbase layer does not necessarily reduce the stresses at the top of that layer, as expected.

Subgrade

The results of the mechanistic analysis for the subgrade included the same parameters used in the combined base and subbase layer analysis, except that the shear stress/strength ratio at the top of the subgrade was calculated. The results are detailed in the full report in Appendix B and indicate that increasing the thickness of the subbase layer (the coarse ASTM #2 aggregate subbase layer given that this is the "strong" material) reduces the stresses (absolute values) at the top of the subgrade soil layer, as expected.

During dry conditions, when the subgrade is relatively dry (or at equilibrium moisture content) and has a nonzero internal friction angle ($\phi \neq 0$), the shear strength of the subgrade soil changes with the thickness of the combined base and subbase layer. Interestingly, the effective shear strength of the subgrade soil decreases slightly as the thickness of the base/subbase layer increases. This is attributed to the effective shear strength of subgrade soils being positively correlated with the normal stress at the failure plane under dry conditions ($\phi \neq 0$) (as defined in Equation 4.3), which provides confinement. An increase in the thickness of the base/subbase layer significantly reduces the normal stress at the failure plane at the top of the subgrade soil layer, and consequently, the effective shear strength of the subgrade soil decreases slightly as the thickness of the base/subbase layer increases.

Under wet conditions (i.e., when the subgrade is soaked and has a zero internal friction angle [$\phi = 0$]), the effective shear strength of subgrade soils does not change with the thickness of the base/subbase layer. This is because the shear strength of materials with zero internal friction angle is independent of the normal stress applied and is determined only by the cohesion of the material (as defined in Equation 4.3). Therefore, soaked subgrade soils will have constant effective shear strength regardless of an increase in the thickness of the base/subbase layer. The effective shear strength will be equal to the cohesion of the material which is slightly lower than the effective shear strength of the subgrade soil under dry conditions.

The normal stress and the shear stress are both higher under wet conditions than those under dry conditions for an identical structure and identical material properties (plots illustrating this are included the full report in Appendix B). The shear stress/strength ratio under wet conditions is also higher than the

shear stress/strength ratio under dry conditions for an identical structure and identical material properties, as expected. This confirms that wet conditions are the most critical condition influencing rutting and permanent deformation in the subgrade in pavements with permeable interlocking concrete paver surfaces.

Thickness of Base/Subbase Layers for Different Shear Stress/Strength Ratio Values

Based on the results discussed above, the base/subbase layer thicknesses with shear stress/strength ratios of 0.8 (i.e., >0.7), 0.5 (i.e., intermediate between 0.3 and 0.7 [0.3 ≤ SSR ≤ 0.7]), and 0.2 (i.e., <0.3), representing different rutting risk levels, were estimated using interpolation of the different material properties and subgrade moisture conditions. The results are presented in Figure 4.3 and Figure 4.4. The main observations with regard to required base/subbase layer thicknesses for PICP include the following:

- Higher shear stress/strength ratios, which equate to a higher risk of rutting, require thicker base/subbase layers, as expected.
- For the same shear stress/strength ratio, an increase in the effective stiffness of the base/subbase layer reduces the required thickness of that layer, especially when the subgrade has a low stiffness.
- An increase in the stiffness of the surface layer reduces the required base/subbase layer thickness to achieve the same shear stress/strength ratio. However, the effect of the surface layer stiffness is not significant due to the relatively low thickness of the pavers (80 mm) and the reduced interlock between them compared to pavers with sand joints.
- For the same shear stress/strength ratio, wet conditions require thicker base/subbase layers compared to the dry condition, confirming that undrained wet conditions are the most critical condition for design.
- The theoretical optimal design base thicknesses (combined bedding, base, and subbase layers) for low, intermediate, and higher risk levels (subgrade shear stress/strength ratios of 0.2, 0.5 and 0.8, respectively) under dry subgrade moisture conditions are approximately 1,300 mm, 800 mm, and 500 mm (51 in., 32 in., and 20 in.), respectively. In wet conditions, the theoretical optimal design thicknesses increase to 1,400 mm, 1,000 mm and 600 mm (55 in., 39 in., and 24 in.), respectively.

4.2.5 Test Track Layer Thickness Design

Empirical Design

The design approach described in the ICPI Permeable Interlocking Concrete Pavements guide *(4)* was followed to determine a benchmark design for the test track that could be used to compare with the results from a mechanistic design. Using the pavement structure detailed in Section 4.2.3, and designing for a subgrade soaked CBR of 4 percent (determined from DCP tests) and lifetime equivalent standard axle loads (ESALs) of 1,000,000 (expected traffic loading with the HVS), a subbase thickness of 675 mm (27 in.) under bedding and base layers of 50 mm (2 in.) and 100 mm (4 in.) respectively, would be required.

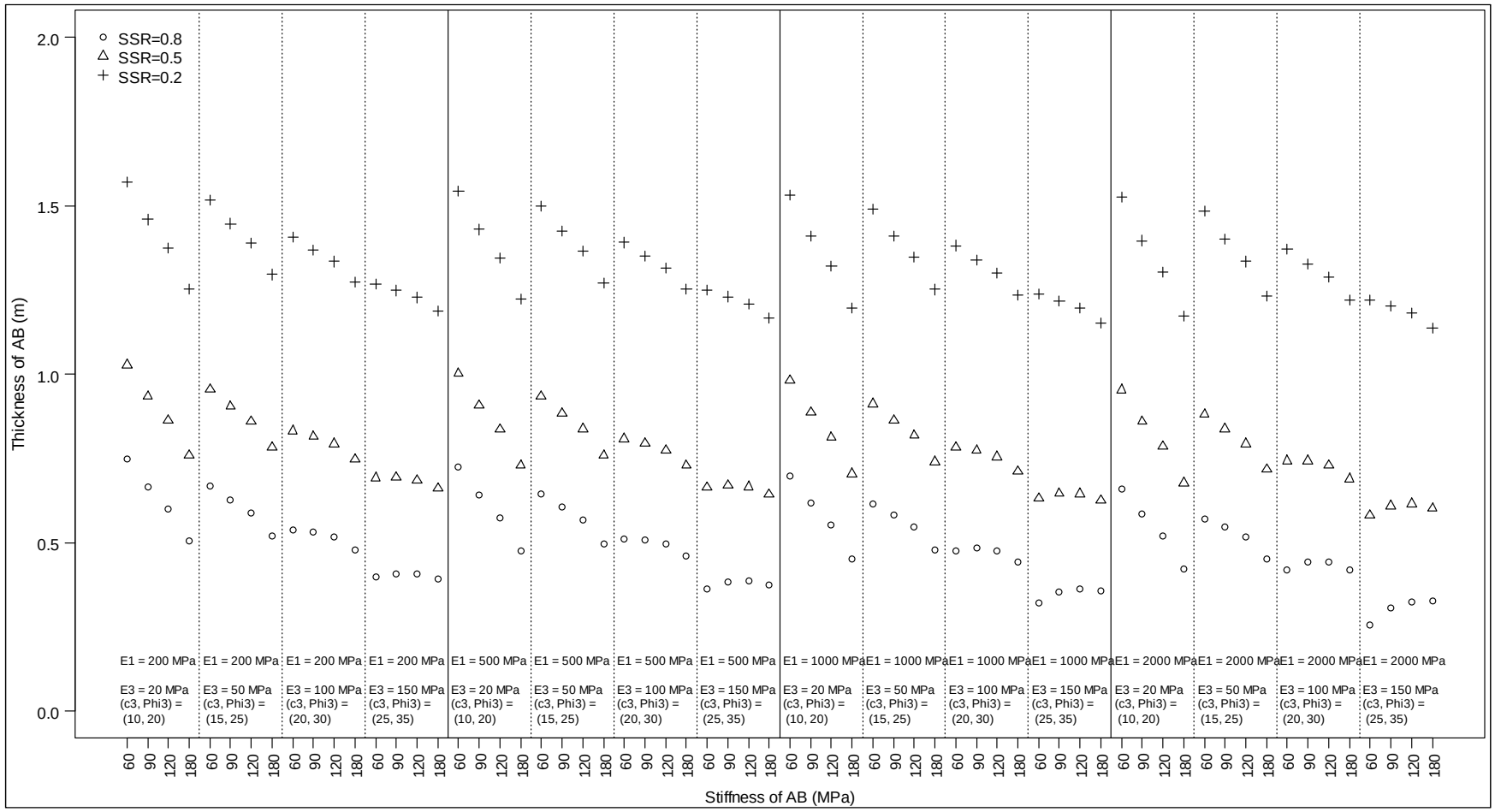

Figure 4.3: Suggested base layer thicknesses for different shear stress/strength ratios ($\phi \neq 0$ [dry]).

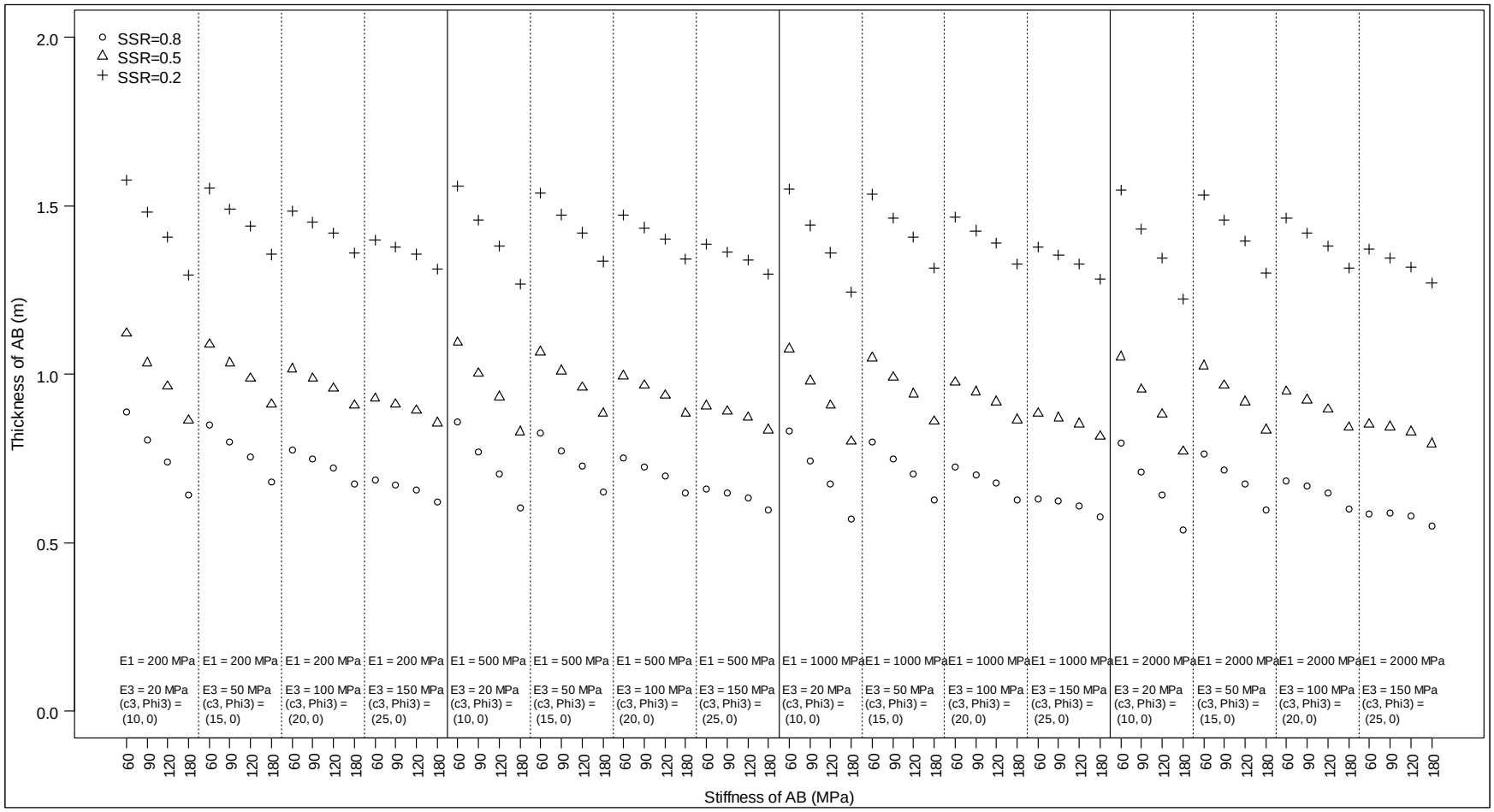

Figure 4.4: Suggested base layer thicknesses for different shear stress/strength ratios (ϕ = 0 [wet]).

Mechanistic Design

The test track design was developed using the results from the mechanistic analysis described above. The theoretical optimal design base thicknesses (combined bedding, base, and subbase layers) for the three different subgrade shear stress/strength ratios (0.8, 0.5 and 0.2) under dry conditions were approximately 500 mm, 800 mm and 1,300 mm (20 in., 32 in., and 51 in.), respectively. In wet conditions, the theoretical optimal design thicknesses increased to 600 mm, 1,000 mm and 1,400 mm (24 in, 40 in., and 56 in.), respectively.

Based on the results of the mechanistic analysis, three subbase (i.e., coarse aggregate [ASTM #2]) thicknesses of 450 mm, 650 mm, and 950 mm (18 in., 26 in., and ~38 in.), were selected for the HVS test track design to provide high, intermediate (similar to the thickness determined using the PICP design process), and low risk scenarios (Figure 4.5). The bedding layer (#8 stone) and base layer (#57 stone) thicknesses were fixed at 50 mm and 100 mm (2 in. and 4 in.), respectively, equating to total structure thicknesses of 600 mm, 800 mm, and 1,100 mm (24 in., 32 in., and 44 in.) for the three subsections. These subbase layer thicknesses are mostly thinner than the theoretical optimal design thicknesses discussed above and were selected to ensure that the performance and behavior of the test track structure could be fully understood within the time and budgetary constraints of the project.

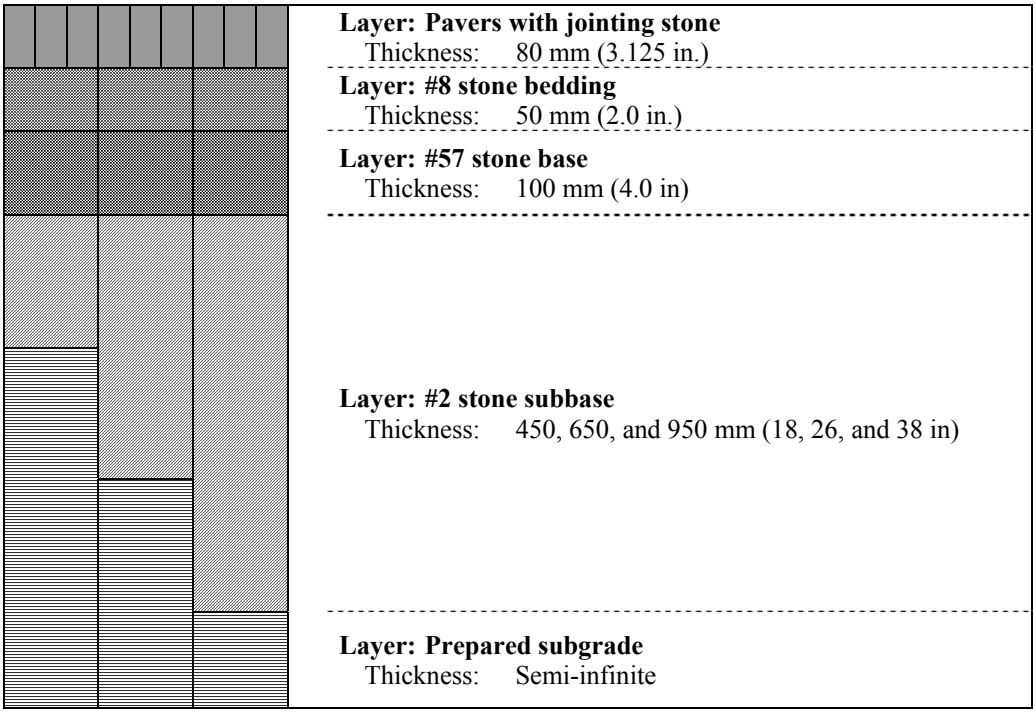

Figure 4.5: Proposed pavement structure for PICP test track (*not to scale*).

The proposed test track design provided to the construction contractor is shown in Figure 4.6. The track dimensions were 30 m long by 8 m wide (98 ft by 26 ft), long enough to accommodate the HVS and wide enough for three side-by-side test sections to allow testing under dry and wet conditions, and if required, a third moisture condition.

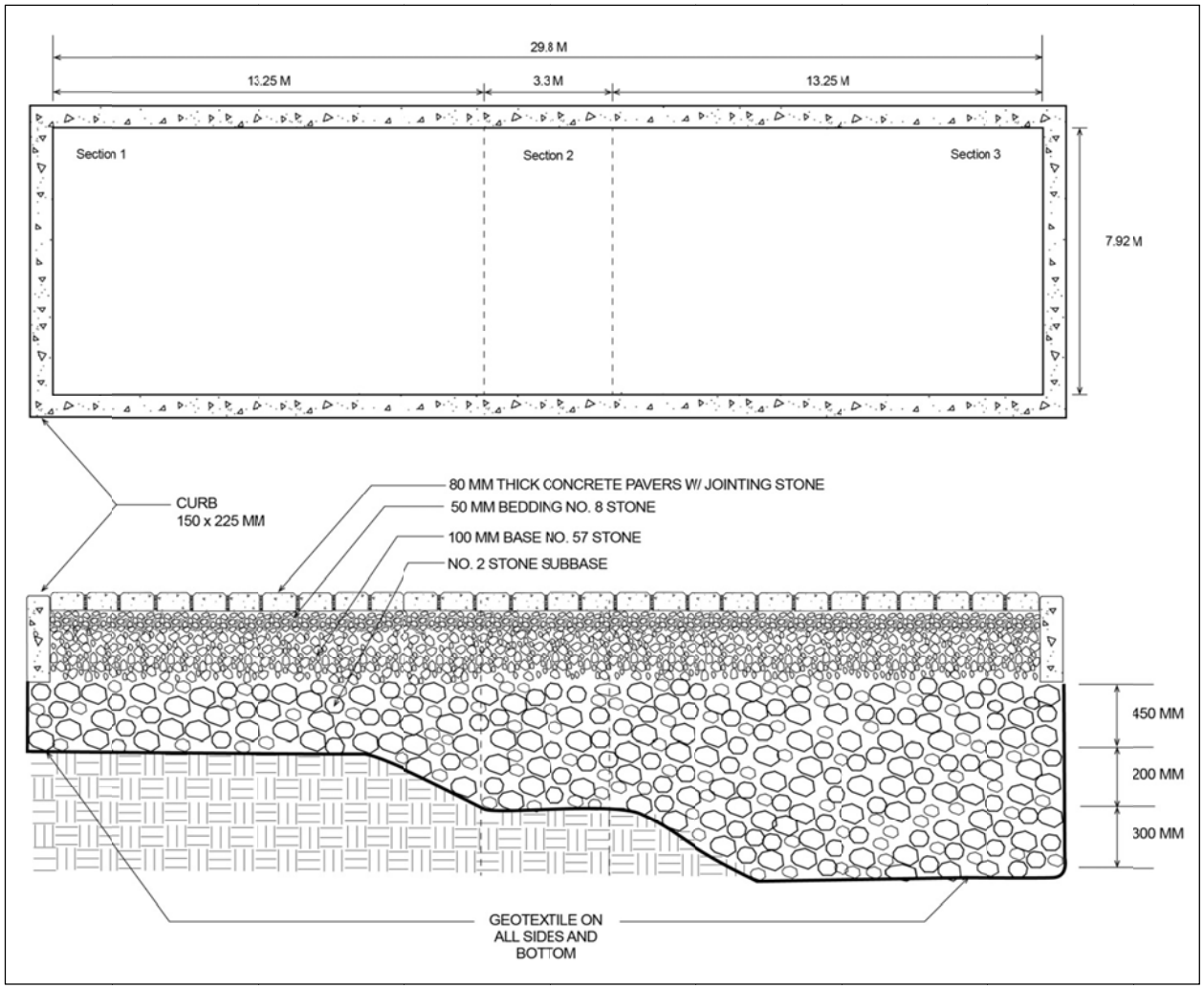

Figure 4.6: Proposed test track design supplied to the contractor.

5. TEST TRACK CONSTRUCTION

5.1 Introduction

Construction of the test track started on January 20, 2014 and was completed on January 29, 2014. The track was constructed by California Pavers, Inc. Construction was overseen by Mr. David Smith from the Interlocking Concrete Pavement Institute. Staff from the UCPRC observed all stages of construction and maintained a photographic record of the process.

5.2 Excavation (01/20/2014 – 01/21/2014)

The test track was laid out with string lines according to the dimensions in the approved test track design. A backhoe loader was used to excavate the soil. Depths and transitions between the different sections were measured with a laser level. Photographs of the excavation process are shown in Figure 5.1. Soil samples were removed during excavation to determine the laboratory maximum dry density and optimum moisture content (tested according to ASTM D1557). These were found to be 1,983 kg/m^3 (124 lb/ft^3) and 11.5 percent, respectively, and considered to be slightly higher than typical for silty-clay soils with low California Bearing Ratio strengths.

Figure 5.1: Excavation.

5.3 Subgrade Preparation (01/21/2014)

After excavation, the subgrade was smoothed with a blade attached to the back of the backhoe loader and then compacted with a 3 ton, 31 kN vibratory smooth drum roller (Figure 5.2). A 60 kN vibratory plate compactor was used to compact around the edges of the excavation. The floor of the excavation was not reworked (i.e., ripped and recompacted) and no water was added before or during compaction.

Permeability measurements were taken before and after compaction using a Modified Philip-Dunne Infiltrometer (100 mm, single ring tube) *(18)* (Figure 5.3). Before compaction, values averaged 0.03 cm/second, but after compaction, the permeability was less than 0.0001 cm/second (essentially not measurable), indicating that infiltration of water into the subgrade would be very slow. A plot of cumulative infiltration for six locations (two before compaction and four after compaction) on the subgrade is shown in Figure 5.4. The plot clearly shows the effect of compaction on infiltration.

Figure 5.2: Subgrade compaction.

Figure 5.3: Permeability measurements.

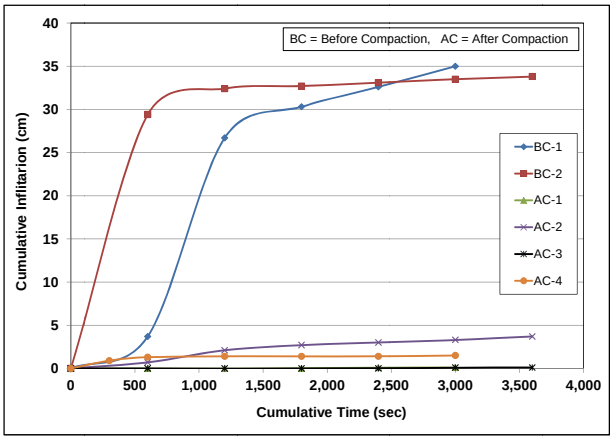

Figure 5.4: Cumulative infiltration of water into subgrade.

In situ density was measured with a nuclear density gauge after compaction (Figure 5.5). Relative compaction (percent of laboratory determined modified Proctor density [ASTM D1557]) varied between 90 percent and 91 percent across the excavation. Compaction of the subgrade is listed as optional in the ICPI guideline document *(4)*, and if required by the designer, compaction to 95 percent of the laboratory determined standard Proctor density (ASTM D698) is recommended.

Shear strength was measured with a dynamic cone penetrometer to a depth of 800 mm (~32 in.) below the surface (Figure 5.6) and used to calculate an approximate in situ California Bearing Ratio (CBR). CBR

values of three percent were consistent across the test track indicating that the subgrade was uniform, but weak, and in line with the design criteria. A series of instruments (pressure cells, permanent deformation gauges, and water level indicators) were also installed at this stage. Details on the instruments and installation are provided in Section 6.3.

Figure 5.5: Density measurements.

Figure 5.6: Dynamic cone penetrometer measurements.

Geotextile (*Mirafi 160N*) was placed on the floor and sides of the excavation to prevent pumping of subgrade fines into the subbase material (Figure 5.7). Orange markers in the excavated area in the photograph indicate location of the subgrade instrumentation on the three different depths.

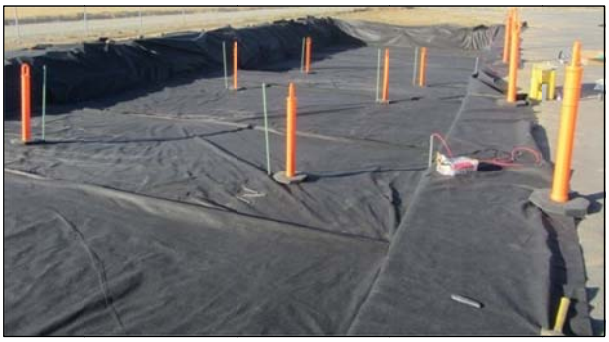

Figure 5.7: Geotextile placement.

5.4 Subbase Placement (01/22/2014 – 01/23/2014)

Subbase aggregate was sourced from a quarry near Valley Springs, CA. The rhyolite aggregate is described by the supplier as "#24 Rail Road Ballast". The properties are summarized in Table 5.1 and for the most part met the requirements for ASTM #2 stone listed in the ICPI guideline *(4)* and applicable ASTM standards. The aggregate was end-dumped into the excavation from trucks or from a front loader, and then spread with a loader into lifts approximately 30 cm (12 in.) thick (Figure 5.8). Each lift was compacted with a 3 ton, 31 kN vibratory steel wheel roller and then a 60 kN vibratory plate compactor.

Thickness of the aggregate was controlled with a laser level. Density and DCP measurements were not taken due to the coarse, open-graded nature of the aggregate, which did not permit penetration. A light-weight deflectometer (*Zorn Instruments ZFG 3000*) was used to obtain an indication of the uniformity in stiffness across the subbase surface. Seventeen measurements were taken, with stiffnesses varying between 38.8 MN/m^2 and 61.3 MN/m^2 with a mean of 51.7 MN/m^2 and a standard deviation of 7.4 MN/m^2. Variability in the results was attributed to poor seating of the instrument on the relatively loose aggregate, and movement of the aggregate when the weight was dropped.

Table 5.1: Subbase Aggregate Properties (ASTM #2)

Property	Result	
	Recommended	Actual
Gradation (mm [in.], ASTM D448) (% passing)		
75.0 (3.0)	100.0	100.0
63.0 (2.5)	90 – 100	97
50.0 (2.0)	35 – 70	–
38.0 (1.5)	0 – 15	53
19.0 (3/4)	0 – 5	7
12.5 (1/2)	–	5
0.075 (#200)	–	1
Specific gravity	–	2.8
Absorption (%)	–	0.1
Soundness (Sodium sulfate, ASTM C88) (%)	< 12	0.35
Abrasion loss (LA abrasion, ASTM C535) (%[1])	< 40	13.8
[1] after 1,000 revolutions		

Figure 5.8: Placing and compacting the subbase.

5.5 Curb Placement (01/23/2014 – 01/24/2014)

A 225 mm by 150 mm (9 in. by 6 in.) curb was included in the design for confinement of the base, bedding layer, and pavers. Formwork for this curb was fabricated on site on top of the subbase (Figure 5.11). Levels for the top of the curb were aligned with the existing road surface on the east side of the track. Reinforcing steel (13 mm (0.5 in.) was included to limit any cracking when the HVS was towed onto the test track. Ready-mix concrete was poured into the formwork and hand finished (Figure 5.10). Removal of the formwork started after approximately four hours when initial set was evident (Figure 5.11).

Figure 5.9: Formwork for curb.

Figure 5.10: Concrete curb placement.

Figure 5.11: Completed curb after removal of formwork (pipes are for instrument wiring).

5.6 Base Placement (01/27/2014)

Base aggregate was sourced from a quarry near Woodland, CA. Aggregate properties are summarized in Table 5.2 and for the most part met the requirements listed in the ICPI guideline *(4)*.

Table 5.2: Base Aggregate Properties (ASTM #57)

Sieve Size		% Passing	
(mm)	(in./# mesh)	Recommended[1]	Actual
37.0	1.5	100	100
25.0	1.0	95 – 100	100
19.0	3/4	–	89
12.5	1/2	25 – 60	24
9.50	3/8	–	3.0
4.75	#4	0 – 10	0.3
2.36	#8	0 – 5	0.3

Aggregate was tipped onto the subbase using a small skid-steer loader, rough-spread with the skid-steer bucket, and then levelled by hand with shovels and rakes (Figure 5.12). After placement, the aggregate was compacted with a 60 kN vibratory plate compactor. Thickness was controlled with a laser level. Density and DCP measurements were not taken due to the coarse, open-graded nature of the aggregate. However, a light-weight deflectometer (*Zorn Instruments ZFG 3000*) was used to obtain an indication of the uniformity in stiffness across the test track (Figure 5.13). Nineteen measurements were taken, with stiffnesses varying between 38.9 MN/m^2 and 76.0 MN/m^2, with a mean of 59.1 MN/m^2 and a standard deviation of 8.5 MN/m^2. Variability in the results was again attributed to poor seating of the instrument on the relatively loose, open-graded aggregate, and movement of the aggregate when the weight was dropped. The instrument did not distinguish between the different subbase thicknesses.

Figure 5.12: Base layer placement.

Figure 5.13: Light-weight deflectometer testing on the base.

5.7 Bedding Layer Placement (01/28/2014)

Bedding layer aggregate was sourced from the same quarry as the base aggregate. Properties are summarized in Table 5.3 and for the most part met the requirements listed in the ICPI guideline *(4)*.

Table 5.3: Bedding Layer Aggregate Properties (ASTM #8)

Sieve Size		% Passing	
(mm)	(in./# mesh)	Recommended	Actual
12.5	1/2	100	100.0
9.50	3/8	85 – 100	86
4.75	#4	10 – 30	4.7
2.36	#8	0 – 10	1.8
1.18	#16	0 - 5	1.7

Aggregate was tipped onto the base using a small skid-steer loader, rough-spread with the skid-steer bucket, then levelled by hand with shovels and rakes (Figure 5.14). Final smoothing was completed with a straight edge run on two pipes that were positioned at the correct height. Depth was checked with a laser level. The bedding layer was not compacted.

Figure 5.14: Bedding layer placement.

Figure 5.13: Bedding layer placement.

5.8 Paver Placement (01/28/2014 – 01/29/2014)

The pavers used to surface the test track were 195 mm x 95 mm x 80 mm (7.7 x 3.7 x 3.2 in.) in size and reportedly met the requirements specified in ASTM C936 (Standard Specification for Solid Concrete Interlocking Paving Units). Pavers were machine placed in a 90° herringbone pattern flush with the curb using custom placing equipment (Figure 5.15).

Figure 5.15: Paver placement and compaction.

Edge (~100 x 100 mm) and full-size stitching pavers were placed by hand where required along the concrete curbs. No pavers were cut. After placement, the pavers were compacted with 60 kN and 22 kN vibratory plate compactors until a level surface was achieved. Jointing stone (crushed aggregate passing a 4.75 mm [#4]/ retained on a 2.36 mm [#8] sieve and meeting the requirements listed in Table 5.3) was spread into the joints with brooms and then the surface was compacted again with a 22 kN plate compactor (Figure 5.16). Photographs of the completed test track are shown in (Figure 5.17).

Figure 5.16: Jointing stone placement and compaction.

Figure 5.17: Completed test track.

5.9 Surface Permeability

Surface permeability was measured according to ASTM C1701 (*Standard Test Method for Infiltration Rate of In Place Pervious Concrete*, which is similar to ASTM C1781 [*Standard Test Method for Surface Infiltration Rate of Permeable Unit Pavement Systems*]). The results are summarized in Figure 5.18. Permeability was consistent across the test track and considered to be rapid, with no water ponding on, or running across, the surface.

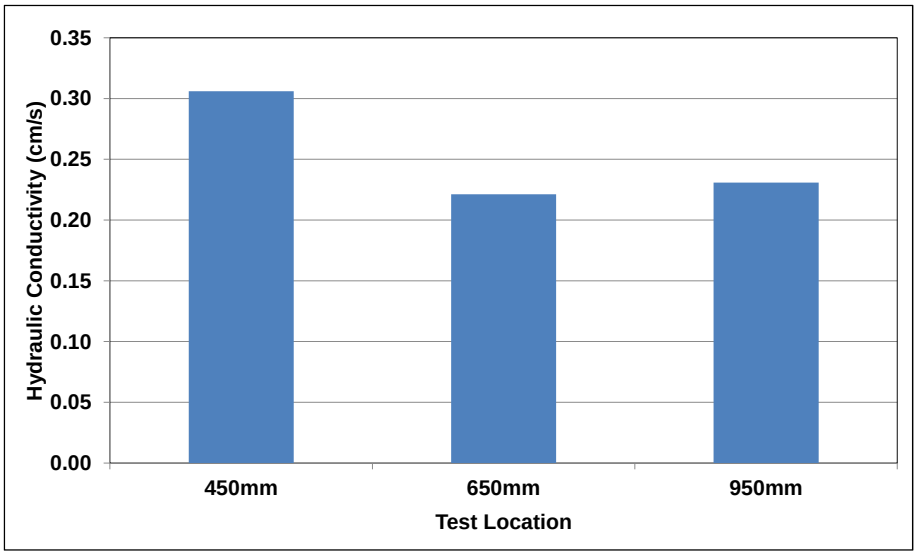

Figure 5.18: Surface permeability after construction.

5.10 Material Sampling

Samples of all layers were collected during construction and retained for future testing if required. The optimum moisture content and maximum dry density of the subgrade material were determined to establish the degree of compaction (see Section 5.3).

6. TRACK LAYOUT, INSTRUMENTATION, AND TEST CRITERIA

The Heavy Vehicle Simulator (HVS) test section layout, test setup, trafficking, and measurements followed standard University of California Pavement Research Center (UCPRC) protocols *(19)*.

6.1 Test Track Layout

The test track layout is shown in Figure 6.1. Three HVS test sections were demarcated on the track, the first for testing under dry conditions, the second for testing under soaked conditions (i.e., water level maintained at the top of the subbase), and the third for testing under drained conditions (i.e., wet subgrade, but no water in the subbase). Test sections were evenly distributed across the test track. The test section numbers were allocated in order of testing sequence as follows (HC refers to the specific HVS equipment used for testing):

- Section 678HC: Dry test
- Section 679HC: Wet test
- Section 680HC: Drained test

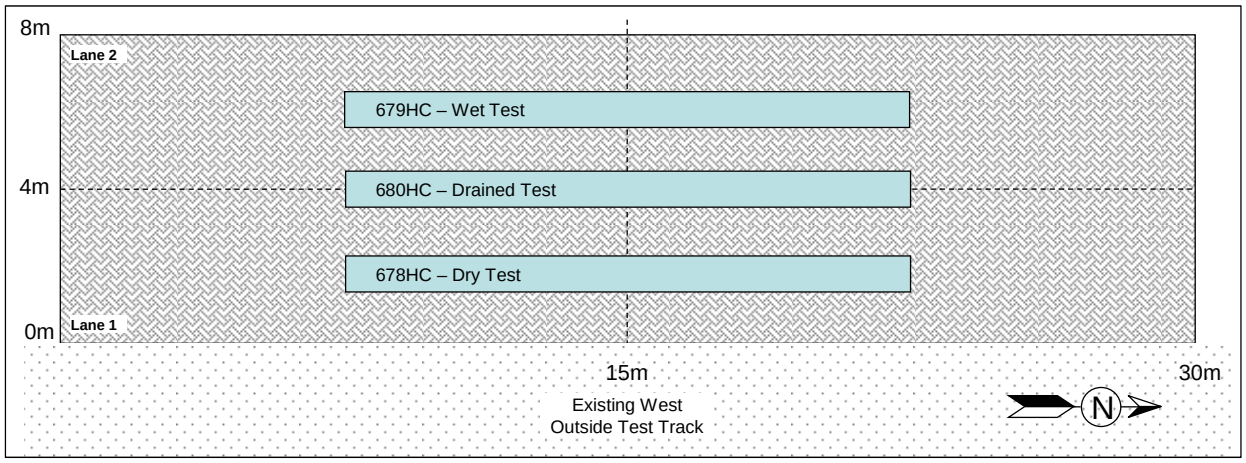

Figure 6.1: Plan view of test track layout.

6.2 HVS Test Section Layout

An extended HVS test section is 15.0 m (49.2 ft) long and 1.0 m (3.3 ft) wide. A schematic in Figure 6.2 shows an HVS test section along with the stationing and coordinate system. Station numbers (0 to 30) refer to fixed points on the test section and are used for measurements and as a reference for discussing performance. Stations are placed at 0.5 m (1.6 ft) increments. A sensor installed at the center of the test section would have an *x*-coordinate of 7,500 mm and a *y*-coordinate of 500 mm.

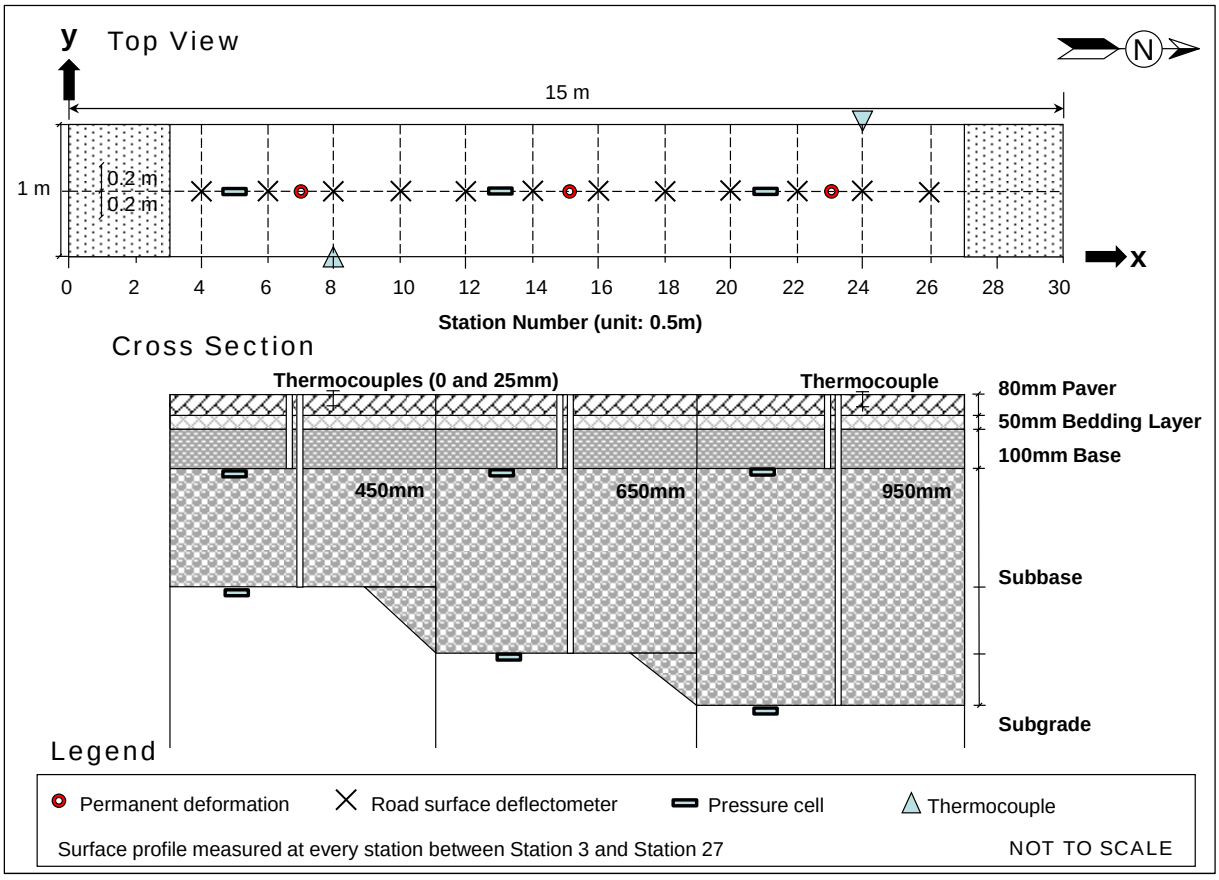

Figure 6.2: Schematic of an extended HVS test section.

6.3 Test Section Instrumentation and Measurements

Measurements were taken with the equipment and instruments listed below. Instrument positions are shown in Figure 6.2.

6.3.1 Temperatures

Type-K thermocouples were used to measure pavement and air temperatures at 60 minute intervals for the duration of the test. Two thermocouples were bundled together to form a "thermocouple tree" for measuring air and paver temperatures. Paver temperature was measured 25 mm below the surface. Thermocouple trees were installed on the edge of each subsection (shaded by the HVS during part of the day) and approximately 2.0 m from the center of the test section on the unshaded western side of the HVS. Additional air temperatures were recorded at a weather station at the northern end of the test track.

6.3.2 Water Level in the Pavement

A perforated pipe (75 mm [3 in.] diameter) was installed on the east and west sides of the test track on each subsection. The bottom of the pipe rested on the subgrade and the top of the pipe extended above the

surface (Figure 6.3). An *Omega PX437-010GI* submersible pressure transmitter (Figure 6.4) was used to measure hydraulic pressure at 30 minute intervals in one of the pipes on the western side of the 950 mm subbase subsection. Water level was calculated from the hydraulic pressure. Dipstick measurements were taken in the other pipes to verify the pressure transmitter measurements and to check consistency of the water level across the test track.

Figure 6.3: Perforated pipe for water level measurements.

Figure 6.4: Submersible water transmitter.

6.3.3 Surface Permanent Deformation (Rut Depth)

A laser profilometer (Figure 6.5) was used to measure surface profile; measurements were taken at each station on the test section. The following rut parameters were determined from the laser profilometer measurements:

- Maximum total rut depth at each station
- Average maximum total rut depth for all stations
- Average deformation for all stations
- Location and magnitude of the maximum rut depth for the section
- Rate of rut development over the duration of the test

Figure 6.5: Laser profilometer.

The difference between the surface profile after HVS trafficking and the initial surface profile before HVS trafficking is the permanent change in surface profile. Based on the change in surface profile, the maximum total rut is determined for each station, as illustrated in Figure 6.6. The average maximum total rut for the section is the average of all of the maximum total ruts measured between Stations 3 and 27 (Stations 0 to 3 and 27 to 30 are in the wheel braking area and are not measured).

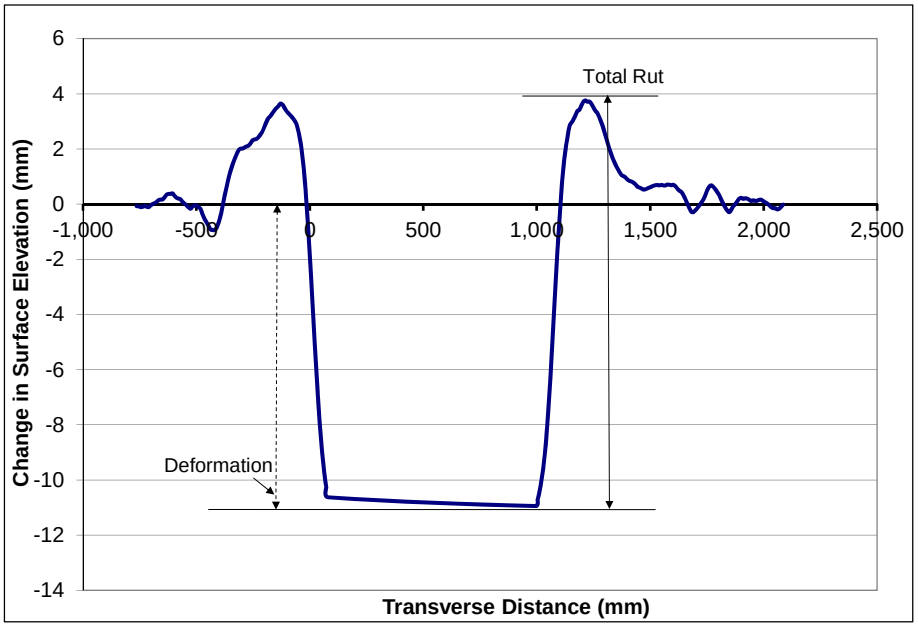

Figure 6.6: Illustration of maximum rut depth and deformation for a leveled profile.
(For HVS test with 1 m wander)

6.3.4 Permanent Deformation in the Underlying Layers

Permanent deformation gauges were installed in each subsection of the dry and wet test sections to measure vertical permanent deformation between the pavement surface and the top of the subbase, and the pavement surface and the top of the subgrade. The gauges were custom fabricated for the experiment, given that instruments that are traditionally used to measure permanent deformation in accelerated pavement testing experiments (e.g., multi-depth deflectometers [MDD]) are not suited to installation and measurements in the coarse aggregates used in the subbase. The gauge consists of a 100 mm (4 in.) square stainless steel target plate that is positioned on a thin layer of bedding sand on the top of the selected layer (Figure 6.7). A 25 mm sleeve is welded to the plate. A stainless steel pipe, cut to a height equivalent to 25 mm below the top of the paver is inserted into the sleeve. The top of this pipe slots into a hole drilled into the paver. A stainless steel rod is inserted into the pipe to measure permanent deformation on a simple measuring jig (Figure 6.8).

Figure 6.7: Permanent deformation gauge.

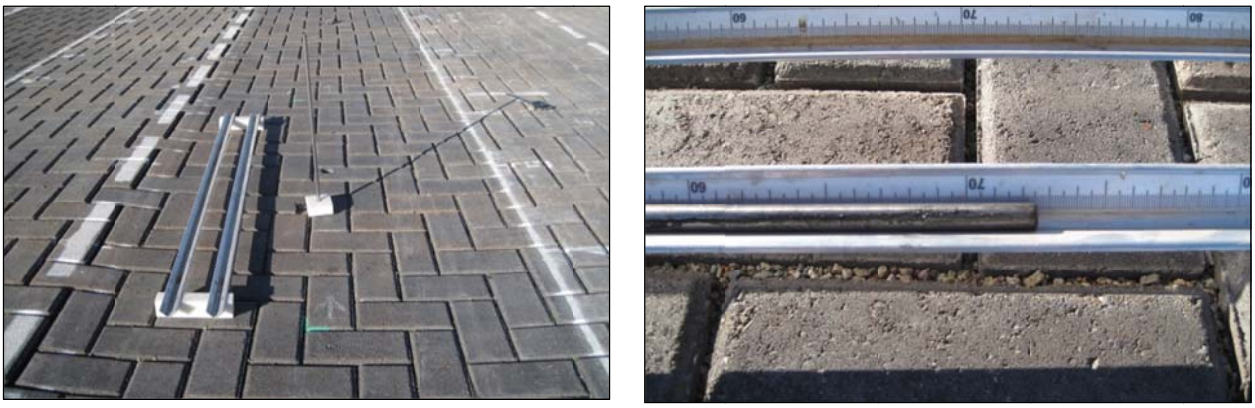

Figure 6.8: Permanent deformation measurements.

6.3.5 Surface Deflection

A road surface deflectometer (RSD [Figure 6.9]) was used to measure surface deflection during the test. RSD measurements were taken under a creep-speed 40 kN half-axle load at regular intervals. Note that RSD measurements under a creep-speed load will not be the same as those recorded under the trafficking speed load (10 km/h). After load changes, deflections were measured under the new load, as well as under the previous lighter loads. Only the results from testing under the 40 kN half-axle load are discussed in this report.

Figure 6.9: Road surface deflectometer.

6.3.6 Vertical Pressure (stress) at the Top of the Subbase and Top of the Subgrade

Pressure cells were installed in each subsection of the dry and wet test sections to measure vertical pressure (stress) under the moving wheel. One *RST Instruments, Model #: LPTPC-09-S* (1 MPa [150 psi] range) pressure cell was installed level with the surface of the subgrade in each subsection after excavation and compaction and before placement of the geotextile (Figure 6.10). A similar pressure cell with 1.4 MPa (200 psi) range was installed on the top of the subbase. Bedding sand for the cells was placed on top of a square of geotextile and used as a leveling course for the instrument to limit any movement on top of the uneven coarse aggregate subbase (Figure 6.11).

Figure 6.10: Pressure cell installation in the subgrade.

Figure 6.11: Pressure cell installation on top of the subbase.

Example data recorded from one of the pressure cells is shown in Figure 6.12. Variation of the pressure reading versus wheel position as the wheel travels from one end of the test section to the other is clearly evident. Several quantities are summarized based on the raw readings. Specifically, the reference value is the reading when the wheel is at the far end of the test section. The peak and valley are maximum and minimum values deviating from the reference value, respectively.

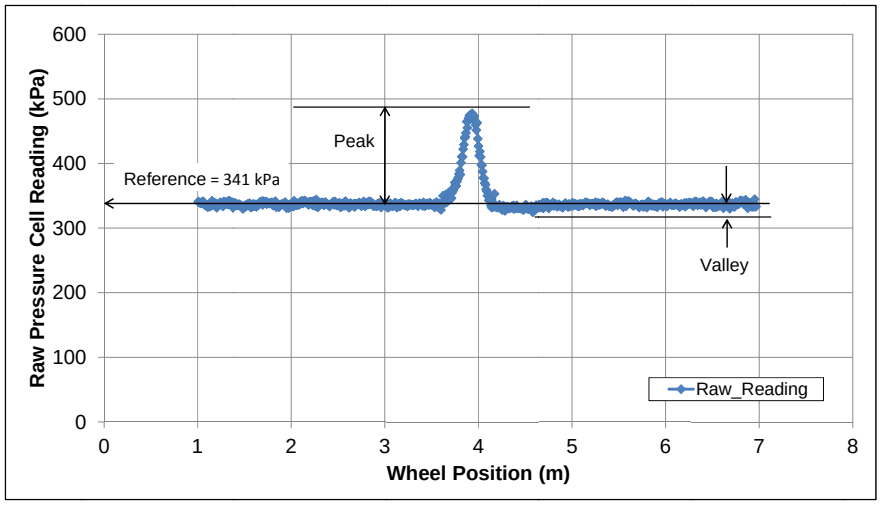

Figure 6.12: Example pressure cell reading and definition of summary quantities.

6.3.7 Jointing Stone Depth

Jointing stone depth relative to the surface was measured with a depth gauge (Figure 6.13) at Stations 4 and 7 on the 450 mm subbase subsection, at Stations 12 and 14 on the 650 mm subbase subsection, at Station 17 in a transition zone, and at Stations 25 and 26 on the 950 mm subbase subsection. Jointing stone was replenished if the measured depth was below 25 mm (1 in.).

Figure 6.13: Jointing stone depth measurement.

6.4 HVS Test Criteria

6.4.1 Test Section Failure Criteria

An average maximum rut depth of 25 mm (1.0 in.) over the length of each subsection (Station 3 to Station 10, Station 10 to Station 20, and Station 20 to Station 27) was set as the failure criteria for the experiment. In some instances, HVS trafficking was continued past these points to fully understand rutting behavior on the entire test section, given than the 450 mm subbase subsection would likely fail before the thicker sections.

6.4.2 Environmental Conditions

Pavement temperatures were not controlled in this experiment since temperature has a minimal effect on the behavior of the concrete pavers in terms of pavement response. All testing was therefore carried out at ambient temperatures.

During the dry test, a number of light rainfall events were recorded, but no change in subgrade moisture condition occurred. In the wet test, water was soaked through the pavers next to the test section and allowed to fill the pavement structure until it overflowed (Figure 6.14). The water level was then allowed to recede to the top of the coarse aggregate subbase, where it was maintained with controlled water flow until the end of the test. In the drained test, no water was added and testing was started once the water level had receded to the top of the subgrade (i.e., there was no water in the coarse aggregate subbase during the test).

Figure 6.14: Flooded section during preparation for wet testing.

6.4.3 Test Duration

HVS trafficking on each test was initiated and completed as shown in Table 6.1.

Table 6.1: Test Duration for Phase 1 HVS Rutting Tests

Section No.	Test	Start Date	Finish Date	Load Repetitions
678HC	Dry	02/12/2014	03/31/2014	340,000
679HC	Wet	04/17/2014	05/21/2014	380,000
680HC	Drained	06/11/2014	07/14/2014	125,000

6.4.4 Loading Program

The HVS loading program for each test is summarized in Table 6.2. Equivalent Standard Axle Loads (ESALs) were determined using the following conversion (Equation 6.1):

$$ESALs = ((axle\ load/40)^{4.0}) \times number\ of\ load\ repetitions \quad \textbf{(6.1)}$$

Table 6.2: Summary of HVS Loading Program

Section	Test	Half-Axle Wheel Load[1] (kN)	Repetitions	ESALs[2]
678HC	Dry	25	100,000	15,259
		40	100,000	100,000
		60	140,000	708,750
		Section Total	340,000	824,009
679HC	Wet	25	100,000	15,259
		40	100,000	100,000
		60	140,000	708,750
		80	40,000	640,000
		Section Total	380,000	1,464,009
680HC	Drained	25	100,000	15,259
		40	25,000	25,000
		Section Total	125,000	40,259
		Project Total	**845,000**	**2,328,277**

[1] 40 kN = 9,000 lb.; 60 kN = 13,500 lb; 80 kN = 18,000 lb.
[2] ESAL: Equivalent standard axle load

All trafficking was carried out with a dual-wheel configuration, using radial truck tires (Goodyear G159 - 11R22.5- steel belt radial) inflated to a pressure of 700 kPa (101 psi), in a bidirectional loading mode with a one meter wide wander pattern (i.e., trafficking in both directions in line with standard procedures for testing base layer performance). Load was checked with a portable weigh-in-motion pad at the beginning of each test, after each load change, and at the end of each test.

Blank page

7. HEAVY VEHICLE SIMULATOR TEST DATA

7.1 Introduction

This chapter provides a summary of the data collected from the three HVS tests (Sections 678HC through 680HC) and a brief discussion of the first-level analysis. In addition to visual assessments, the following data were collected:

- Rainfall
- Temperatures
- Water level in the pavement
- Surface permanent deformation (rutting)
- Permanent deformation in the underlying layers
- Surface deflection
- Vertical pressure (stress) at the top of the subbase and top of the subgrade
- Jointing stone depth

7.2 Rainfall

Figure 7.1 shows the monthly rainfall data from January 2014 through August 2014 measured at the weather station close to the test track. This period spans construction of the test track and the three HVS tests. Rainfall was recorded during dry and wet testing, but not during the drained test. Daily rainfall was very low with 6.4 mm (0.26 in.) being the highest recorded on any one day during testing. During the dry test, the test section was protected from direct rainfall by the HVS. The area surrounding the HVS was covered with plastic sheeting to prevent any infiltration of water.

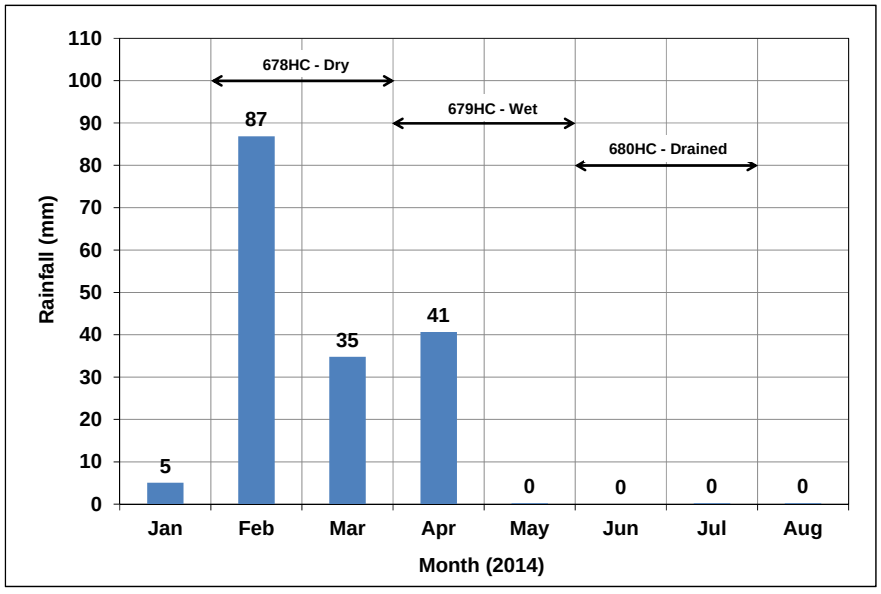

Figure 7.1: Measured rainfall during the study period.

7.3 Section 678HC: Dry Test

7.3.1 Test Summary

Loading commenced with a 25 kN (4,500 lb) half-axle load on February 12, 2014, and ended with a 60 kN (13,500 lb) load on March 31, 2014. A total of 340,000 load repetitions were applied and 26 datasets were collected. Load was increased from 25 kN to 40 kN (9,000 lb) and then to 60 kN (13,500 lb) after 100,000 and 200,000 load repetitions, respectively. One breakdown (test carriage bearing failure) occurred during testing on this section. The HVS loading history for testing on the dry section is shown in Figure 7.2.

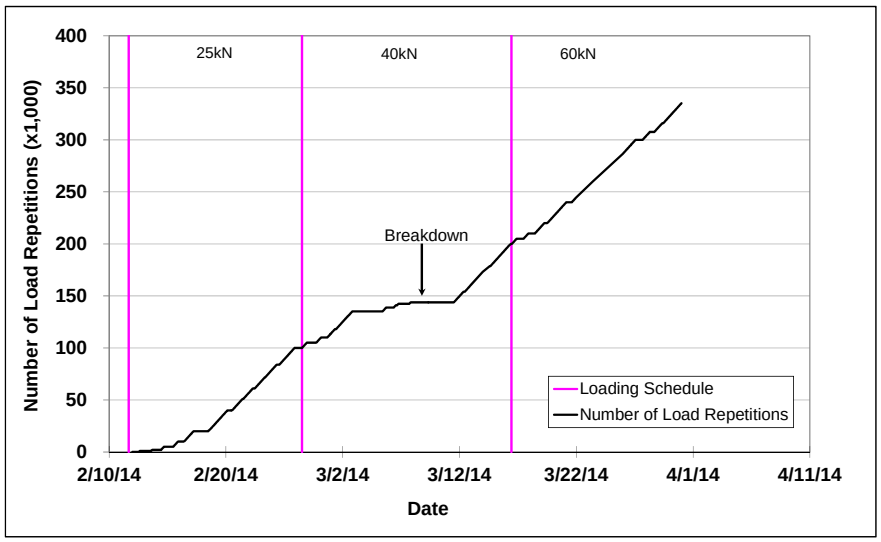

Figure 7.2: 678HC: HVS loading history.

7.3.2 678HC: Water Level in the Pavement

Measurements showed no water in the subbase for the duration of the test.

7.3.3 678HC: Temperatures

Daily average air temperatures and paver temperatures 25 mm below the surface are summarized in Figure 7.3. Vertical error bars show the daily temperature range in the unshaded pavers. Temperature did not appear to influence the performance of the test section in any way. Key measurements include the following:

- Air temperatures above the test section (i.e., shaded by the HVS during periods of the day) ranged from 7.5°C to 20.5°C (46°F to 69°F) during the course of HVS testing, with a daily average of 14.1°C (58°F).
- Air temperatures in the unshaded area ranged from 10.4°C to 21.5°C (51°F to 71°F) during the course of HVS testing, with a daily average of 15.7°C (60°F).
- Paver temperatures in the test section (i.e., shaded by the HVS during periods of the day) ranged from 9.9°C to 22.6°C (50°F to 73°F) with a daily average of 15.5°C (60°F).

- Paver temperatures in the unshaded area of the test track ranged from 7.9°C to 44.0°C (46°F to 111°F) with a daily average of 18.8°C (66°F).

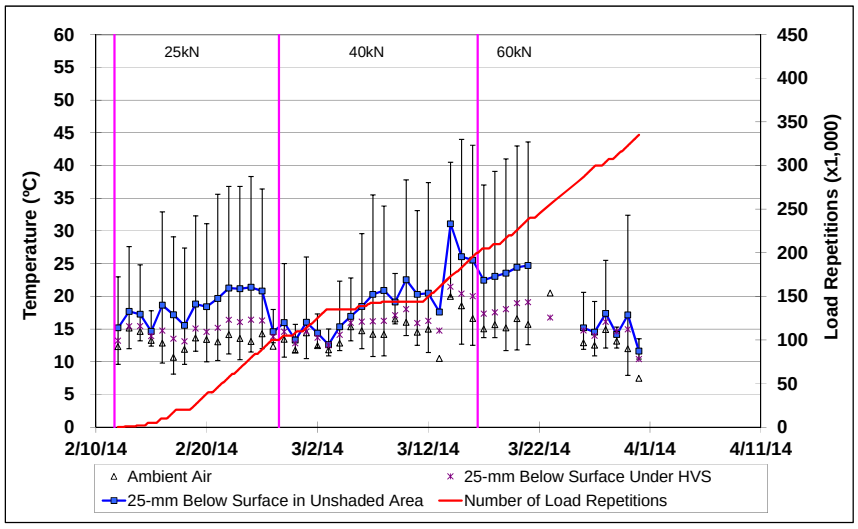

Figure 7.3: 678HC: Daily average air and pavement temperatures.

7.3.4 678HC: Permanent Deformation on the Surface (Rutting)

Figure 7.4 through Figure 7.6 show the average transverse cross sections measured with the laser profilometer at various stages of the test for each of the three thickness design subsections. The plots clearly show the increase in rutting and deformation over time. The plots also show that most of the deformation was in the form of a depression (i.e., deformation was below the zero elevation point at the surface [Figure 6.6]) rather than upward and outward displacement of the material above the zero elevation point.

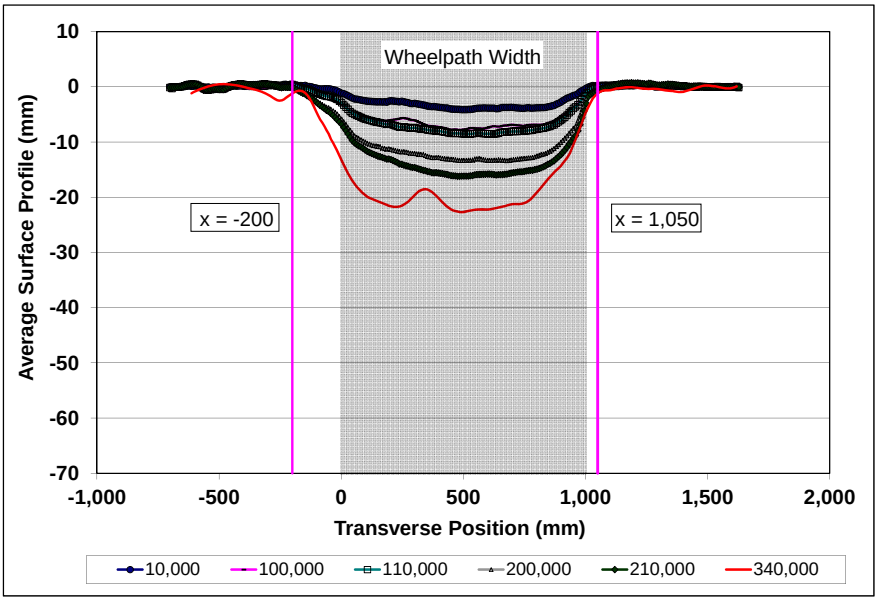

Figure 7.4: 678HC (450 mm): Profilometer cross section at various load repetitions.

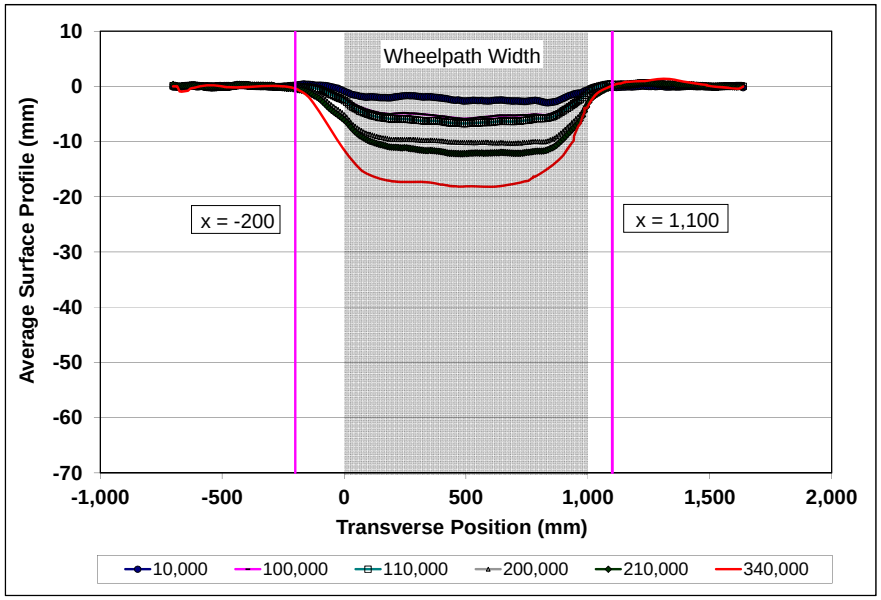

Figure 7.5: 678HC (650 mm): Profilometer cross section at various load repetitions.

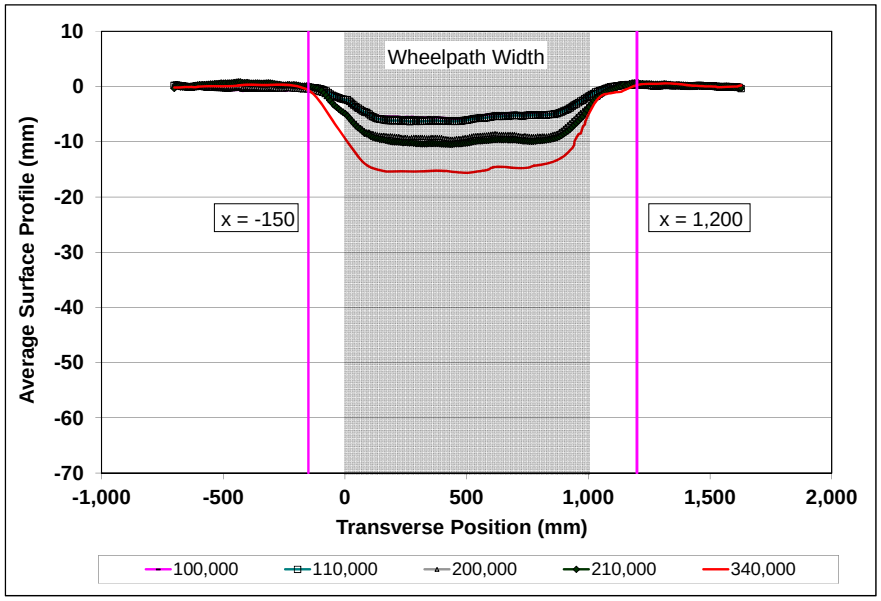

Figure 7.6: 678HC (950 mm): Profilometer cross section at various load repetitions.

Figure 7.7 shows the development of surface permanent deformation (average maximum total rut) with load repetitions for the three subsections. Observations of surface rutting for each wheel load during the dry test include the following:

- 25 kN (4,500 lb) Wheel Load
  - During HVS testing, rutting usually occurs at a high rate initially, and then it typically diminishes as trafficking progresses until reaching a steady state. This initial phase is referred to

as the "embedment" phase. The initial embedment phase in this test, although relatively short in terms of the number of load repetitions (i.e., ± 5,000), ended with a fairly significant early rut of about 5.0 mm (0.2 in.) that was attributed to bedding in of the pavers under the wheel load. The rate of rut depth increase after the initial embedment phase was uniform until the load change.

- 40 kN (9,000 lb) Wheel Load
  - A second small embedment phase was recorded after the load change to 40 kN. The section with the 450 mm subbase was most sensitive to the load change, as expected. After embedment, the rate of rut depth increase was again uniform, but faster than the rate recorded with the 25 kN load, indicating that the pavement was sensitive to very heavy loads (i.e., at or above legal design loads.
- 60 kN (13,500 lb) Wheel Load
  - A third embedment phase was recorded after the load change to 60 kN. The change in rut rate was more severe during this embedment, and the rate of rut depth increase accelerated. The change in rut rate was larger on the 450 mm and 650 mm subbase sections compared to that on the 950 mm subbase section. After completion of trafficking, the average maximum rut depth (average of the total rut recorded at each station) for the 450 mm, 650 mm, and 950 mm subbase subsections was 24.5 mm (0.96 in.), 21.4 mm (0.84 in), and 17.7 mm (0.70 in.), respectively.

The test was stopped after 340,000 load repetitions (equivalent to 824,009 ESALs) when the average maximum rut on the 450 mm subbase subsection reached 25 mm (1 in.), which was the terminal rut depth set for the test (see Section 6.4.1).

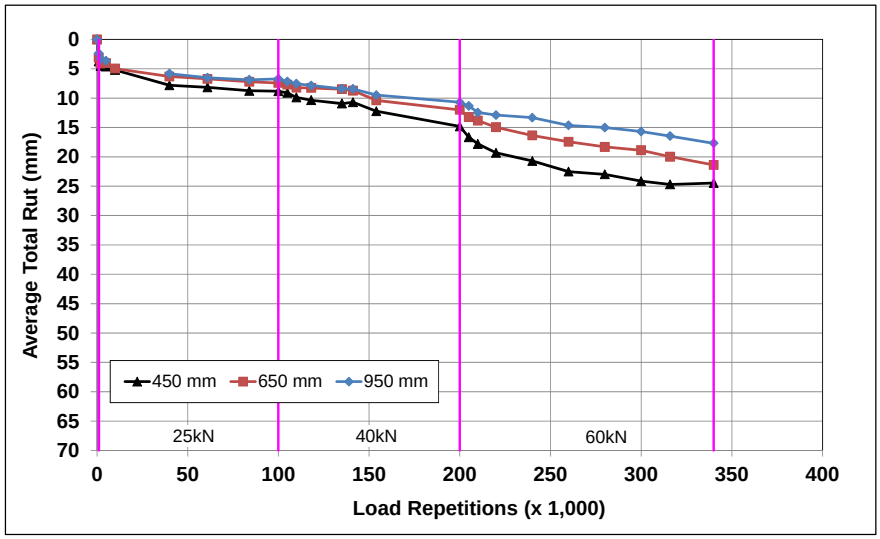

Figure 7.7: 678HC: Average maximum total rut.

Figure 7.8 shows a contour plot of the pavement surface at the end of the test (340,000 load repetitions). The figure illustrates the deeper ruts on the 450 mm and 650 mm subbase subsections compared to the rut on the 950 mm subbase subsection.

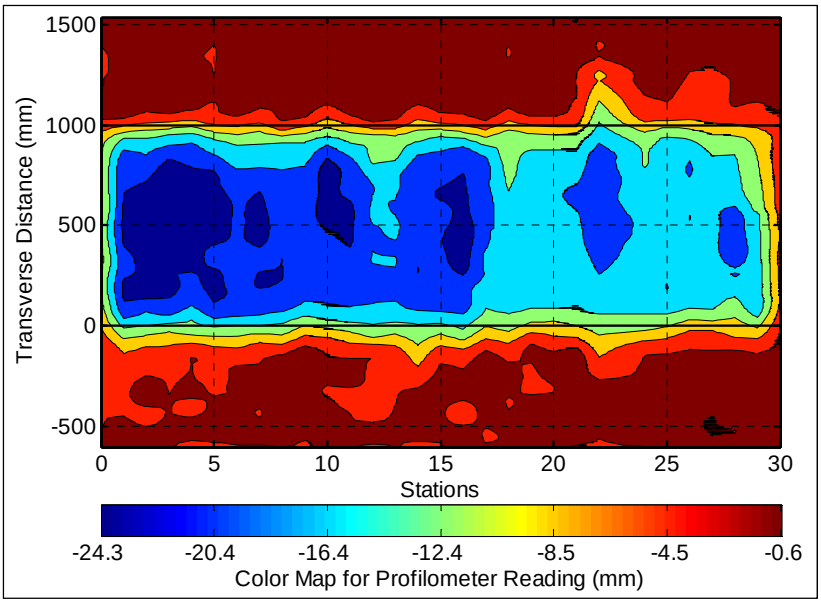

Figure 7.8: 678HC: Contour plot of permanent surface deformation (340,000 repetitions).

7.3.5 678HC: Permanent Deformation in the Underlying Layers

Permanent deformation in the underlying layers, recorded with a gauge in each subsection, and compared to the surface layer (laser profilometer deformation [not total rut] measurement at the same measuring stations), is shown in Figure 7.9, Figure 7.10, and Figure 7.11, for the 450 mm, 650 mm, and 950 mm subbase subsections, respectively. The measurements were consistent with the laser profilometer measurements. Deformation in each of the layers is summarized in Table 7.1. After 340,000 load repetitions, permanent deformation in the bedding and base layer was consistent at about 3.8 mm (0.15 in.) and was attributed to densification under the initial load. Other observations for the three subsections include the following:

- Subsection with 450 mm subbase layer
  - During the 25 kN wheel loading, most of the rutting occurred in the subbase, with very little recorded in the subgrade.
  - After the load change to 40 kN, the rate of increase in permanent deformation in the subbase remained relatively constant, but increased in the subgrade.
  - After completion of trafficking, permanent deformation was relatively evenly distributed between the subbase (10.2 mm [0.4 in.]) and the subgrade (13.4 mm [0.53 in.]).
- Subsection with 650 mm subbase layer
  - Throughout the test, most of the permanent deformation was recorded in the subbase, with 13.2 mm (0.52 in.) of deformation measured in this layer at the end of the test, with a smaller proportion recorded in the subgrade (6.0 mm [0.24 in.]). This implies that the thicker subbase limited deformation in the subgrade.
- Subsection with 950 mm subbase layer
  - Almost all of the permanent deformation was recorded in the subbase on this subsection. At the end of the test, the permanent deformation in the subbase was 12.5 mm (0.49 in.), with just

0.7 mm (0.03 in.) recorded in the subgrade. Permanent deformation in the 650 mm and 950 mm subbase was therefore similar under dry conditions, but the thicker subbase essentially prevented any deformation in the subgrade.

- Total permanent deformation measured with the gauge was 27.4 mm (1.08 in.), 23.0 mm (0.91 in.), and 17.0 mm (0.67 in.) on the three subsections (450 mm, 650 mm, and 950 mm subbase), respectively, implying a generally linear trend of increasing permanent deformation with decreasing subbase thickness.
- There was a minor discrepancy between the permanent deformation measured on the surface with the laser profilometer and the gauge on the subsection with the 450 mm subbase, attributed to leveling of the baseline used as the zero measuring point.

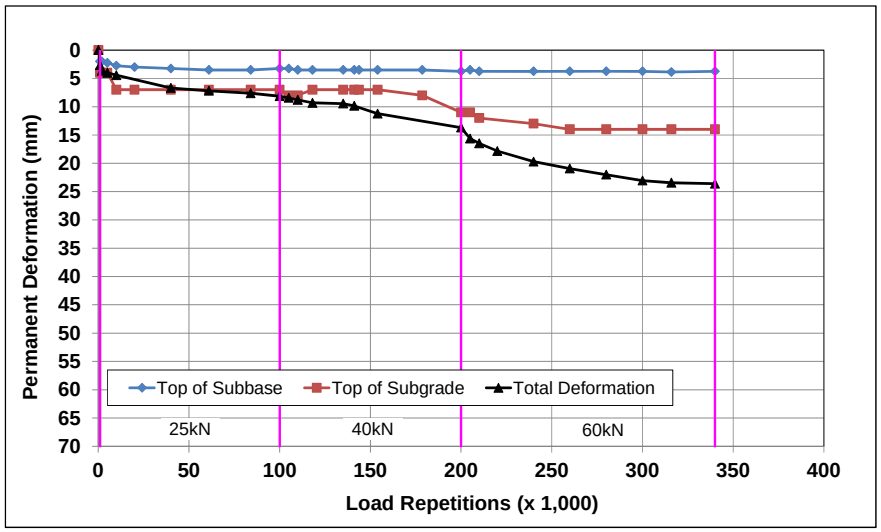

Figure 7.9: 678HC (450 mm): Permanent deformation in the underlying layers.

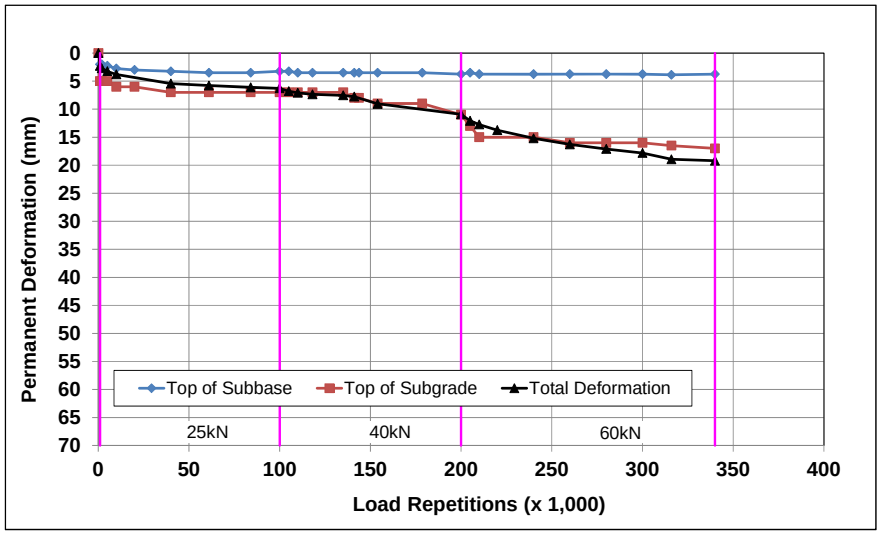

Figure 7.10: 678HC (650 mm): Permanent deformation in the underlying layers.

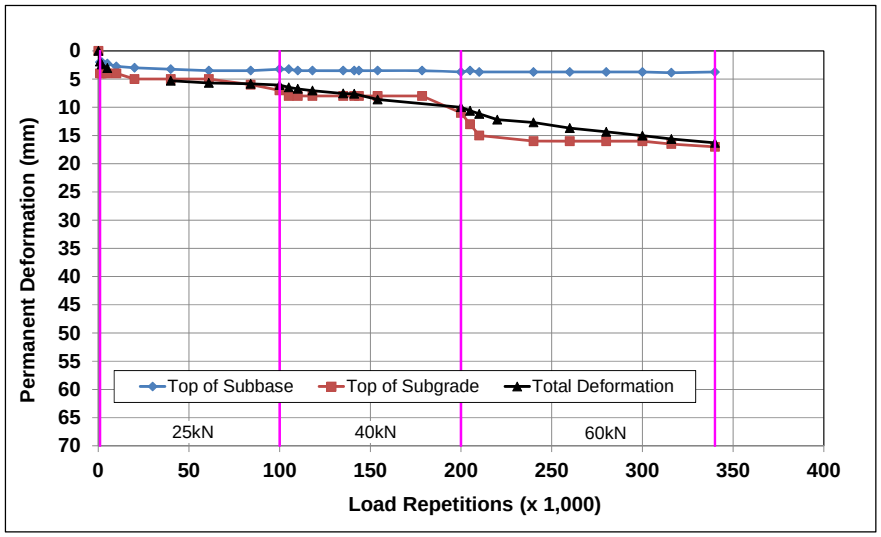

Figure 7.11: 678HC (950 mm): Permanent deformation in the underlying layers.

Table 7.1: 678HC: Deformation in Each Layer

Layer	Layer Thickness		Deformation after 340,000 Load Repetitions					
			450 mm		650 mm		950 mm	
	(mm)	(in.)	(mm)	(in.)	(mm)	(in.)	(mm)	(in.)
Surface	80	3.1	0.0	0.00	0.0	0.00	0.0	0.00
Bedding and Base	150	6.0	3.8	0.15	3.8	0.15	3.8	0.15
Subbase	Variable	-	10.2	0.40	13.2	0.52	12.5	0.49
Subgrade	-	-	13.4	0.53	6.0	0.24	0.7	0.03
Total Gauge Measured Deformation			27.4	1.08	23.0	0.91	17.0	0.67
Total Laser Measured Deformation			25.0	0.98	23.6	0.93	17.7	0.70
Load repetitions at terminal rut (25 mm)			340,000		Rut < 25mm		Rut < 25mm	
ESALs at terminal rut			824,009					

7.3.6 678HC: Surface Deflection

Figure 7.12 compares elastic surface deflections measured with a road surface deflectometer (RSD) under a 40 kN half-axle load for the three subsections. Note that RSD measurements were taken under a creep-speed load and would not be the same as those recorded under the trafficking speed load. The lines on the plot show a trend of increasing deflection over time and with increasing wheel load. Deflections increased with decreasing subbase thickness, while the differences between the three subsections also increased with increasing load. Slight increases in absolute surface deflection were recorded on all subsections after each load change, as expected, but they remained stable thereafter, indicating that there was no significant stiffness change in the pavement structure over time. The deflections recorded were generally double those that would be typically recorded on a dense graded, impermeable structure. However, this is not considered significant given that interlocking concrete pavers are not as susceptible to deflection related distresses (e.g., fatigue cracking) compared to traditional asphalt and portland cement concrete pavements.

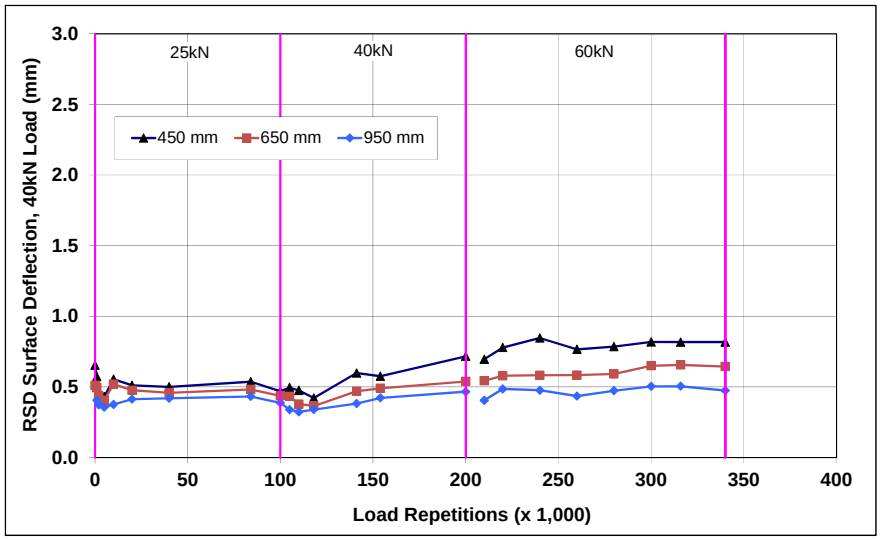

Figure 7.12: 678HC: Surface deflection (RSD).

7.3.7 678HC: Vertical Pressure at the Top of the Subbase and Subgrade

Figure 7.13 and Figure 7.14 show comparisons of traffic-induced vertical pressure at the top of the subbase and top of the subgrade, respectively (note that different y-axis scales are used in the two plots). Observations from the results include the following:

- Pressure readings were sensitive to load changes, and showed a generally linear relationship with increasing pressure associated with an increase in load. There were some inconsistencies in the data during the 40 kN loading cycle, attributed to a change in the support immediately under the instrument probably due to large aggregate movement/settlement after the load change.

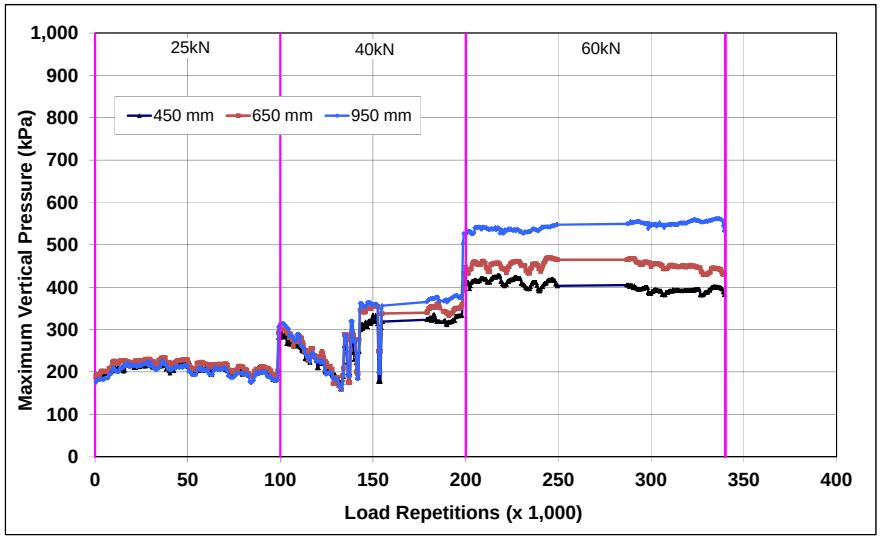

Figure 7.13: 678HC: Vertical pressure at the top of the subbase.

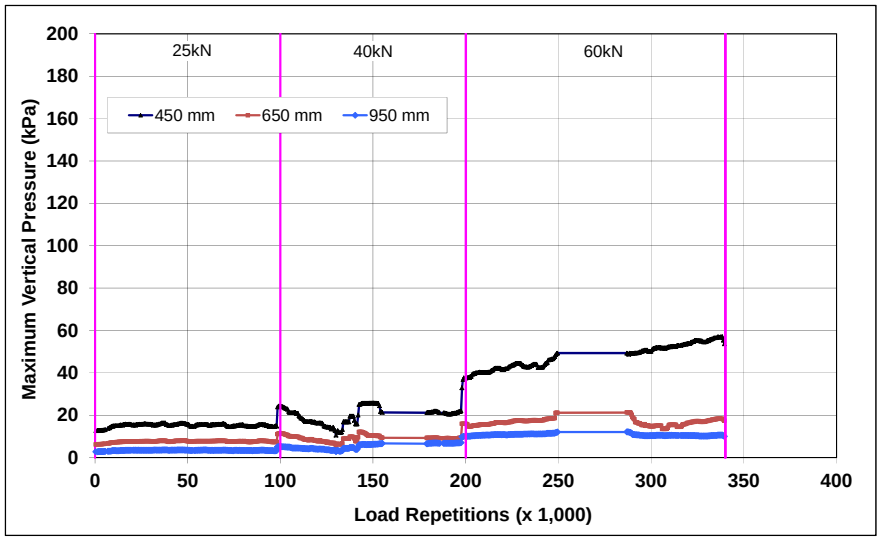

Figure 7.14: 678HC: Vertical pressure at the top of the subgrade.

- At the top of the subbase, there was very little difference between the readings from the three subsections at the 25 kN and 40 kN load levels. After the load change to 60 kN, there was a more distinct difference between the three subsections, with higher pressures recorded on the thicker sections. This was attributed to the higher stiffnesses associated with the support from the thicker subbase layers.
- Very low pressures were recorded at the top of the subgrade as expected; with higher pressures recorded under the 450 mm subbase subsection compared to those recorded under the 650 mm and 950 mm subbase subsections, respectively. The difference in the pressure recorded between the three subsections also increased with an increase in load, especially on the 450 mm subbase subsection, which relates to the permanent deformation measurements recorded on this subsection (Figure 7.9).

7.3.8 678HC: Jointing Stone Depth

Jointing stone depth at seven different locations for the duration of the test is shown in Figure 7.15. Stone depth did not drop below 25 mm and the stone was not replenished. Stone loss was generally uniform along the length of the section, with slightly higher stone loss on the 950 mm subbase subsection after the load change to 60 kN. There were no known contributing factors to this higher stone loss and it did not appear to influence behavior or performance on this subsection.

7.3.9 678HC: Visual Assessment

Apart from rutting, no other distress was recorded on the section. No cracked pavers were observed. Some darkening of the paver surfaces was noted, attributed to rubber deposits and polishing from the HVS tires. Photographs of the test section after HVS testing are shown in Figure 7.16.

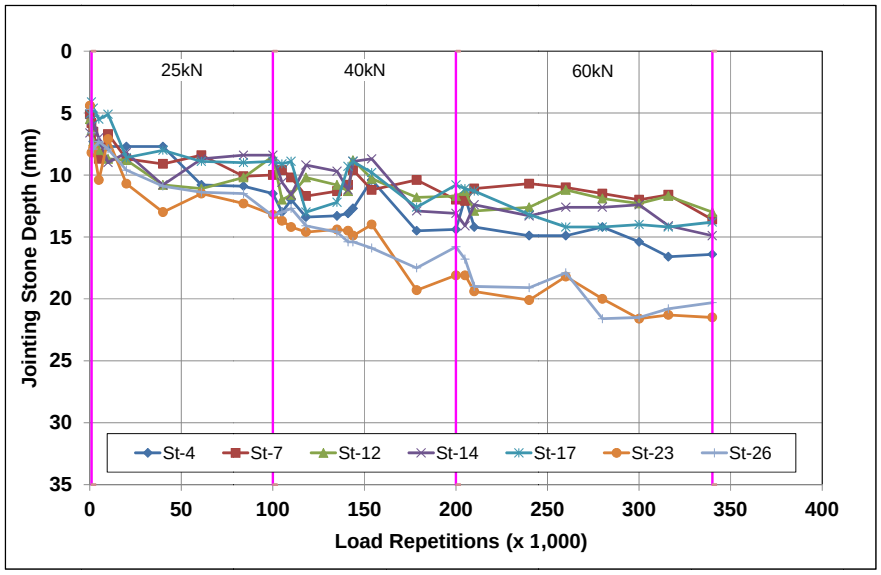

Figure 7.15: 678HC: Jointing stone depth.

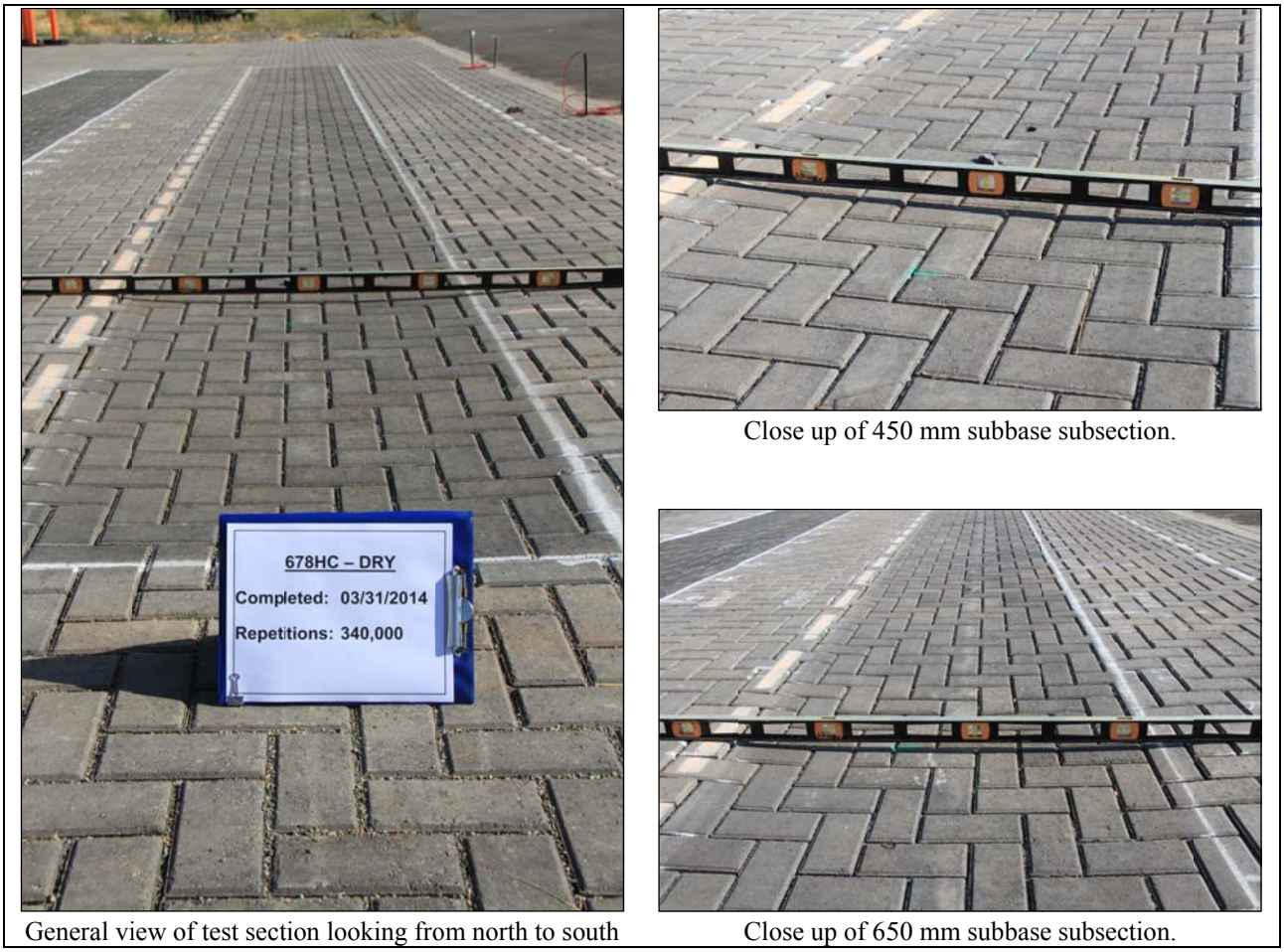

General view of test section looking from north to south

Close up of 450 mm subbase subsection.

Close up of 650 mm subbase subsection.

Figure 7.16: 678HC: Test section photographs.

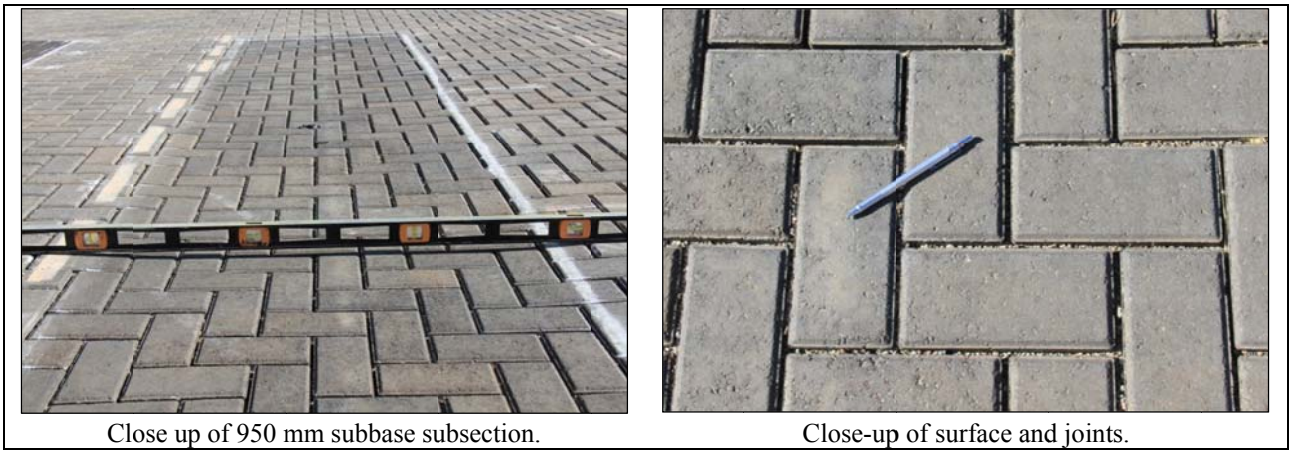

Figure 7.16: 678HC: Test section photographs.

7.4 Section 679HC: Wet Test

7.4.1 Test Summary

Loading commenced with a 25 kN (4,500 lb) half-axle load on April 17, 2014, and ended with an 80 kN (18,000 lb) load on May 21, 2014. A total of 380,000 load repetitions were applied and 36 datasets were collected. Load was increased from 25 kN to 40 kN (9,000 lb) and then to 60 kN (13,500 lb) and 80 kN (18,000 lb) after 100,000 and 340,000 load repetitions, respectively. The HVS loading history for testing on the dry section is shown in Figure 7.17.

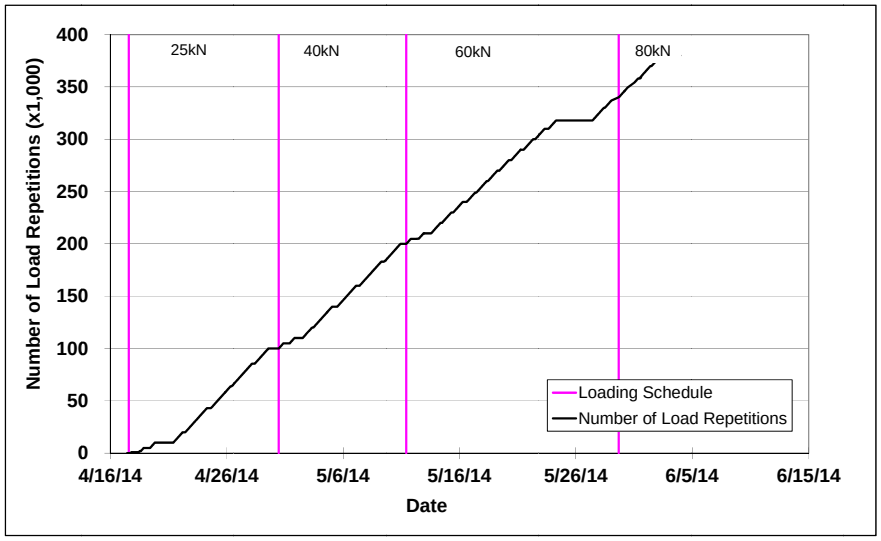

Figure 7.17: 679HC: HVS loading history.

7.4.2 679HC: Water Level in the Pavement

The water level was approximately maintained at the approximate top of the subbase for the duration of the wet test. A plot of the average water level measured in the 950 mm subbase subsection is shown in Figure 7.18. The average water depth below the track surface was 274 mm (standard deviation of

62 mm), or 44 mm below the top of the subbase. This confirms that the subbase served as a reservoir layer during traffic loading, which can be considered as a "worst-case" traffic loading scenario.

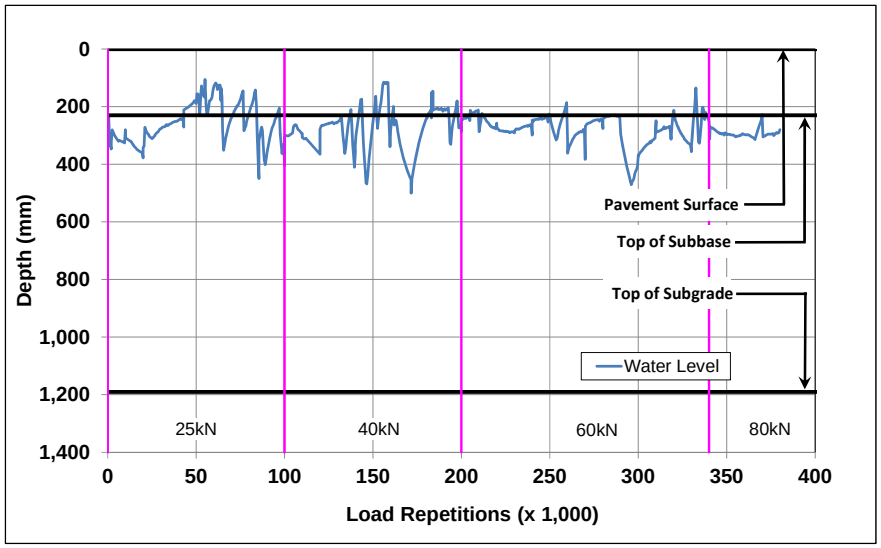

Figure 7.18: 679HC: Water level in the pavement (950 mm subbase subsection).

7.4.3 679HC: Temperatures

Daily average air temperatures and paver temperatures 25 mm below the surface are summarized in Figure 7.19. Vertical error bars show the daily temperature range in the unshaded pavers. Key measurements include the following:

- Air temperatures above the test section (i.e., shaded by the HVS during periods of the day) ranged from 12.8°C to 24.8°C (55°F to 77°F) during the course of HVS testing, with a daily average of 19.9°C (68°F).

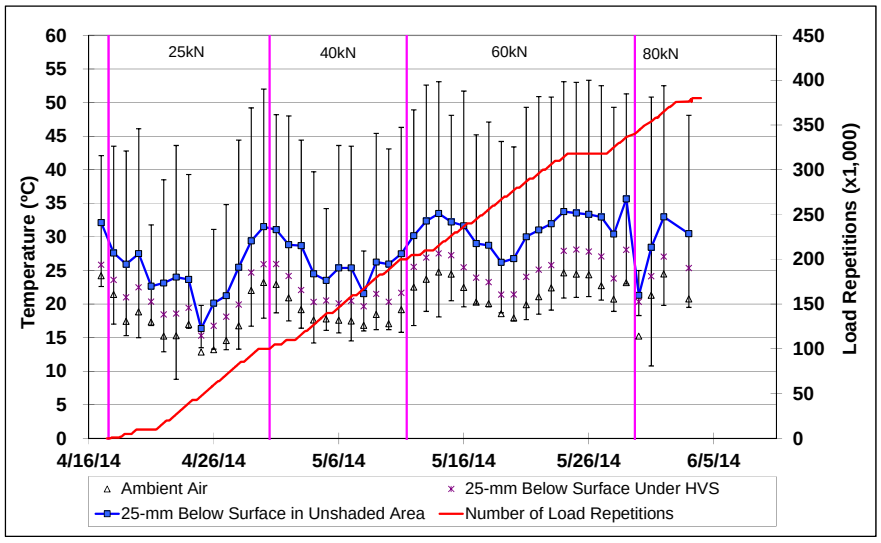

Figure 7.19: 679HC: Daily average air and pavement temperatures.

- Air temperatures in the unshaded area ranged from 15.3°C to 28.1°C (60°F to 83°F) during the course of HVS testing, with a daily average of 23.1°C (74°F).
- Paver temperatures in the test section (i.e., shaded by the HVS during periods of the day) ranged from 14.5°C to 29.8°C (58°F to 86°F) with a daily average of 23.6°C (75°F).
- Paver temperatures in the unshaded area of the test track ranged from 16.4°C to 35.6°C (62°F to 96°F) with a daily average of 28.0°C (82°F).

7.4.4 679HC: Permanent Deformation on the Surface (Rutting)

Figure 7.20 through Figure 7.22 show the average transverse cross sections measured with the laser profilometer at various stages of the test for each of the three thickness design subsections.

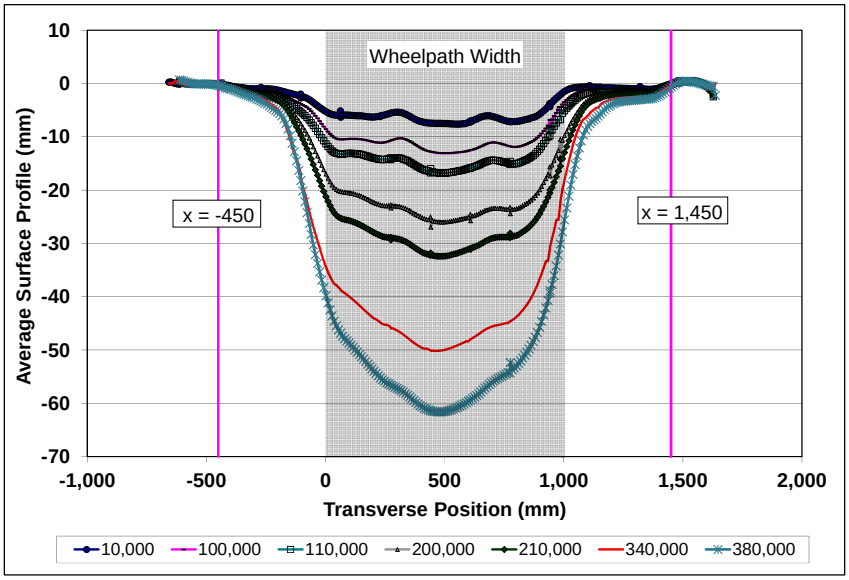

Figure 7.20: 679HC (450 mm): Profilometer cross section at various load repetitions.

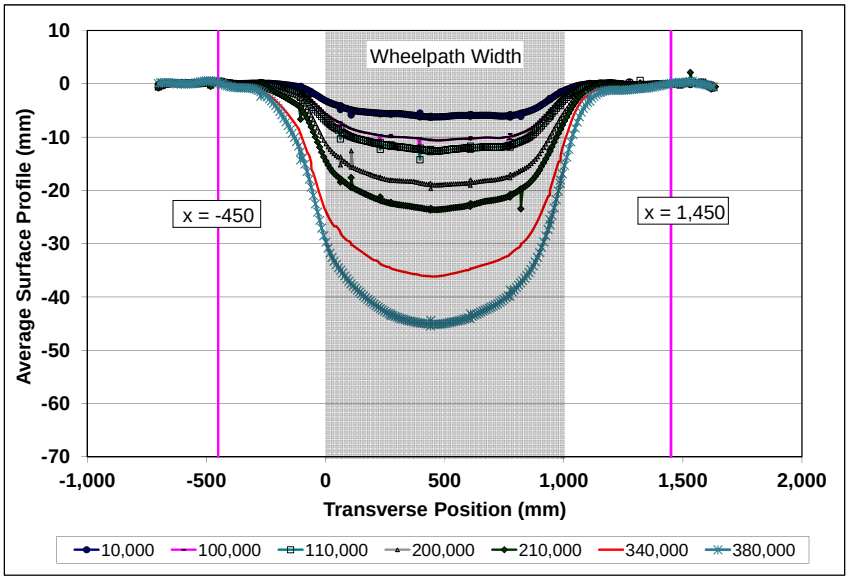

Figure 7.21: 679HC (650 mm): Profilometer cross section at various load repetitions.

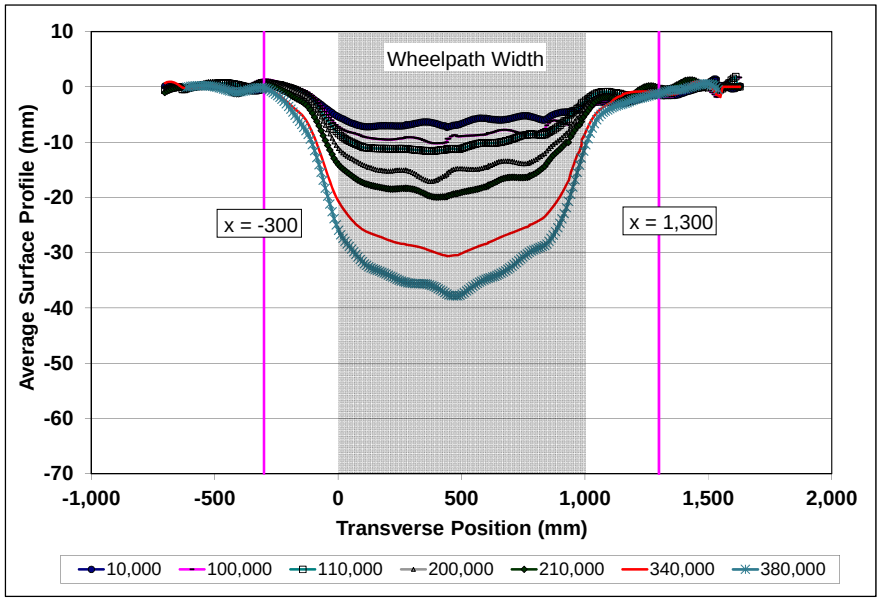

Figure 7.22: 679HC (950 mm): Profilometer cross section at various load repetitions.

The plots clearly show the increase in rutting and deformation over time. The plots also show that most of the deformation was in the form of a depression rather than upward and outward displacement of the material above the zero elevation point.

Figure 7.23 shows the development of permanent deformation (average maximum total rut and average deformation) with load repetitions for the three subsections. This was significantly quicker compared to the rut depths recorded during testing under dry conditions. Observations of surface rutting for each wheel load during the wet test include the following:

- 25 kN (4,500 lb) Wheel Load
  - The initial embedment phase in this test, although relatively short in terms of the number of load repetitions (i.e., ± 5,000), ended with much deeper ruts (6.5 mm on the 450 mm and 650 mm subbase subsections and 9.5 mm on the 950 mm subbase subsection) compared to the dry test. This was attributed partly to bedding in of the pavers under the wheel load and partly to early rutting in the underlying layers due to reorientation of the water-lubricated aggregates. The rate of rut depth increase after the initial embedment phase was uniform until the load change to 40 kN, but faster than that recorded on the dry section.
- 40 kN (9,000 lb) Wheel Load
  - A second small embedment phase was recorded after the load change to 40 kN. After embedment, the rate of rut depth increase was again uniform, but faster than the rate recorded with the 25 kN load and with the 40 kN load on the dry test. The subsection with 450 mm subbase was notably more sensitive to loading compared to the subsections with 650 mm and 950 mm subbases.

- 60 kN (13,500 lb) Wheel Load
  - A short but significant third embedment phase was recorded after the load change to 60 kN. The rate of rut depth increase also accelerated compared to the 40 kN loading cycle, and to the dry test. The difference between the subsection with the 450 mm subbase and the subsections with the 650 mm and 950 mm subsections was again significant. After completion of trafficking at this load level (340,000 load repetitions), the average maximum rut depth for the 450 mm, 650 mm, and 950 mm subbase subsections was 50.5 mm (1.99 in.), 37.9 mm (1.49 in), and 33.7 mm (1.33 in.), respectively. These rut depths are approximately double those recorded on the dry test after the same traffic loading, indicating poorer performance when the subbase layer is serving as a reservoir for water that has drained through the pavers.
- 80 kN (18,000 lb) Wheel Load
  - A short test was conducted at an 80 kN wheel load to continue the assessment of load sensitivity of the pavement structure under extreme moisture conditions. As expected, the rate of rut depth increase continued at a faster pace on all three subsections compared to that measured during the 60 kN loading. After completion of trafficking (additional 40,000 load repetitions [total 380,000]), the average maximum rut depth for the 450 mm, 650 mm, and 950 mm subbase subsections was 62.1 mm (2.44 in.), 46.8 mm (1.84 in), and 39.8 mm (1.57 in.), respectively.

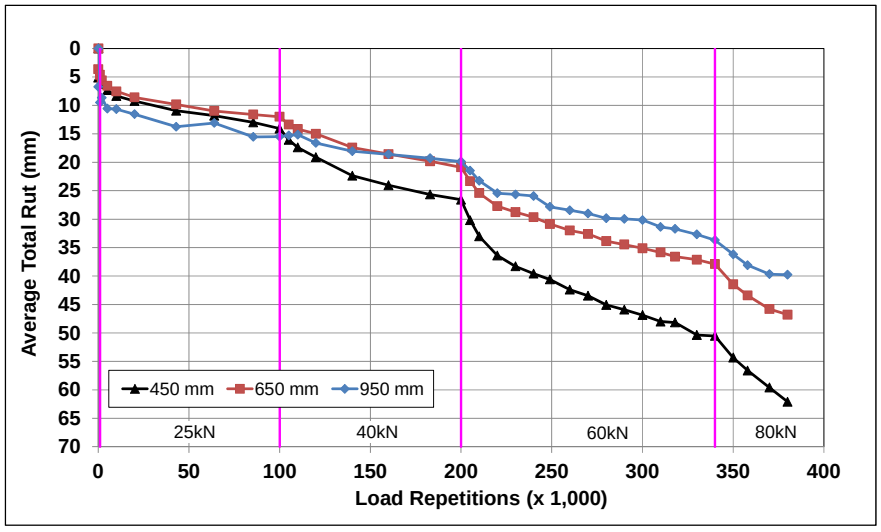

Figure 7.23: 679HC: Average maximum total rut.

Terminal rut (25 mm [1 in.]) was reached after 180,000 load repetitions (95,259 ESALs) on the 450 mm subbase subsection, after 210,000 load repetitions (165,884 ESALs) on the 650 mm subbase subsection, and after 220,000 load repetitions (216,519 ESALs) on the 950 mm subbase subsection.

Figure 7.24 shows contour plots of the pavement surface after 340,000 load repetitions and at the end of the test (380,000 load repetitions). The figures illustrate the deeper ruts on the 450 mm and 650 mm subbase subsections compared to the rut on the 950 mm subbase subsection.

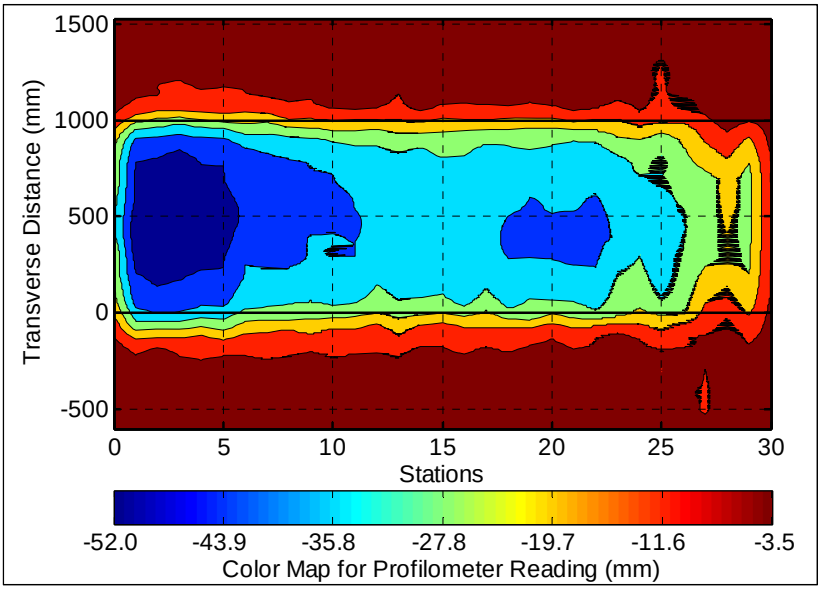

Figure 7.24: 679HC: Contour plots of permanent surface deformation (340,000 repetitions).

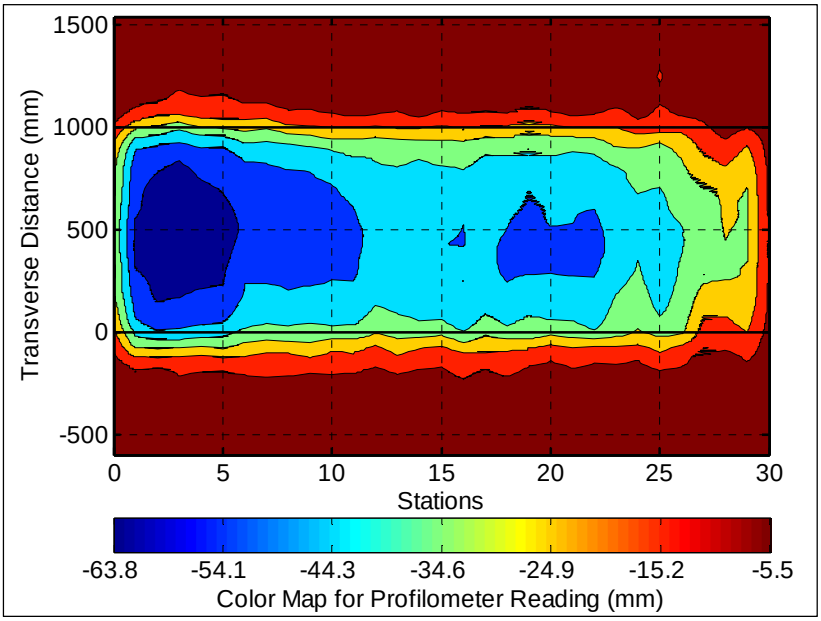

Figure 7.25: 679HC: Contour plots of permanent surface deformation (380,000 repetitions).

7.4.5 679HC: Permanent Deformation in the Underlying Layers

Permanent deformation in the underlying layers, recorded with a gauge in each subsection, and compared to the surface layer (laser profilometer deformation [not total rut] measurement at the same measuring stations), is shown in Figure 7.26, Figure 7.27, and Figure 7.28, for the 450 mm, 650 mm, and 950 mm

subbase sections, respectively. The measurements were consistent with the laser profilometer measurements. Deformation in each of the layers after 340,000 load repetitions (i.e., end of testing at 60 kN) is summarized in Table 7.2.

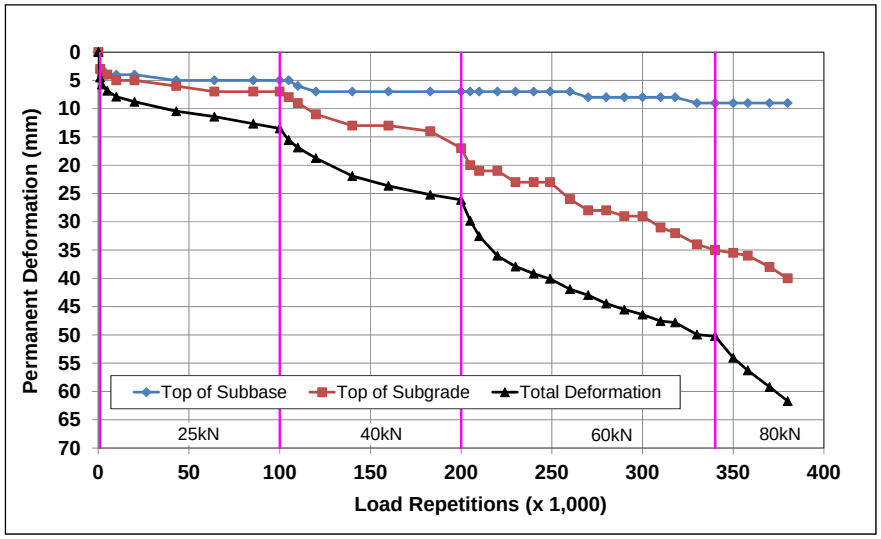

Figure 7.26: 679HC (450 mm): Permanent deformation in the underlying layers.

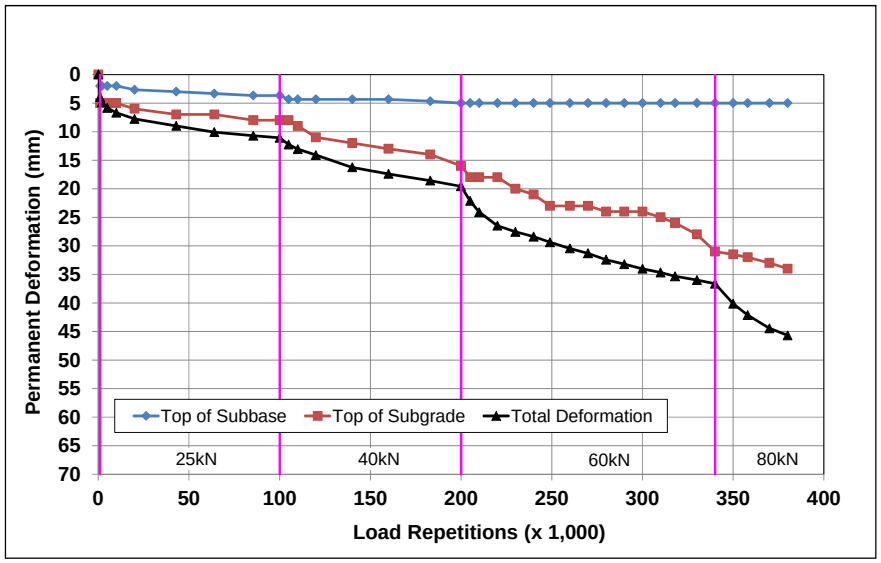

Figure 7.27: 679HC (650 mm): Permanent deformation in the underlying layers.

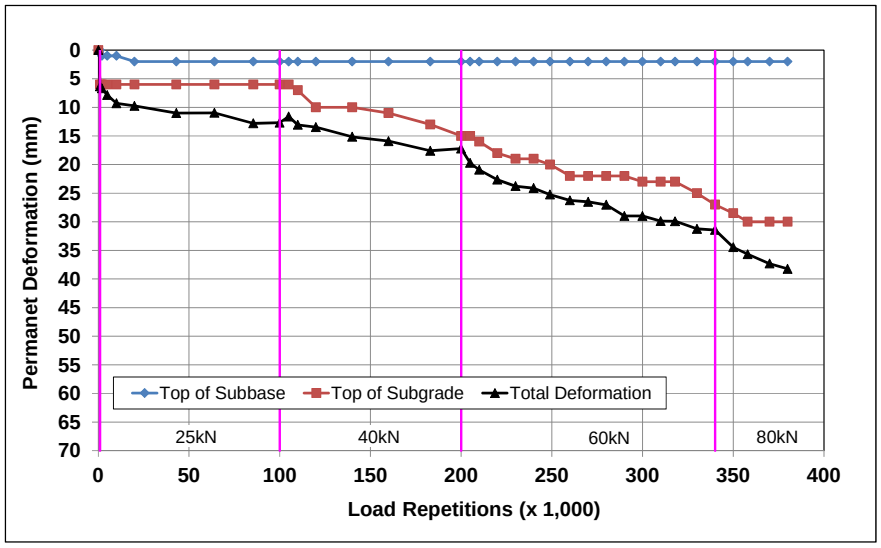

Figure 7.28: 679HC (950 mm): Permanent deformation in the underlying layers.

Table 7.2: 679HC: Deformation in Each Layer

Layer	Layer Thickness		Deformation after 340,000 Load Repetitions					
			450 mm		650 mm		950 mm	
	(mm)	(in.)	(mm)	(in.)	(mm)	(in.)	(mm)	(in.)
Surface	80	3.1	0.0	0.00	0.0	0.00	0.0	0.00
Bedding and Base	150	6.0	9.0	0.35	5.0	0.20	2.0	0.08
Subbase	Variable	-	26.0	1.02	26.0	1.02	25.0	0.98
Subgrade	-	-	15.2	0.60	5.6	0.22	4.1	0.16
Total Gauge Measured Deformation			50.2	1.98	36.6	1.44	31.4	1.24
Total Laser Measured Deformation			50.5	1.99	37.8	1.49	33.7	1.33
Load repetitions at terminal rut (25 mm)			180,000		210,000		220,000	
ESALs at terminal rut			95,259		165,884		216,519	

Other observations for the three subsections include the following:

- Subsection with 450 mm subbase layer
  - The combined bedding and base layer was susceptible to loading, with a distinct initial embedment phase and one after the first load change, indicating some moisture sensitivity and settlement associated with deformation in the underlying subbase layer. Permanent deformation measured in this layer at the end of the test was 9.0 mm (0.35 in), significantly more than the 3.8 mm (0.15 in.) recorded on the dry test, and consistent with the deformation recorded in the subbase.
  - During trafficking with the 25 kN wheel load, very little permanent deformation was recorded in the subbase, with deformation relatively evenly distributed between the combined bedding and base layer (5.0 mm [0.20 in.]) and the subgrade (6.5 mm [0.26 in.]).
  - After the load change to 40 kN, there was a considerable, but similarly trending rate of increase in permanent deformation in both the subbase and subgrade, with deformation relatively evenly distributed between the two layers (10.0 mm [0.39 in.] and 9.1 mm [0.36 in.]) at the end of the loading cycle.

- After the load change to 60 kN, permanent deformation in both the subbase and subgrade continued to increase at a much faster rate than that recorded in the dry test, with this trend continuing after the load change to 80 kN. However, unlike the dry test, more deformation was recorded in the subbase (26.0 mm [1.02 in.]) after 340,000 load repetitions than in the subgrade (15.2 mm [0.6 in.]), possibly indicating that the water-lubricated particles were susceptible to reorientation and further densification.
- Increasing the load to 80 kN resulted in an increase in the rate of deformation, as expected, with a higher rate of deformation occurring in the subgrade, compared to the subbase. After the additional 40,000 load repetitions at 80 kN, deformation in the subbase had increased by 5.0 mm to 31.0 mm (1.2 in.), while deformation in the subgrade had increased by 6.4 mm to 21.7 mm (0.85 in.).

- Subsection with 650 mm subbase layer
  - The combined bedding and base layer had less permanent deformation at the end of the test compared to the thinner section, which was attributed to less deformation in the underlying layers. A small embedment was recorded after the first two load changes and thereafter permanent deformation in this layer remained relatively constant at 5.0 mm (0.2 in.)
  - In the first part of the test with 25 kN wheel loading, deformation was equally distributed between the base (3.7 mm [0.15 in.]), subbase (4.3 mm [0.17 in.]), and subgrade (3.1 mm [0.12 in.]).
  - After the load change to 40 kN, the rate of increase in permanent deformation was faster, with most occurring in the subbase (11 mm [0.43 in.]) rather than in the subgrade (3.6 mm [0.14 in.]) by the end of the loading cycle. This again implies that the thicker base limited deformation in the subgrade at design maximum axle loadings.
  - A similar trend continued after the load changes to 60 kN and 80 kn, but as with the 450 mm subbase subsection, the rate of increase in deformation with the subgrade started to increase at a faster rate, especially after the load change to 80 kN, indicating some load sensitivity in the soaked conditions. Permanent deformation of 26 mm (1.02 in.) and 5.6 mm (0.22 in.) was recorded in the subbase and subgrade respectively after 340,000 load repetitions, increasing to 29 mm (1.14 in.) and 11.7 mm (0.46 in.) respectively, after the additional 40,000 load repetitions.
  - Although considerably less permanent deformation was recorded on this subsection compared to the thinner subsection, it was still significantly higher than that recorded on the same subsection in the dry test. However, more deformation was recorded in the subbase compared to the subgrade in this subsection compared to the thinner one. The higher deformation recorded in the subbase compared to the subgrade was also consistent with the dry test.
- Subsection with 950 mm subbase layer
  - Apart from minor embedment at the start of the test, permanent deformation in the combined bedding and base layer (2 mm [0.08 in.]) did not increase during the test.
  - Similar trends to those recorded on the 650 mm subbase subsection were observed, although the increase in the rate of deformation was slower, as expected. Most of the deformation again occurred in the subbase, with measurements of 25 mm (1.0 in) and 4.4 mm (0.17 in.) recorded in the subbase and subgrade respectively, after 340,000 load repetitions, and 28 mm (1.1 in.) and 8.2 mm (0.32 in.) respectively, after the additional 40,000 load repetitions at 80 kN.

- Total permanent deformation measured with the gauge was 50.2 mm (1.98 in.), 36.6 mm (1.44 in.), and 31.4 mm (1.24 in.) on the three subsections (450 mm, 650 mm, and 950 mm subbase), respectively. This trend was not linear, with considerably more permanent deformation on the thin subsection compared to the thicker subsections, implying that thicker subbase layers will be necessary if water levels are maintained in the subbase.
- There was a minor discrepancy between the permanent deformation measured on the surface with the laser profilometer and the gauge on the subsections with 450 mm and 650 mm subbase, which was again attributed to leveling of the baseline used as the zero measuring point.

7.4.6 679HC: Surface Deflection

Figure 7.29 compares elastic surface deflections under a 40 kN half-axle load for the three subsections. The lines on the plot show a trend of increasing deflection over time and with increasing wheel load. Deflections were considerably higher during all stages of this wet test compared to measurements during the dry test, as expected. Deflections on the 450 mm subbase subsection were significantly higher than those recorded on the subsections with thicker subbases, especially after the load changes, indicating a load-sensitive, weaker overall structure as a result of the wet subgrade. The difference in deflection between the 650 mm and 950 mm subbase subsections was distinct, but less significant.

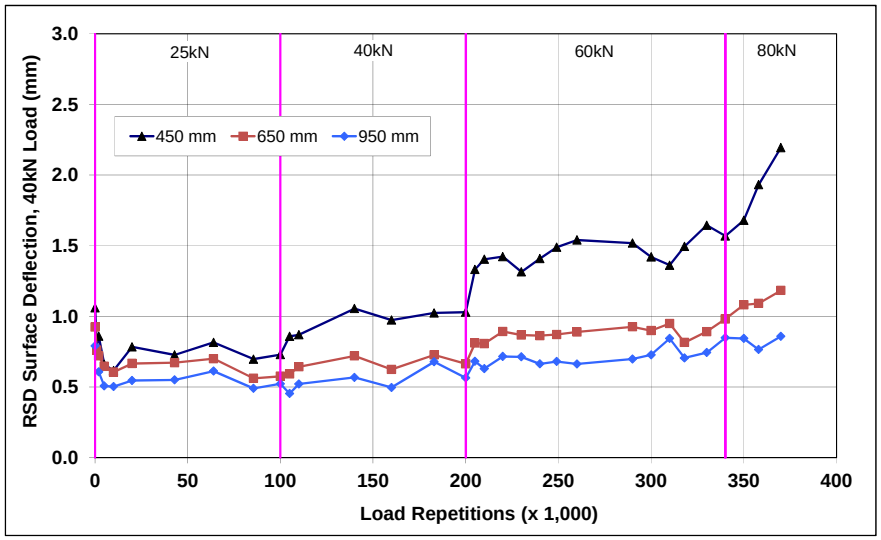

Figure 7.29: 679HC: Surface deflection (RSD).

7.4.7 679HC: Vertical Pressure at the Top of the Subbase and Subgrade

Figure 7.30 and Figure 7.31 show comparisons of traffic-induced vertical pressure at the top of the subbase and top of the subgrade, respectively (note that different y-axis scales are used in the two plots). Observations from the results include the following:

- Pressure readings were sensitive to load changes, and showed a generally linear relationship with increasing pressure associated with an increase in load. Inconsistencies (noise) in the data were

attributed to changes in the support immediately under the instrument due to the presence of the water and slight movements of the instrument as the load moved over it. These trends are consistent with other results from pressure cells used in similar conditions.

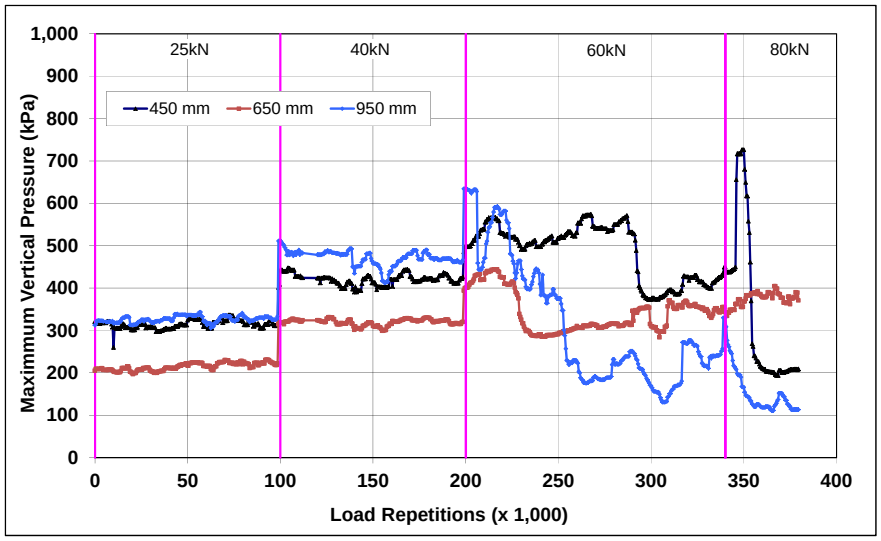

Figure 7.30: 679HC: Vertical pressure at the top of the subbase.

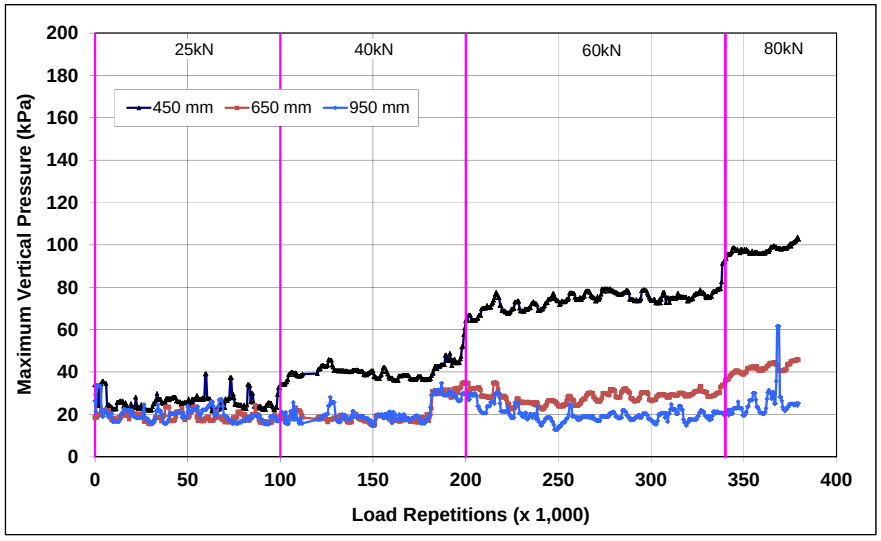

Figure 7.31: 679HC: Vertical pressure at the top of the subgrade.

- At the top of the subbase, there was very little difference between the readings from the 450 mm and 950 mm subbase subsections at the 25 kN and 40 kN load levels; however, the pressure was approximately 100 kPa higher than the pressure recorded at these stages of the testing on the dry test. Pressure on the 650 mm subbase subsection was the same as that recorded during the dry test. This was attributed in part to the two water inflow areas being at the ends of the test section adjacent to the 450 mm and 950 mm subbase subsection, which implies that the water level may have been slightly lower under the pressure cell in the 650 mm subbase subsection. After the load change to 60 kN, the data is inconsistent.

- Very low pressures were recorded at the top of the subgrade; with higher pressures recorded under the 450 mm subbase subsection compared to those recorded under the 650 mm and 950 mm subbase subsections, respectively. The difference in the pressure recorded between the three subsections also increased with an increase in load. Pressure on the 450 mm subbase subsection increased significantly after the load increases to 60 kN and 80 kN, which is consistent with the higher permanent deformation measurements recorded in the subgrade on this subsection (Figure 7.26).

7.4.8 679HC: Jointing Stone Depth

Jointing stone depth at seven different locations for the duration of the test is shown in Figure 7.32. Stone depth dropped below or was close to 25 mm on the 450 mm subbase subsection on two occasions during the test, and was therefore replenished back to original levels. This stone loss was attributed to the severe rutting and consequent downward movement of the pavers on this subsection. Stone loss on the 650 mm and 950 mm subbase subsections was generally uniform.

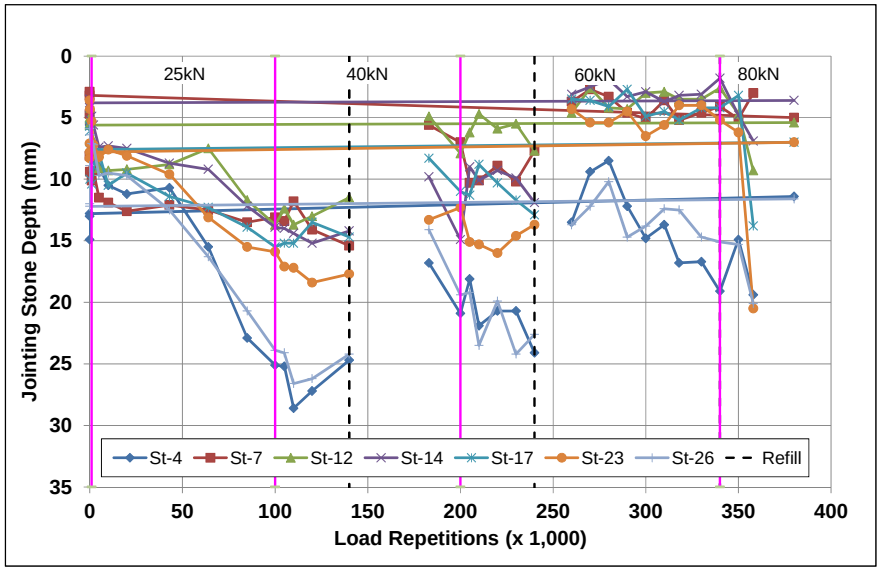

Figure 7.32: 679HC: Jointing stone depth.

7.4.9 679HC: Visual Assessment

Apart from rutting, no other distress was recorded on the section. No cracked pavers were observed. Some darkening of the paver surfaces was noted, attributed to rubber deposits and polishing from the HVS tires. Photographs of the test section after HVS testing are shown in Figure 7.33.

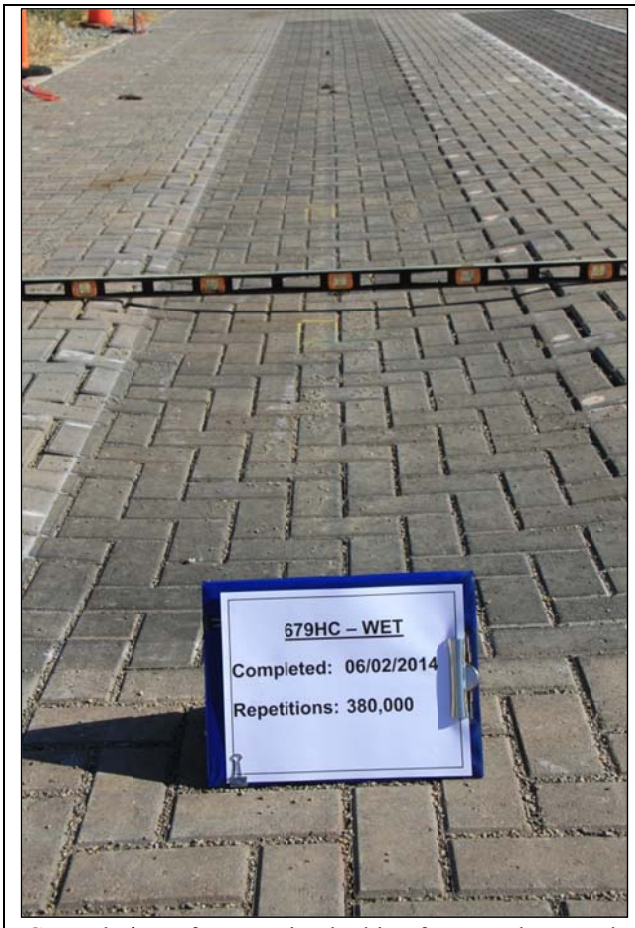

General view of test section looking from north to south


Close up of 450 mm subbase subsection.


Close up of 650 mm subbase subsection.


Close up of 950 mm subbase subsection.


Close-up of surface and joints.

Figure 7.33: 679HC: Test section photographs.

7.5 Section 680HC: Drained Test

7.5.1 Test Summary

This test was included to compare rate of rut increase on the section with no water in the subbase with rate of rut increase on the dry and wet tests. This section did not contain pressure cells or permanent deformation gauges. A limited number of load repetitions were applied, sufficient to compare surface

rutting trends with those on the other two sections. Loading commenced with a 25 kN (4,500 lb) half-axle load on June 11, 2014, and ended with a 40 kN (9,000 lb) load on July 14, 2014. A total of 140,000 load repetitions were applied and nine datasets were collected. Load was increased from 25 kN to 40 kN (9,000 lb) after 100,000 load repetitions. The HVS loading history for testing on the dry section is shown in Figure 7.34.

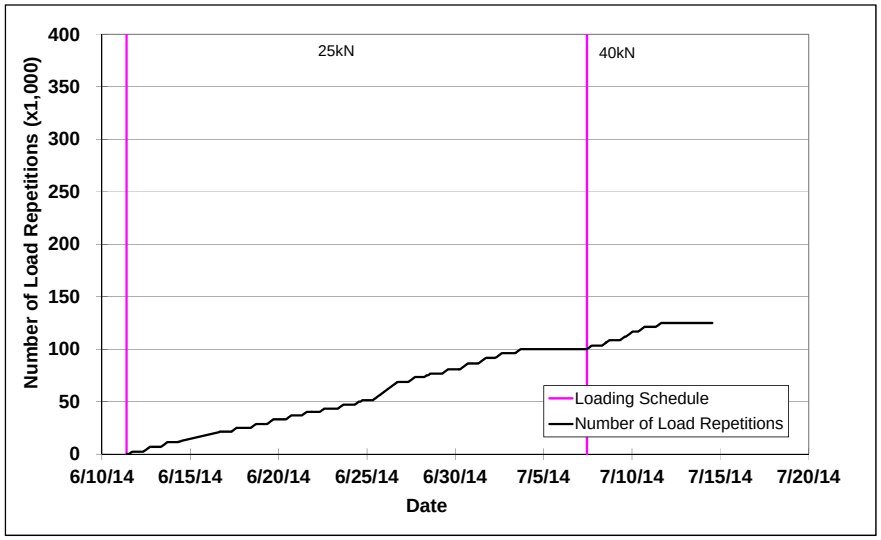

Figure 7.34: 680HC: HVS loading history.

7.5.2 680HC: Water Level in the Pavement

No water was measured in the subbase for the duration of the test.

7.5.3 680HC: Temperatures

Daily average air temperatures and paver temperatures 25 mm below the surface are summarized in Figure 7.35. Vertical error bars show the daily temperature range in the unshaded pavers. Key measurements include the following:

- Air temperatures above the test section (i.e., shaded by the HVS during periods of the day) ranged from 20.1°C to 28.8°C (68°F to 84°F) during the course of HVS testing, with a daily average of 23.5°C (74°F).
- Air temperatures in the unshaded area ranged from 22.8°C to 32.9°C (73°F to 91°F) during the course of HVS testing, with a daily average of 28.1°C (83°F).
- Paver temperatures in the test section (i.e., shaded by the HVS during periods of the day) ranged from 21.9°C to 36.0°C (71°F to 97°F) with a daily average of 28.6°C (84°F).
- Paver temperatures in the unshaded area of the test track ranged from 26.0°C to 42.0°C (79°F to 108°F) with a daily average of 34.6°C (98°F).

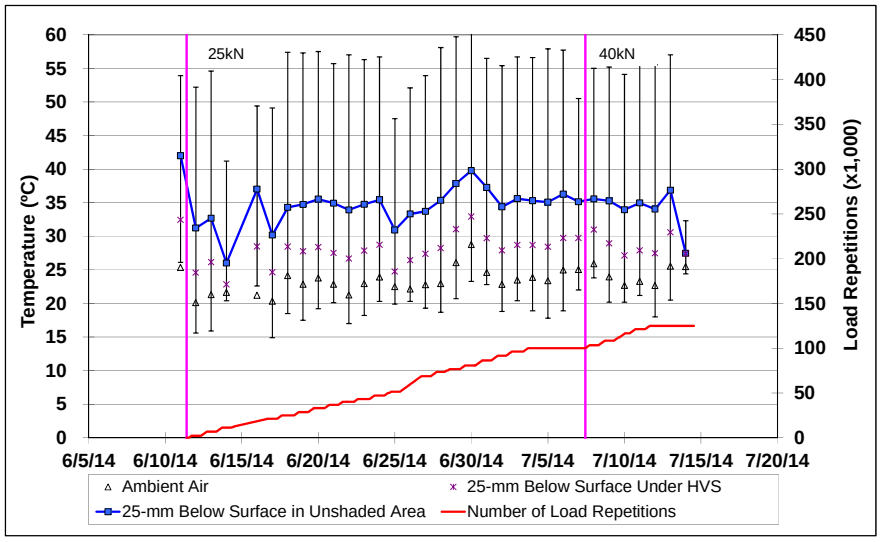

Figure 7.35: 680HC: Daily average air and pavement temperatures.

7.5.4 680HC: Permanent Deformation on the Surface (Rutting)

Figure 7.36 through Figure 7.38 show the average transverse cross sections measured with the laser profilometer at various stages of the test for each of the three thickness design subsections. The plots show similar rutting behavior to that recorded on the dry test, with considerably less rutting compared to the wet test after similar numbers of load repetitions. As with the other tests, the plots show that most of the deformation was in the form of a depression rather than upward and outward displacement of the material above the zero elevation point.

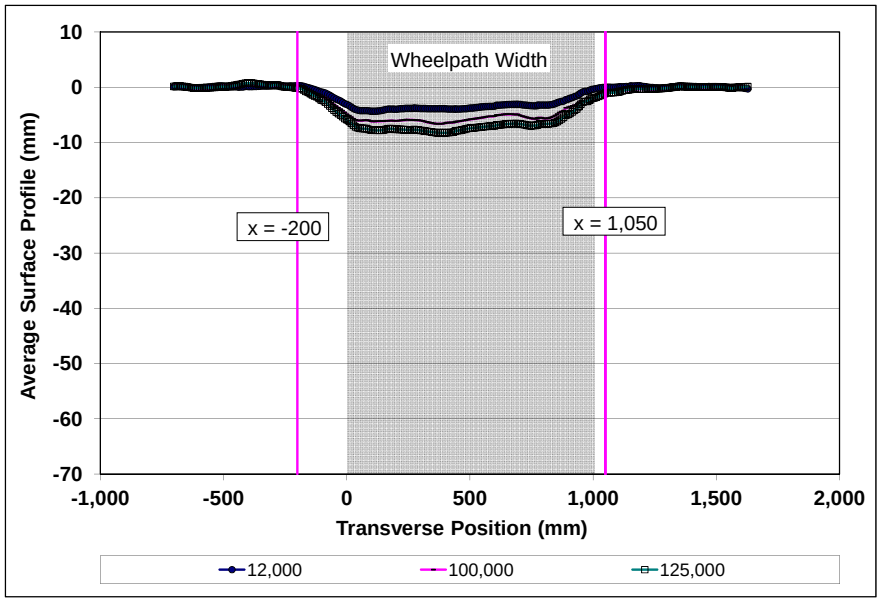

Figure 7.36: 680HC (450 mm): Profilometer cross section at various load repetitions.

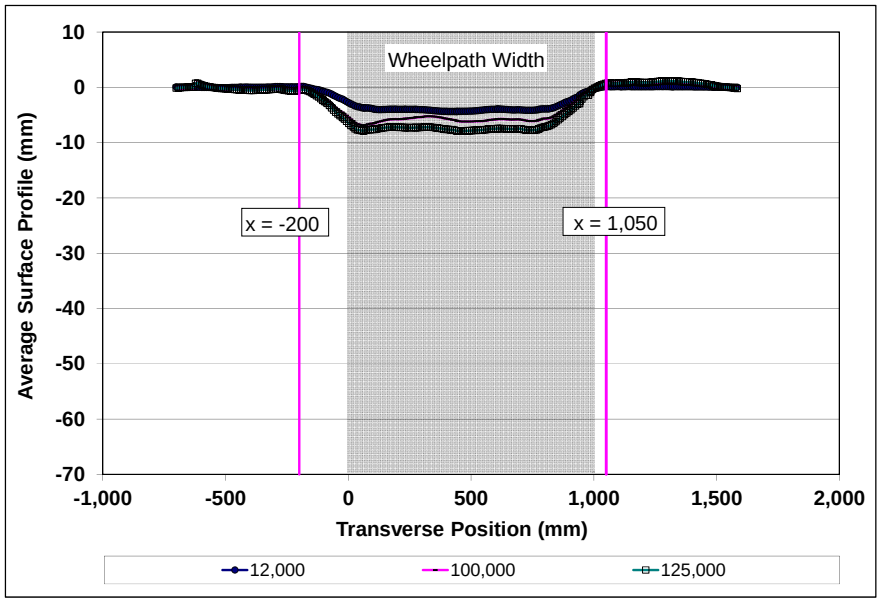

Figure 7.37: 680HC (650 mm): Profilometer cross section at various load repetitions.

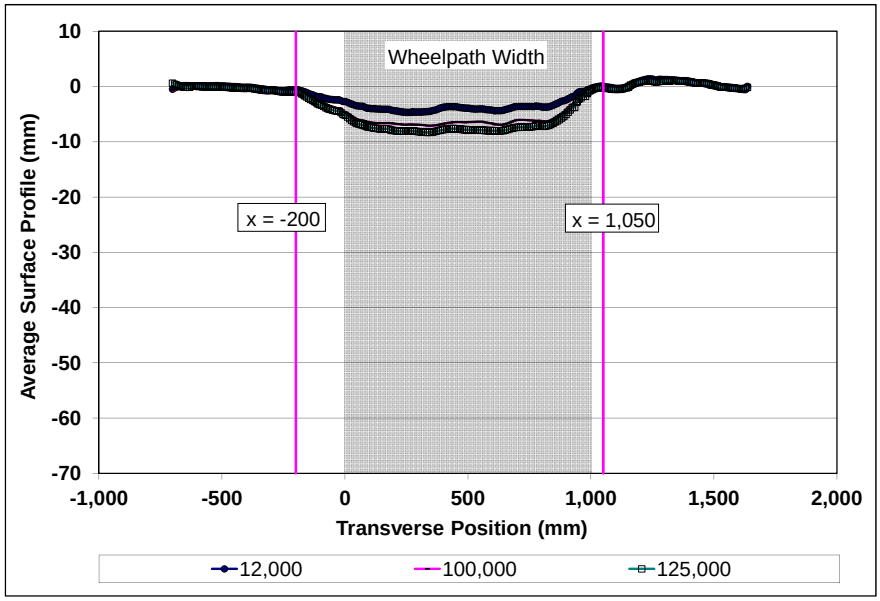

Figure 7.38: 680HC (950 mm): Profilometer cross section at various load repetitions.

Figure 7.39 shows the development of permanent deformation (average maximum total rut and average deformation) with load repetitions for the three subsections. The plots show that rutting trends and rut depths were similar to those recorded on the dry section.

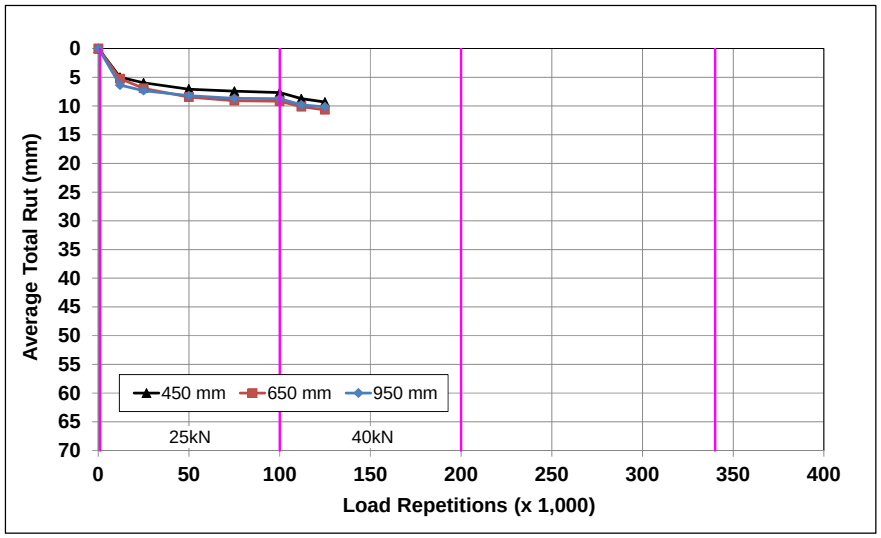

Figure 7.39: 680HC: Average maximum total rut.

7.5.5 680HC: Permanent Deformation in the Underlying Layers

Permanent deformation in the underlying layers was not measured in this test.

7.5.6 680HC: Surface Deflection

Figure 7.40 compares elastic surface deflections under a 40 kN half-axle load for the three subsections. Deflections were generally in between those recorded during the dry and wet tests, indicating that the still-wet subgrade influenced the behavior of the structure, although not to the same extent as when the subbase was serving as a reservoir.

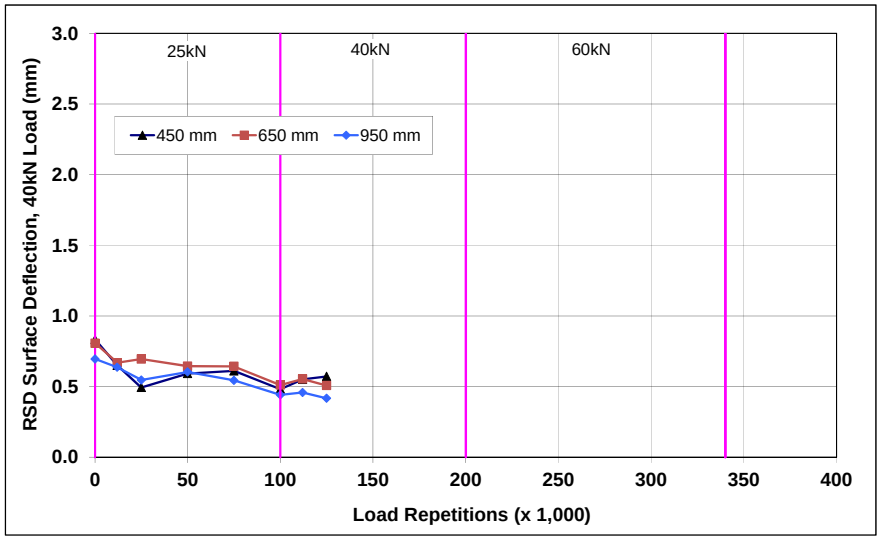

Figure 7.40: 680HC: Surface deflection (RSD).

7.5.7 680HC: Vertical Pressure at the Top of the Subbase and Subgrade

Pressure cells were not installed in the test section and vertical pressure was therefore not monitored in this test.

7.5.8 680HC: Jointing Stone Depth

Jointing stone depth was not monitored in this test.

7.5.9 680HC: Visual Assessment

Apart from rutting, no other distress was recorded on the section. No cracked pavers were observed. Some darkening of the paver surfaces was noted, attributed to rubber deposits and polishing from the HVS tires. Photographs of the test section after HVS testing are shown in Figure 7.41.

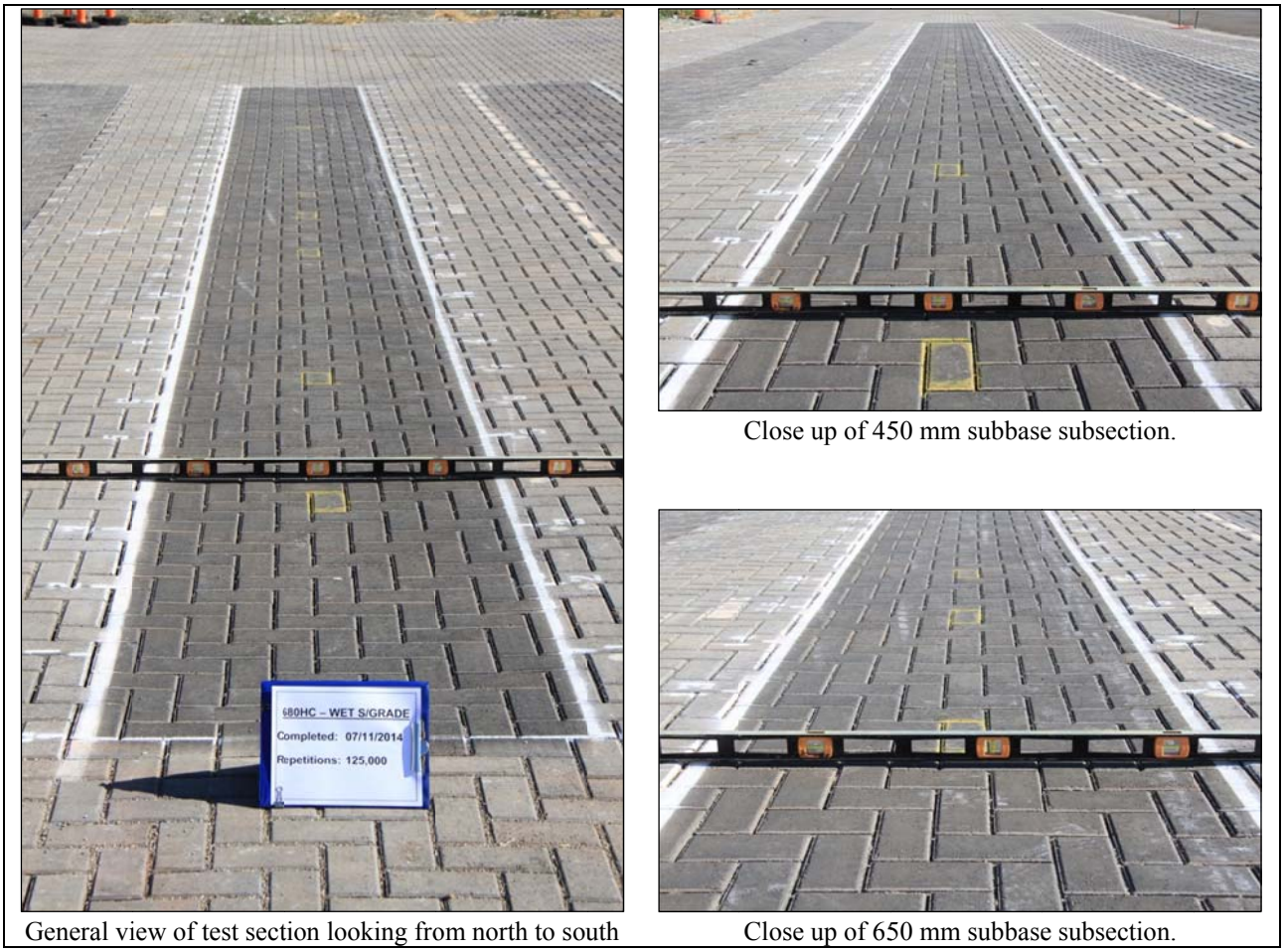

General view of test section looking from north to south

Close up of 450 mm subbase subsection.

Close up of 650 mm subbase subsection.

Figure 7.41: 680HC: Test section photographs.

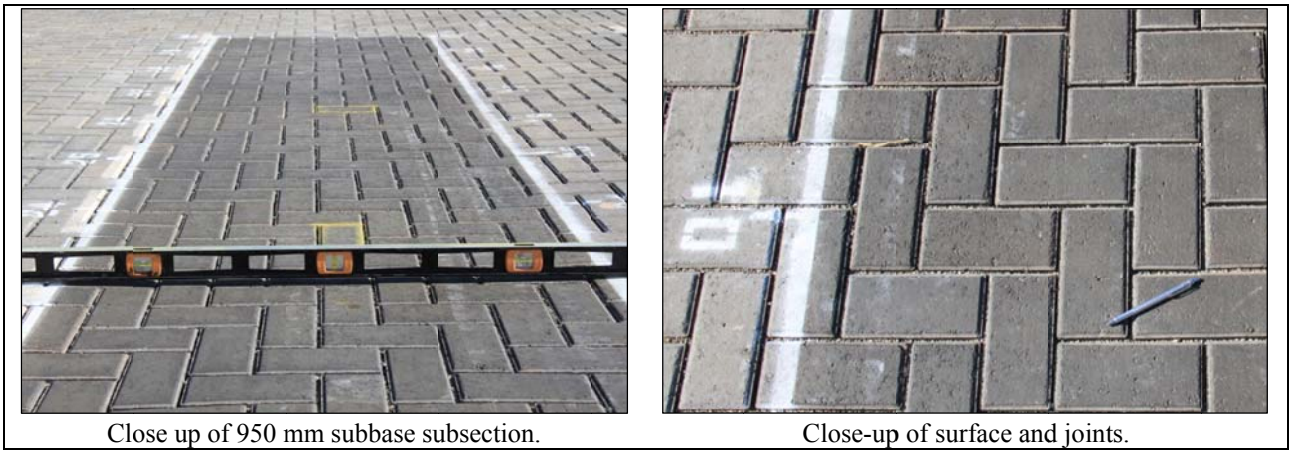

Close up of 950 mm subbase subsection. Close-up of surface and joints.

Figure 7.41: 680HC: Test section photographs.

7.6 Surface Permeability

Surface permeability was measured after completion of testing on Section 678HC (dry test) according to ASTM C1701 (Standard Test Method for Infiltration Rate of In Place Pervious Concrete, which is similar to ASTM C1781 [Standard Test Method for Surface Infiltration Rate of Permeable Unit Pavement Systems]). The results were compared with the measurements taken after construction and are summarized in Figure 7.42. A large drop in measured permeability was recorded; however, there was no visibly noticeable observed difference in the rate of water infiltration, which was still considered to be rapid.

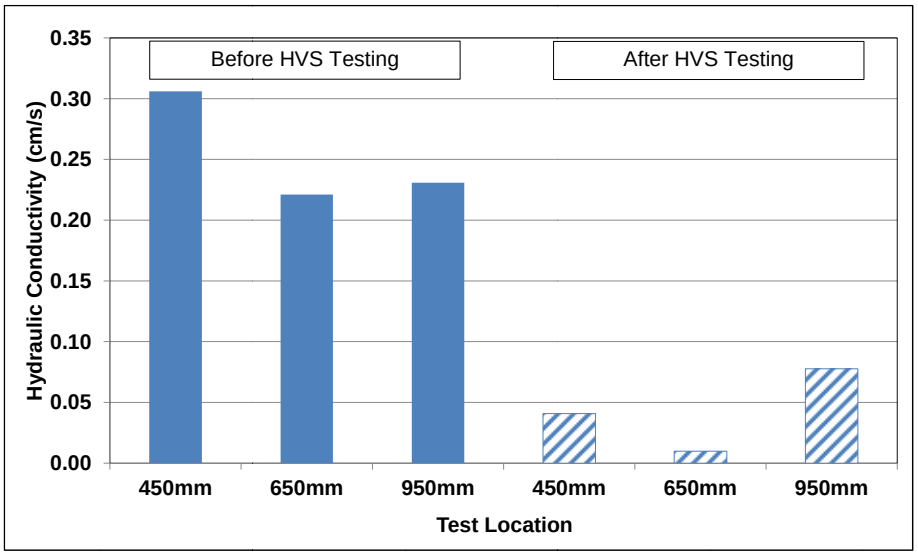

Figure 7.42: Surface permeability before and after HVS testing.

7.7 HVS Test Summary

Key observations from HVS testing include the following:

- There was a significant difference in rutting performance and rutting behavior between the wet and dry tests, as expected.
- A large proportion of the rutting on all three sections occurred as initial embedment in the first 2,000 to 5,000 load repetitions of the test and again after each of the load changes, implying that much of the rutting in the base and subbase layers was attributed to bedding in, densification, and/or reorientation of the aggregate particles. Although, this behavior is consistent with rutting behavior on other types of structures, better compaction of the base and subbase may have limited the extent.
- During testing under dry conditions, limited permanent deformation (< 4 mm) was recorded in the bedding and base layers on all three subsections, and most occurred very early in the test. On the subsection with the 450 mm subbase, rutting occurred in both the subbase (10 mm rut) and subgrade (13 mm rut). On the 650 mm and 950 mm subbase subsections, rutting occurred mostly in the subbase. Total permanent deformation on the 450 mm, 650 mm, and 950 mm subbase subsections was 27 mm, 23 mm and 17 mm respectively, implying a generally linear trend of increasing permanent deformation with decreasing subbase thickness.
- During testing under wet conditions, rutting in the bedding and base layers was dependent on the thickness of the subbase (9 mm, 5 mm and 2 mm on the 450 mm, 650 mm, and 950 mm subbase subsections, respectively). Rutting occurred in both the subbase and the subgrade on all subsections, with rutting in the subbase consistent across all three sections (~ 25 mm). Rutting in the subgrade differed between sections relative to subbase thickness, with 15 mm, 6 mm, and 4 mm of rut recorded on the 450 mm, 650 mm, and 950 mm subbase subsections, respectively.
- Although only limited testing was undertaken under drained conditions (i.e., no water in the subbase), rutting behavior appeared to show similar trends and behavior to the test under dry conditions.
- The thickness of the subbase influenced rut depth in the subgrade, as expected, but did not influence the rutting behavior in the subbase itself. Rutting in this layer therefore appears to be governed by the aggregate properties and construction methods and quality.
- The rate of rut depth increase escalated with increasing load, indicating that the pavement structure was load sensitive, especially at load levels close to and above the legal design load.
- Deflection during dry testing was dependent on subbase thickness and it increased with increasing load. Deflections were relatively high compared to more traditional pavements with dense graded layers. Deflection during wet testing was higher compared to that recorded during dry testing, with deflection on the 450 mm subbase subsection significantly higher compared to that recorded on the 650 mm and 950 mm subbase subsections, indicating a load-sensitive, weaker overall structure as a result of the wet subgrade.
- No distress was noted on any individual pavers and no pavers were dislodged from the pavement during testing.
- The measured infiltration rate of water through the joints between the pavers reduced marginally over the course of HVS testing; however, visually it was still considered to be both rapid and effective.

Blank page

8. DATA ANALYSIS

This chapter covers the development of a mechanistic-empirical (M-E) design method for permeable interlocking concrete pavements (PICP) based on mechanistic analysis and partial validation with the accelerated pavement testing results discussed in Chapter 7. The same approach to that described in Chapter 4 was followed, but some of the assumptions were adjusted based on the results from the HVS testing.

8.1 Design Criteria, Design Variables, and Critical Responses

The design criteria, design variables, and critical responses used in the original test track design and discussed in Chapter 4 (Section 4.2) were used in the mechanistic analysis. However, in the initial design, the bedding, base, and subbase layers were combined into a single aggregate base layer for purposes of the design. The results of HVS testing indicated that rutting behavior in the bedding and base layers differed from that in the subbase layer during the wet test, and consequently, the bedding and base layers were combined into a single layer and analyzed separately from the subbase layer in this stage of the analysis.

8.2 Rut Models for Different Layers

Based on the observations made and measurements taken during HVS testing, it was concluded that no deformation or distress occurred in the pavers, only in the underlying layers, which resulted in measurable deformation on the surface. Consequently, although surface rutting is the primary criterion designed for and predicted in the analysis, it is assumed that the pavers themselves would not deform. It should also be noted that, although individual pavers have a relatively high stiffness, a permeable surface layer constructed of pavers does not, due to the wider spacing and reduced interlock between the pavers compared to pavers with sand joints.

8.2.1 Combined Bedding and Base Layer

During testing under dry conditions (see Section 7.3), a rapid embedment of about 4 mm was recorded in the combined bedding and base layer on the three subsections in the first 2,000 load repetitions. Thereafter, no further significant rutting was recorded for the remainder of the test on any of the subsections. The rut depth model of this combined layer under dry conditions was therefore set as a constant (4 mm).

Under wet conditions (see Section 7.4), the rut depth in the combined bedding and base layers varied depending on the subgrade thickness. On the 650 mm and 950 mm subbase subsections, most of the

rutting occurred during early embedment after which it remained relatively constant. On the 450 mm subbase subsection, rutting was influenced by changes in the load. The rut depth model of this combined layer for wet conditions was therefore set as a linear function of the subbase thickness (Table 8.1).

8.2.2 Subbase Layer

A typical mechanistic approach using the general formula in Equation 8.1 was used to develop the rutting model for the subbase layer.

$$RD_{SB} = aN^b \quad \textbf{(8.1)}$$

Where: RD_{SB} is the rut depth of the subbase layer,
N is the number of load repetitions,
a and b are constants and are a function of the shear stress/strength ratio (SSR_{SB}) at the top of the subbase layer, calculated using Equations 4.1 through 4.4.

A two-step model development process was followed:

- Step 1. Fit $RD_{SB} = a(dN+N_0)^b$ for each testing case with different subbase thickness (*h_SB*), test load (*L*), and test moisture condition (*Dry* and *Wet*), considering the effect of early embedment in the initial stages of trafficking. RD_{SB} is the total rut depth in the subbase for a load level *i*; *dN* is the incremental repetition under that load level *i;* N_0 is a model constant for considering the effect of earlier loading.
- Step 2. Fit $a \sim f(SSR_{SB})$ and $b \sim f(SSR_{SB})$ for all testing cases.

Using the rut test data from the HVS testing, it was found that the rut depth showed an approximately linear relationship with load repetitions after early initial embedment for all testing cases. Consequently, the power constant *b* was set as 1. The constant *a* is a function of SSR_{SB}, calculated for each case using Equations 4.1 through 4.4. The subbase rut model is summarized in Table 8.1.

8.2.3 Subgrade

The procedure for developing the rutting model for the subgrade was similar to that used for the subbase layer. The general formula for the rut model is (Equation 8.2):

$$RD_{SG} = aN^b \quad \textbf{(8.2)}$$

Where: RD_{SG} is the rut depth in the subgrade,
N is the number of load repetitions,
a and b are constants and are a function of the shear stress/strength ratio (SSR_{SG}) at the top of the subgrade, calculated using Equations 4.1 through 4.4.

A two-step model development process similar to that described above was followed:

- Step 1. Fit $RD_{SG} = a(dN+N_0)^b$ for each testing case with different subbase thickness (*h_SB*), test load (*L*), and test moisture condition (*Dry* and *Wet*), considering the effect of early embedment.

RD_{SG} is the total rut depth in the subgrade for a load level i; dN is the incremental repetition under that load level i; N_0 is a model constant for considering the effect of earlier loading.

- Step 2. Fit $a \sim f(SSR_{SG})$ and $b \sim f(SSR_{SG})$ for all testing cases.

Using the rut test data from the HVS testing, it was found that the rut depth in the subgrade had a power relationship of approximately 0.5 with load repetitions after early embedment for all testing cases. Consequently, the power constant c was set as 0.5. The constant a is a function of SSR_{SB}, calculated for each case using Equations 4.1 through 4.4. The subgrade rut model is summarized in Table 8.1.

Table 8.1: Summary of Rut Models Developed for Different Layers in a PICP

Layer	Rut Model[1]	Moisture Condition	Model Parameters		
			a	*b*	*c*
Combined bedding and base	$RD_{BB} = a \times h\_SB + b$	Dry Wet	0 -0.012	4.0 13.1	- -
Subbase	$RD_{SB} = (a \times SSR^b) \times N^c$	Dry Wet	3.10E-06 3.10E-06	2.70 2.70	1 1
Subgrade (Silty clay)	$RD_{SG} = (a \times SSR + b) \times N^c$	Dry Wet	0.03 0.03	-0.01 -0.01	0.5 0.5

[1] RD_{xx}, rut depth of *xx* layer (BB=surface(paver, bedding and base); SB=subbase; SG=subgrade), mm;
h_SB, thickness of subbase, mm;
SSR, shear stress/strength ratio at the top of the layer;
N, load repetition;
a, b, c, model constants.

Given that rutting in the subbase cannot be prevented simply by increasing the thickness of this layer, only rutting in the subgrade was used in the development of the example design tables. Changing the rutting behavior of the subbase would require tighter specifications for the properties of the materials used in this layer, and/or the construction methods (e.g., higher relative compaction/lower air void content). Consideration for these alternatives would require laboratory and additional accelerated pavement testing to quantify the effects of the changes, which was beyond the scope of this study.

8.3 Input Parameters for M-E Design of PICP

The default input parameters for mechanistic-empirical design of PICP were revised from those used in the earlier study (see Table 4.1) based on the HVS test results and are summarized in Table 8.2 and discussed in the following sections.

8.3.1 Pavement Structure

The same standard permeable interlocking concrete pavement structure used in the initial analysis was used. However, as discussed above, for this analysis, the bedding and base layers were combined with the pavers into a single surface layer, and the subbase was analyzed as a separate layer.

Table 8.2: Summary of Inputs for Performance Modeling and M-E Design of PICP

Variable		Surface (Paver, bedding & base)		Subbase			Subgrade	
		Thickness (mm)	Stiffness (MPa[1])	Thickness (mm)	Stiffness (MPa)	c, ϕ (kPa, °)	Stiffness (MPa)	c, ϕ (kPa, °)
Pavement Structure and Materials	Label	h1	E1	h2	E2	c, ϕ	E3	c, ϕ
	Value	230	110 (dry) 87 (wet)	Varying (450 default)	122 (dry) 73 (wet)	0, 45 (dry) 0, 30 (wet)	60 (dry) 37 (wet)	15, 25 (dry) 9, 15 (wet)
Climate	**Variable**	**Wet Days [2]**	[2] Number of days in a calendar year when the subbase has standing water					
	Label	W						
	Value	50						
Traffic	**Variable**	**Axle Type**	**Axle Load[2] (kN[3])**	**Stress Location**	[2] The total truck traffic volume was divided into different axle loads according to an axle-load distribution factor. Group 1 WIM truck traffic data from California was used as the default axle-load distribution factor.			
	Label	AT	AL	SL				
	Value	Single (S) Tandem (T)	10 to 160 (S) 20 to 200 (T)	Under Wheel Between Wheel				
[1] 1,000 psi = 6.890 MPa			[3] 1,000 lb = 4.448 kN					

8.3.2 Material Properties

The same material properties used in the earlier analysis were used; however, the values were adjusted to match the materials and layer thicknesses used in the test track. The following default stiffnesses were selected for each layer under both wet and dry conditions based on the backcalculated effective stiffnesses from the deflection data collected during HVS testing:

- Combined surface layer:
  - Dry: 110 MPa
  - Wet: 87 MPa
- Subbase:
  - Dry: 122 MPa
  - Wet: 73 MPa
- Subgrade:
  - Dry: 60 MPa
  - Wet: 37 MPa

The same Poisson's ratio used in the original analysis (0.35) was used for this phase of the analysis. The default cohesion (c) of the subbase material remained the same at 0 kPa under both dry and wet conditions. However, in this phase of the analysis, different default internal friction angles (ϕ) were assumed for dry and wet conditions. Selected values were 45° under dry conditions and 30° under wet conditions, based on differences in rutting performance in this layer in the dry and wet tests and a review of the literature *(10,12)*.

The default cohesion and internal friction angles of the subgrade were revised as follows, based on the HVS testing results:

- Dry: 15 kPa and 25°
- Wet: 9 kPa and 15°

8.3.3 Climate

Based on the HVS test results, the worse-case design condition for PICP would be when the subbase contains standing water (i.e., the subbase is serving as a reservoir for collected rainwater while that water infiltrates the subgrade or drains through a subsurface drainage system). The number of wet days when the subbase contains standing water is required to distribute the traffic between dry and wet periods. The default number of wet days was set at 50.

8.3.4 Traffic

Traffic input was expanded from that used in the original analysis. An axle load spectrum for single and tandem axles with dual wheels was used to characterize traffic. Twelve single axle loads ranging between 10 kN and 160 kN (2,250 lb and 36,000 lb) and ten tandem axle loads ranging between 20 kN and 200 kN (4,500 lb and 45,000 lb) were considered. Tire pressure was set at 700 kPa (101 psi). The tandem axle load was treated as two independent single axle loads. The distance between the two tire centers was set at 340 mm (13.4 in.). The stress under the wheel and the stress between the wheels were both calculated to identify the most critical stress.

The total truck traffic volume was calculated from two-way annual average daily traffic (AADT), percentage of trucks, direction distribution factor, lane distribution factor, annual growth rate, design life, and traffic safety factor. The total truck traffic volume was divided into different axle loads according to the axle-load distribution factor. The equivalent single axle load (ESAL) was then calculated using the 4^{th}-power law.

8.4 Design Tool and Validation

A mechanistic-empirical design tool for permeable interlocking concrete pavements was created in an *Excel*® spreadsheet and used to run the analyses and prepare the example design tables provided in Chapter 9. The critical responses, including the major and minor principal stresses (σ_1 and σ_3) on top of the subbase and subgrade layers, required for calculating the shear stress/strength ratio (*SSR*), were calculated with the inputs listed above using multilayer linear elastic theory. The *OpenPave* software program *(5)* was used for these analyses. An incremental recursive analysis method *(20*) was then used to calculate the rut depth in the M-E design tool. The user interface for this design tool is shown in Figure 8.1. The tool was used in two ways in this analysis to provide the following:

- The expected total rut depth (derived from the predicted rut depth in the subgrade) based on the input values of pavement structure, material properties, climate, and traffic.
- The required minimum thickness of the subbase layer for a given allowable rut depth.

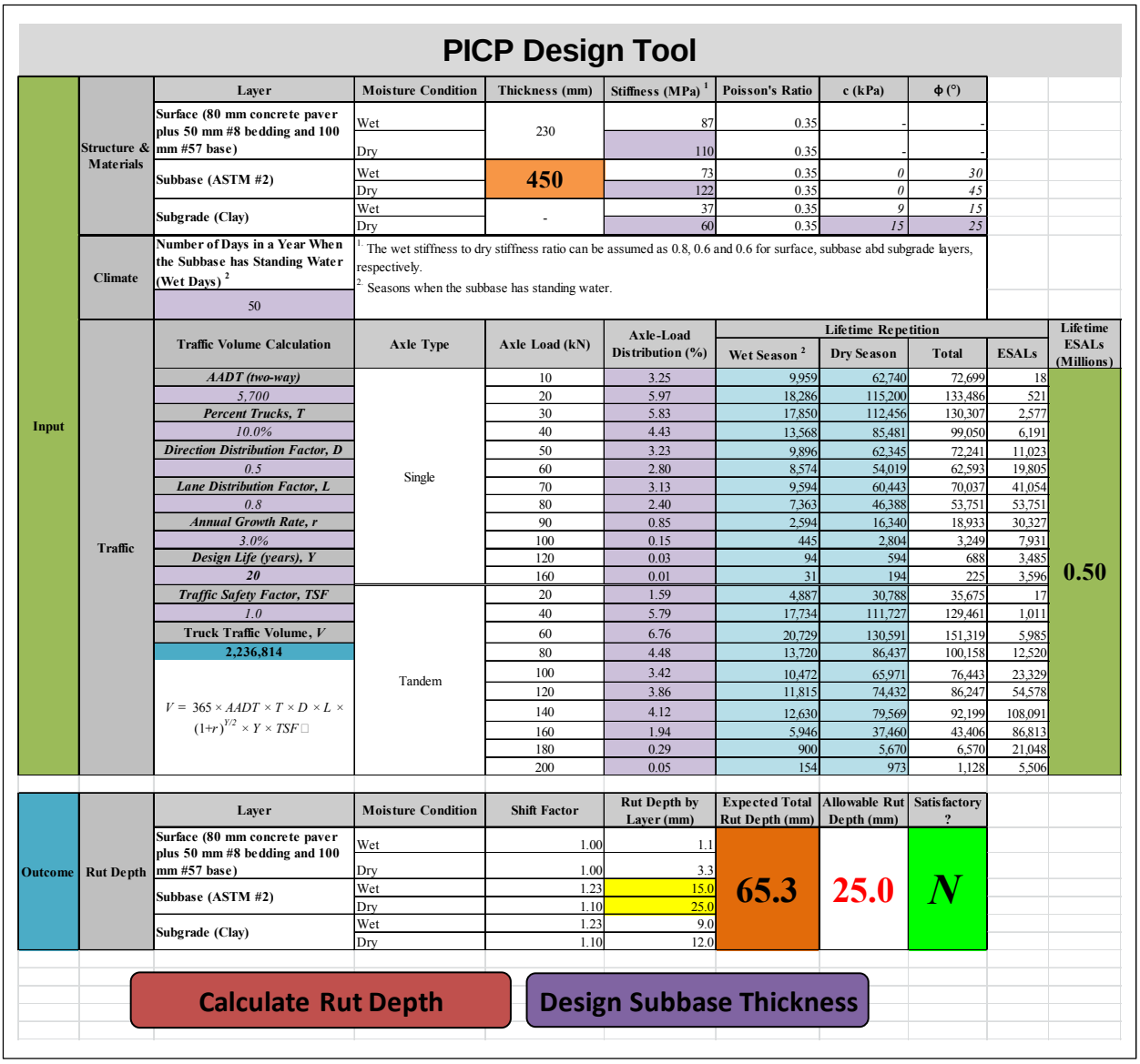

Figure 8.1: User interface for the PICP design tool.

The design tool was validated and the results calibrated with the data collected during the three HVS tests. No independent validation of the calibration was undertaken since only one set of HVS test data, and no comprehensive long-term performance measurements with traffic and subbase water content data from in-service pavements were available.

The comparison of measured and calculated rut depth for the HVS test sections is presented in Table 8.3 and Figure 8.2 for both dry and wet conditions. The maximum error between the measured and calculated rut depths ranged from -4 percent to +5 percent, with rut depth shift factors of 1.10 for dry conditions and 1.23 for wet conditions.

Table 8.3: Comparison of Measured and Calculated Rut Depth for the HVS Testing Sections

Section	Moisture Condition	Measured Rut Depth for Three Subsections (mm)			Calculated Rut Depth for Three Subsections (mm)			Error for the Three Subsections (%)		
		450	650	950	450	650	950	450	650	950
678HC	Dry	24	19	16	27	19	14	2	0	-3
679HC	Wet	62	47	40	68	54	43	-4	5	3

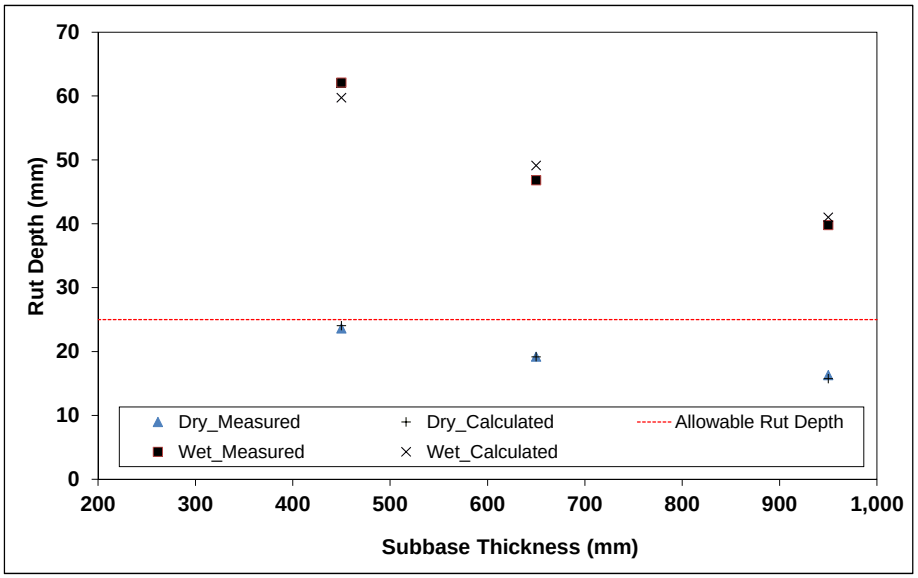

Figure 8.2: Comparison of measured and calculated rut depth for the HVS testing sections.

The main observations from the earlier mechanistic analysis discussed in Section 4.2.4 were refined as follows after this analysis as follows:

- Higher shear stress/strength ratios at the top of the subgrade, which equate to a higher risk of rutting in the subgrade, require thicker subbase layers, as expected.
- An increase in the stiffness of the surface layer reduces the required subbase layer thickness to achieve the same shear stress/strength ratio. However, the effect of the surface layer stiffness on overall pavement performance is not significant due to the relatively low thickness of the pavers (80 mm) and the reduced interlock between them compared to pavers with sand joints.
- For the same shear stress/strength ratio at the top of the subbase, an increase in the stiffness of the subbase layer reduces the required thickness of that subbase layer, especially when the subgrade has a low stiffness.
- For the same shear stress/strength ratio at the top of the subgrade, wet conditions require thicker subbase layers compared to the dry condition, confirming that wet conditions are the most critical condition for design.

8.5 Design Tool Analysis of a Theoretical Structure with Pervious Concrete Subbase

A theoretical permeable pavement structure similar to the structure analyzed in the preceding sections, but with a 150 mm (6 in.) pervious concrete subbase on top of the subgrade, was evaluated to determine the

influence of having a stiff layer underneath the coarse aggregate subbase. This layer would typically serve as a platform on which to compact the coarse aggregate subbase as well as contributing to the overall stiffness of the structure, thereby potentially allowing for a reduction in the thickness of the coarse aggregate layer. The same input values listed in Table 8.2 were used for this analysis. A stiffness of 6 GPa (870 ksi) was used for the pervious concrete layer.

The analysis found that for annual traffic up to two million ESALs, the 150 mm pervious concrete layer could be used as an alternative to the coarse aggregate subbase in the example design tables. No field testing was undertaken to validate this finding. The influence of the stiff pervious concrete platform on improved compaction of the coarse aggregate subbase and resulting reduced rutting in the subbase could not be determined without field data. Based on these findings, the use of a pervious concrete subbase to replace or supplement the coarse aggregate subbase should be investigated.

9. PROPOSED EXAMPLE DESIGN TABLES

Two versions of the proposed example design tables were compiled using the design tool discussed in Chapter 8. Both versions use a table format that is similar to the current table in the ICPI guide *(4)*, but in addition to the subgrade shear strength/resilient modulus as a governing factor dictating subbase thickness, the revised versions also include the number of days in a year that the subbase will contain standing water above the top of the subgrade (i.e., the subbase is serving as a reservoir). The first set of tables, Table 9.1 (metric) and Table 9.2 (U.S. units), uses a target number of days and includes eight options (0, 10, 30, 50, 70, 90, 110, and 130 days). The second set of tables, Table 9.3 (metric) and Table 9.4 (U.S. units), uses a range of days and also includes eight options (0, <10, 10-29, 30-49, 50-69, 70-89, 90-109, and 110-130). The values listed in this second set of tables are the same as those listed in the first set, which implies that there is added conservatism in the lower range of the days in each column. If a layer thickness is critical, a more realistic subbase thickness can be determined either by using the same *Excel*® spreadsheet-based design tool used to develop the tables, or by extrapolation using the corresponding value in the previous column. A column with zero days is included in both tables for comparison purposes to show the designer the additional subbase thickness that would be required for trafficking under wet conditions and/or water storage.

Traffic classes and subgrade modulus remain the same as in the current table in the ICPI guide; however, only four of the subgrade modulus categories are included in the example table (40, 60, 80, and 100 MPa [5.8, 8.7, 11.6, and 14.5 ksi] for dry conditions and 24, 36, 48, and 60 MPa [3.5, 5.2, 6.7, and 8.7 ksi] for wet conditions). A range of corresponding cohesion and internal friction angles for subgrade materials are also included in the tables for refining the selection. Designs for a specific set of project circumstances can be undertaken by using the same *Excel*® spreadsheet-based design tool used to develop the tables in conjunction with the hydrological design procedures provided in the ICPI guide *(4)*.

The design tool output and corresponding values in the tables should be considered as best estimate designs, since they were developed from the results of only two HVS tests. Designers should continue to use sound engineering judgment when designing permeable interlocking concrete pavements and can introduce additional conservatism/reliability by altering one or more of the design inputs, namely the material properties, number of days that the subbase will contain standing water, and/or traffic.

The new recommended minimum subbase thicknesses required to prevent subgrade rutting do not differ significantly from the values in the table in the ICPI guide *(4)*; there are new thicknesses which are slightly thinner or slightly thicker depending on the design traffic, resilient modulus, and number of days

that the subbase contains water. In scenarios where lower numbers of days with standing water in the subbase are selected, the new recommended minimum subbase thicknesses are mostly less conservative than the thicknesses proposed in the current ICPI guide. If the maximum number of days with standing water in the subbase is selected (i.e., 130), then the new recommended minimum subbase thickness is slightly more conservative (e.g., 700 mm [27.6 in.] versus 675 mm [27.0 in.] for a design traffic of 1 million ESALs on the weakest subgrade).

Table 9.1: Example Design Table with Target Number of Days with Water Stored in Subbase (Metric)

Number of Days in a Year When the Subbase Has Standing Water		0				10				30				50			
Subgrade Resilient Modulus (MPa)	Dry	40	60	80	100	40	60	80	100	40	60	80	100	40	60	80	100
	Wet	24	36	48	60	24	36	48	60	24	36	48	60	24	36	48	60
Subgrade Cohesion (kPa)/ Internal Friction Angle (°)[1]	Dry	10/20	15/25	20/30	25/35	10/20	15/25	20/30	25/35	10/20	15/25	20/30	25/35	10/20	15/25	20/30	25/35
	Wet	6/12	9/15	12/22	15/25	6/12	9/15	12/22	15/25	6/12	9/15	12/22	15/25	6/12	9/15	12/22	15/25
Lifetime ESALs (Traffic Index)		Minimum Subbase Thickness in mm ASTM #2 for 25 mm Allowable Rut Depth (All designs have 80 mm Paver, 50 mm ASTM #8 Bedding Layer, & 100 mm ASTM #57 Base Layer.)															
50,000 (6.3)		150	150	150	150	150	150	150	150	150	150	150	150	175	150	150	150
100,000 (6.8)		150	150	150	150	210	150	150	150	260	150	150	150	285	180	150	150
200,000 (7.4)		230	150	150	150	315	210	150	150	365	255	160	150	395	285	185	150
300,000 (7.8)		290	180	150	150	375	265	170	150	425	315	215	150	455	340	240	160
400,000 (8.1)		330	220	150	150	420	305	210	150	470	350	255	175	500	380	280	200
500,000 (8.3)		360	250	160	150	450	335	240	160	500	380	280	205	530	410	305	230
600,000 (8.5)		385	275	185	150	475	360	260	180	525	405	305	225	555	435	330	250
700,000 (8.6)		410	295	205	150	495	380	280	200	550	425	325	245	580	455	350	270
800,000 (8.8)		425	310	220	150	515	395	295	215	565	440	340	260	600	470	365	285
900,000 (8.9)		440	325	235	155	530	410	310	230	585	455	355	270	615	485	380	295
1,000,000 (9.0)		455	340	250	165	545	425	325	240	600	470	365	285	630	500	390	310

[1] Default values based on testing cited in the literature *(10,12)*.

Table 9.1: Example Design Table with Target Number of Days with Water Stored in Subbase (Metric) *(continued)*

Number of Days in a Year When the Subbase Has Standing Water		70				90				110				130			
Subgrade Resilient Modulus (MPa)	Dry	40	60	80	100	40	60	80	100	40	60	80	100	40	60	80	100
	Wet	24	36	48	60	24	36	48	60	24	36	48	60	24	36	48	60
Subgrade Cohesion (kPa)/ Internal Friction Angle (°)[1]	Dry	10/20	15/25	20/30	25/35	10/20	15/25	20/30	25/35	10/20	15/25	20/30	25/35	10/20	15/25	20/30	25/35
	Wet	6/12	9/15	12/22	15/25	6/12	9/15	12/22	15/25	6/12	9/15	12/22	15/25	6/12	9/15	12/22	15/25
Lifetime ESALs (Traffic Index)		Minimum Subbase Thickness in mm ASTM #2 for 25 mm Allowable Rut Depth (All designs have 80 mm Paver, 50 mm ASTM #8 Bedding Layer, & 100 mm ASTM #57 Base Layer.)															
50,000 (6.3)		195	150	150	150	210	150	150	150	225	150	150	150	235	150	150	150
100,000 (6.8)		310	200	150	150	325	215	150	150	335	230	150	150	350	240	150	150
200,000 (7.4)		415	305	205	150	430	320	215	150	445	330	230	150	455	340	240	160
300,000 (7.8)		475	360	260	180	495	375	275	195	505	390	285	210	520	400	295	220
400,000 (8.1)		520	400	295	220	535	415	310	235	550	430	325	245	565	440	335	255
500,000 (8.3)		550	430	325	245	570	445	340	260	585	460	350	270	595	470	360	280
600,000 (8.5)		580	455	350	270	595	470	360	280	610	485	375	295	625	495	385	305
700,000 (8.6)		600	475	365	285	620	490	380	300	635	505	395	310	645	515	405	320
800,000 (8.8)		620	490	385	300	640	505	395	315	655	520	410	330	665	535	420	340
900,000 (8.9)		635	505	395	315	655	525	410	330	670	535	425	340	685	550	435	350
1,000,000 (9.0)		650	520	410	325	670	535	425	340	685	550	435	355	700	560	445	365

[1] Default values based on testing cited in the literature *(10,12)*.

Table 9.2: Example Design Table with Target Number of Days with Water Stored in Subbase (U.S.)

Number of Days in a Year When the Subbase Has Standing Water		0				10				30				50			
Subgrade Resilient Modulus (ksi)	Dry	5.8	8.7	11.6	14.5	5.8	8.7	11.6	14.5	5.8	8.7	11.6	14.5	5.8	8.7	11.6	14.5
	Wet	3.5	5.2	6.7	8.7	3.5	5.2	6.7	8.7	3.5	5.2	6.7	8.7	3.5	5.2	6.7	8.7
Subgrade Cohesion (psi)/ Internal Friction Angle (°)[1]	Dry	1.5/ 20	2.2/ 25	2.9/ 30	3.6/ 35	1.5/ 20	2.2/ 25	2.9/ 30	3.6/ 35	1.5/ 20	2.2/ 25	2.9/ 30	3.6/ 35	1.5/ 20	2.2/ 25	2.9/ 30	3.6/ 35
	Wet	0.9/ 12	1.3/ 15	1.7/ 22	2.2/ 25	0.9/ 12	1.3/ 15	1.7/ 22	2.2/ 25	0.9/ 12	1.3/ 15	1.7/ 22	2.2/ 25	0.9/ 12	1.3/ 15	1.7/ 22	2.2/ 25
Lifetime ESALs (Traffic Index)		**Minimum Subbase Thickness in inches[2] ASTM #2 for 1 in. Allowable Rut Depth (All designs have 3.2 in. Paver, 2 in. ASTM #8 Bedding Layer, & 4 in. ASTM #57 Base Layer.)**															
50,000 (6.3)		6.0	6.0	6.0	6.0	6.0	6.0	6.0	6.0	6.0	6.0	6.0	6.0	7.0	6.0	6.0	6.0
100,000 (6.8)		6.0	6.0	6.0	6.0	8.5	6.0	6.0	6.0	10.5	6.0	6.0	6.0	11.5	7.0	6.0	6.0
200,000 (7.4)		9.0	6.0	6.0	6.0	12.5	8.5	6.0	6.0	14.5	10.0	6.5	6.0	16.0	11.5	7.5	6.0
300,000 (7.8)		11.5	7.0	6.0	6.0	15.0	10.5	7.0	6.0	17.0	12.5	8.5	6.0	18.0	13.5	9.5	6.5
400,000 (8.1)		13.0	9.0	6.0	6.0	17.0	12.0	8.5	6.0	19.0	14.0	10.0	7.0	20.0	15.0	11.0	8.0
500,000 (8.3)		14.5	10.0	6.5	6.0	18.0	13.5	9.5	6.5	20.0	15.0	11.0	8.0	21.0	16.5	12.0	9.0
600,000 (8.5)		15.5	11.0	7.5	6.0	19.0	14.5	10.5	7.0	21.0	16.0	12.0	9.0	22.0	17.5	13.0	10.0
700,000 (8.6)		16.5	12.0	8.0	6.0	20.0	15.0	11.0	8.0	22.0	17.0	13.0	10.0	23.0	18.0	14.0	11.0
800,000 (8.8)		17.0	12.5	9.0	6.0	20.5	16.0	12.0	8.5	22.5	17.5	13.5	10.5	24.0	19.0	14.5	11.5
900,000 (8.9)		17.5	13.0	9.5	6.0	21.0	16.5	12.5	9.0	23.5	18.0	14.0	11.0	24.5	19.5	15.0	12.0
1,000,000 (9.0)		18.0	13.5	10.0	6.5	22.0	17.0	13.0	9.5	24.0	19.0	14.5	11.5	25.0	20.0	15.5	12.5

[1] Default values based on testing cited in the literature *(10,12)*.

Table 9.2: Example Design Table with Target Number of Days with Water Stored in Subbase (U.S.) *(continued)*

Number of Days in a Year When the Subbase Has Standing Water		70				90				110				130			
Subgrade Resilient Modulus (ksi)	Dry	5.8	8.7	11.6	14.5	5.8	8.7	11.6	14.5	5.8	8.7	11.6	14.5	5.8	8.7	11.6	14.5
	Wet	3.5	5.2	6.7	8.7	3.5	5.2	6.7	8.7	3.5	5.2	6.7	8.7	3.5	5.2	6.7	8.7
Subgrade Cohesion (psi)/ Internal Friction Angle (°)[1]	Dry	1.5/ 20	2.2/ 25	2.9/ 30	3.6/ 35	1.5/ 20	2.2/ 25	2.9/ 30	3.6/ 35	1.5/ 20	2.2/ 25	2.9/ 30	3.6/ 35	1.5/ 20	2.2/ 25	2.9/ 30	3.6/ 35
	Wet	0.9/ 12	1.3 /15	1.7/ 22	2.2/ 25	0.9/ 12	1.3 /15	1.7/ 22	2.2/ 25	0.9/ 12	1.3 /15	1.7/ 22	2.2/ 25	0.9/ 12	1.3 /15	1.7/ 22	2.2/ 25
Lifetime ESALs (Traffic Index)		Minimum Subbase Thickness in inches[2] ASTM #2 for 1 in. Allowable Rut Depth (All designs have 3.2 in. Paver, 2 in. ASTM #8 Bedding Layer, & 4 in. ASTM #57 Base Layer.)															
50,000 (6.3)		8.0	6.0	6.0	6.0	8.5	6.0	6.0	6.0	9.0	6.0	6.0	6.0	9.5	6.0	6.0	6.0
100,000 (6.8)		12.0	8.0	6.0	6.0	13.0	8.5	6.0	6.0	13.0	9.0	6.0	6.0	14.0	9.5	6.0	6.0
200,000 (7.4)		16.5	12.0	8.0	6.0	17.0	13.0	8.5	6.0	17.5	13.0	9.0	6.0	18.0	13.5	9.5	6.5
300,000 (7.8)		18.5	14.0	10.0	7.0	20.0	15.0	11.0	8.0	20.0	15.5	11.0	8.5	20.5	15.5	11.5	8.5
400,000 (8.1)		20.5	15.5	11.5	8.5	21.5	16.5	12.5	9.5	21.5	17.0	13.0	9.5	22.0	17.5	13.0	10.0
500,000 (8.3)		21.5	17.0	13.0	9.5	23.0	18.0	13.5	10.5	23.0	18.0	14.0	10.5	23.5	18.5	14.0	11.0
600,000 (8.5)		23.0	18.0	14.0	10.5	24.0	19.0	14.5	11.0	24.0	19.0	15.0	11.5	24.5	19.5	15.0	12.0
700,000 (8.6)		23.5	18.5	14.5	11.0	25.0	19.5	15.0	12.0	25.0	20.0	15.5	12.0	25.5	20.5	16.0	12.5
800,000 (8.8)		24.5	19.5	15.0	12.0	25.5	20.0	16.0	12.5	26.0	20.5	16.0	13.0	26.0	21.0	16.5	13.5
900,000 (8.9)		25.0	20.0	15.5	12.5	26.0	21.0	16.5	13.0	26.5	21.0	16.5	13.5	27.0	21.5	17.0	14.0
1,000,000 (9.0)		25.5	20.5	16.0	13.0	27.0	21.5	17.0	13.5	27.0	21.5	17.0	14.0	27.5	22.0	17.5	14.5

[1] Default values based on testing cited in the literature *(10,12)*.

Table 9.3: Example Design Table with Range of Days with Water Stored in Subbase (Metric)

Number of Days in a Year When the Subbase Has Standing Water		0				≤10				11 - 30				31 - 50			
Subgrade Resilient Modulus (MPa)	Dry	40	60	80	100	40	60	80	100	40	60	80	100	40	60	80	100
	Wet	24	36	48	60	24	36	48	60	24	36	48	60	24	36	48	60
Subgrade Cohesion (kPa)/ Internal Friction Angle (°)[1]	Dry	10/20	15/25	20/30	25/35	10/20	15/25	20/30	25/35	10/20	15/25	20/30	25/35	10/20	15/25	20/30	25/35
	Wet	6/12	9/15	12/22	15/25	6/12	9/15	12/22	15/25	6/12	9/15	12/22	15/25	6/12	9/15	12/22	15/25
Lifetime ESALs (Traffic Index)		Minimum Subbase Thickness in mm ASTM #2 for 25 mm Allowable Rut Depth (All designs have 80 mm Paver, 50 mm ASTM #8 Bedding Layer, & 100 mm ASTM #57 Base Layer.)															
50,000 (6.3)		150	150	150	150	150	150	150	150	150	150	150	150	175	150	150	150
100,000 (6.8)		150	150	150	150	210	150	150	150	260	150	150	150	285	180	150	150
200,000 (7.4)		230	150	150	150	315	210	150	150	365	255	160	150	395	285	185	150
300,000 (7.8)		290	180	150	150	375	265	170	150	425	315	215	150	455	340	240	160
400,000 (8.1)		330	220	150	150	420	305	210	150	470	350	255	175	500	380	280	200
500,000 (8.3)		360	250	160	150	450	335	240	160	500	380	280	205	530	410	305	230
600,000 (8.5)		385	275	185	150	475	360	260	180	525	405	305	225	555	435	330	250
700,000 (8.6)		410	295	205	150	495	380	280	200	550	425	325	245	580	455	350	270
800,000 (8.8)		425	310	220	150	515	395	295	215	565	440	340	260	600	470	365	285
900,000 (8.9)		440	325	235	155	530	410	310	230	585	455	355	270	615	485	380	295
1,000,000 (9.0)		455	340	250	165	545	425	325	240	600	470	365	285	630	500	390	310

[1] Default values based on testing cited in the literature *(10,12)*.

Table 9.3: Example Design Table with Range of Days with Water Stored in Subbase (Metric) *(continued)*

Number of Days in a Year When the Subbase Has Standing Water		51 - 70				71 - 90				91 - 110				111 - 130			
Subgrade Resilient Modulus (MPa)	Dry	40	60	80	100	40	60	80	100	40	60	80	100	40	60	80	100
	Wet	24	36	48	60	24	36	48	60	24	36	48	60	24	36	48	60
Subgrade Cohesion (kPa)/ Internal Friction Angle (°)[1]	Dry	10/20	15/25	20/30	25/35	10/20	15/25	20/30	25/35	10/20	15/25	20/30	25/35	10/20	15/25	20/30	25/35
	Wet	6/12	9/15	12/22	15/25	6/12	9/15	12/22	15/25	6/12	9/15	12/22	15/25	6/12	9/15	12/22	15/25
Lifetime ESALs (Traffic Index)		Minimum Subbase Thickness in mm ASTM #2 for 25 mm Allowable Rut Depth (All designs have 80 mm Paver, 50 mm ASTM #8 Bedding Layer, & 100 mm ASTM #57 Base Layer.)															
50,000 (6.3)		195	150	150	150	210	150	150	150	225	150	150	150	235	150	150	150
100,000 (6.8)		310	200	150	150	325	215	150	150	335	230	150	150	350	240	150	150
200,000 (7.4)		415	305	205	150	430	320	215	150	445	330	230	150	455	340	240	160
300,000 (7.8)		475	360	260	180	495	375	275	195	505	390	285	210	520	400	295	220
400,000 (8.1)		520	400	295	220	535	415	310	235	550	430	325	245	565	440	335	255
500,000 (8.3)		550	430	325	245	570	445	340	260	585	460	350	270	595	470	360	280
600,000 (8.5)		580	455	350	270	595	470	360	280	610	485	375	295	625	495	385	305
700,000 (8.6)		600	475	365	285	620	490	380	300	635	505	395	310	645	515	405	320
800,000 (8.8)		620	490	385	300	640	505	395	315	655	520	410	330	665	535	420	340
900,000 (8.9)		635	505	395	315	655	525	410	330	670	535	425	340	685	550	435	350
1,000,000 (9.0)		650	520	410	325	670	535	425	340	685	550	435	355	700	560	445	365

[1] Default values based on testing cited in the literature *(10,12)*.

Table 9.4: Example Design Table with Range of Days with Water Stored in Subbase (U.S.)

Number of Days in a Year When the Subbase Has Standing Water		0				≤10				11 - 30				31 - 50			
Subgrade Resilient Modulus (ksi)	Dry	5.8	8.7	11.6	14.5	5.8	8.7	11.6	14.5	5.8	8.7	11.6	14.5	5.8	8.7	11.6	14.5
	Wet	3.5	5.2	6.7	8.7	3.5	5.2	6.7	8.7	3.5	5.2	6.7	8.7	3.5	5.2	6.7	8.7
Subgrade Cohesion (psi)/ Internal Friction Angle (°)[1]	Dry	1.5/ 20	2.2/ 25	2.9/ 30	3.6/ 35	1.5/ 20	2.2/ 25	2.9/ 30	3.6/ 35	1.5/ 20	2.2/ 25	2.9/ 30	3.6/ 35	1.5/ 20	2.2/ 25	2.9/ 30	3.6/ 35
	Wet	0.9/ 12	1.3/ 15	1.7/ 22	2.2/ 25	0.9/ 12	1.3/ 15	1.7/ 22	2.2/ 25	0.9/ 12	1.3/ 15	1.7/ 22	2.2/ 25	0.9/ 12	1.3/ 15	1.7/ 22	2.2/ 25
Lifetime ESALs (Traffic Index)		**Minimum Subbase Thickness in inches[2] ASTM #2 for 1 in. Allowable Rut Depth (All designs have 3.2 in. Paver, 2 in. ASTM #8 Bedding Layer, & 4 in. ASTM #57 Base Layer.)**															
50,000 (6.3)		6.0	6.0	6.0	6.0	6.0	6.0	6.0	6.0	6.0	6.0	6.0	6.0	7.0	6.0	6.0	6.0
100,000 (6.8)		6.0	6.0	6.0	6.0	8.5	6.0	6.0	6.0	10.5	6.0	6.0	6.0	11.5	7.0	6.0	6.0
200,000 (7.4)		9.0	6.0	6.0	6.0	12.5	8.5	6.0	6.0	14.5	10.0	6.5	6.0	16.0	11.5	7.5	6.0
300,000 (7.8)		11.5	7.0	6.0	6.0	15.0	10.5	7.0	6.0	17.0	12.5	8.5	6.0	18.0	13.5	9.5	6.5
400,000 (8.1)		13.0	9.0	6.0	6.0	17.0	12.0	8.5	6.0	19.0	14.0	10.0	7.0	20.0	15.0	11.0	8.0
500,000 (8.3)		14.5	10.0	6.5	6.0	18.0	13.5	9.5	6.5	20.0	15.0	11.0	8.0	21.0	16.5	12.0	9.0
600,000 (8.5)		15.5	11.0	7.5	6.0	19.0	14.5	10.5	7.0	21.0	16.0	12.0	9.0	22.0	17.5	13.0	10.0
700,000 (8.6)		16.5	12.0	8.0	6.0	20.0	15.0	11.0	8.0	22.0	17.0	13.0	10.0	23.0	18.0	14.0	11.0
800,000 (8.8)		17.0	12.5	9.0	6.0	20.5	16.0	12.0	8.5	22.5	17.5	13.5	10.5	24.0	19.0	14.5	11.5
900,000 (8.9)		17.5	13.0	9.5	6.0	21.0	16.5	12.5	9.0	23.5	18.0	14.0	11.0	24.5	19.5	15.0	12.0
1,000,000 (9.0)		18.0	13.5	10.0	6.5	22.0	17.0	13.0	9.5	24.0	19.0	14.5	11.5	25.0	20.0	15.5	12.5

[1] Default values based on testing cited in the literature *(10,12)*.

Table 9.4: Example Design Table with Range of Days with Water Stored in Subbase (U.S.) *(continued)*

Number of Days in a Year When the Subbase Has Standing Water		51 - 70				71 - 90				91 - 110				111 - 130			
Subgrade Resilient Modulus (ksi)	Dry	5.8	8.7	11.6	14.5	5.8	8.7	11.6	14.5	5.8	8.7	11.6	14.5	5.8	8.7	11.6	14.5
	Wet	3.5	5.2	6.7	8.7	3.5	5.2	6.7	8.7	3.5	5.2	6.7	8.7	3.5	5.2	6.7	8.7
Subgrade Cohesion (psi)/ Internal Friction Angle (°)[1]	Dry	1.5/ 20	2.2/ 25	2.9/ 30	3.6/ 35	1.5/ 20	2.2/ 25	2.9/ 30	3.6/ 35	1.5/ 20	2.2/ 25	2.9/ 30	3.6/ 35	1.5/ 20	2.2/ 25	2.9/ 30	3.6/ 35
	Wet	0.9/ 12	1.3 /15	1.7/ 22	2.2/ 25	0.9/ 12	1.3 /15	1.7/ 22	2.2/ 25	0.9/ 12	1.3 /15	1.7/ 22	2.2/ 25	0.9/ 12	1.3 /15	1.7/ 22	2.2/ 25
Lifetime ESALs (Traffic Index)		**Minimum Subbase Thickness in inches[2] ASTM #2 for 1 in. Allowable Rut Depth (All designs have 3.2 in. Paver, 2 in. ASTM #8 Bedding Layer, & 4 in. ASTM #57 Base Layer).**															
50,000 (6.3)		8.0	6.0	6.0	6.0	8.5	6.0	6.0	6.0	9.0	6.0	6.0	6.0	9.5	6.0	6.0	6.0
100,000 (6.8)		12.0	8.0	6.0	6.0	13.0	8.5	6.0	6.0	13.0	9.0	6.0	6.0	14.0	9.5	6.0	6.0
200,000 (7.4)		16.5	12.0	8.0	6.0	17.0	13.0	8.5	6.0	17.5	13.0	9.0	6.0	18.0	13.5	9.5	6.5
300,000 (7.8)		18.5	14.0	10.0	7.0	20.0	15.0	11.0	8.0	20.0	15.5	11.0	8.5	20.5	15.5	11.5	8.5
400,000 (8.1)		20.5	15.5	11.5	8.5	21.5	16.5	12.5	9.5	21.5	17.0	13.0	9.5	22.0	17.5	13.0	10.0
500,000 (8.3)		21.5	17.0	13.0	9.5	23.0	18.0	13.5	10.5	23.0	18.0	14.0	10.5	23.5	18.5	14.0	11.0
600,000 (8.5)		23.0	18.0	14.0	10.5	24.0	19.0	14.5	11.0	24.0	19.0	15.0	11.5	24.5	19.5	15.0	12.0
700,000 (8.6)		23.5	18.5	14.5	11.0	25.0	19.5	15.0	12.0	25.0	20.0	15.5	12.0	25.5	20.5	16.0	12.5
800,000 (8.8)		24.5	19.5	15.0	12.0	25.5	20.0	16.0	12.5	26.0	20.5	16.0	13.0	26.0	21.0	16.5	13.5
900,000 (8.9)		25.0	20.0	15.5	12.5	26.0	21.0	16.5	13.0	26.5	21.0	16.5	13.5	27.0	21.5	17.0	14.0
1,000,000 (9.0)		25.5	20.5	16.0	13.0	27.0	21.5	17.0	13.5	27.0	21.5	17.0	14.0	27.5	22.0	17.5	14.5

[1] Default values based on testing cited in the literature *(10,12)*.

10. CONCLUSIONS

10.1 Summary

This report details the research undertaken to develop revised design tables for permeable interlocking concrete pavement using a mechanistic-empirical design approach. The study included a literature review, field testing of existing projects and test sections, estimation of the effective stiffness of each layer in permeable interlocking concrete pavement structures, mechanistic analysis and structural design of a test track incorporating three different subbase thicknesses (low, medium, and higher risk), tests on the track with a Heavy Vehicle Simulator (HVS) to collect performance data to validate the design approach using accelerated loading, refinement and calibration of the design procedure using the test track data, development of a spreadsheet based design tool, and development of revised design tables using the design tool.

Rut development rate as a function of the shear strength to shear stress ratios at the top of the subbase and the top of the subgrade was used as the basis for the design approach. This approach was selected given that low shear strengths of saturated and often poorly compacted subgrades are common in permeable pavements and that higher allowable ruts are usually tolerated due to the absence of ponding on the surface during rainfall. The alternative approach of using a vertical strain criterion was considered inappropriate for permeable pavements.

Key observations from the study include:

- Infiltration of water into the subgrade is significantly reduced when the subgrade is compacted prior to placing the subbase. In this study, compaction added very little to the structural performance of the pavement and would not have permitted reducing the thickness of the subbase layer.
- There was a significant difference in rutting performance and rutting behavior between the wet and dry tests, as expected.
- A large proportion of the rutting on all three sections occurred as initial embedment in the first 2,000 to 5,000 load repetitions of the test and again after each of the load changes, indicating that much of the rutting in the base and subbase layers was attributed to bedding in, densification, and/or reorientation of the aggregate particles. This behavior is consistent with rutting behavior on other types of structures.
- During testing under dry conditions, limited permanent deformation (< 4 mm) was recorded in the bedding and base layers on all three subsections, and most occurred very early in the test. On the subsection with the 450 mm subbase, rutting occurred in both the subbase (10 mm rut) and subgrade (13 mm rut). On the 650 mm and 950 mm subbase subsections, rutting occurred mostly in the subbase. Total permanent deformation on the 450 mm, 650 mm, and 950 mm subbase subsections was 27 mm, 23 mm and 17 mm respectively, implying a generally linear trend of increasing permanent deformation with decreasing subbase thickness.

- During testing under wet conditions (i.e., water level maintained at the top of the subbase), rutting in the bedding and base layers was dependent on the thickness of the subbase (9 mm, 5 mm and 2 mm on the 450 mm, 650 mm, and 950 mm subbase subsections, respectively). Rutting occurred in both the subbase and the subgrade on all subsections, with rutting in the subbase consistent across all three sections (~ 25 mm). Rutting in the subgrade differed between sections relative to subbase thickness, with 15 mm, 6 mm, and 4 mm of rut recorded on the 450 mm, 650 mm, and 950 mm subbase subsections, respectively at the end of the test. The number of load repetitions and equivalent standard axles required to reach the terminal rut depth (25 mm [1 in.]) set for the project is summarized in Table 10.1. The sensitivity of the pavement structure to water (i.e., standing water in the subbase) and to load is clearly evident.

Table 10.1: Repetitions and ESALs Required to Reach Terminal Rut

Test	Load repetitions at terminal rut (25 mm)			ESALs at terminal rut		
	450 mm	650 mm	950 mm	450 mm	650 mm	950 mm
Dry	340,000	Rut < 25mm	Rut < 25mm	824,009	Rut < 25mm	Rut < 25mm
Wet	95,259	180,000	210,000	165,884	220,000	216,519

- Although only limited testing was undertaken under drained conditions (i.e., wet subgrade but no standing water in the subbase), rutting behavior appeared to show similar trends and behavior to the test under dry conditions.
- The thickness of the subbase influenced rut depth in the subgrade, as expected, but did not influence the rutting behavior in the subbase itself. Rutting in this layer therefore appears to be governed by the aggregate properties, and construction methods and quality.
- The increase in rate of rut depth increased with increasing load, indicating that the pavement structure was load sensitive, especially at load levels close to and above the legal load limit.
- Deflection during dry testing was dependent on subbase thickness and it increased with increasing load. Deflections were relatively high compared to more traditional pavements with dense graded layers. Deflection during wet testing was higher compared to that recorded during dry testing, with deflection on the 450 mm subbase subsection significantly higher compared to that recorded on the 650 mm and 950 mm subbase subsections, indicating a load-sensitive, weaker overall structure as a result of the wet subgrade.
- No distress was noted on any individual pavers and no pavers were dislodged from the pavement during testing.
- The measured infiltration rate of water through the joints between the pavers reduced over the course of HVS testing; however, it was still considered to be both rapid and effective.

Key findings from the mechanistic analysis include:

- The use of the shear stress to shear strength ratios at the top of the subbase and top of the subgrade as inputs for modelling the rut development rate at the top of these layers is considered to be an appropriate design approach for PICP.
- Higher shear stress/strength ratios at the top of the subgrade, which equate to a higher risk of rutting in the subgrade, require thicker subbase layers, as expected.

- An increase in the stiffness of the surface layer reduces the required subbase layer thickness to achieve the same shear stress/strength ratio. However, the effect of the surface layer stiffness on overall pavement performance is not significant due to the relatively small thickness of the pavers (80 mm) and the reduced interlock between them compared to pavers with sand joints.
- For the same shear stress/strength ratio at the top of the subbase, an increase in the stiffness of the subbase layer reduces the required thickness of that subbase layer, especially when the subgrade has a low stiffness.
- For the same shear stress/strength ratio at the top of the subgrade, wet conditions require thicker subbase layers compared to the dry condition, confirming that wet conditions are the most critical condition for design.

New example design tables, based on the number of days with standing water in the subbase (target days including 0, 10, 30, 50, 70, 90, 110, and 130 days and range of days including 0, <10, 10-29, 30-49, 50-69, 70-89, 90-109, and 110-130), have been developed. The tables use a similar format to the one currently used in the ICPI Permeable Interlocking Concrete Pavements guideline. The design thicknesses proposed in the new tables do not differ significantly from those in the current ICPI table. Designs for a specific set of project circumstances can be undertaken by using the same *Excel*® spreadsheet-based design tool used to develop the tables in conjunction with the hydrological design procedures provided in the ICPI guide. The design tool output and corresponding values in the tables should be considered as best estimate designs since they were developed from the results of only two HVS tests. Designers should continue to use sound engineering judgment when designing permeable interlocking concrete pavements and can introduce additional conservatism/reliability by altering one or more of the design inputs, namely the material properties, number of days that the subbase will contain standing water, and/or traffic.

10.2 Recommendations

Given that a large proportion of the permanent deformation measured on the test track occurred in the subbase and that increasing the thickness of the subbase did not reduce this rutting, it is recommended that the specifications of the aggregate properties used in this layer and the methods used to construct it are reviewed to determine whether any reductions in rutting can be achieved by changing them. Further research into stabilization of the subbase aggregate using geogrids, geocells, or cement, and the use of a pervious concrete subbase on top of the subgrade to reduce the thickness of the coarse aggregate subbase, or to replace it, should also be considered.

The pavement tested in this study appeared to be sensitive to very heavy loads and care should therefore be taken when designing projects that will carry large numbers of heavy or overloaded trucks.

Blank page

REFERENCES

1. JONES, D., Li, H. and Harvey, J.T. 2013. **Development and HVS Validation of Design Tables for Permeable Interlocking Concrete Pavement: Literature Review.** Davis and Berkeley, CA: University of California Pavement Research Center. UCPRC-TM-2013-03)
2. JONES, D., Li, H. and Harvey, J.T. 2013. **Development and HVS Validation of Design Tables for Permeable Interlocking Concrete Pavement: Field Testing and Test Section Structural Design.** Davis and Berkeley, CA: University of California Pavement Research Center. (UCPRC-TM-2013-09).
3. METCALF, J.B. 1996. **NCHRP Synthesis of Highway Practice 235: Application of Full-Scale Accelerated Pavement Testing.** Washington, DC: Transportation Research Board.
4. SMITH, D.R. 2011. **Permeable Interlocking Concrete Pavements (4th Edition).** Herndon VA: Interlocking Concrete Pavement Institute.
5. LEA, J. undated. **OpenPave: An N-Layer, N-Load, N-Point Multi-Layer Elastic Half Space Calculation.** www.OpenPave.org. Accessed 2013/09/10.
6. CHOI, J.W., Wu, R., Pestana, J.H. and Harvey, J. 2010. New Layer-Moduli Back-Calculation Method Based on the Constrained Extended Kalman Filter. **Journal of Transportation Engineering, 136(1).** (pp 20–30).
7. TUTUMLUER, E. and Seyhan, U. 1999. Laboratory Determination of Anisotropic Aggregate Resilient Moduli Using an Innovative Test Device. **Transportation Research Record: Journal of the Transportation Research Board, Vol. 1687.** (pp. 13-21).
8. THOMPSON, M., Gomez-Ramirez, F. and Bejarano, M. 2002. Illi-Pave Based Flexible Pavement Design Concepts for Multiple Wheel Heavy Gear Load Aircraft. **Proceedings 9th International Conference on Asphalt Pavements.** Copenhagen, Denmark. International Society of Asphalt Pavements.
9. TUTUMLUER, E., Kim, I. and Santoni, R. 2004. Modulus Anisotropy and Shear Stability of Geofiber-Stabilized Sands. **Transportation Research Record: Journal of the Transportation Research Board, Vol. 1874.** (pp. 125-135).
10. KIM, I. and Tutumluer, E. 2006. Field Validation of Airport Pavement Granular Layer Rutting Predictions. **Transportation Research Record: Journal of the Transportation Research Board, Vol. 1952.** (pp. 48-57).
11. LI, H., Harvey J.T. and Jones, D. 2010. **Summary of a Computer Modeling Study to Understand the Performance Properties of Fully Permeable Pavements.** Davis and Berkeley, CA: University of California Pavement Research Center. (UCPRC-TM-2010-04).

12. CHOW, L.C. and Tutumluer, E. 2014. Framework for Improved Unbound Aggregate Base Rutting Model Development for Mechanistic-Empirical Pavement Design. **Proceedings Transportation Research Board 93rd Annual Meeting.** Washington, D.C: Transportation Research Board.
13. DAS, B.M. 2007. **Advanced Soil Mechanics.** New York, NY: Taylor and Francis.
14. NOVA, R. 2012. **Soil Mechanics.** Hoboken, NJ: John Wiley and Sons.
15. CARTER, M. and Bentley, S.P. 1991. **Correlations of Soil Properties.** London, UK: Pentech Press.
16. WNEK, M., Tutumluer, E., Moaveni, M. and Gehringer, E. 2013. Investigation of Aggregate Properties Influencing Railroad Ballast Performance. **Transportation Research Record: Journal of the Transportation Research Board, Vol. 2374.** (pp. 180-189).
17. HUANG, H., Tutumluer, E. and Dombrow, W. 2009. Laboratory Characterization of Fouled Railroad Ballast Behavior. **Transportation Research Record: Journal of the Transportation Research Board, Vol. 2117.** (pp. 93-101).
18. AHMED, F., Nestingen, R., Nieber, J.L., Gulliver, J.S., and Hozalski, R.M. 2014. A Modified Philip-Dunne Infiltrometer for Measuring the Field-Saturated Hydraulic Conductivity of Surface Soil. **Vadose Zone Journal, 10/2136.** Soil Science Society of America.
19. JONES, D. 2005. **Quality Management System for Site Establishment, Daily Operations, Instrumentation, Data Collection and Data Storage for APT Experiments.** Pretoria, South Africa: CSIR Transportek. (Contract Report CR-2004/67-v2.).
20. ULLIDTZ, P, Harvey, J.T., Basheer, I., Jones, D., Wu, R., Lea, J., and Lu, Q. 2010. *CalME*, a Mechanistic-Empirical Program to Analyze and Design Flexible Pavement Rehabilitation. **Transportation Research Record: Journal of the Transportation Research Board, Vol. 2153.** (pp. 143-152).

APPENDIX A: LITERATURE REVIEW REPORT

Blank page

May 2013
Technical Memorandum: UCPRC-TM-2013-03

Development and HVS Validation of Design Tables for Permeable Interlocking Concrete Pavement: Literature Review

Authors:
D. Jones, H. Li and J.T. Harvey

Concrete Masonry Association of California and Nevada. Grant Agreement UCPRC-PP-2011-01

PREPARED FOR:

Concrete Masonry Association of
California and Nevada

PREPARED BY:

University of California
Pavement Research Center
UC Davis, UC Berkeley

DOCUMENT RETRIEVAL PAGE			**Technical Memorandum: UCPRC-TM-2013-03**
Title: Development and HVS Validation of Design Tables for Permeable Interlocking Concrete Pavement: Literature Review			
Authors: David Jones, Hui Li, and John T. Harvey			
Prepared for: Concrete Masonry Association of California and Nevada	**FHWA Report No:** Not applicable	**Work submitted:** May 2013	**Date:** June 2013
UC Davis Contract No: UCPRC-PP-2011-01	**Status:** Final		**Version No.:** 2

Abstract:

This report details a review of the recent literature on permeable interlocking concrete pavements. Field surveys were not conducted as part of this task, but will be incorporated in Task #2, which covers field testing of existing projects. Only a few organizations worldwide have undertaken detailed research on the topic, with many studies focusing on infiltration on low volume traffic roads, rather than structural design of roads carrying truck traffic. Laboratory studies have focused on resilient modulus of saturated and unsaturated materials. Well graded materials with no fines appeared to perform best under both conditions. Permeable pavements will need to be designed for the worst case condition (i.e., base/reservoir layer is full of water) indicating that a reduction in resilient modulus of about 50 percent of the dry material value can be expected. The use of cemented materials and geogrids in the base to compensate for this lower stiffness is gaining interest. Failure mechanisms appear to be mostly rutting of the surface layer due to shearing in the bedding and/or base layers. Choice of paver and paver laying pattern can limit this to a certain extent, but optimizing the base material grading and thickness, stabilizing base materials, quality of construction, and the use of geofabrics on top of the subgrade to prevent contamination of the base with fines will have the biggest influence. Mechanistic-empirical design has been considered in Australian and United Kingdom design procedures to some extent, with the work done in Australia appearing to be the most comprehensive.

The Australian and United Kingdom design procedures should be used in conjunction with the ICPI and UCPRC design approaches in developing the design tables, choice of design for the test track, and in the analysis of test track performance when validating the final design tables.

Keywords:
Permeable interlocking concrete pavement, permeable pavement, mechanistic-empirical design, accelerated pavement testing.

Proposals for implementation:

Related documents:
None

Signatures:

D. Jones **1st Author**	J. Harvey **Technical Review**	D. Jones **Principal Investigator**	D. Smith **For CMACN**

DISCLAIMER

The contents of this report reflect the views of the authors who are responsible for the facts and accuracy of the data presented herein. The contents do not necessarily reflect the official views or policies of the Concrete Masonry Association of California and Nevada (CMACN), the California Nevada Cement Association (CNCA), or the Interlocking Concrete Pavement Institute (ICPI). This report does not constitute a standard, specification, or regulation.

PROJECT OBJECTIVES/GOALS

The objective of this project is to produce design tables for permeable interlocking concrete pavement (PICP) based on mechanistic analysis and partially validated with accelerated pavement testing (APT). The following tasks will be completed to achieve this objective:

1. Perform a literature and field survey to identify critical responses, failure mechanisms, appropriate performance transfer functions and modeling assumptions for mechanistic analysis of PICP under truck loading.
2. Measure deflections in the field on several PICP locations to characterize effective stiffness of layers for use in modeling.
3. Perform mechanistic analyses of PICP to develop design tables following the approach documented in California Department of Transportation (Caltrans) Research Report CTSW-RR-09-249.04 for development of structural design tables for pervious concrete and porous asphalt.
4. Prepare a plan for validation with accelerated pavement testing based on the results of the mechanistic analysis.
5. Test responses and, if possible, failure of up to three PICP structures in dry and wet condition with the Heavy Vehicle Simulator (HVS), and revise the tables as needed.
6. Analyze the results of the HVS testing to update the structural design tables where necessary.
7. Write a final report documenting the results of all tasks in the study and demonstrating the design tables.
8. Present findings to Caltrans Office of Concrete Pavements and Foundation Program and Office of Stormwater - Design staff in Sacramento, CA.

This report covers Task 1.

TABLE OF CONTENTS

SI* (MODERN METRIC) CONVERSION FACTORS

APPROXIMATE CONVERSIONS TO SI UNITS

Symbol	When You Know	Multiply By	To Find	Symbol
		LENGTH		
In	inches	25.4	Millimeters	mm
Ft	feet	0.305	Meters	m
Yd	yards	0.914	Meters	m
Mi	miles	1.61	Kilometers	Km
		AREA		
in^2	square inches	645.2	Square millimeters	mm^2
ft^2	square feet	0.093	Square meters	m^2
yd^2	square yard	0.836	Square meters	m^2
Ac	acres	0.405	Hectares	ha
mi^2	square miles	2.59	Square kilometers	km^2
		VOLUME		
fl oz	fluid ounces	29.57	Milliliters	mL
Gal	gallons	3.785	Liters	L
ft^3	cubic feet	0.028	cubic meters	m^3
yd^3	cubic yards	0.765	cubic meters	m^3
		NOTE: volumes greater than 1000 L shall be shown in m^3		
		MASS		
Oz	ounces	28.35	Grams	g
Lb	pounds	0.454	Kilograms	kg
T	short tons (2000 lb)	0.907	megagrams (or "metric ton")	Mg (or "t")
		TEMPERATURE (exact degrees)		
°F	Fahrenheit	5 (F-32)/9 or (F-32)/1.8	Celsius	°C
		ILLUMINATION		
Fc	foot-candles	10.76	Lux	lx
Fl	foot-Lamberts	3.426	candela/m^2	cd/m^2
		FORCE and PRESSURE or STRESS		
Lbf	poundforce	4.45	Newtons	N
lbf/in^2	poundforce per square inch	6.89	Kilopascals	kPa

APPROXIMATE CONVERSIONS FROM SI UNITS

Symbol	When You Know	Multiply By	To Find	Symbol
		LENGTH		
mm	millimeters	0.039	Inches	in
m	meters	3.28	Feet	ft
m	meters	1.09	Yards	yd
Km	kilometers	0.621	Miles	mi
		AREA		
mm^2	square millimeters	0.0016	square inches	in^2
m^2	square meters	10.764	square feet	ft^2
m^2	square meters	1.195	square yards	yd^2
Ha	Hectares	2.47	Acres	ac
km^2	square kilometers	0.386	square miles	mi^2
		VOLUME		
mL	Milliliters	0.034	fluid ounces	fl oz
L	liters	0.264	Gallons	gal
m^3	cubic meters	35.314	cubic feet	ft^3
m^3	cubic meters	1.307	cubic yards	yd^3
		MASS		
g	grams	0.035	Ounces	oz
kg	kilograms	2.202	Pounds	lb
Mg (or "t")	megagrams (or "metric ton")	1.103	short tons (2000 lb)	T
		TEMPERATURE (exact degrees)		
°C	Celsius	1.8C+32	Fahrenheit	°F
		ILLUMINATION		
lx	lux	0.0929	foot-candles	fc
cd/m^2	candela/m^2	0.2919	foot-Lamberts	fl
		FORCE and PRESSURE or STRESS		
N	newtons	0.225	Poundforce	lbf
kPa	kilopascals	0.145	poundforce per square inch	lbf/in^2

*SI is the symbol for the International System of Units. Appropriate rounding should be made to comply with Section 4 of ASTM E380 (Revised March 2003)

1. INTRODUCTION

1.1 Project Scope

This project is being coordinated through the Interlocking Concrete Pavement Institute (ICPI) and the Concrete Masonry Association of California and Nevada with additional support from the California Nevada Cement Association. The objective of this project is to produce design tables for permeable interlocking concrete pavement (PICP) based on mechanistic analysis and partially validated with accelerated pavement testing (APT).

1.2 Background to the Study

Although permeable pavements are becoming increasingly common across the United States, they are mostly used in parking lots, basic access streets, recreation areas, and landscaped areas, all of which carry very light, slow moving traffic. Only limited research has been undertaken on the mechanistic design and long-term performance monitoring of permeable pavements carrying higher traffic volumes and heavier loads, and the work that has been done has focused primarily on pavements with open-graded asphalt or portland cement concrete surfacings. Very little research has been undertaken on the use of permeable concrete paver surfaces on these more heavily trafficked pavements.

1.3 Study Objective/Goal

The objective of this project is to produce design tables for permeable interlocking concrete pavement (PICP) based on mechanistic analysis and partially validated with accelerated pavement testing (APT).

The following tasks will be completed to achieve this objective:

1. Perform a literature and field survey to identify critical responses, failure mechanisms, appropriate performance transfer functions and modeling assumptions for mechanistic analysis of PICP under truck loading.
2. Measure deflections in the field on several PICP locations to characterize effective stiffness of layers for use in modeling.
3. Perform mechanistic analyses of PICP to develop design tables following the approach documented in California Department of Transportation (Caltrans) Research Report CTSW-RR-09-249.04 for development of structural design tables for pervious concrete and porous asphalt pavements.
4. Prepare a plan for validation with APT based on the results of the mechanistic analysis.
5. Test responses and, if possible, failure of up to three PICP structures in dry and wet condition with the Heavy Vehicle Simulator (HVS), and revise the tables as needed.
6. Analyze the results of the HVS testing to update the structural design tables where necessary.

7. Write a final report documenting the results of all tasks in the study and demonstrating the design tables.
8. Present findings to Caltrans Office of Concrete Pavements and Foundation Program and Office of Stormwater - Design staff in Sacramento, CA.

This report covers the literature review work completed in Task #1. Field surveys will be conducted as part of Task #2.

1.4 Approach to the Literature Review

The ICPI regularly tracks the literature on the use of interlocking concrete pavers in pavement applications. A list of publications and copies of available documents was provided to the UCPRC. In addition to this, the UCPRC conducted a separate search using the University of California (UC) library system to search journal articles, the Transportation Research Board (TRB) publications index to search for papers in the Transportation Research Record and Annual Meeting Compendiums, and *Google Scholar* and other internet searchers to identify papers, reports, and articles not located in the ICPI, UC and TRB searches. Research conducted in the United States as well as internationally was reviewed. Reference lists in sourced publications were also checked to identify any other potentially relevant publications that were missed in the earlier searches. Searches of state and county departments of transportation and university research center sites were not attempted.

1.5 Report Layout

The ICPI routinely updates their state-of-the-practice documentation with the latest research and it was not the intent of this study to duplicate this effort. Instead, the available literature was reviewed in the context of its relevance and contribution to the objectives of this UCPRC study. Consequently, this report is limited to a brief description of the research conducted relevant to each objective and how the findings of that research could be used to refine the UCPRC study, specifically in terms of developing the design tables, designing the test track, the type of data collected, data analysis, and validation of the design tables.

2. BACKGROUND

2.1 Permeable Pavement Design

Permeable pavements are defined for the purposes of this study as those in which all layers are intended to be permeable and water infiltrates into the underlying soil. The three major permeable pavement types are porous asphalt, pervious concrete and permeable interlocking concrete pavement. Since the late 1970s, a variety of permeable pavement projects have been constructed for low traffic areas carrying light vehicles and occasional truck traffic. There have been both failures and successes. Sources of failures have been described anecdotally. Variables contributing to successes have not been completely identified beyond seemingly conservative hydrologic and structural designs. Unlike conventional pavements, permeable pavements do not yet have decades of research and experience, Therefore, permeable pavements and the benefits they potentially provide have been limited largely because of a lack of performance data and the ability to consider different materials, climates, subgrades and structural cross-sections. Because of durability concerns, most applications of permeable pavements in North America have been for parking lots and very low-volume streets that are not subjected to high-speed traffic or to repeated truck traffic. This data gap is in part being addressed by the American Society of Civil Engineers (ASCE) Technical Committee on Permeable Pavements. This committee plans a 2013 release of a manual on permeable pavement design, construction and maintenance. Performance information is largely experienced-based and structural design methods for pervious concrete, porous asphalt and ICPI relies on industry recommendations. This publication identifies structural design research as a pressing need.

The National Asphalt Pavement Association (NAPA), the American Concrete Pavement Association (ACPA), and the Interlocking Concrete Pavement Institute (ICPI) have each produced a design manual for permeable pavements for their surface type and for this type of low-volume traffic application. The ICPI manual and the ACPA manual both include some consideration of structural design for trucks using modifications of the AASHTO 1993 empirical design approach. These manuals, and the pavement designs used to date, have been empirical in nature with little or no long-term monitoring data to support the empiricism. These designs have, to date, generally been used in low-risk pavements, such as parking lots, alleys, and low-speed, low-traffic roads. This approach and these designs may not work well for pavements intended to carry any heavy truck traffic.

The Caltrans Office of Storm Water Management has drafted a design guide and construction specifications for PICP, pervious concrete, and porous asphalt. These resources are intended for design of non-highway facilities such as parking lots and low-speed, low-traffic roads. The guide includes information on hydrologic design, which follows that for other infiltration practices used by Caltrans.

Structural design limits applications to a Caltrans Traffic Index less than nine or one million 80 kN (18,000 lb.) equivalent single axle loads. This recommendation was developed from permeable pavement industry literature and experience, which is largely empirical in nature with little full-scale load testing to validate this limit or potentially raise it.

2.2 California Department of Transportation/UCPRC Study

The UCPRC completed a project in early 2010 for the California Department of Transportation (Caltrans) Division of Environmental Analysis to develop structural design tables for the design of porous asphalt, pervious concrete, and permeable concrete slabs to carry heavy trucks. Permeable interlocking concrete pavements (i.e., permeable joints between the paving units) were excluded from the scope of this project by Caltrans. The project report presents a summary of the results of laboratory testing, computer performance modeling, and life-cycle cost analysis (LCCA) on permeable pavements. The LCCA compared permeable pavements with alternative stormwater management best management practices currently used by Caltrans, given that permeable pavements are being considered as a potential best management practice for managing stormwater on California highways. The deliverables from this research were a preliminary design procedure and an example set of catalog-type design tables that can be used to design permeable pavement pilot and experimental test sections in California.

Because of concerns with high-speed traffic on different types of permeable pavement, the report considered two applications: low- to medium-speed facilities such as streets, parking lots, rest areas, etc; and, retrofit of the shoulders of high-speed roads. For the shoulder retrofit application, the report includes considerations for drainage and protection of the adjacent existing impermeable pavement. Maintenance recommendations are also included in the report, based on discussions with Caltrans district maintenance engineers.

2.3 Mechanistic Pavement Design

The approach used for development of the permeable pavement designs in the California study is referred to as “mechanistic-empirical” or “ME.” The Federal Highway Administration and state departments of transportation, including Caltrans, are in the process of implementing this approach as a replacement for older empirical design methods. The structural properties of interest include stiffness, strength, durability, fatigue, and rutting (where applicable) performance, which differ from the assumptions of empirical based designs that use “structural coefficients” of generic material types without considering actual mechanical properties.

The UCPRC is assisting Caltrans with transition to the ME pavement design approach. The goal is to transition to an ME design and analysis system with a software package, databases, guidelines, and test methods that result in pavements with more cost-effective and environmentally sustainable life-cycles.

2.4 Environmental Considerations for Permeable Pavements

The UCPRC is completing an initial project, and beginning a continuation project, for Caltrans developing an environmental life-cycle assessment (LCA) framework and models for pavements. LCA analyzes the total energy and resource requirements, and environmental impacts of human-designed systems using an approach that measures the inputs to (e.g., energy, resources, etc.) and outputs from (e.g., environmental impacts such as air emissions, water releases, etc.) a system over its life cycle. The goal is to capture the environmental impacts from a cradle-to-grave perspective by determining the impact from each life-cycle phase.

LCA phases for pavements include raw material extraction and production of paving materials, as well as construction, use, maintenance, and end-of-life processes. Both policymakers and industry have shown a great deal of interest in applying LCA as a decision-making criterion during planning and design for new pavement construction, maintenance, and rehabilitation activities. In addition to the work for Caltrans, the UCPRC will be incorporating the LCA approach into pavement sustainability guidelines for the Federal Highway Administration (FHWA) as part of a recently signed agreement, and is using the results of the Caltrans funded work in a pooled-effort project for a group consisting of Caltrans and eight European national highway laboratories looking at the net effects of pavement roughness.

For the LCA work, the UCPRC is studying the effects of permeable pavements on local urban heat island temperatures (near the pavement structure, not the entire urban area). As part of this study, nine 4 m by 4 m (13.1 ft x 13.1 ft.) sections were built in 2011 at the UCPRC test site at UC Davis. These consist of three interlocking concrete paver sections, three concrete sections and three asphalt sections. Each set of three sections includes one impermeable and two permeable pavements, which are being tested both dry and with water to assess the insulation effects of porous materials on near surface temperatures, cooling effects of evaporation, and the effects of surface absorptivity (albedo) *(1)*.

Although not included in the proposal for this study, LCA is a likely framework for future decision-making regarding pavement type selection policies for agencies interested in including energy use, green-house gas emissions, and other environmental considerations into their practice.

Blank page

3. LITERATURE REVIEW

3.1 Introduction

There is limited literature discussing research into the structural design of permeable interlocking concrete pavements. Most research on these types of pavements appears to focus on hydrological performance over time, with investigations typically on parking lots and low traffic volume access streets. This research is not discussed below as it does not form part of the objectives of the study. There is also considerable documented research on the use of interlocking concrete pavers in heavily trafficked impermeable pavements, mostly with reference to ports and other industrial loading areas. This research is not discussed below. Research into the structural properties of the concrete pavers alone is also not discussed as this does not form part of the objectives of the study, which are to focus on the pavement structure. A number of newer references discussing pervious concrete and porous asphalt surfacings were reviewed and are discussed if components of this research were considered relevant (e.g., base course materials, deflection measurements, climatic influences, etc.).

A brief summary of each document reviewed is provided in the following sections. Research in the United States is covered first, followed by Australia, the United Kingdom, and other countries. A brief discussion of the relevance to the ICPI/UCPRC study is also provided. The literature that was reviewed, but has no relevance to permeable interlocking concrete pavement structures, is not discussed.

Comprehensive literature reviews were undertaken as part of the UCPRC study conducted in 2009 and 2010 and documented in the Caltrans reports summarized in Section 3.3, and relevant findings were factored into the outcomes of that research. This literature is not documented again in this report.

3.2 Interlocking Concrete Pavement Institute (ICPI) *(2)*

The ICPI document is a comprehensive and detailed guide to the design, construction (including example specifications), and maintenance of permeable interlocking concrete pavements. It is based on industry experience in North America and internationally. The ICPI manual uses the AASHTO 1993 empirical design method for designs up to one million ESALs (Caltrans Traffic Index of 9). This empirical design method is conservative with little or no long-term monitoring data to support it. While conservative in developing base/subbase thickness recommendations, the design approach is useful in providing recommendations to designers and agencies. The ICPI also uses the AASHTO design procedure in the *Permeable Design Pro* software as well as an FHWA drainage model called *Drainage Requirements in Pavements*.

3.2.1 Relevance to this Study

This guide will be the starting point for the development of the design tables based on mechanistic-empirical design approaches. Results from the current research study will be used to validate and/or update the design procedures and tables in this guide, with specific reference to truck traffic.

3.3 University of California Pavement Research Center (UCPRC)

3.3.1 Summary Report *(3)*

This report summarizes the results of laboratory testing, computer performance modeling, and life-cycle cost analysis of permeable pavements with porous asphalt, pervious concrete and permeable cast concrete slab surfacing alternatives. The deliverables included a preliminary, mechanistic-based design procedure and an example set of catalog-type design tables that can be used to design pilot and experimental permeable pavement test sections. The catalog considers both structural and hydrologic design to produce pavements that handle storm water from storms with different return periods and truck traffic. The designs also consider the use of pervious concrete as a subbase layer to reduce stresses at the top of the subgrade and to provide confinement to the granular reservoir layer, increasing its stiffness and rutting resistance. Although PICP was not investigated, the underlying layers would be similar. The results obtained from the analyses indicated that permeable pavements could be a cost-effective stormwater best management practice alternative as a shoulder retrofit on highways, and for maintenance yards, parking lots, and other areas with slow moving truck traffic in California climates. However, the study noted that the results needed to be validated in controlled experimental test sections and pilot studies before wider-scale implementation is considered.

Recommendations included accelerated pavement tests and monitored pilot studies on in-service roadways designed using the procedure developed. The findings from these full-scale experiments would be used to identify situations where permeable pavements are an appropriate best management practice, validate and refine the design method, undertake detailed life-cycle cost and environmental life-cycle assessments, and to prepare guideline documentation for the design and construction of permeable pavements. To date, these recommendations have not been implemented by Caltrans.

3.3.2 Laboratory Testing Report *(4)*

This report summarizes the laboratory testing to assess the mechanical properties of permeable pavement materials. Testing focused on subgrade and base course materials, and pervious concrete and porous asphalt concrete wearing courses. Key findings include:

- The results of tests on two different subgrade soils common in the Central Valley of California (clay and silt) indicate that both soil types will offer very little support to a pavement structure, and that

the stiffness and the associated strength of the materials will decrease significantly as the moisture content increases. The tests assumed minimal compaction of the subgrade to maintain the highest possible permeability. Any permeable pavement structure on these materials will need to compensate for this poor bearing capacity with thicker base and surfacing layers.

- The results of tests on four different commercially available permeable base-course aggregates indicate that these materials will probably provide sufficient support for typical traffic loads in parking lots, basic access streets and driveways, and on highway shoulders, while serving as a reservoir layer for the pavement structure. Although three of the four materials tested had smaller maximum aggregate sizes than those typically discussed in the literature, the permeability was still adequate for California rainfall events.

3.3.3 Computer Modeling Report *(5)*

This report summarizes the computer modeling of the expected pavement performance of permeable pavements using laboratory test results described in the above report, and development of pavement designs for critical distresses. Full-factorial experimental designs were followed, taking pavement type, material type, pavement geometry (thicknesses, and slab dimensions for concrete pavement only), climate, truck axle type, traffic load, and traffic speed (HMA only) into consideration. This resulted in almost 20,000 analysis cases using layer elastic theory for HMA and finite element analysis for concrete. The results indicated that sufficient structural strength can be obtained with appropriate and reasonable pavement designs for pervious concrete and porous hot mix asphalt pavements.

3.3.4 Life-Cycle Cost Analysis and Environmental Life-Cycle Assessment *(6)*

This report presents a summary of the methods and results from a life-cycle cost analysis (LCCA), undertaken to understand the cost implications of constructing and maintaining permeable pavements. Input data for the models were obtained from the comprehensive laboratory investigation of porous asphalt and pervious concrete with computer performance modeling described above, from Caltrans databases, and from interviews with contractors. A framework for environmental life-cycle assessment (LCA) for permeable pavements was also developed. However, a detailed LCA study could not be performed because of insufficient available data on the construction, long-term performance, maintenance, and ability to rehabilitate permeable pavements and currently used alternative best management practices (BMPs) for stormwater management. The results indicate that permeable pavements are potentially more cost-effective than currently available BMP technologies in terms of the cost per cubic meter of water treated. Factors influencing this finding included construction costs as well as annual maintenance costs.

3.3.5 Hydraulic Performance *(7)*

Hydraulic performance was assessed by determining the minimum required thickness of the aggregate base course to capture and retain stormwater during rainfall events. Performance was evaluated by simulation under varying hydrological, material, and geometric conditions using the *HYDRUS* software, which uses unsaturated flow theory and a finite element analysis process. The simulations were

performed using data from three representative rainfall regions in California (Eureka, Sacramento and Riverside) and 24-hour rainfall intensity based on actual or mechanically generated rainfall. Critical aggregate reservoir layer thickness was determined for two-, fifty- and one-hundred year storm recurrence duration.

Results obtained from the hydraulic simulations, which were used as inputs in developing the design procedure discussed above, are summarized as follows *(7)*:

- The critical aggregate reservoir layer thickness to capture all the runoff generated by typical rainfall events in California ranges from less than 1.0 m (3.0 ft.) to about 3.0 m (10 ft.), dependent in part on the number of impermeable lanes that need to be drained into the permeable pavement.
- The minimum aggregate thickness in Eureka was about 50 percent higher than the minimum aggregate thickness required for the Sacramento and Riverside areas. Longer recurrence periods (50 and 100 years) required thicker aggregate bases (i.e., reservoir layers) compared with the two-year period. Simulations using natural rainfall required slightly thicker base layers compared to those where mechanically generated rainfall simulations were used. The use of actual data is therefore recommended to obtain a more conservative layer thickness estimation.
- Saturated soil hydraulic conductivity is the most sensitive factor when determining critical aggregate layer thickness. A soil permeability of less than 10^{-5} cm/sec (0.014 in./hr) was found to be impractical for the design of permeable pavements.
- In general, the required thickness of the aggregate base doubles with additional lanes (i.e., increasing a two-lane road to a four-lane road requires a doubling of the base layer thickness). The increase in aggregate thickness for Eureka was higher compared to Sacramento and Riverside.
- If the subgrade soil is still wet from earlier rainfall events and additional rainfall occurs, then the aggregate layer thickness needs to be increased by an additional 80 percent (compared to the dry condition). Alternatively, allowance needs to be made for two or three surface overflows on an annual basis.
- The critical layer thicknesses determined during 24-hour rainfall simulations were verified through annual storm event simulations. The results show that the critical aggregate thicknesses determined in the study are sufficient. A reduction in layer thickness would result in periodic overflows. These overflows will increase significantly when the subgrade soil hydraulic conductivity is less than 10^{-4} cm/sec (0.14 in./hr).
- The simulation results showed that a significant reduction in the air-voids in the pavement surface layer (i.e., severe clogging) and consequent significant reduction in the surface pavement hydraulic conductivity would be needed before the pavement would be classified as impermeable (i.e., water flows over the permeable surfacing and off the edge of the road instead of through the road). Surface permeability of the porous asphalt and pervious concrete is therefore not the critical factor for design for the surface types considered in the study.

3.3.6 Relevance to this Study

The design tables will be used as a basis together with other design approaches for developing new design tables for permeable interlocking concrete pavements. The findings from the laboratory testing on base and subgrade materials and hydraulic performance are relevant to this study and the work does not need to be repeated. The frameworks for LCCA and LCA are also relevant to this study; however, the LCCA will need to be re-run with PICP surfacing to obtain appropriate and comparative cost-benefits.

3.4 Minnesota Department of Transport Study (MnROAD) *(8,9,10)*

This study was started in 2008 and completed in 2012. Although permeable interlocking concrete pavers were not investigated, open-graded aggregate bases with porous asphalt and pervious concrete surfacings were subjected to heavy truck traffic, which is considered relevant to this study. The base for the section consisted of 100 mm (4 in.) of railway ballast over 250 mm (12 in.) of Minnesota DOT specification open-graded aggregate (CA-15) similar in gradation to ASTM No. 57. In most permeable pavement structures, the particle size of aggregate layers generally increases with the depth of each layer. The Minnesota DOT investigation placed a layer of larger-sized aggregates (railway ballast) over the smaller due to instability of the CA-15 under construction equipment. Two subgrades were assessed, one sandy and one clay. Final reports on the pervious concrete and porous asphalt test sections were completed in 2011 and 2012, respectively.

Interim results on the pervious concrete test sections in 2011 after 12,000 truck passes (27,000 80 kN [18,000 lb.] ESALs) indicated that the permeable base was still performing well. Falling weight deflectometer results for the base and subgrade indicated lower stiffness values compared to conventional pavements, as expected.

The porous asphalt test sections performed well over the monitoring period, despite what was considered to be significant loading for this type of pavement. The only significant pavement distresses observed were some rutting in the loaded lane, and shallow surface raveling. Other pavement distress including ride quality, permeability, stiffness modulus, strain response, skid resistance, and noise were considered to be minimal.

The monitoring of climatic effects on both pavements indicated that the permeable pavement froze later and thawed earlier compared to the conventional pavement. Maintenance techniques and their effect on permeability were also assessed, during which it was noted that regular vacuuming was necessary to prevent clogging. Once clogged, vacuuming was not effective.

3.4.1 Relevance to this Study

Although interlocking pavers were not assessed, the base and subgrade stiffness data collected after loaded truck trafficking, as well as climatic and hydraulic performance and maintenance techniques, will be taken into consideration in the test track design and performance analysis.

3.5 University of Illinois *(11)*

In this study, an advanced triaxial testing machine was used for determining the vertical and horizontal resilient moduli of thirteen "good" and "poor" performing base/subbase materials received from eight different states. The materials included open-graded aggregates. The fines content dictated performance, with materials with high percentages (i.e. >12 percent) passing the 0.075 mm (ASTM No.200) sieve having lower resilient moduli. In general, much lower anisotropic modular ratios were obtained for the "good quality" materials than those of the "poor quality" materials at low, intermediate, and high stress states. As the stress states applied on the specimen increased from low to high, the modular ratios consistently increased for the "good quality" materials and consistently decreased for the "poor quality" materials. This implies that a good performing base/subbase material hardens and gets stronger under applied stresses increasing its horizontal stiffness relative to the vertical and thus reducing its tendency to spread laterally under wheel loads. The open-graded materials with no or little fines were considered as "good" materials.

3.5.1 Relevance to this Study

The findings are relevant to this study and will be taken into consideration for understanding the behavior of the open-graded base when developing the design tables.

3.6 Applied Research Associates *(12)*

This report summarized a laboratory study, undertaken on behalf of ICPI, to investigate the resilient modulus of open-graded drainage layer aggregates. Nine different gradations were assessed. Tests were restricted to a maximum aggregate size of 37 mm (1.5 in.). Test results were generally consistent with other similar research and indicated that well-graded coarse aggregates, such as the ASTM No. 57 stone recommended by ICPI for use as a base in permeable interlocking concrete pavement structures, had relatively high resilient moduli, similar to those of dense-graded aggregate base materials. Tutumluer (personal communication with ICPI) agreed with most of the results from this study, but warned of a decrease in resilient modulus with increasing fines content (i.e., above 12 percent). He disagreed with the finding that resilient modulus values do not change with increasing deviator stresses and noted his experience that good quality aggregate materials show an increase in modulus with increasing deviator stresses under appropriate confining stress, which is inherent for the stress-hardening nature of granular materials if they are of good quality.

3.6.1 Relevance to this Study

The findings are relevant to this study and will be taken into consideration for understanding the behavior of the open-graded drainage layer aggregate base when developing the design tables.

3.7 Texas A and M University *(13)*

This guideline covers the design of permeable interlocking concrete pavements using the *UNI Eco-Stone*® system. The procedure considers water drainage and structural capacity (i.e., rutting performance), but focuses on parking lot applications with slow moving truck traffic. Stabilized bases are recommended for heavy truck traffic. It is organized to give the reader a brief review of basic hydrological concepts relevant to the design of pavements with specific reference to the *Eco-Stone*® system. Information is provided on how runoff infiltration can be controlled in the pavement subsurface and its interaction with the performance of the pavement system. A method is provided to determine the amount of infiltration and the storage capacity of a permeable base relative to the time of retention and degree of saturation associated with the characteristics of the base. A step-by-step guide covers the process for selecting the best pavement alternative in terms of base materials and gradations for the given drainage, subgrade strength conditions, and the criteria for maximum allowable rutting. The design method is empirical.

3.7.1 Relevance to this Study

This guide is relevant to the study and the design process will be compared against the ICPI and UCPRC processes described above. Given that the document covers one manufacturer's pavers, applicability to other types of pavers will need to be checked.

3.8 University of Alaska Fairbanks *(14)*

This study was limited to a laboratory investigation comparing behavior of open- and dense-graded materials under saturated, undrained, repeated triaxial loading conditions. The effect of aggregate gradation on the cyclic stress-strain behavior, pore pressure, damping, resilient modulus, compressibility, and permeability was studied. Results indicate that saturated granular materials will develop excess pore water pressure under undrained repeated triaxial loading, which can lead to a decrease in resilient modulus and a potential increase in volume compressibility. Open-graded aggregates were more resistant to pore water pressure buildup than dense-graded aggregates and are therefore less likely to induce damage in pavements under saturated conditions. In this respect, the estimated damage per repetition was estimated to be as much as 70 to 100 times more for pavements with dense-graded bases compared to permeable pavements with open-graded bases.

3.8.1 Relevance to this Study

The findings from this study are in line with those used in the UCPRC design process. The theoretical findings of less pore pressure buildup and relatively less damage in open-graded aggregates can be examined during APT testing if project funding and time permits.

3.9 University of New South Wales, Australia *(15-20)*

The University of New South Wales (Shackel) has conducted extensive laboratory and field research into interlocking concrete block pavements, both permeable and impermeable, and has published widely on the topic. Individual references are not discussed in this literature review. A number of design procedures and design software packages (*PERMPAVE* for hydraulic performance and *LOCKPAVE* for structural performance [not evaluated in this review]) have been developed and a range of projects, built using these procedures, have been monitored for periods of 10 years and longer. Considerable work was completed on base course properties and similar findings to those documented in the UCPRC study were noted with respect to the good performance of graded materials as opposed to single sized materials. Resilient moduli of saturated permeable bases were found to be typically 50 percent of those of the equivalent unsaturated bases and structural designs have to be selected accordingly. The successful use of cemented materials in the base course was also investigated to compensate for the lower moduli of the saturated unbound materials. In recent years their work has focused more on stormwater management issues rather than structural design.

3.9.1 Relevance to this Study

The work undertaken by Shackel et al. is very relevant to this study and their design procedures will be considered in the development of the design tables. Cemented base materials should be considered in a comparative study to unbound materials if project funding and time permit.

3.10 University of South Australia *(21)*

This study investigated three commercially available permeable pavers in low traffic applications and included both laboratory testing and field evaluation focusing on change in permeability and modulus, determined with a falling weight deflectometer, over time. Findings were consistent with other research referenced in this report and in the general literature on PICP.

3.10.1 Relevance to this Study

No new information relevant to the study is contained in this report. Insufficient information on deflection testing was provided to understand any implications for structural design.

3.11 Interpave (Precast Concrete Paving and Kerb Association), United Kingdom *(22)*

This comprehensive guide, developed by Knapton, covers all forms of heavy duty pavement for ports and other industries, of which permeable interlocking concrete pavers is one option. Pavement design is based on a finite element modeling approach. This guide uses a cement-stabilized, open-graded base and open-graded bedding course under the concrete pavers to offer additional structural support from heavy wheel loads. A series of design tables is used to select an appropriate pavement structure for a given set of conditions. The design method for PICP using a cement-stabilized, open-graded base has not been validated with full-scale load testing. As noted in Section 3.9.1, this design approach holds promise for addressing axle loads higher than the one million ESALs typically cited in ICPI literature. This may provide additional momentum for combining PICP surfacing with a pervious concrete base.

3.11.1 Relevance to this Study

This guide is relevant to the study and the design process will be compared against the ICPI and UCPRC processes described above.

3.12 John Knapton Consulting Engineers *(23,24)*

Two papers were reviewed from this author. The first describes a full scale trial comparing permanent deformation on four short (6.0 m [20 ft.]) test sections constructed with different permeable bases commonly used in the United Kingdom and trafficked by heavy trucks over a two-month period. Base types included unreinforced 20 mm/6 mm (0.75 by 0.25 in.) coarse-graded aggregate, 20 mm/6 mm coarse-graded aggregate stabilized with three percent cement, dense bitumen macadam (five percent binder content), and coarse-graded aggregate reinforced with two layers of geogrid. The sections were sealed with polythene to maintain a constant water content in the base and limit the influence of the subgrade. The stabilized layers out-performed the unstabilized layers in terms of surface rut depth measured at the end of the test.

The second paper provides design guidance for permeable pavements based upon the authors' experience over a ten-year period. The use of geogrids to enhance the structural performance of the pavement is encouraged on all projects. An appendix contains new design solutions in the form of a catalogue of designs based on subgrade strain calculations and the properties of the base material and pavers. The design method combines two design methodologies. For lightly trafficked pavements, the loads applied by wheels are the critical factor and the guidance for those pavements is based upon wheel loads and is termed the "ultimate load design". More heavily trafficked highway pavements are designed on the basis of the cumulative number of standard 8,000 kg (18,000 lb) axles, in line with the UK Highway Agency

design. The approach is called the "serviceability design". Pavements trafficked by vehicles applying greater loads than those commonly encountered on highways are not covered. Instead, the British Ports Association heavy duty pavement design manual *(22)* would be adopted.

3.12.1 Relevance to this Study

The guide discussed in the second paper is relevant to the study and will be compared against the ICPI and UCPRC processes described above. The findings of the first paper have limited relevance given that subgrade conditions were isolated from the experiment.

3.13 University of Canterbury *(25)*

Although this study did not investigate permeable interlocking concrete pavers, it did use accelerated pavement testing and Benkelman Beam measurements to assess the performance of conventional interlocking concrete pavement, both of which are relevant to the current study. One of the key findings from the Canterbury study was that compaction of the bedding layer influenced the rutting performance of pavers. Likewise, the density of the bedding layer in PICP typically relies on compaction of the paving units placed on it. The extent of compaction and resulting density within the bedding layer (as well as choking into the underlying base layer) is not known, but could influence rutting in the surface.

3.13.1 Relevance to this Study

Details on behavior of the interlocking pavers under accelerated pavement testing and use of a Benkelman Beam for deflection measurements are relevant to the accelerated testing part of this study. Special attention will need to be paid to the change in deflection over time under repeated wheel loads. An unpublished ICPI FWD study found that PICP stiffened when repeatedly loaded in the same location. Therefore, a high Benkelman Beam deflection measurement from a single load test may not be indicative of smaller deflections as a result of repeated loads. This will be carefully monitored in the accelerated load testing phase.

4. CONCLUSIONS AND RECOMMENDATIONS

4.1 Review of Report Objective

Perform a literature and field survey to identify critical responses, failure mechanisms, appropriate performance transfer functions and modeling assumptions for mechanistic analysis of PICP under truck loading.

The preceding chapters detail a review of the recent literature on permeable interlocking concrete pavements. Field surveys were not conducted as part of this task, but will be incorporated in Task #2, which covers field testing of existing projects.

Only a few organizations worldwide have undertaken detailed research on the topic under review, with many studies focusing on infiltration on low volume traffic roads, rather than structural design of roads carrying truck traffic.

Laboratory studies have focused on resilient modulus of saturated and unsaturated materials. Well-graded materials with no fines (typical of that used under PICP) appeared to perform best under both conditions. Permeable pavements will need to be designed for the worst case condition (i.e., a saturated soil subgrade and possibly a base/reservoir layer immersed in water). These conditions may (conservatively) require a reduction in resilient modulus as much as 50 percent of the dry material value. The use of cemented materials and geogrids in the base to compensate for this lower subgrade and aggregate base stiffness is gaining interest.

Failure mechanisms appear to be mostly rutting of the surface layer due to shearing in the bedding and/or base layers. Choice of paver and paver laying pattern can limit this to a certain extent. However, optimizing the base material grading and thickness, material hardness, stabilization of the base materials with cement, asphalt, or a geogrid, quality of construction, and the use of geosynthetics to prevent contamination of the base are all design considerations with substantial influence on control of rutting and failure.

Mechanistic-empirical design has been considered in Australian and United Kingdom design procedures to some extent, with the work done in Australia appearing to be the most comprehensive. For unstabilized aggregates, these procedures typically characterize repetitive compressive strain at the top of the soil subgrade as the failure mechanism. Tension is generally not considered since these materials are not in tension. However, the measurement and understanding of stress distribution within and at the bottom of

an open-graded base is not well documented or understood (compared to dense-graded materials), and this topic will likely require further research, modeling, and full-scale verification beyond the scope of this project. The challenge ahead is measuring stiffness and stress distributions within the open-graded bedding/base/subbase from repeated loads. Such research would better enable development of models/ tools that can predict permeable pavement performance, including surface distresses, maintenance/ rehabilitation remedies, and ultimate structural life. For this project, the field testing and full-scale PICP accelerated load testing will provide some basis for validation/calibration of UCPRC design approaches, especially for worst case conditions. Australian and United Kingdom studies and design approaches can help inform the validation process as well as contribute to the development of PICP design tables.

4.2 Recommendations

The Australian and United Kingdom design procedures should be used in conjunction with the ICPI and UCPRC design approaches in developing the design tables, choice of design for the test track, and in the analysis of test track performance when validating the final design tables.

REFERENCES

1. LI, H., Harvey, J. and Kendall, A. 2012. Field Measurement of Albedo for Different Land Cover Materials and Effects on Thermal Performance. **Journal of Building and Environment, 59(0)**. pp 536-46.
2. SMITH, D.R. 2011. **Permeable Interlocking Concrete Pavements.** Herndon. VA: Interlocking Concrete Pavement Institute.
3. JONES, D. Harvey, J., Li, H., Wang, T., Wu, R. and Campbell, B. 2010. **Laboratory Testing and Modeling for Structural Performance of Fully Permeable Pavements under Heavy Traffic: Final Report.** Davis and Berkeley, CA: University of California Pavement Research Center. (CTSW-RR-09-249.04 / RR-2010-05).
4. JONES, D., Harvey, J., Li, H. and Campbell, B. 2009. **Summary of Laboratory Tests to Assess Mechanical Properties of Permeable Pavement Materials.** Davis and Berkeley, CA: University of California Pavement Research Center. (CTSW-TM-09-249.01 / UCPRC-TM-2009-05).
5. LI, H., Harvey J. and Jones, D. 2010. **Summary of a Computer Modeling Study to Understand the Performance Properties of Fully Permeable Pavements.** Davis and Berkeley, CA: University of California Pavement Research Center. (CTSW-TM-09-249.02 / UCPRC-TM-2010-04).
6. WANG, T., Jones, D. and Harvey, J. 2010. **A Framework for Life-Cycle Cost Analyses and Environmental Life-Cycle Assessments for Fully Permeable Pavements.** Davis and Berkeley, CA: University of California Pavement Research Center. (CTSW-TM-09-249.03 / UCPRC-TM-2010-05).
7. KAYHANIAN, M., Chai, L. and Givens, B. 2010. **Hydraulic Performance Evaluation of Permeable Pavement under Heavy Load and Heavy Traffic.** Davis, CA: University of California, Davis. (CTSW-RT-10-247.03D).
8. IZEVBEKHAI, B. 2011. **Pervious Concrete Test Cells on MnROAD Low-Volume Road.** Minneapolis, MN: Minnesota Department of Transportation. (Report No. MN/RC 2011-23).
9. VANCURA, M., Khazanovich, L. and MacDonald, K. 2010. **Performance Evaluation of In-Service Pervious Concrete Pavements in Cold Weather.** Minneapolis, MN: University of Minnesota.
10. LEBENS, M.A. and Troyer, B. 2012. **Porous Asphalt Pavement Performance in Cold Regions.** Minneapolis, MN: Minnesota Department of Transportation. (Report No. MN/RC 2012-12).
11. TUTUMLUER, E. and Seyhan, U. 2000. Directional Dependency of Aggregate Stiffnesses: An Indicator of Granular Base Performance. **Proceedings 8th Annual Symposium of the International Center for Aggregates Research.** Denver, CO.

12. APPLIED RESEARCH ASSOCIATES. 2005. **Resilient Modulus Testing of Open Graded Drainage Layer Aggregates.** Toronto, Canada.
13. CAO, S.L., Poduska, D. and Zollinger, D.G. 1998. **Drainage Design and Performance Guidelines for *Uni Eco-Stone*® Permeable Pavement.** Palm Beach Gardens, FL: Uni-Group USA.
14. RAAD, L., Minassian, G.H. and Gartin, S. 1992. Characterization of Saturated Granular Bases under Repeated Loads. **Transportation Research Record #1369.** Washington, DC: Transportation Research Board.
15. SHACKEL, B. 2010. The Design, Construction and Evaluation of Permeable Pavements in Australia. **Proceedings 24th Australian Road Research Board Conference.** Melbourne, Australia.
16. SHACKEL, B. and Pezzaniti, D. 2010. Development of Design Procedures and Software for Permeable Interlocking Concrete Pavements. **Proceedings 5th Australian Road Engineering and Maintenance Conference.** Melbourne, Australia.
17. SHACKEL, B. and Pezzaniti, D. 2009. Development of Design Software for Permeable Interlocking Concrete Pavements. **Proceedings 9th International Conference on Concrete Block Paving.** Buenos Aires, Argentina.
18. SHACKEL, B. 2006. Design of Permeable Pavements Subject to Traffic. **Proceedings 8th International Conference on Concrete Block Paving.** San Francisco, CA.
19. SHACKEL, B., Jitakeerul, P. and Prasetyo, S.B. 2001. An Experimental Study of Unbound Base Material for Use in Permeable Pavements. **Proceedings 16th Australian Road Research Board Conference.** Melbourne, Australia.
20. OESER, M., Shackel, B., Kabitzke, U. and Da Luz, G. 2009. A Pilot Study of Cement-Treated Basecourses for Use in Permeable Interlocking Concrete Pavements. **Proceedings 9th International Conference on Concrete Block Paving.** Buenos Aires, Argentina.
21. Urban Water Resources Center. 2002. **Research into "Effective Life" of Permeable Pavement Source Control Installations.** Adelaide, Australia: University of South Australia.
22. KNAPTON, J. 2007. **The Structural Design of Heavy Duty Pavements for Ports and Other Industries, 4th Edition.** Leicester, UK: Interpave.
23. KNAPTON, J. and McBride, C. 2009. Permeable Pavements for Heavily Trafficked Roads – A Full Scale Trial. **Proceedings 9th International Conference on Concrete Block Paving.** Buenos Aires, Argentina.
24. KNAPTON, J., Morrell, D. and Simeunovich, M. 2012. **Structural Design Solutions for Permeable Pavements.** Whitley Bay, UK: John Knapton Consulting Engineers.

25. SEDDON, P.A. 1980. The Behavior of Concrete Block Paving under Repetitive Loading. **Proceedings 10th Australian Road Research Board Conference.** Sydney, Australia.

Blank page

APPENDIX B: DEFLECTION TESTING REPORT

Blank page

December 2013
Technical Memorandum: UCPRC-TM-2013-09

Development and HVS Validation of Design Tables for Permeable Interlocking Concrete Pavement: Field Testing and Test Section Structural Design

Authors:
H. Li, D. Jones, R. Wu and J. Harvey

Concrete Masonry Association of California and Nevada. Grant Agreement UCPRC-PP-2011-01

PREPARED FOR:

Concrete Masonry Association of California and Nevada

PREPARED BY:

University of California
Pavement Research Center
UC Davis, UC Berkeley

DOCUMENT RETRIEVAL PAGE		**Technical Memorandum: UCPRC-TM-2013-09**
Title: Development and HVS Validation of Design Tables for Permeable Interlocking Concrete Pavement: Field Testing and Test Section Structural Design		
Authors: H. Li, D. Jones, R. Wu and J. Harvey		
Prepared for: Concrete Masonry Association of California and Nevada	**Work submitted:**	**Date:** December 2013
UC Davis Contract No: UCPRC-PP-2011-01	**Status:** Final	**Version No.:** 2nd revision with comments addressed

Abstract:

This report details field testing of existing permeable interlocking concrete pavement projects and test sections, estimation of the effective stiffness of each layer in the structures, and mechanistic analysis and structural design of a test track to validate the design approach using accelerated loading. Key findings from the study include: (a) Higher shear stress/strength ratios, which equate to a higher risk of rutting, require thicker base layers, as expected. (b) For the same shear stress/strength ratio, an increase in the stiffness of the base layer reduces the required thickness of the base layer, especially when the subgrade has a low stiffness. (c) An increase in the stiffness of the surface layer reduces the required base layer thickness to achieve the same shear stress/strength ratio. However, the effect of the surface layer stiffness is not significant due to the relatively low thickness of the pavers. (d) For the same shear stress/strength ratio, undrained wet conditions require thicker base layers compared to the dry condition, confirming that wet conditions are the most critical condition for design. (e) The theoretical optimal design base thicknesses (combined base, and subbase layers) under dry subgrade moisture conditions for low, intermediate, and higher rutting risk levels (subgrade shear stress/strength ratios of 0.2, 0.5 and 0.8, respectively) are approximately 1,300 mm, 800 mm, and 500 mm, respectively. Under wet conditions, the theoretical optimal design thicknesses increase to 1,400 mm, 1,000 mm and 600 mm, respectively. The following interim recommendations are made based on the findings from this study: (a) Based on the mechanistic analysis, three coarse aggregate (ASTM #2) layer thicknesses of 950 mm, 650 mm, and 450 mm should be tested to assess low, intermediate, and higher risk designs. The bedding layer (#8 stone) and base layer (#57 stone) thicknesses should be fixed at 50 mm and 100 mm, respectively. (b) The shear stress/strength ratio is considered to be an appropriate parameter for assessing the rutting risk in the subgrade in permeable interlocking concrete pavement, and needs to be validated and calibrated in the accelerated load testing phase. (c) The mechanistic analysis predicted that an increase in base layer thickness will theoretically not reduce the shear stress/strength ratio of the base/subbase layer. This finding needs to be validated in the accelerated load testing phase. (d) Models are needed to quantify rut depth on permeable interlocking concrete paver structures for a given number of load repetitions for various base and subgrade configurations. Preliminary models should be developed using the results from accelerated pavement testing.

Keywords:
Interlocking concrete pavement, fully permeable pavement, mechanistic-empirical design, accelerated pavement testing.

Proposals for implementation:
Proceed with construction of the test track and accelerated load testing

Related documents:
UCPRC-TM-2013-03

Signatures:

H. Li **1st Author**	J. Harvey **Technical Review**	D. Jones **Principal Investigator**	D. Smith **For CMACN**

DISCLAIMER

The contents of this report reflect the views of the authors who are responsible for the facts and accuracy of the data presented herein. The contents do not necessarily reflect the official views or policies of the Concrete Masonry Association of California and Nevada (CMACN) or the Interlocking Concrete Pavement Institute (ICPI). This report does not constitute a standard, specification, or regulation.

PROJECT OBJECTIVES/GOALS

The objective of this project is to produce thickness design tables for permeable interlocking concrete pavement (PICP) based on mechanistic analysis and partially validated with accelerated load testing (ALT). The following tasks will be completed to achieve this objective:

1. Perform a literature and field survey to identify critical responses, failure mechanisms, appropriate performance transfer functions, and modeling assumptions for mechanistic analysis of PICP under truck loading.
2. Measure pavement deflection in the field on several PICP locations to characterize effective stiffness of the different layers in the structure for use in modeling.
3. Perform mechanistic analyses of PICP to develop design tables following the approach documented in California Department of Transportation (Caltrans) Research Report CTSW-RR-09-249.04 for development of structural design tables for permeable/pervious/porous asphalt and concrete pavement.
4. Prepare a plan for validation with accelerated load testing based on the results of the mechanistic analysis.
5. Test responses and, if possible, failure of up to three PICP structures in dry and wet condition with a Heavy Vehicle Simulator (HVS).
6. Analyze the results of the HVS testing to revise/update the structural design tables where necessary.
7. Write a final report documenting the results of all tasks in the study and demonstrating the design tables.
8. Present findings to Caltrans Office of Concrete Pavements and Foundation Program and Office of Stormwater - Design staff in Sacramento, CA.

This report covers Tasks 2 through 4.

TABLE OF CONTENTS

LIST OF TABLES

LIST OF FIGURES

SI* (MODERN METRIC) CONVERSION FACTORS

APPROXIMATE CONVERSIONS TO SI UNITS

Symbol	When You Know	Multiply By	To Find	Symbol
		LENGTH		
in	inches	25.4	Millimeters	mm
ft	feet	0.305	Meters	m
yd	yards	0.914	Meters	m
mi	miles	1.61	Kilometers	Km
		AREA		
in^2	square inches	645.2	Square millimeters	mm^2
ft^2	square feet	0.093	Square meters	m^2
yd^2	square yard	0.836	Square meters	m^2
ac	acres	0.405	Hectares	ha
mi^2	square miles	2.59	Square kilometers	km^2
		VOLUME		
fl oz	fluid ounces	29.57	Milliliters	mL
gal	gallons	3.785	Liters	L
ft^3	cubic feet	0.028	cubic meters	m^3
yd^3	cubic yards	0.765	cubic meters	m^3
		NOTE: volumes greater than 1000 L shall be shown in m^3		
		MASS		
oz	ounces	28.35	Grams	g
lb	pounds	0.454	Kilograms	kg
T	short tons (2000 lb)	0.907	megagrams (or "metric ton")	Mg (or "t")
		TEMPERATURE (exact degrees)		
°F	Fahrenheit	5 (F-32)/9 or (F-32)/1.8	Celsius	°C
		ILLUMINATION		
fc	foot-candles	10.76	Lux	lx
fl	foot-Lamberts	3.426	$candela/m^2$	cd/m^2
		FORCE and PRESSURE or STRESS		
lbf	poundforce	4.45	Newtons	N
lbf/in^2	poundforce per square inch	6.89	Kilopascals	kPa

APPROXIMATE CONVERSIONS FROM SI UNITS

Symbol	When You Know	Multiply By	To Find	Symbol
		LENGTH		
mm	millimeters	0.039	Inches	in
m	meters	3.28	Feet	ft
m	meters	1.09	Yards	yd
km	kilometers	0.621	Miles	mi
		AREA		
mm^2	square millimeters	0.0016	square inches	in^2
m^2	square meters	10.764	square feet	ft^2
m^2	square meters	1.195	square yards	yd^2
ha	Hectares	2.47	Acres	ac
km^2	square kilometers	0.386	square miles	mi^2
		VOLUME		
mL	Milliliters	0.034	fluid ounces	fl oz
L	liters	0.264	Gallons	gal
m^3	cubic meters	35.314	cubic feet	ft^3
m^3	cubic meters	1.307	cubic yards	yd^3
		MASS		
g	grams	0.035	Ounces	oz
kg	kilograms	2.202	Pounds	lb
Mg (or "t")	megagrams (or "metric ton")	1.103	short tons (2000 lb)	T
		TEMPERATURE (exact degrees)		
°C	Celsius	1.8C+32	Fahrenheit	°F
		ILLUMINATION		
lx	lux	0.0929	foot-candles	fc
cd/m^2	$candela/m^2$	0.2919	foot-Lamberts	fl
		FORCE and PRESSURE or STRESS		
N	newtons	0.225	Poundforce	lbf
kPa	kilopascals	0.145	poundforce per square inch	lbf/in^2

*SI is the symbol for the International System of Units. Appropriate rounding should be made to comply with Section 4 of ASTM E380 (Revised March 2003)

1. INTRODUCTION

1.1 Project Scope

This project is being coordinated through the Interlocking Concrete Pavement Institute (ICPI) and the Concrete Masonry Association of California and Nevada with additional support from the California Nevada Cement Association. The objective of this project is to produce thickness design tables for permeable interlocking concrete pavement (PICP) based on mechanistic analysis and partially validated with accelerated load testing (ALT).

1.2 Background to the Study

Although permeable pavements are becoming increasingly common across the United States, they are mostly used in parking lots, basic access streets, recreation areas, and landscaped areas, all of which carry very light, slow moving traffic. Only limited research has been undertaken on the mechanistic design and long-term performance monitoring of permeable pavements carrying higher traffic volumes and heavier loads, and the work that has been done has focused primarily on pavements with open-graded asphalt or portland cement concrete surfacings. Very little research has been undertaken on the use of permeable concrete paver surfaces on these more heavily trafficked pavements.

1.3 Study Objective

The objective of this project is to produce design tables for permeable interlocking concrete pavement (PICP) based on mechanistic analysis and partially validated with accelerated load testing (ALT).

The tasks to complete this objective include the following:

1. Perform a literature and field survey to identify critical responses, failure mechanisms, appropriate performance transfer functions, and modeling assumptions for mechanistic analysis of PICP under truck loading. This task has been completed and a summary report prepared *(1)*.
2. Measure pavement deflection in the field on several PICP locations to characterize effective stiffness of the different layers in the structure for use in modeling.
3. Perform mechanistic analyses of PICP to develop design tables following the approach documented in California Department of Transportation (Caltrans) Research Report CTSW-RR-09-249.04 for development of structural design tables for permeable/pervious/porous asphalt and concrete pavement *(2)*.
4. Prepare a plan for validation with accelerated load testing based on the results of the mechanistic analysis.
5. Test responses and, if possible, failure of up to three PICP structures in dry and wet condition with a Heavy Vehicle Simulator (HVS).

6. Analyze the results of the HVS testing to revise/update the structural design tables where necessary.
7. Write a final report documenting the results of all tasks in the study and demonstrating the design tables.
8. Present findings to Caltrans Office of Concrete Pavements and Foundation Program and Office of Stormwater - Design staff in Sacramento, CA.

The report covers Tasks 2 through 4.

1.4 Report Layout

This report covers the pavement deflection measurement and stiffness backcalculation work completed in Task #2, mechanistic analyses and structural design completed in Task #3, and the accelerated loading test plan for validation of the structural designs completed in Task #4. Chapters include:

- Chapter 2 includes a brief description of pavement deflection testing and details the experiment plan for field deflection testing of existing PICP sections.
- Chapter 3 summarizes the results of the deflection testing.
- Chapter 4 presents the results and analyses of the mechanistic analysis and preliminary structural designs.
- Chapter 5 presents the test plan for thickness validation with a Heavy Vehicle Simulator.
- Chapter 6 presents conclusions and recommendations.
- Appendix A contains summary plots of the mechanistic analysis results.

1.5 Measurement Units

Metric units are always used by the UCPRC in mechanistic design, the design and layout of HVS test tracks, for laboratory, accelerated load testing, and field measurements, and for data storage. Where appropriate in this report, both U.S. customary and metric units are provided. In other cases where data is collected, analyzed, and discussed, only metric units are used. A conversion table is provided on page vi at the beginning of this report.

2. DEFLECTION TESTING PLAN

2.1 Introduction

This chapter describes the experiment plan for deflection testing of existing PICP projects in northern California. A brief background to deflection testing is provided, followed by a description of the equipment used in this study to measure deflections, the testing procedure followed, and details on supplementary testing of subgrade shear strengths in dry and soaked conditions. A description of the test section locations and pavement structures is also provided.

2.2 Background to Deflection Testing

Pavement surface deflection measurements are a primary method of evaluating the behavior of pavement structures when subjected to a load. These measurements, which are non-destructive, are used to assess a pavement's structural condition, by taking most relevant factors into consideration, including traffic type and volume, pavement structural section, temperature, and moisture condition. Deflection measurements can be used in backcalculation procedures to determine:

- Pavement structural layer stiffness, used as an indicator to determine what level of traffic loading the pavement can withstand (i.e., design life or remaining life in terms of number of axle loads), and
- Subgrade resilient modulus, used to determine the thickness of the pavement that will be required to prevent subgrade failures over the expected design life.

Deflection measurements are used by most departments of transportation as the basis for rehabilitation designs and often as a trigger for when rehabilitation or reconstruction is required.

All pavements bend under loading to some degree. Although this bending can normally not be distinguished with the naked eye (measurements are typically recorded in microns or mils) it has a significant effect on the integrity of the different layers over time. Repeated bending and then relaxation as the load moves onto and then off a point on a pavement is analogous to repeatedly bending a piece of wire back and forth – it eventually breaks. In pavements, the "damage" usually materializes as reorientation of the material particles, cracks and/or shearing, which leads to a reduction in stiffness over time, which in turn leads to moisture ingress, rutting, and other associated problems.

2.3 Deflection Measurement Method

Pavement deflection is most commonly measured with a falling weight deflectometer (FWD). However, this equipment is designed for continuous asphalt concrete and portland cement concrete pavements built

on dense-graded aggregate bases, and was not considered appropriate for testing deflection on pavements constructed with interlocking concrete pavers (because of the segmented nature of the pavement surface), overlying open-graded aggregate bases. An FWD also applies an instantaneous dynamic load onto the pavement surface to simulate a truck wheel load passing over that point at a speed of about 60 km/h (40 mph). Deflection in the pavement is measured under this load. Open-graded aggregate bases used in permeable pavements, are usually more stress dependent than dense-graded bases, and can therefore have a bigger range of stiffness increase and relaxation as the wheel load passes over it. Backcalculating stiffnesses based on these measurements may therefore provide incorrect results when analyzing PICP. A review of the literature on PICP *(1)* revealed that other researchers had experienced problems with accurately analyzing the stiffness of PICP from FWD deflection measurements.

Based on these concerns, a modified Benkelman beam (road surface deflectometer [RSD]) was instead used to measure deflection on the test sections. This device, which is standard equipment for measuring surface deflections on accelerated load tests at the UCPRC, measures the actual deflection between the dual wheels of a truck as it passes at slow speed over the instrument (Figure 2.1).

Figure 2.1: Road surface deflectometer.

The instrument is not influenced by the segmental nature of the pavers (provided that the four points are in contact with the surface and not on a joint) and is considered more appropriate for accommodating the

stress dependent nature of the open-graded aggregate base. These deflection measurements were used to backcalculate the effective stiffnesses of the individual pavement layers based on multilayer linear elastic theory. A comparison between the FWD and RSD was undertaken on a fully permeable pavement with a continuous open-graded asphalt surface to compare the backcalculated stiffnesses of the open-graded base using the two deflection methods. Testing was done under both dry and wet conditions on this section. Dynamic cone penetrometer measurements were also taken on this pavement to obtain an indication of the subgrade shear strength under dry and wet conditions to further verify the results.

2.4 Testing Equipment

2.4.1 Test Vehicle

A single rear axle, dual-wheel dump truck loaded with aggregate was used as the test vehicle (Figure 2.2). The load area of this truck was dividable, which allowed a load change on the rear axle by distributing the aggregate (Figure 2.3). Measurements were taken with wheel loads of 35 kN and 45 kN (8,000 lb and 10,000 lb). Axle loads were measured using a weigh-in-motion pad (Figure 2.4 and Figure 2.5).

Figure 2.2: Test vehicle.

Figure 2.3: Re-distribution of aggregate to change load.

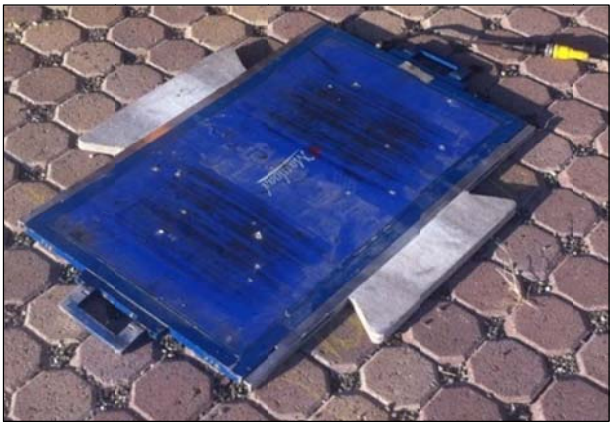

Figure 2.4: Weigh-in-motion pad.

Figure 2.5: Measuring the wheel load.

2.4.2 Road Surface Deflectometer (RSD)

A road surface deflectometer (RSD) was used to measure the deflection basin caused by the moving load on the pavement surface (Figure 2.1). An encoder was designed and constructed to precisely measure the wheel location/distance (Figure 2.6), which is a critical input for backcalculating the pavement stiffness. Air and pavement surface temperatures were measured using Type-K thermocouple sensors. All data was collected on a customized data acquisition system (DAS). A setup at a test section is shown in Figure 2.7.

Figure 2.6: Encoder for measuring wheel location.

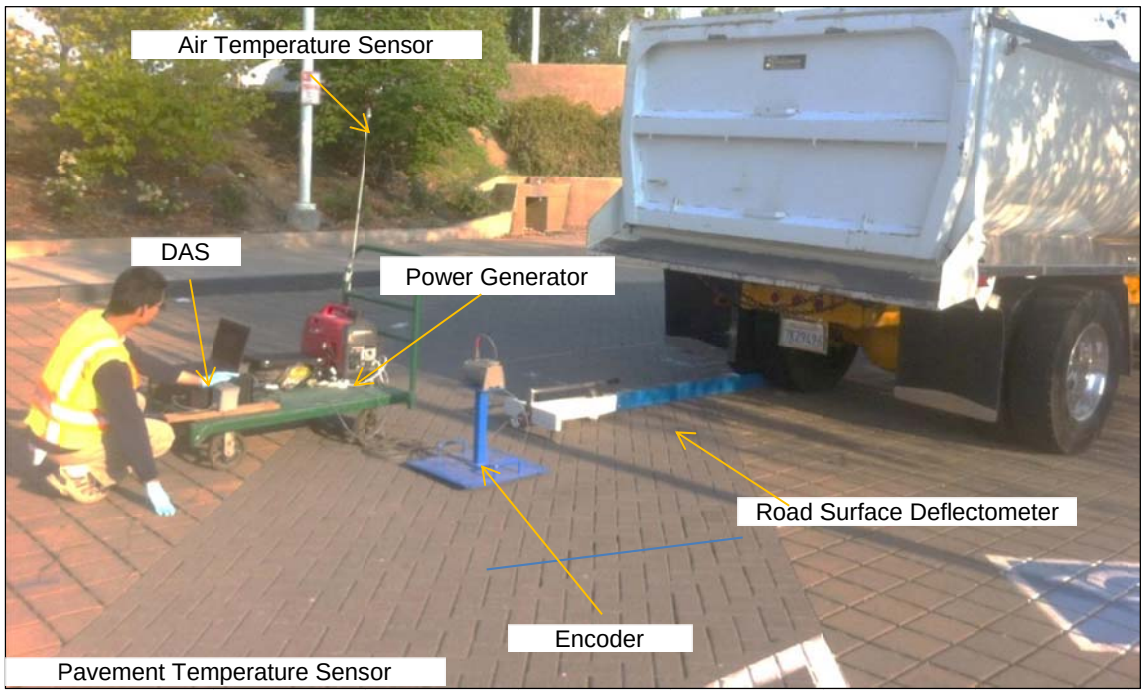

Figure 2.7: Test section setup.

2.5 Deflection Testing Procedure

Deflection measurements were taken at various locations at each test site on two different lines on the pavement: the centerline (CL) and approximate outside wheelpath (WP). Five replicate measurements

were taken at each test location with each test load. Testing was carried out at the end of the summer in the dry condition.

2.6 Test Section Locations

2.6.1 Existing PICP Projects

Three sites in northern California were selected for the deflection measurements, two in Davis and one in Sacramento (Figure 2.8). Construction records indicated that the pavement structures at the different sites consisted of an ASTM No. 57 aggregate base layer 300 to 400 mm (12 to 16 in.) thick, underneath an ASTM No. 8 aggregate bedding layer 25 to 50 mm (1 to 2 in.) thick. The surface pavers used at all three sites were 80 mm (3.2 in.) thick. Different laying patterns were used at each site (Figure 2.9). Additional information on the test sites is summarized in Table 2.1. Actual pavement structures were not verified in the field with coring or test pits.

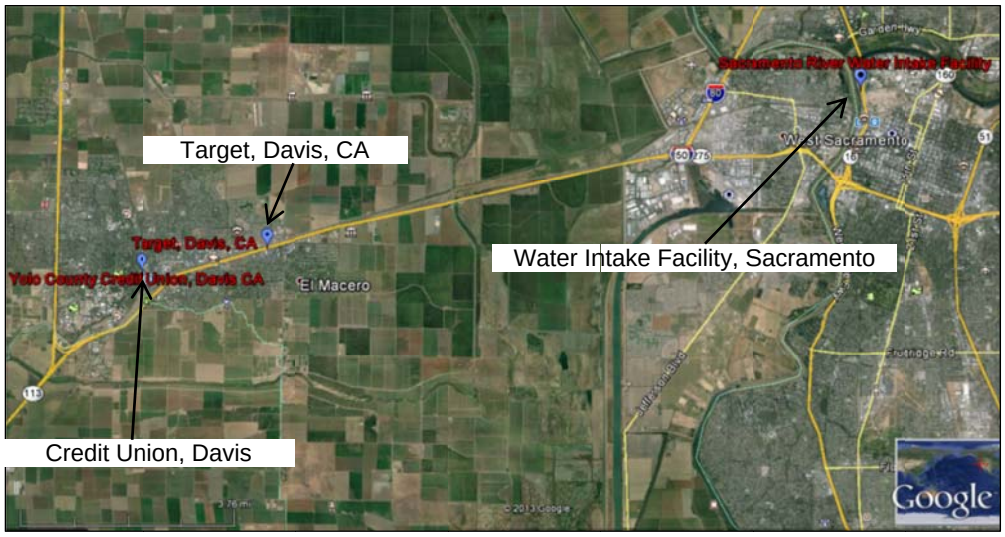

Figure 2.8: Test sites for field deflection measurement.

Davis (Target) Davis (Credit Union) Sacramento

Figure 2.9: Paver laying patterns at the different test sites.

Table 2.1: PICP Test Section Details

#	Site Name/Location/Traffic	Pavement Structure	Construction Date
1	Target Store 4601 2nd St., Davis Apparent minimal vehicular traffic (fire lane)	80 mm (3.2 in.) Uni Eco Stone Paver 50 mm (2 in.) #8 stone bedding layer 300 mm (12 in.) #57 stone base Subgrade not documented	2010
2	Yolo Federal Credit Union 501 G Street, Davis Regular vehicle traffic	80 mm (3.2 in.) concrete pavers 25 mm (1 in.) #8 stone bedding layer 375 mm (15 in.) #7 stone base Subgrade is native soil (silty clay) with an R-value < 5 Non-woven geotextile was placed on the subgrade and a BX1200 geogrid was placed on top of the fabric.	2012
3	Sacramento River Water Intake Facility (Matsui Park) Jibbom Street, Sacramento Intermittent vehicular traffic	80 mm (3.2 in.) SF-Rima™ permeable concrete pavers 50 mm (2 in.) 6 to 9 mm (1/4" to 3/8") stone bedding layer Aggregate base gradation not documented 400 mm (16 in.) type B Fill, placed in 200 mm (8in.) lifts.	Unknown

2.6.2 UCPRC Experimental Section

Since the testing on the existing PICP projects discussed above was all undertaken at the end of the dry season, only best case scenario measurements were obtained. Any pavement will exhibit high stiffnesses when all the materials are dry. However, these stiffnesses can drop significantly when the materials get wet, and consequently, most pavements are designed for wet conditions rather than dry (i.e., layers are thicker to prevent rutting in the subgrade), and considerable effort is placed into ensuring that water is effectively drained away from the road. Given that permeable pavements allow rain water to flow through the structure and into the subgrade, and that the base layers may actually be used to "store" water while it infiltrates into the subgrade, it is important to fully understand how the pavement will behave under these soaked conditions before thickness design tables can be prepared.

The existing PICP sections could not be flooded with water to assess moisture conditions, and time did not allow for a second round of tests at the end of the rain season. As an alternative, deflection testing was undertaken on a permeable pavement structure with a porous asphalt concrete surface at the UCPRC test facility. This experiment is close to the site selected for construction of the test track for accelerated load testing of PICP. Deflection testing was done under both dry and wet conditions (water was allowed to flow through the surface until it overtopped). Deflection measurements were taken with both the RSD and the FWD and the results backcalculated to assess the difference in stiffnesses of the open-graded aggregate base and the subgrade under the two moisture conditions. This UCPRC test section was originally constructed as part of a larger experiment to measure the influence of permeable pavements on near surface temperature, albedo, and evaporation. Although not truly representative of typical PICP projects in terms of base thickness design and base aggregate properties, it was considered suitable for

comparing the change in uncompacted subgrade properties under an open-graded aggregate base when conditions changed from dry to wet. Test section details are summarized in Table 2.2.

Table 2.2: UCPRC Test Section Details

#	Site Name/Location	Pavement Structure	Construction Date
4	UCPRC Facility porous asphalt	4 in. (100 mm) porous asphalt 1 in. (25 mm) #8 stone bedding layer 12 in. (300 mm) graded aggregate base Silty-clay subgrade (uncompacted)	2011

Blank page

3. DEFLECTION MEASUREMENT ANALYSIS

3.1 Introduction

This chapter discusses the analysis of the deflection measurement data collected at the four test locations discussed in Chapter 2. The primary component of this analysis was the backcalculation of the stiffnesses of the different pavement layers. Backcalculation is a mechanistic evaluation of pavement surface deflection basins generated by pavement deflection devices (i.e., the RSD and FWD in this study). In the backcalculation process, measured surface deflections are matched, within some tolerable error, with a calculated surface deflection generated from an identical pavement structure using assumed layer stiffnesses (moduli). The assumed layer moduli in the calculated model are adjusted until they produce a surface deflection that closely matches the measured one. The combination of assumed layer stiffnesses that results in this match is then assumed to be near the actual in situ moduli for the various pavement layers. The backcalculation process is usually iterative and normally done with computer software.

In this study, layer stiffness backcalculation using RSD data was conducted using a *Matlab* script (*KalmanBack*) developed by the UCPRC. *KalmanBack* uses *OpenPave* (www.openpave.org) for the deflection calculation and then uses a Kalman Filter as the search algorithm *(3)*. When matching surface deflections measured with the RSD, the deflection at the RSD anchoring feet was also accounted for.

3.2 Backcalculation of Stiffness

The pavement structures were simplified into three layers for the backcalculation of stiffness: surface layer (paver), base layer (aggregate, including bedding layers and base layer), and subgrade layer (soil). The as-designed layer thicknesses summarized in Table 2.1 and Table 2.2 were used for the backcalculation analysis. The effective stiffnesses of these three layers were optimized through minimizing the error between the calculated and the measured deflection basin curves based on multilayer linear elastic theory, which is commonly used as the basis for pavement design procedures.

3.2.1 Example Deflection Basin Curves

The measured deflection basin curves had some noise, consistent with deflection measurements on pavements with uneven surfaces. The data were therefore processed using center-moving-average filtering to reduce this noise. Examples of the raw deflection basin curve and the filtered deflection basin curve are shown in Figure 3.1.

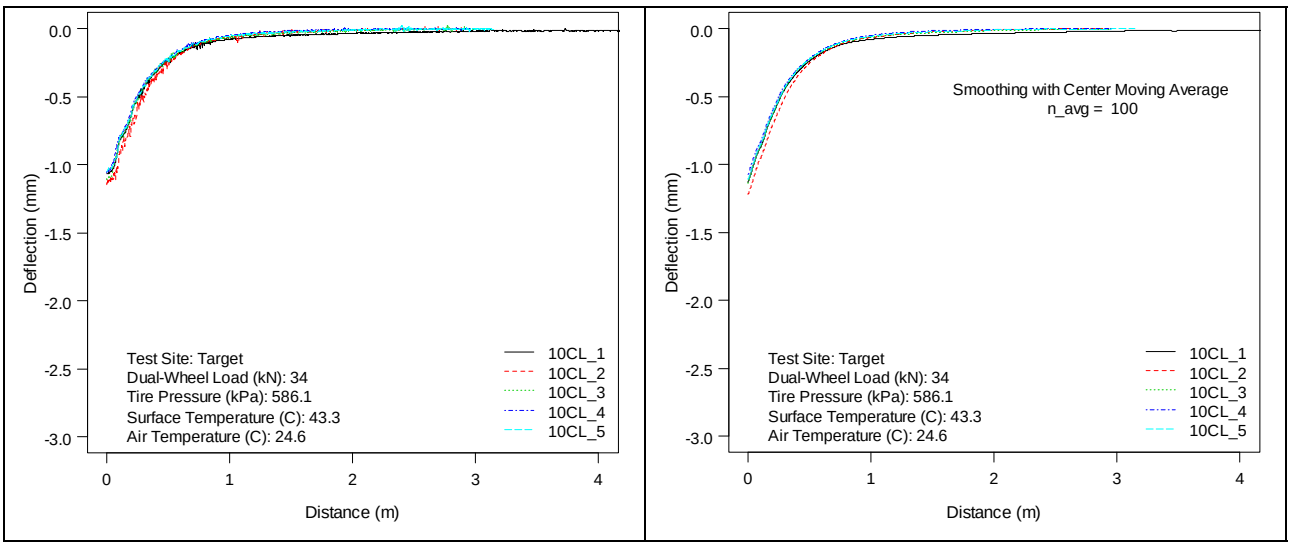

(a) Raw deflection basin curve (b) Filtered deflection basin curve

Figure 3.1: Raw and filtered deflection basin curves.

3.2.2 Backcalculated Effective Stiffness of the Surface Layers

Effective stiffnesses were backcalculated from the deflection measurements using layer elastic theory. The effective stiffness of the surface layers under two different load levels and for two testing lines (centerline [CL] and wheelpath [WP]) at the three test sites (Target, Yolo Credit Union, and Matsui Park) are presented in Figure 3.2 through Figure 3.4. The main observations from this analysis include:

- There was a significant variation in surface effective stiffness among the three test sections, with very low stiffnesses measured at Matsui Park, intermediate stiffnesses measured at Yolo Credit Union, and higher stiffnesses measured at the Target site. Variation in stiffness was attributed to paver shape, paving laying pattern, degree of interlock between pavers, and confinement. For example, the lower stiffnesses at Matsui Park were attributed in part to the choice of paver (square) and the laying pattern (no interlocking pattern [see Figure 2.9]).
- Variations in surface effective stiffness were noted along the length of each test section on both the centerline and the wheelpath. This was attributed in part to construction variability and loosening of the paver interlock under traffic.
- The mean effective stiffness of the surface layer under the heavier load was generally slightly higher than that under the lighter load on all three sections.
- Lower variation in effective stiffness was measured along the wheelpath compared to the centerline. This was attributed to the stronger and more uniform confining effect from the concrete curb and underlying edge walls close to the wheelpath.

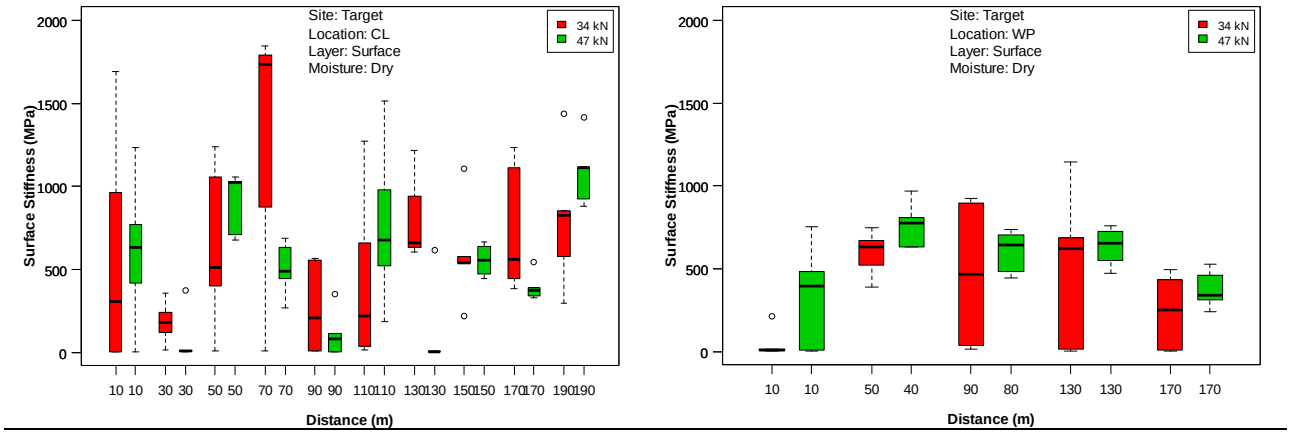

Centerline Wheelpath

Figure 3.2: Effective surface layer stiffness at Target test site (1 MPa = 145 psi).

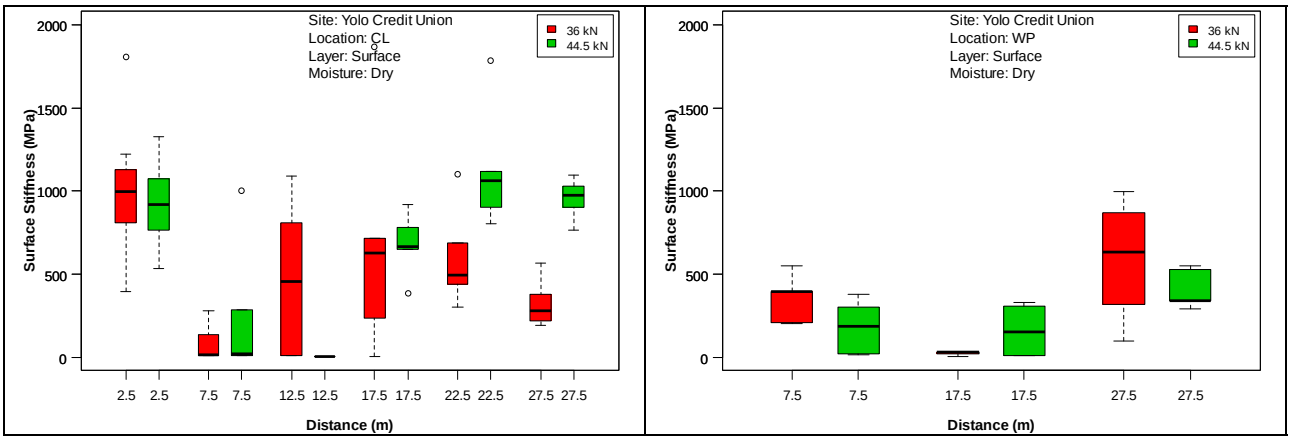

Centerline Wheelpath

Figure 3.3: Effective surface layer stiffness at Yolo Credit Union test site.

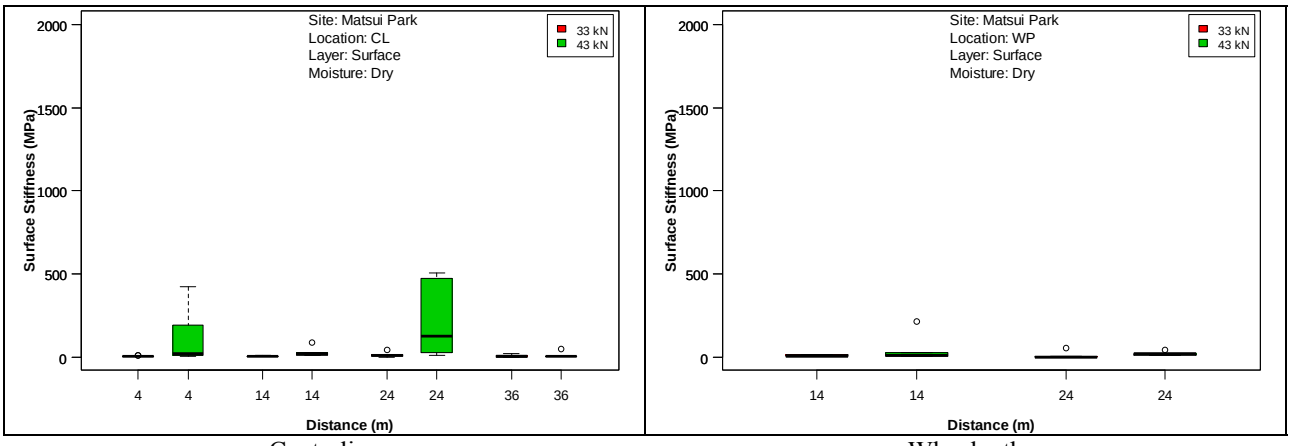

Centerline Wheelpath

Figure 3.4: Effective surface layer stiffness at Matsui Park test site.

3.2.3 Backcalculated Effective Stiffness of the Base Layers

The effective stiffness of the base layers for the two load levels and two testing paths (centerline and wheelpath) at all three test sites are presented in Figure 3.5 through Figure 3.7. The main observations from this analysis include:

- The mean effective stiffnesses of the base layers calculated for the three sites were in the range of 20 MPa to 120 MPa (2.9 ksi to 17.4 ksi). However, average effective base layer stiffnesses were more consistent across the three sections compared to the surface stiffnesses. It should be noted that calculated stiffnesses will be influenced by and are sensitive to layer thickness and that design thicknesses were used in the analysis. These were not verified with on-site excavation. Consequently, actual layer stiffnesses could be lower or higher if the as-built thicknesses were thinner or thicker than the design.
- Effective stiffness along the wheelpath had lower variation compared to the centerline, which was again attributed to constraining effects of the curb and edge walls. The Matsui Park test section had the highest variability.
- In most instances, the effective stiffness of the base layer was slightly higher under the heavier load, as expected. This was attributed to the higher confining stresses under the heavier load.

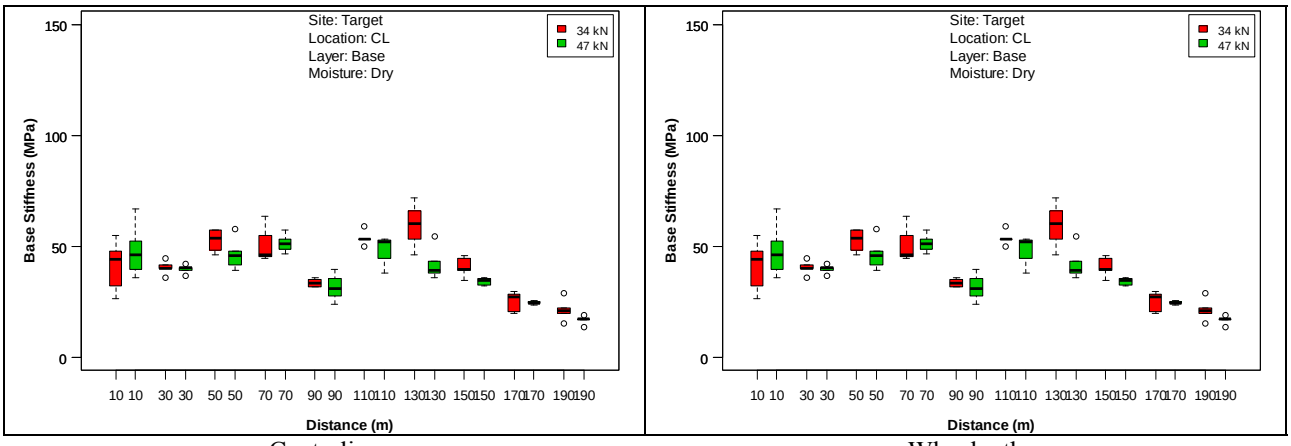

Centerline Wheelpath

Figure 3.5: Effective base stiffness at Target test site.

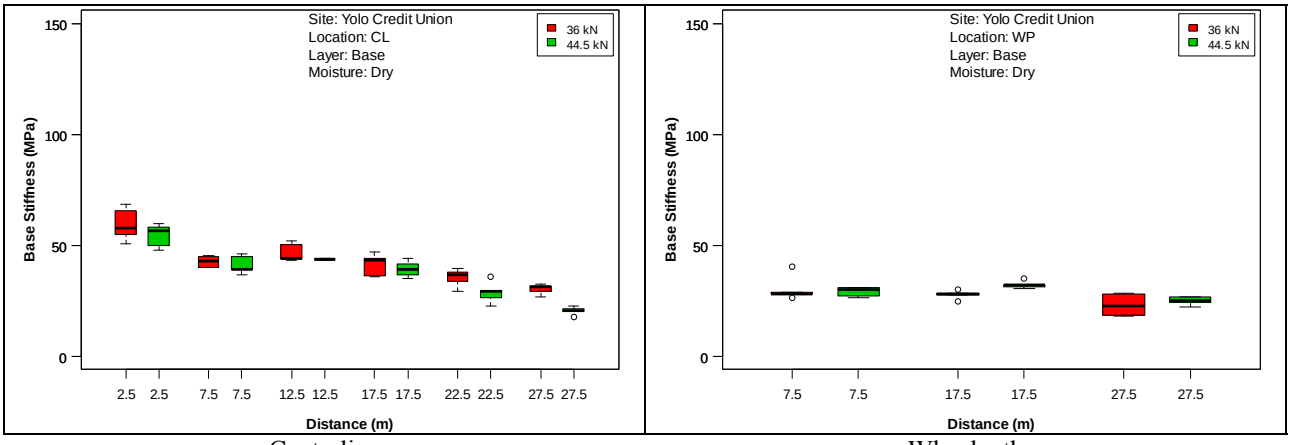

Centerline Wheelpath

Figure 3.6: Effective base stiffness at Yolo Credit Union test site.

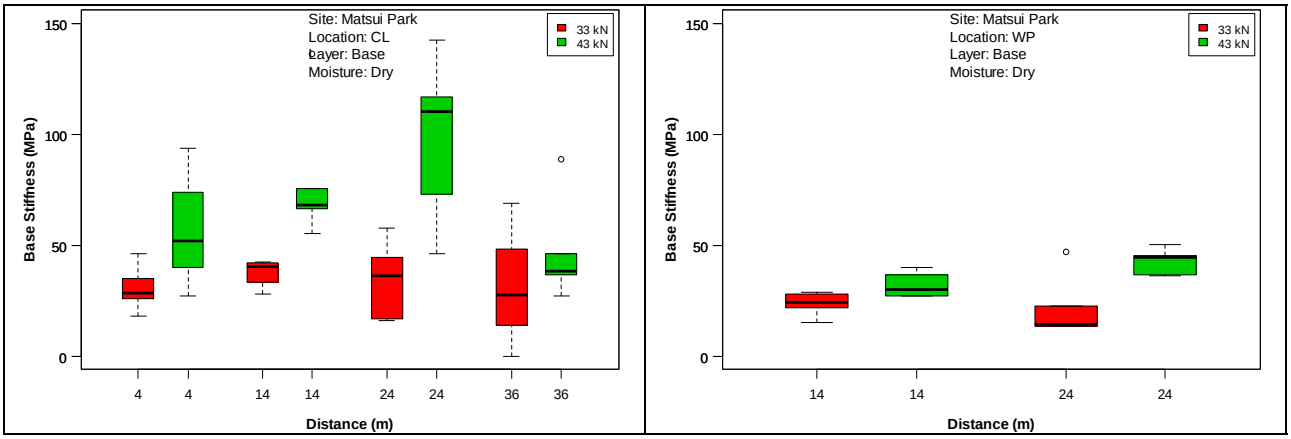

Centerline Wheelpath

Figure 3.7: Effective base stiffness at Matsui Park test site.

3.2.4 Backcalculated Effective Stiffness of the Subgrade Layers

The effective stiffnesses of the subgrade layers under dry conditions for the three test sites are presented in Figure 3.8 through Figure 3.10. The main observations include:

- The mean effective stiffnesses of the subgrade layers varied between 20 MPa and 100 MPa (2.9 ksi and 14.5 ksi) for the three test sites.
- The Matsui Park section had the highest effective subgrade stiffness of the three sections, but also the highest variability. This was attributed to the likely alluvial (river gravel) nature of the subgrade material. The Target and Yolo Credit Union sites had a similar range of subgrade stiffnesses consistent with silty-clay materials common in this area.
- Trends and variation along the two test paths were similar to those observed for the surface and base layers.
- The effect of the different load levels was less apparent on the subgrade stiffness compared to the effect it had on base and surface layer stiffnesses. This was attributed to the subgrade materials being of a less granular nature than the base materials and therefore less susceptible to confining stress.

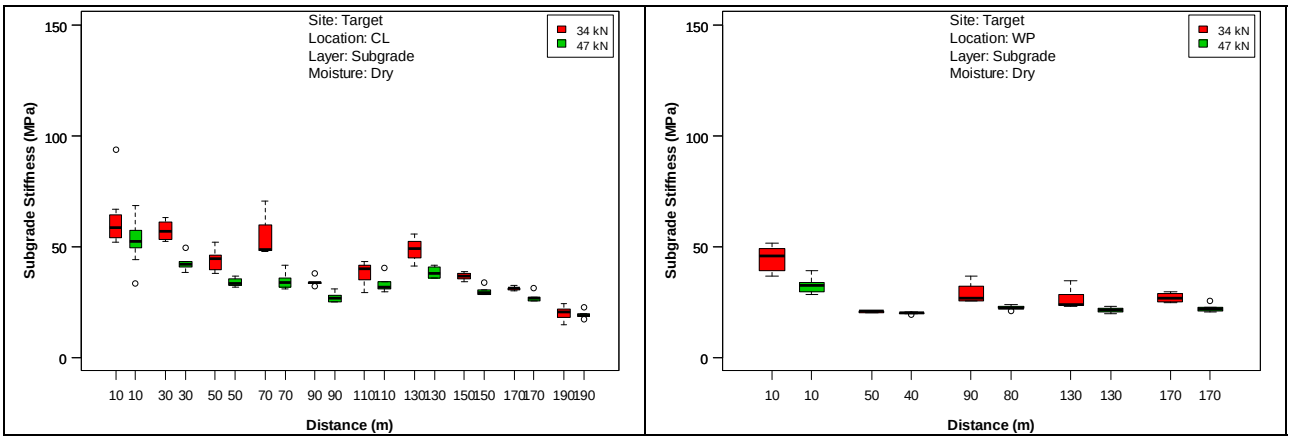

Centerline Wheelpath

Figure 3.8: Effective subgrade stiffness at Target test site.

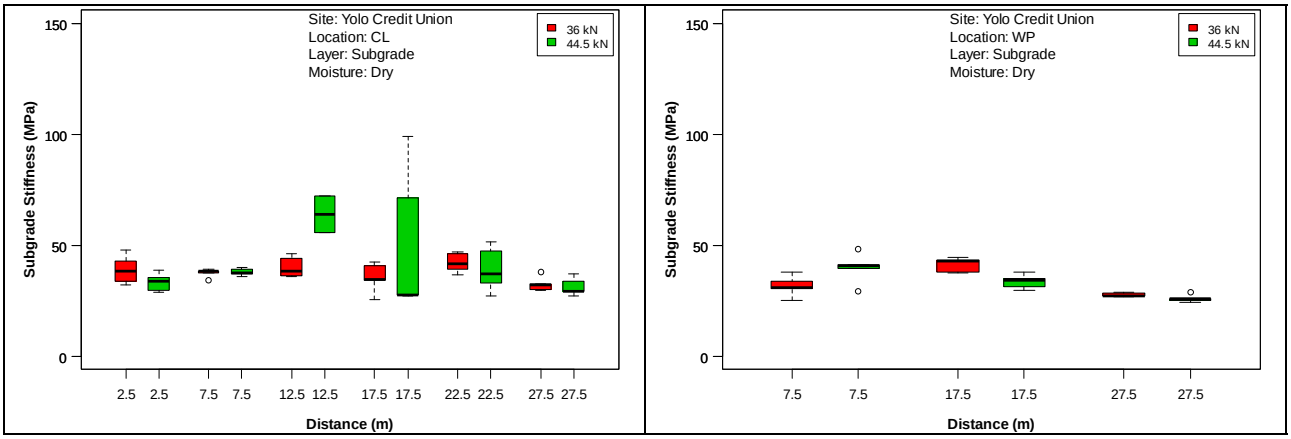

Centerline Wheelpath

Figure 3.9: Effective subgrade stiffness at Yolo Credit Union test site.

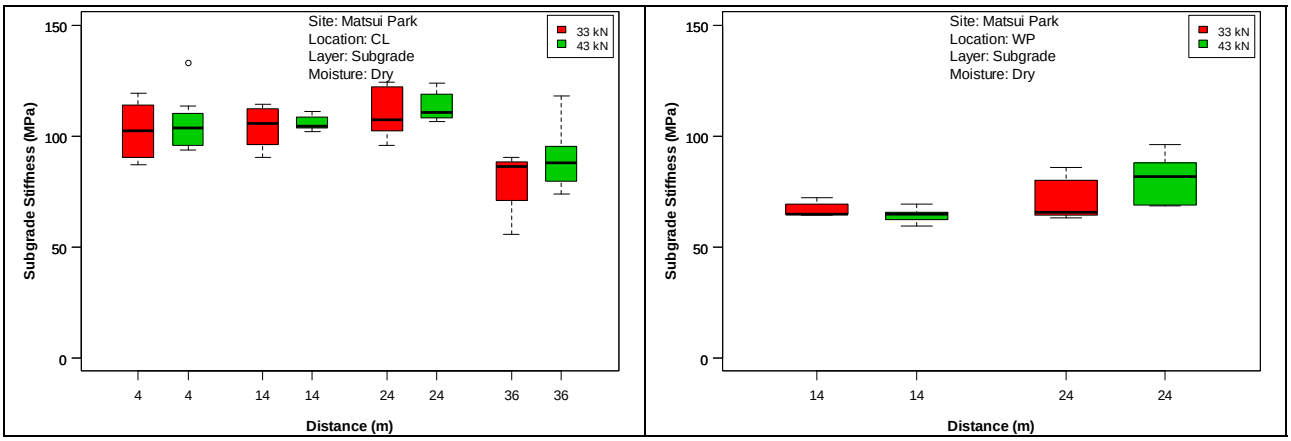

Centerline Wheelpath

Figure 3.10: Effective subgrade stiffness at Matsui Park test site.

3.2.5 Effective Stiffness Analysis

The distributed backcalculated effective stiffnesses of the surface layers, base layers, and subgrades at the three test sites were analyzed using empirical cumulative distribution functions (CDF). The empirical distribution function, or empirical CDF, is the cumulative distribution function associated with the empirical measure of the sample. This CDF is a step function that increases by 1/n at each of the n data points. The empirical distribution function estimates the true underlying CDF of the points in the sample and converges with a probability of one according to the Glivenko–Cantelli theorem.

The effective stiffnesses of each layer were grouped and summarized for the three sites and are shown in Figure 3.11 through Figure 3.13. The median effective stiffnesses (50th percentile) for the surface and base layers and the subgrade were approximately 400 MPa, 40 MPa, and 40 MPa (58 ksi, 5.8 ksi, and 5.8 ksi), respectively. Given that subgrade conditions at the Davis sites were likely different to the Sacramento site, the exercise was repeated for the two Davis sites only (Figure 3.14 through Figure 3.16).

Effective stiffness values changed to approximately 500 MPa, 35 MPa and 35 MPa (73 ksi, 5.1 ksi, and 5.1 ksi), respectively.

The results indicate that the effective stiffnesses at the 50th percentile of the surface layers at the Davis sites were higher than that at the Sacramento site, which was again attributed to paver type, laying pattern, and degree of paver interlock. The effective stiffnesses at 50 percent CDF of the base and subgrade layers at the Davis sites were slightly lower than that of the Sacramento site, which was attributed to different base aggregate sources and the likelihood that the Sacramento site had an alluvial aggregate subgrade, compared to the silty-clay subgrades common in the Davis area. These effective stiffnesses are comparable to the results obtained during earlier laboratory testing *(1,2)* and results cited in the literature (e.g., *4-6*).

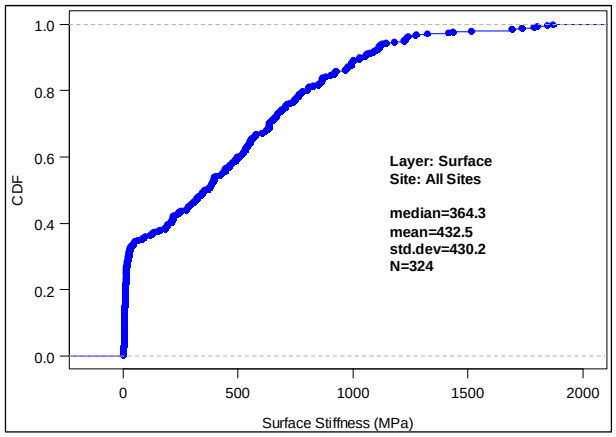

Figure 3.11: Cumulative distribution of effective surface stiffness at all three test sites.

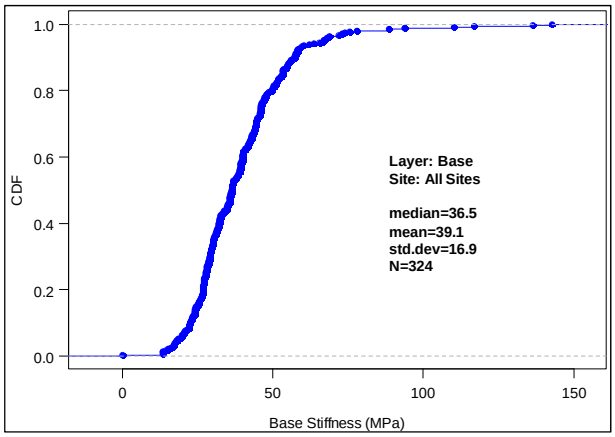

Figure 3.12: Cumulative distribution of effective base stiffness at all three test sites.

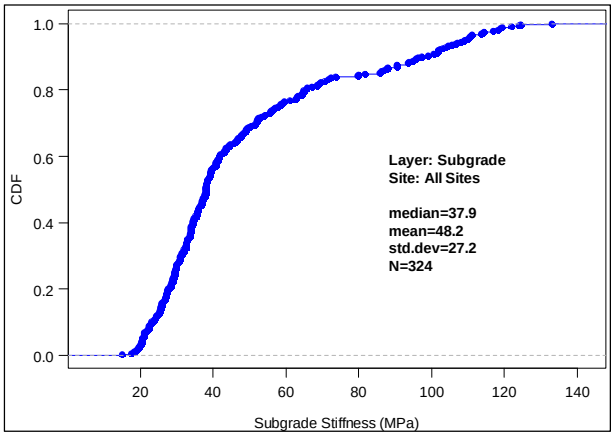

Figure 3.13: Cumulative distribution of effective subgrade stiffness at all three test sites.

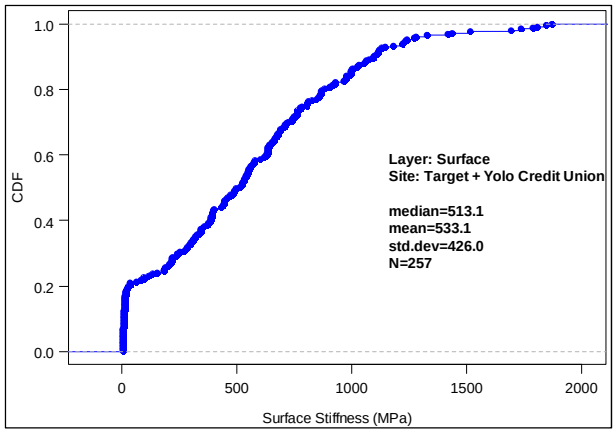

Figure 3.14: Cumulative distribution of effective surface stiffness at the two Davis sites.

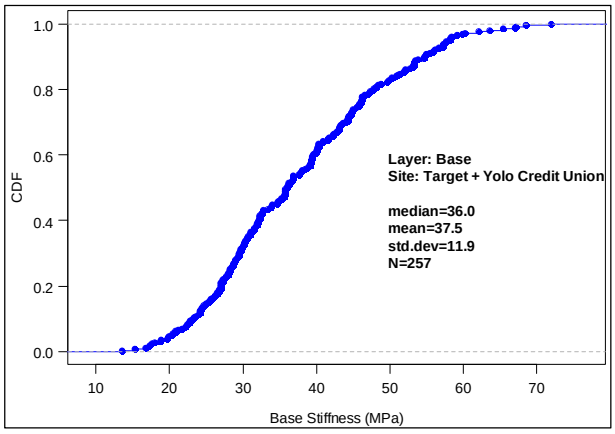

Figure 3.15: Cumulative distribution of effective base stiffness at the two Davis sites.

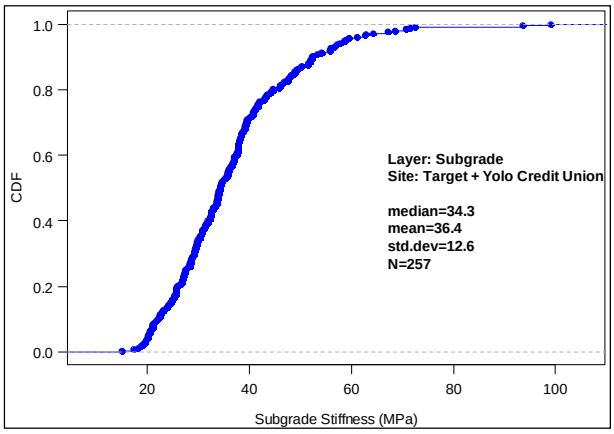

Figure 3.16: Cumulative distribution of effective subgrade stiffness at the two Davis sites.

3.3 UCPRC Test Section

3.3.1 Backcalculated Effective Stiffness from RSD Measurements

The results of the backcalculated effective stiffness from RSD measurements on the porous asphalt section are presented in Figure 3.17 though Figure 3.19. Observations include:

- There was no significant difference between the stiffnesses measured under the two different wheel loads.
- The stiffnesses of the base layer across the test section were relatively uniform, but relatively low compared to the results from the Davis and Sacramento test sections described above. This was attributed to the small size of the UCPRC test section (lack of confinement), different base aggregates, very light compaction of the base materials during construction, the absence of any subgrade compaction, and the absence of any trafficking on the sections after construction.
- Stiffnesses under soaked conditions were lower than those measured under dry conditions, as expected.

3.3.2 Backcalculated Effective Stiffness from FWD Measurements

The effective base and subgrade stiffnesses backcalculated from FWD measurements under dry and wet conditions at two different temperatures are presented in Figure 3.20. FWD-determined base and subgrade stiffnesses were comparable, but higher than those determined from RSD measurements, especially for the subgrade.

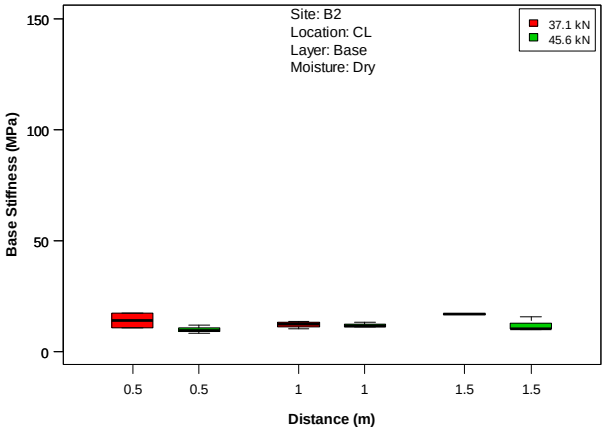

Figure 3.17: Effective base stiffness under different loads (dry condition).

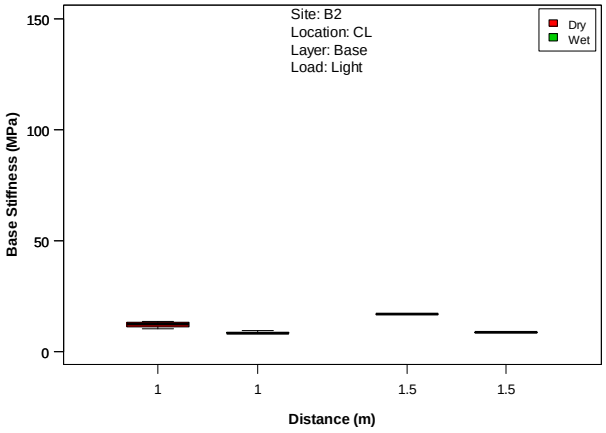

Figure 3.18: Effective base stiffness under dry and wet conditions (37 kN load).

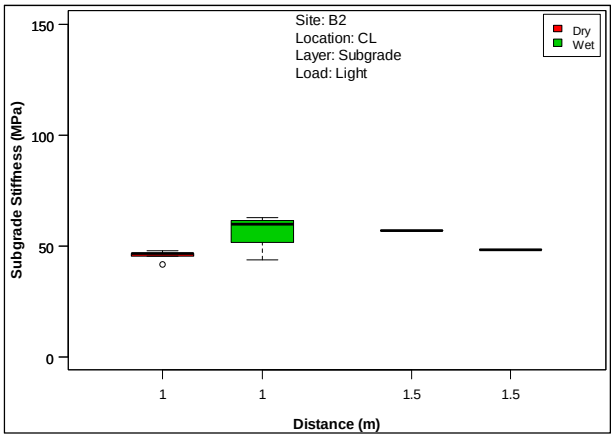

Figure 3.19: Effective subgrade stiffness in dry and wet conditions (37 kN load).

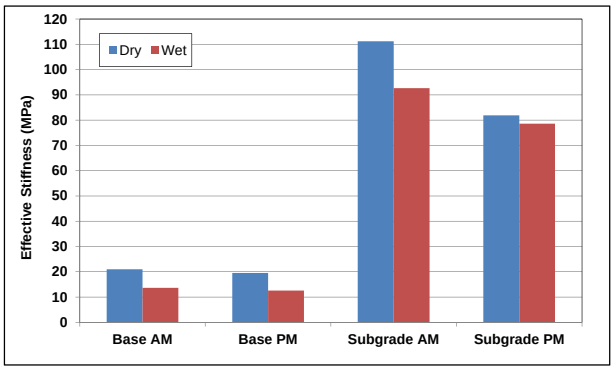

Figure 3.20: Effective base and subgrade stiffness (FWD) of the porous asphalt section.

3.4 DCP Tests on the UCPRC Sections

Dynamic cone penetrometer tests were used to empirically characterize the thickness and strength of the base and subgrade layers after completion of the deflection testing on the UCPRC section to obtain a different measure of strength and stiffness for comparison purposes. The strength characteristics of the base and subgrade materials were estimated from the DCP measurements using the *EasyDCP* program *(7)*. Results are presented in Table 3.1. The slightly higher subgrade strengths on the test section compared to the adjacent area was attributed to the confinement provided by the pavement structure. The results are consistent with silty clay subgrade materials in the Davis area.

Table 3.1: DCP-Determined Strength Characteristics of Base and Subgrade Materials.

Surface Type	Moisture Condition	DCP-Determined Strength Characteristic					
		Base			Subgrade		
		CBR[1] (%)	UCS[2] (kPa)	Su[3] (kPa)	CBR (%)	UCS (kPa)	Su (kPa)
100 mm porous asphalt	Wet	14	151	76	4	47	24
Adjacent subgrade, no surface	Wet	-	-	-	1	21	11

[1] CBR = California Bearing Ratio [2] UCS = Uniaxial Compressive Strength [3] Su = Undrained Shear Strength
[4] Low confinement compared to PCC and AC.

4. MECHANISTIC ANALYSES AND STRUCTURAL DESIGN

4.1 Introduction

This chapter summarizes the results of the mechanistic analyses and theoretical structural designs for permeable interlocking concrete pavements (PICP). This study was essentially a sensitivity analysis considering a range of values from worst to best case scenarios. Design criteria, design variables, critical responses, inputs for the mechanistic modelling and structural analysis, and the range of pavement structure options are discussed.

4.2 Design Criteria

The most likely failure mode of permeable interlocking concrete pavements is permanent deformation in the base, subbase, and/or subgrade layers, which will manifest as rutting and/or paver displacement on the surface. The design criteria for this analysis therefore focused on this type of distress.

4.3 Design Variables

4.3.1 Background

Shear stress/strength ratio (SSR or τ_f / τ_{max}) was used as the main design variable in this study for permeable interlocking concrete pavements. The basis for the use of shear strength to shear stress/strength ratio for design comes from work done at the University of Illinois, primarily under Prof. Marshall Thompson and carried out by Prof. Erol Tutumleur *(8-10)*. It is based on decades of laboratory testing for permanent deformation, followed by field validation. The concept was primarily developed for use in airfields where the shear stresses from aircraft loads and tire pressures are high relative to the strengths of the subgrade materials. It was selected for use on this permeable pavement project because of the low shear strengths of saturated, poorly compacted subgrades (which are common conditions in permeable pavements) where the ratio between shear stresses and strengths can also be high given highway loads and tire pressures.

The alternative approach considered was the use of a vertical strain criterion, which is typically used where the shear stresses relative to shear strains are relatively low, which results in relatively low overall rutting. In this approach, vertical strains are typically calculated from pavement deflection measured over the full pavement structure. Strains in the localized areas at the top of the base and subgrade layers cannot be directly measured unless a strain gauge has been specifically installed in that position. Consequently, the damage and stiffness is calculated from measured deflections and then the strain is calculated from the

calibrated damage and stiffness model. Vertical strain based approaches are difficult to calibrate when high shear stress to strength ratios occur in high water content environments, which in turn lead to large ruts. This has been learned from UCPRC experience on other projects that investigated pavement performance under soaked conditions and consequently the vertical strain approach was not considered appropriate for designing permeable pavements.

Shear stress data has not been directly measured for ANY materials in the field because there is currently no instrument that can effectively measure shear stresses in a pavement structure. In the laboratory, shear stresses for all materials are calculated based on assumptions about the material and mechanics. Only limited shear strength data is available from laboratory tests on open-graded bases. Similarly, there is very little laboratory or field data to support a strain based rutting model for open graded bases. Given these limitations, the stress/strength ratio concept was considered the most robust approach to accommodate the high stress to strength ratios, and higher allowable ruts that are part of designing permeable pavements.

4.3.2 Shear Stress/Strength Ratio

Shear stress/strength ratio is defined as the ratio between the applied shear stress (τ_f) and the material shear strength (τ_{max} [$\tau_{max} = c + \sigma_f \tan\phi$ in a triaxial strength test, where c is the cohesion of the material]) on the failure plane at a specific applied normal and confining stress state *(8)*. The normal and shear stresses (σ_f and τ_{max}) acting on a failure plane (oriented at an angle of $45° + \phi/2$, where ϕ is the internal friction angle of the material) can be calculated according to the Mohr-Coulomb failure theory for specific confining (σ_3) and deviator (σ_d) stresses applied to a laboratory specimen during triaxial testing.

Materials with lower shear stress/strength ratios are less likely to fail due to shear (i.e., rutting and permanent deformation) than materials with higher shear stress/strength ratios. Research studies *(11,12)* have shown that materials subjected to shear stress/strength ratios higher than 0.7 are likely to accumulate high permanent deformation and present a higher rutting risk, leading to rapid shear failure in the pavement. Materials with shear stress/strength ratios between 0.3 and 0.7 represent a medium risk with a steady but reasonable rate of rutting, while those with shear stress/strength ratios less than about 0.3 are expected to have little or no rutting after an initial small "bedding-in" rut. Based on these findings, the following three shear stress/strength ratio design variable categories aligned to the level of rutting risk were defined for permeable interlocking concrete pavements *(1,9)*:

- SSR < 0.3, low risk of rutting;
- 0.3 ≤ SSR ≤ 0.7, medium risk of rutting;
- SSR > 0.7, high risk of rutting.

The equations used to calculate the SSR corresponding to the stress state applied during triaxial testing or other conditions are listed below:

$$Shear\ Stress/strength\ Ratio\ (SSR) = \frac{\tau_f}{\tau_{max}} \quad (4.1)$$

$$\tau_f = \frac{\sigma_1 - \sigma_3}{2} cos\phi = \frac{\sigma_d}{2} cos\phi \quad (4.2)$$

$$T_{max} = c + \sigma_f tan\phi \quad (4.3)$$

$$\sigma_f = \frac{\sigma_1 + \sigma_3}{2} - \frac{\sigma_1 - \sigma_3}{2} sin\phi = \frac{\sigma_d + 2\sigma_3}{2} - \frac{\sigma_d}{2} sin\phi \quad (4.4)$$

Where: τ_{max} is applied shear stress acting on the failure plane oriented at an angle of 45° + ϕ/2;
σ_f is applied normal stress acting on the failure plane oriented at an angle of 45° + ϕ/2;
τ_f is shear strength of the material under a certain stress state;
σ_1 and σ_3 are the major and minor principal stresses, respectively;
σ_d is the deviator stress, $\sigma_d = \sigma_1 - \sigma_3$;
c is the cohesion of the material;
ϕ is the internal friction angle of the material (ϕ = 0 for stress-independent materials).

4.4 Critical Responses

In mechanistic analyses, the major and minor principal stresses (σ_1 and σ_3) on top of the base and subgrade layers are the critical responses required for calculating the shear stress/strength ratio for designing permeable interlocking concrete pavements. These stresses can be calculated using multilayer linear elastic theory. The *OpenPave* software program *(13)* was used for these analyses.

4.5 Input Parameters for Mechanistic Modeling and Structural Analysis

The input parameters used in the mechanistic modelling and structural analysis are summarized in Table 4.1 and discussed in the following sections. Where appropriate, worst case conditions were assumed (i.e., soaked subgrade, maximum legal axle load, etc.).

4.5.1 Pavement Structure

A standard permeable interlocking concrete pavement structure with the following layers was used in the mechanistic analysis:

- Surface (interlocking concrete paver, 80 mm thick)
- Bedding layer (ASTM #8 aggregate, 50 mm thick)
- Base layer (ASTM #57 aggregate, 100 mm thick)
- Subbase layer (ASTM #2 aggregate, with varying thickness)
- Subgrade soil

Table 4.1: Summary of Input Factorials for Performance Modeling of PICP

Variable	Surface		Base			Subgrade		Axle Type	Axle Load (kN)	Stress Location
	Thickness (mm)	Stiffness (MPa)	Thickness (mm)	Stiffness (MPa)	c, ϕ (kPa, °)	Stiffness (MPa)	c, ϕ (kPa, °)			
Label	h1	E1	h2	E2	c, ϕ	E3	c, ϕ	AT	AL	SL
Value	80	200 500 1,000 2,000	300 450 600 750 900 1,050 1,200 1,350 1,500	60 90 120 180	45, 0	20 50 100 150	10, 20 and 0 15, 25 and 0 20, 30 and 0 25, 35 and 0	Dual Single	89	UW[1] BW[2]
Factorial Levels	1	4	9	4	1	4	2	1	1	2
Total Calculations	2,304									

[1] UW = under wheel [2] BW=between wheel

Given that the bedding and base layers are more a function of construction, providing intermediate levelling layers between the coarse subbase aggregate and the concrete pavers, rather than different shear strengths, all of the aggregate layers (bedding, base, and subbase) were integrated into one nominal aggregate base (AB) layer and assumed to have similar strength properties (a range of strength properties was used). Nine different thicknesses of this nominal aggregate base (AB) layer, ranging from 300 mm to 1,500 mm (12 in. to 59 in.), were used in the mechanistic analysis.

4.5.2 Materials Properties

The material properties used in the mechanistic analysis include stiffness and Poisson's ratio for each layer in the pavement structure, and cohesion and internal friction angle of the base aggregate and subgrade soil materials. These properties were selected from the analyses discussed in Chapter 3 and from the results of other studies documented in the literature. No laboratory testing to measure actual material properties were undertaken in this study.

Four different stiffnesses were selected for each layer (surface, base and subgrade) based on the backcalculated effective stiffnesses discussed in Chapter 3:

- Surface (pavers): 200, 500, 1,000, and 2,000 MPa
- Base (combined bedding and base layers): 60, 90, 120, and 180 MPa
- Subgrade: 20, 50, 100, and 150 MPa

The Poisson's ratio for each layer was assumed to be 0.35 based on measurements documented in other studies *(8,10)*.

The cohesion and internal friction angle (c, ϕ) of the aggregate base material was assumed to be 0 kPa and 45° respectively, based on a review of the literature *(8,10)*. For the subgrade material, both non-zero ($\phi \neq 0$) and zero ($\phi = 0$) internal friction angles were used in the analysis for all stiffness levels to simulate drained and soaked, undrained soil conditions, respectively. Based on a review of the literature *(14-18)*, the subgrade cohesion and internal friction angles (c, ϕ) were set at the following levels for each of the four subgrade stiffnesses:

- 20 MPa: 10 kPa and 20° and 0°
- 50 MPa: 15 kPa and 25° and 0°
- 100 MPa: 20 kPa and 30° and 0°
- 150 MPa: 25 kPa and 35° and 0°

4.5.3 Traffic Load

A single rear axle with dual wheels was used in the analysis. The axle load was set at 89 kN (20,000 lb.) and the tire pressure was set at 700 kPa (101 psi, which is the tire pressure used in accelerated

load tests). The distance between the two tire centers was set at 340 mm (13.4 in.). The stress under the wheel and the stress between the wheels were both calculated to identify the most critical stress.

4.6 Mechanistic Analysis Results

4.6.1 Base Layer

The results of the mechanistic analysis for the different base layer (combined bedding and base layers) stiffness values and thicknesses include the major and minor principal stresses, normal stress at the failure plane, shear strength at the selected stress state, shear stress at the failure plane, and the shear stress/ strength ratio at the failure plane at the top of the base layer. The results are plotted in Figure A.1 though Figure A.6 in Appendix A. The results indicate that, according to the multilayer linear elastic design theory, an increase in the thickness of the base layer does not necessarily reduce the stresses at the top of that layer.

4.6.2 Subgrade Layer

The results of the mechanistic analysis for the subgrade layer included the same parameters used in the base layer analysis, except that the shear stress/strength ratio at the top of the subgrade was calculated. The results are plotted against the different stiffness values for each layer, the different base thicknesses (combined bedding and base layers), and the internal friction angle of the subgrade in Figure A.7 through Figure A.18 in Appendix A. The results indicate that increasing the thickness of the base layer (specifically the coarse ASTM #2 aggregate layer given that this is the "strong" material) reduces the stresses (absolute values) at the top of the subgrade soil layer, as expected.

During dry conditions, when the subgrade is relatively dry (or at equilibrium moisture content) and has a nonzero internal friction angle ($\phi \neq 0$), the shear strength of the subgrade soil changes with the thickness of the base layer (Figure A.11). Interestingly, the effective shear strength of the subgrade soil decreases slightly as the thickness of the base layer increases. This is attributed to the effective shear strength of subgrade soils being positively correlated with the normal stress at the failure plane under dry conditions ($\phi \neq 0$) (as defined in Equation 4.3). An increase in the thickness of the base layer significantly reduces the normal stress at the failure plane at the top of the subgrade soil layer (Figure A.9), and consequently, the effective shear strength of the subgrade soil decreases slightly as the thickness of the base layer increases.

Under wet conditions (i.e., when the subgrade is soaked and has a zero internal friction angle [$\phi = 0$]), the effective shear strength of subgrade soils does not change with the thickness of the base layer (as shown in Figure A.12). This is because the shear strength of materials with zero internal friction angle is

independent of the normal stress applied and is determined only by the cohesion of the material (as defined in Equation 4.3). Therefore, soaked subgrade soils will have constant effective shear strength regardless of an increase in the thickness of the base layer. The effective shear strength will be equal to the cohesion of the material which is slightly lower than the effective shear strength of the subgrade soil under dry conditions.

The normal stress and the shear stress are both higher under wet conditions than those under dry conditions for an identical structure and identical material properties (Figure A.9, Figure A.10, Figure A.13, and Figure A.14). The shear stress/strength ratio under wet conditions is also higher than the shear stress/strength ratio under dry conditions for an identical structure and identical material properties (Figure A.15 and Figure A.17), as expected. This confirms that wet conditions are the most critical condition influencing rutting and permanent deformation in subgrade layers in pavements with permeable interlocking concrete paver surfaces.

Figure A.16 and Figure A.18 show that the shear stress/strength ratio in log scale has a good linear relationship with the thickness of the base layer (combined bedding and base layers).

4.6.3 Thickness of Base Layers for Different Shear Stress/Strength Ratio Values

Based on the results discussed above, the base layer thicknesses with shear stress/strength ratios of 0.8 (i.e., >0.7), 0.5 (i.e., intermediate between 0.3 and 0.7 [$0.3 \leq SSR \leq 0.7$]), and 0.2 (i.e., <0.3), representing different rutting risk levels, were estimated using interpolation of the different material properties and subgrade moisture conditions. The results are presented in Figure 4.1 and Figure 4.2. The main observations with regard to required base layer thicknesses include:

- Higher shear stress/strength ratios, which equate to a higher risk of rutting, require thicker base layers, as expected.
- For the same shear stress/strength ratio, an increase in the effective stiffness of the base layer reduces the required thickness of that base layer, especially when the subgrade layer has a low stiffness.
- An increase in the stiffness of the surface layer reduces the required base layer thickness to achieve the same shear stress/strength ratio. However, the effect of the surface layer stiffness is not significant due to the relatively low thickness of the pavers (80 mm).
- For the same shear stress/strength ratio, wet conditions require thicker base layers compared to the dry condition, confirming that undrained wet conditions are the most critical condition for design.
- The theoretical optimal design base thicknesses (combined bedding, base, and subbase layers) for low, intermediate, and higher risk levels (subgrade shear stress/strength ratios of 0.2, 0.5 and 0.8, respectively) under dry subgrade moisture conditions are approximately 1,300 mm, 800 mm, and 500 mm (51 in., 32 in., and 20 in.), respectively. In wet conditions, the theoretical optimal design thicknesses increase to 1,400 mm, 1,000 mm and 600 mm (55 in., 39 in., and 24 in.), respectively.

4.7 Preliminary Design Tables

Given that no laboratory testing was undertaken in this study, that only limited data was collected from the field sections, and that all testing on pavers was done under dry conditions, the development of preliminary design tables (part of Task 3 of this study) was postponed until additional response data under controlled prolonged trafficking on the test track has been collected.

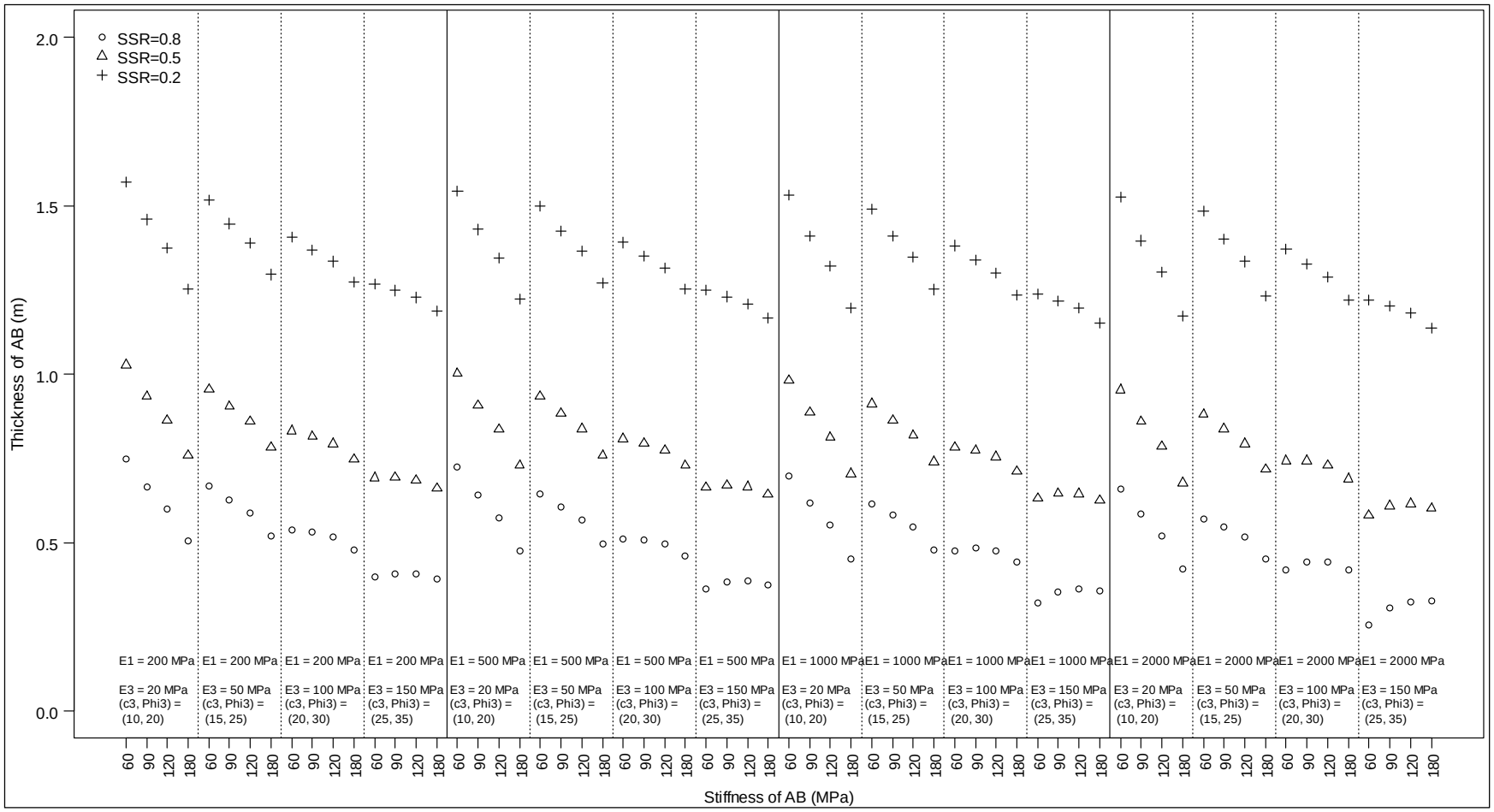

Figure 4.1: Suggested base layer thicknesses for different shear stress/strength ratios ($\phi \neq 0$ [dry]).

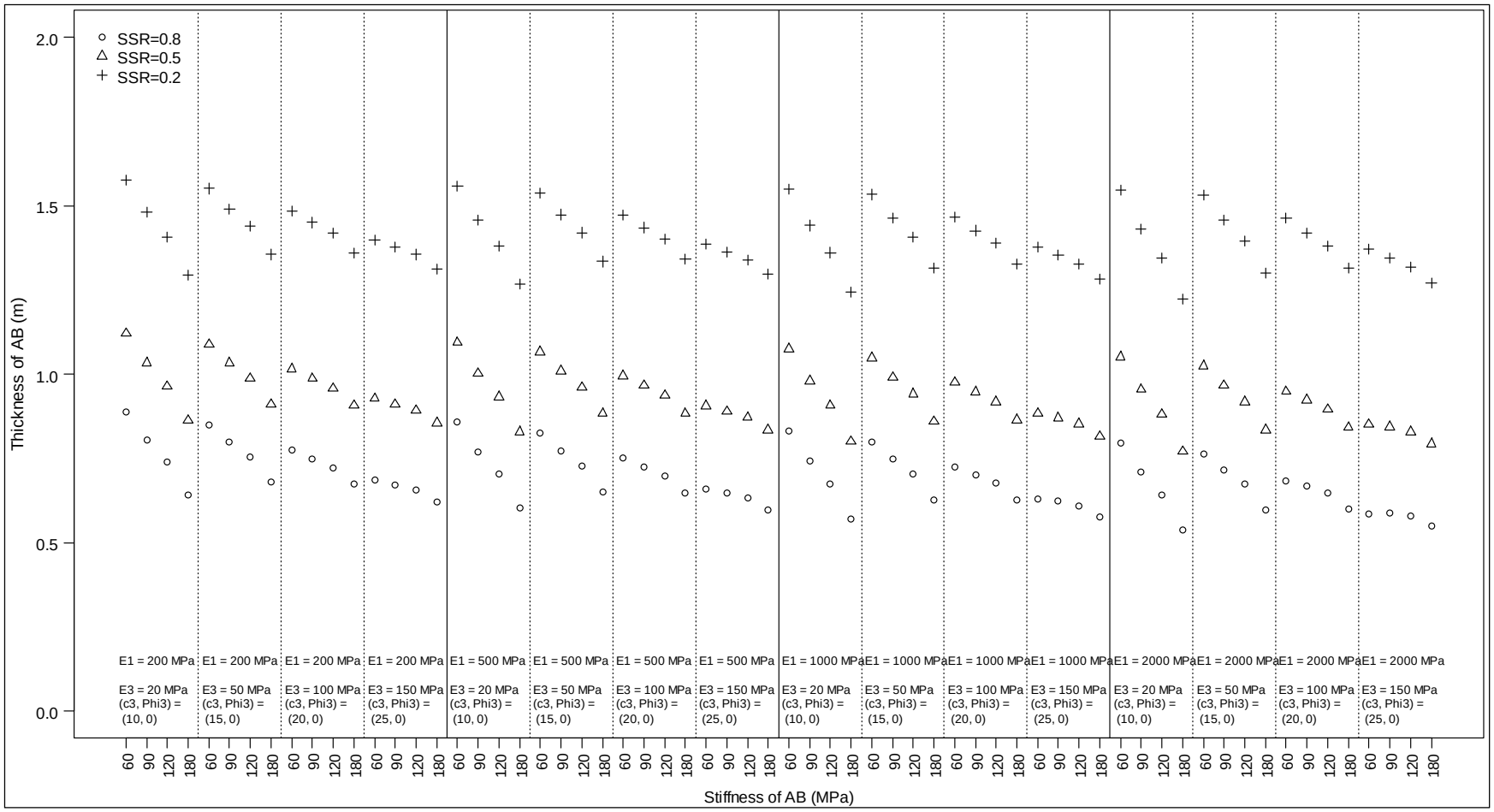

Figure 4.2: Suggested base layer thicknesses for different shear stress/strength ratios (ϕ = 0 [wet]).

5. TEST PLAN FOR THICKNESS VALIDATION

5.1 Thickness Design

A test track design was developed using the results from the mechanistic analysis. The theoretical optimal design base thicknesses (combined bedding, base, and subbase layers) for the three different subgrade shear stress/strength ratios (0.8, 0.5 and 0.2) under dry conditions are approximately 500 mm, 800 mm and 1,300 mm (20 in., 32 in., and 51 in.), respectively. In wet conditions, the theoretical optimal design thicknesses increase to 600 mm, 1,000 mm and 1,400 mm (24 in, 40 in., and 56 in.), respectively. Based on these results, three subbase (i.e., coarse aggregate [ASTM #2]) thicknesses of 450 mm, 650 mm, and 950 mm (18 in., 26 in., and ~38 in.), were selected for the accelerated load test pavement design to provide high, intermediate, and low risk scenarios (Figure 5.1). The bedding layer (#8 stone) and base layer (#57 stone) thicknesses were fixed at 50 mm and 100 mm (2 in. and 4 in.), respectively, equating to total structure thicknesses of 600 mm, 800 mm, and 1,100 mm (24 in., 32 in., and 44 in.) for the three sections. These subbase layer thicknesses are mostly thinner than the theoretical optimal design thicknesses and were selected to ensure that the performance and behavior of the test track structure could be fully understood within the time and budgetary constraints of the project. The proposed test track design provided to the construction contractor is shown in Figure 5.2. The track design is wide enough for three side-by-side test sections to allow testing under dry and wet conditions, and if required, a third moisture condition.

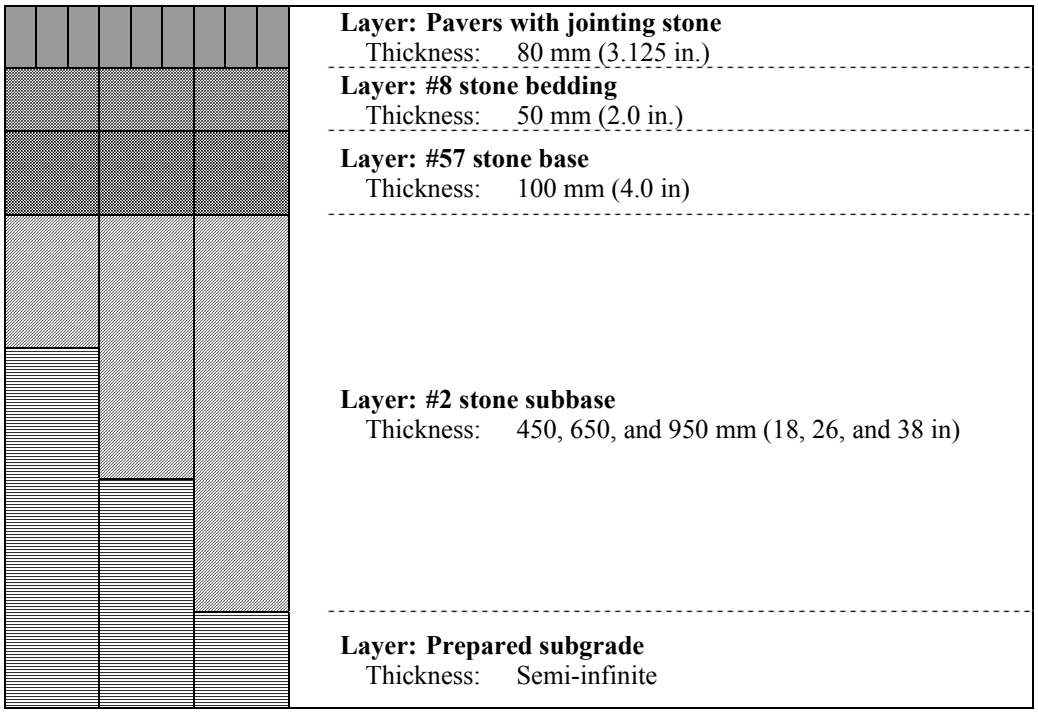

Figure 5.1: Proposed pavement structure for PICP test track (*not to scale*).

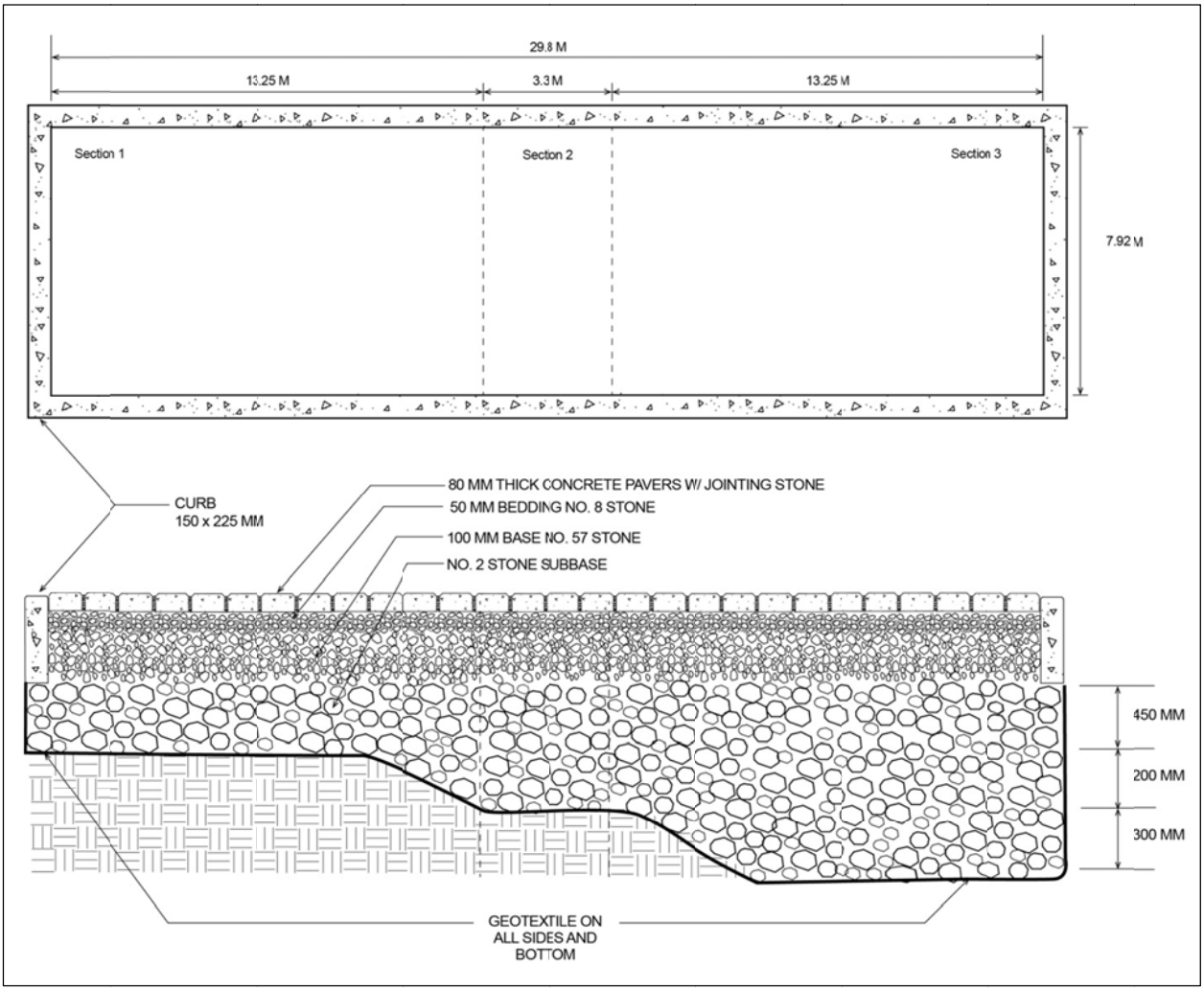

Figure 5.2: Proposed test track design.

5.2 Test Track Instrumentation

Each subsection in each test section will have pressure cells on top of the subgrade and top of the #57 aggregate base layers to measure vertical stress, and a steel reference plate to measure the location of any permanent deformation. Temperatures will be measured at two different locations on the test track (east and west side of the test section). At each location, ambient temperatures and temperatures of the pavement surface and pavement at 25 mm depth will be measured.

Additional manual measurements include profile (laser profilometer) to evaluate surface rutting, surface deflection (road surface deflectometer), and subbase water content (dipstick).

5.3 Heavy Vehicle Simulator Test Plan

5.3.1 Test Sections

At least two test sections, with three subsections in each section, will be tested. The first section will be tested dry, the second after soaking with water. Space for a third test is available between these two sections if additional testing is required; however, this third section is not instrumented.

5.3.2 Loading Plan

Test loads will start at 25 kN (5,600 lb). This load will be maintained until responses (deflection and strain) and rut depth rate increase have stabilized. The load will then be increased to 40 kN (9,000 lb) and maintained at that level until responses and rut depth rate increase have again stabilized. Depending on test track performance, the load may be increased to higher levels to accelerate the loading. Load increment levels will be 60 kN (13,500 lb), 80 kN (18,000 lb), and 100 kN (22,500 lb). The same loading plan will be followed on the dry and wet tests.

All testing will be done with a dual wheel configuration with a tire pressure of 700 kPa (101 psi). Trafficking will be bi-directional at a speed of 10 km/h (6 mph).

5.3.3 Environmental Control

All testing will be conducted at ambient conditions. Water levels in the subbase will be monitored with dipsticks. In the wet test, water will be applied to the surface of the test track and allowed to infiltrate until it overtops the surface. Thereafter, the water level will be maintained at the top of the #2 stone subbase (i.e., top of the reservoir layer) for the duration of load testing to simulate worst case conditions. If time and funds permit, a third test will be conducted after water has drained from the #2 stone subbase (i.e., no water in the reservoir layer, but subgrade will be moist) to simulate intermediate conditions.

5.3.4 Measurements

Measurements will be taken after every 10,000 load repetitions, or more regularly if dictated by performance. These periodic measurements include a visual evaluation, profile, deflections, and permanent deformation at the top of the #57 aggregate base and top of the subgrade. Temperatures and strain measurements from the pressure cells will be measured continuously during trafficking.

Blank page

6. SUMMARY AND RECOMMENDATIONS

6.1 Summary

This report details field testing of existing projects and test sections, estimation of the effective stiffness of each layer in permeable interlocking concrete pavement structures, and mechanistic analysis and structural design of a test track to validate the design approach using accelerated loading. Key findings from the study include:

- Higher shear stress/strength ratios, which equate to a higher risk of rutting, require thicker base layers, as expected.
- For the same shear stress/strength ratio, an increase in the stiffness of the base layer reduces the required thickness of that base layer, especially when the subgrade layer has a low stiffness.
- An increase in the stiffness of the surface layer reduces the required base layer thickness to achieve the same shear stress/strength ratio. However, the effect of the surface layer stiffness is not significant due to the relatively low thickness of the pavers (80 mm).
- For the same shear stress/strength ratio, wet conditions require thicker base layers compared to the dry condition, confirming that wet conditions are the most critical condition for design.
- The theoretical optimal design base thicknesses (combined bedding, base, and subbase layers) for low, intermediate, and higher risk levels (subgrade shear stress/strength ratios of 0.2, 0.5 and 0.8, respectively) under dry subgrade moisture conditions are approximately 1,300 mm, 800 mm, and 500 mm (51 in., 32 in., and 20 in.), respectively. In wet conditions, the theoretical optimal design thicknesses increase to 1,400 mm, 1,000 mm and 600 mm (55 in., 39 in., and 24 in.), respectively.

6.2 Recommendations

The following interim recommendations are made based on the findings from this study:

- Based on the mechanistic analysis, three subbase (i.e., coarse aggregate [ASTM #2]) thicknesses of 950 mm, 650 mm, and 450 mm (~38 in., 26 in., and 18 in.) should be tested to assess low, intermediate, and higher risk designs. The bedding layer (#8 stone) and base layer (#57 stone) thicknesses should be fixed at 50 mm and 100 mm (2 in. and 4 in.), respectively.
- The shear stress/strength ratio is considered to be an appropriate parameter for assessing the rutting risk in subgrade layers in permeable interlocking concrete pavement. This approach needs to be validated and calibrated in the accelerated load testing phase of this study.
- The mechanistic analysis predicted that an increase in base layer thickness will theoretically not reduce the stresses and the shear stress/strength ratio value of the base/subbase layer in permeable interlocking concrete pavements. This finding needs to be validated in the accelerated load testing phase of this study.
- Models are needed to quantify the rut depth on permeable interlocking concrete pavements for a given number of load repetitions for various base and subgrade configurations. Preliminary models should be developed using the results from the accelerated load testing phase of this study.

Blank page

REFERENCES

1. JONES, D., Li, H. and Harvey, J.T. 2013. **Development and HVS Validation of Design Tables for Permeable Interlocking Concrete Pavement: Literature Review.** Davis and Berkeley, CA: University of California Pavement Research Center. (UCPRC-TM-2013-03).
2. JONES, D., Harvey, J.T., Li, H., Wang, T., Wu, R. and Campbell, B. 2010. **Laboratory Testing and Modeling for Structural Performance of Fully Permeable Pavements under Heavy Traffic: Final Report.** Davis and Berkeley, CA: University of California Pavement Research Center. (UCPRC-RR-2010-05).
3. CHOI, J.W., Wu, R., Pestana, J.H. and Harvey, J. 2010. New Layer-Moduli Back-Calculation Method Based on the Constrained Extended Kalman Filter. **Journal of Transportation Engineering, 136(1).** (pp 20–30).
4. JONES, D., Harvey, J.T., Li, H. and Campbell, B. 2009. **Summary of Laboratory Tests to Assess Mechanical Properties of Permeable Pavement Materials.** Davis and Berkeley, CA: University of California Pavement Research Center. (UCPRC-TM-2009-01).
5. TUTUMLUER, E. and Seyhan, U. 1999. Laboratory Determination of Anisotropic Aggregate Resilient Moduli Using an Innovative Test Device. **Transportation Research Record: Journal of the Transportation Research Board, Vol. 1687.** (pp. 13-21).
6. AYITHI, A. and Hiltunen, D. 2013. Characterization of Moisture-Dependent Changes in Stiffness of Unbound Aggregate Base Materials in Florida. **Transportation Research Record: Journal of the Transportation Research Board, Vol. 2349.** (pp. 25-31).
7. LEA, J.D. Undated. ***EasyDCP*: An Easy Tool for DCP Data Processing.** www.OpenPave.org. Accessed 2013/09/10.
8. CHOW, L.C. and Tutumluer, E. 2014. Framework for Improved Unbound Aggregate Base Rutting Model Development for Mechanistic-Empirical Pavement Design. **Proceedings Transportation Research Board 93rd Annual Meeting.** Washington, D.C: Transportation Research Board.
9. THOMPSON, M., Gomez-Ramirez, F. and Bejarano, M. 2002. Illi-Pave Based Flexible Pavement Design Concepts for Multiple Wheel Heavy Gear Load Aircraft. **Proceedings 9th International Conference on Asphalt Pavements.** Copenhagen, Denmark. International Society of Asphalt Pavements.
10. TUTUMLUER, E., Kim, I. and Santoni, R. 2004. Modulus Anisotropy and Shear Stability of Geofiber-Stabilized Sands. **Transportation Research Record: Journal of the Transportation Research Board, Vol. 1874.** (pp. 125-135).

11. KIM, I. and Tutumluer, E. 2006. Field Validation of Airport Pavement Granular Layer Rutting Predictions. **Transportation Research Record: Journal of the Transportation Research Board, Vol. 1952.** (pp. 48-57).
12. LI, H., Harvey J.T. and Jones, D. 2010. **Summary of a Computer Modeling Study to Understand the Performance Properties of Fully Permeable Pavements.** Davis and Berkeley, CA: University of California Pavement Research Center. (UCPRC-TM-2010-04).
13. LEA, J. undated. **OpenPave: An N-Layer, N-Load, N-Point Multi-Layer Elastic Half Space Calculation.** www.OpenPave.org. Accessed 2013/09/10.
14. DAS, B.M. 2007. **Advanced Soil Mechanics.** New York, NY: Taylor and Francis.
15. NOVA, R. 2012. **Soil Mechanics.** Hoboken, NJ: John Wiley and Sons.
16. CARTER, M. and Bentley, S.P. 1991. **Correlations of Soil Properties.** London, UK: Pentech Press.
17. WNEK, M., Tutumluer, E., Moaveni, M. and Gehringer, E. 2013. Investigation of Aggregate Properties Influencing Railroad Ballast Performance. **Transportation Research Record: Journal of the Transportation Research Board, Vol. 2374.** (pp. 180-189).
18. HUANG, H., Tutumluer, E. and Dombrow, W. 2009. Laboratory Characterization of Fouled Railroad Ballast Behavior. **Transportation Research Record: Journal of the Transportation Research Board, Vol. 2117.** (pp. 93-101).

APPENDIX A: MECHANISTIC ANALYSIS PLOTS

The following mechanistic analysis plots are included in this Appendix:

- Figure A.1: Major principal stress σ_1
- Figure A.2: Minor principal stress σ_3.
- Figure A.3: Normal stress at the failure plane σ_f
- Figure A.4: Shear strength τ_{max}
- Figure A.5: Shear stress at the failure plane τ_f
- Figure A.6: Shear stress/strength ratio at the failure plane SSR
- Figure A.7: Major principal stress σ_1
- Figure A.8: Minor principal stress σ_3
- Figure A.9: Normal stress at the failure plane σ_f ($\phi \neq 0$)
- Figure A.10: Normal stress at the failure plane σ_f ($\phi = 0$)
- Figure A.11: Shear strength τ_{max} ($\phi \neq 0$)
- Figure A.12: Shear strength τ_{max} ($\phi = 0$)
- Figure A.13: Shear stress at the failure plane τ_f ($\phi \neq 0$)
- Figure A.14: Shear stress at the failure plane τ_f ($\phi = 0$)
- Figure A.15: Shear stress/strength ratio at the failure plane SSR ($\phi \neq 0$)
- Figure A.16: Shear stress/strength ratio at the failure plane SSR ($\phi \neq 0$, log scale for SSR)
- Figure A.17: Shear stress/strength ratio at the failure plane SSR ($\phi = 0$)
- Figure A.18: Shear stress/strength ratio at the failure plane SSR ($\phi = 0$, log scale for SSR)

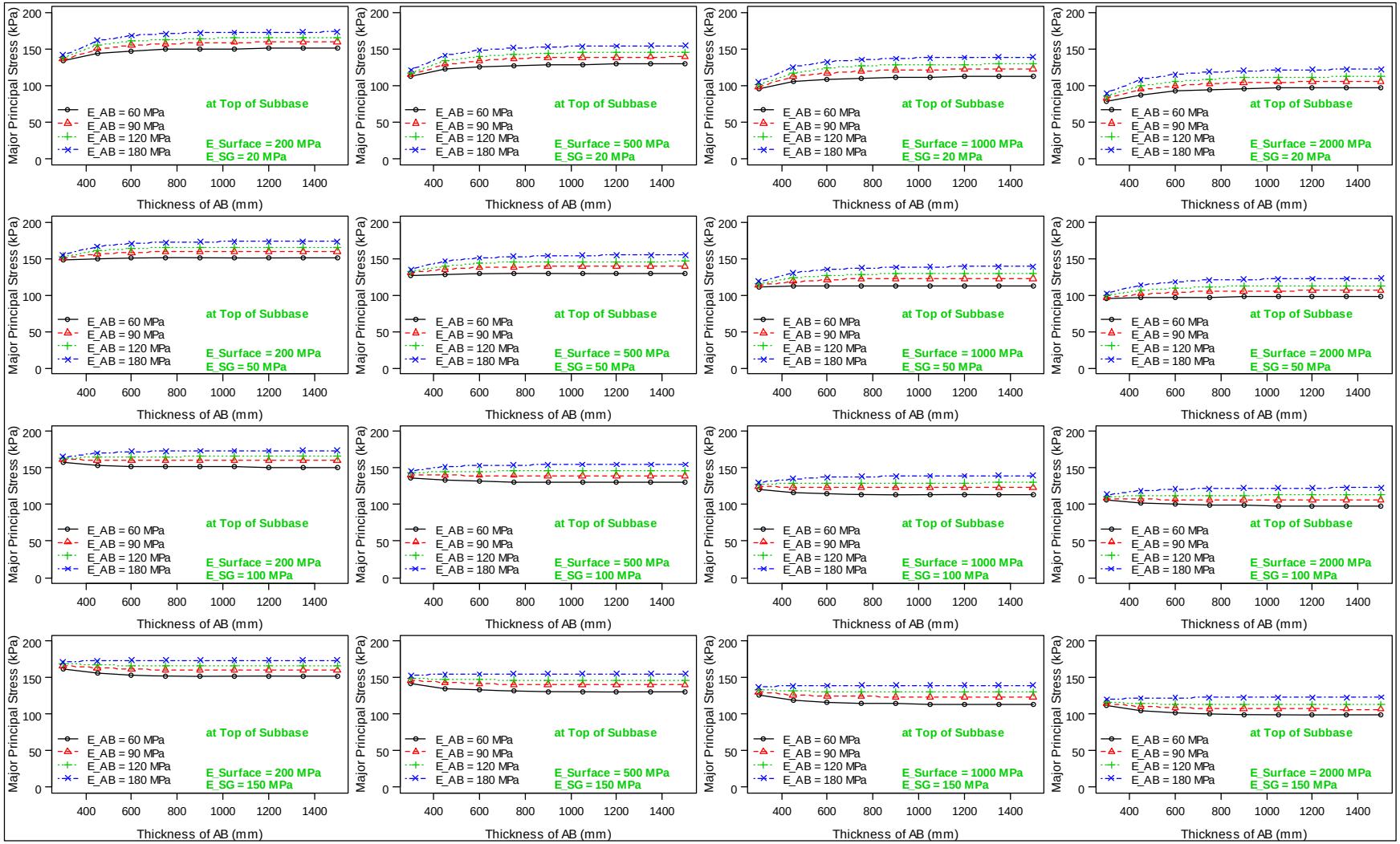

Figure A.1: Major principal stress σ_1.

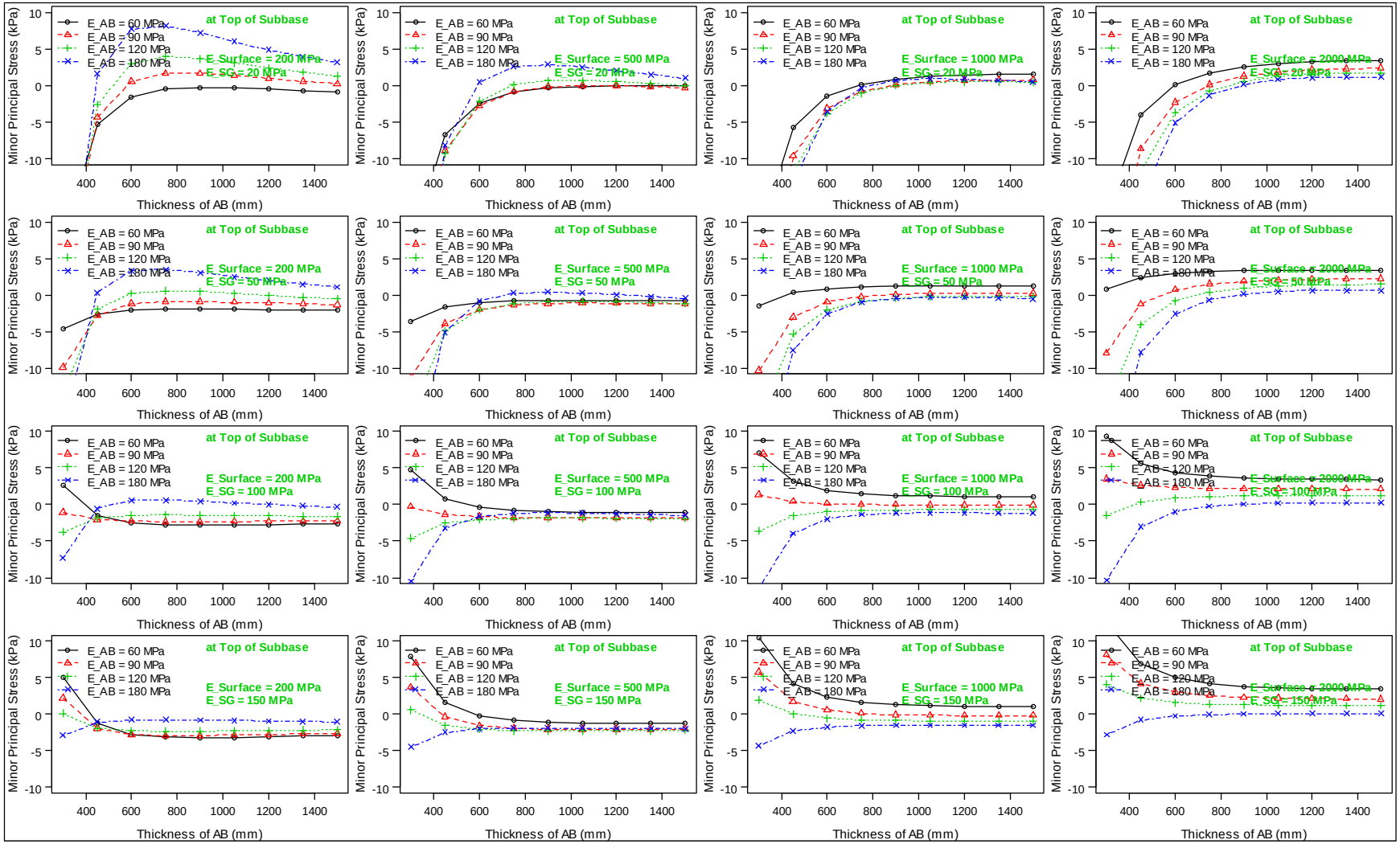

Figure A.2: Minor principal stress σ_3.

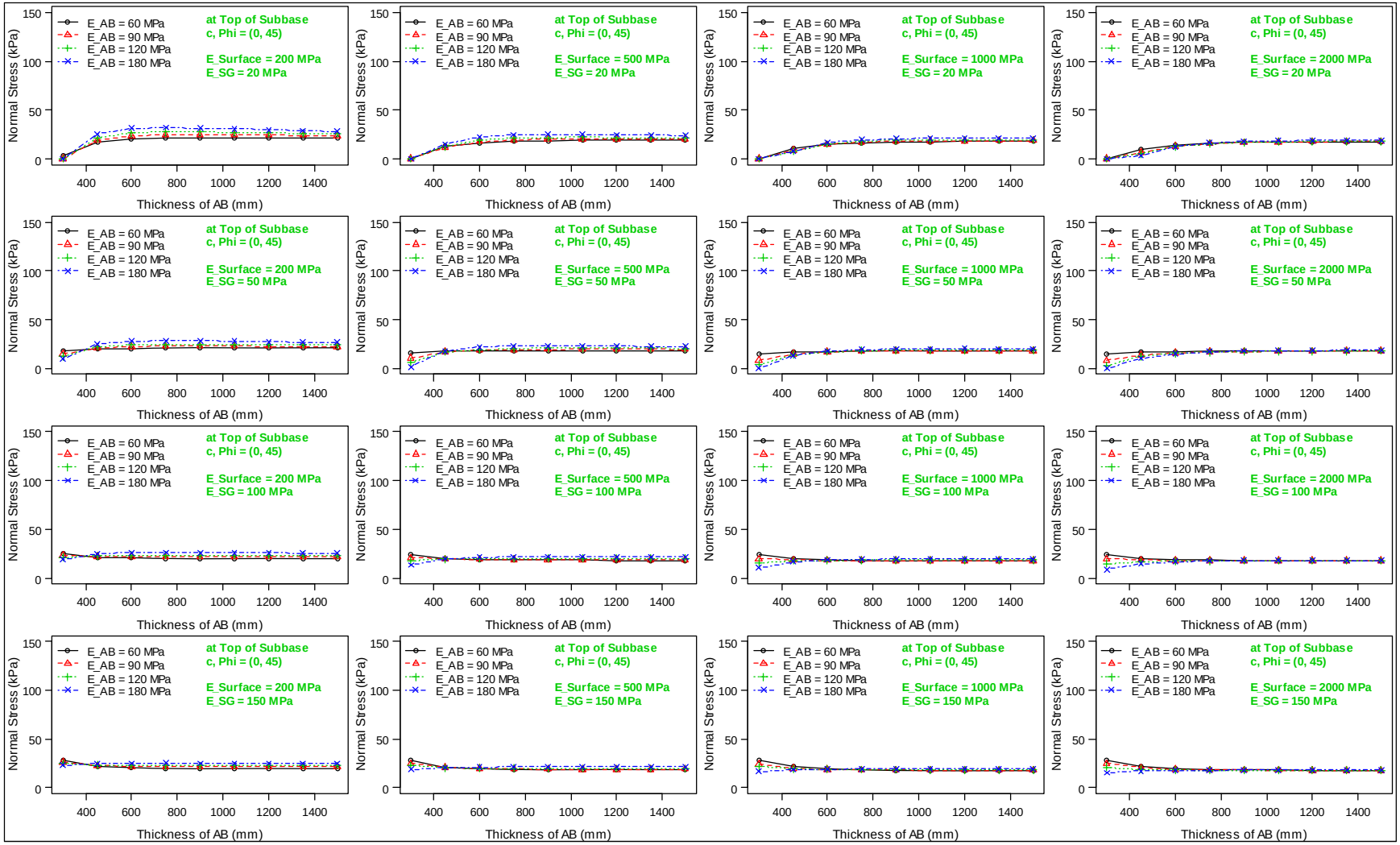

Figure A.3: Normal stress at the failure plane σ_f.

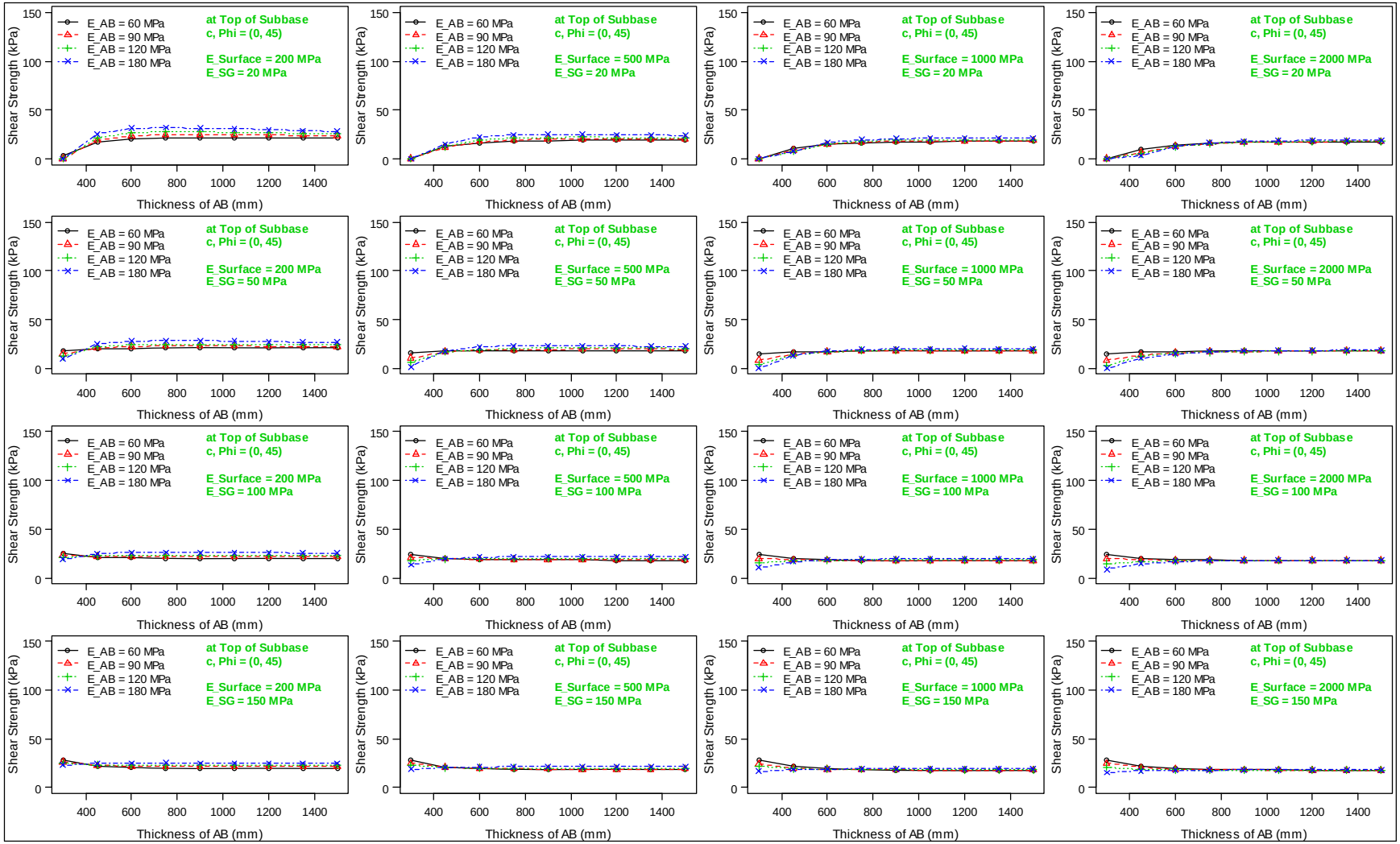

Figure A.4: Shear strength τ_{max}.

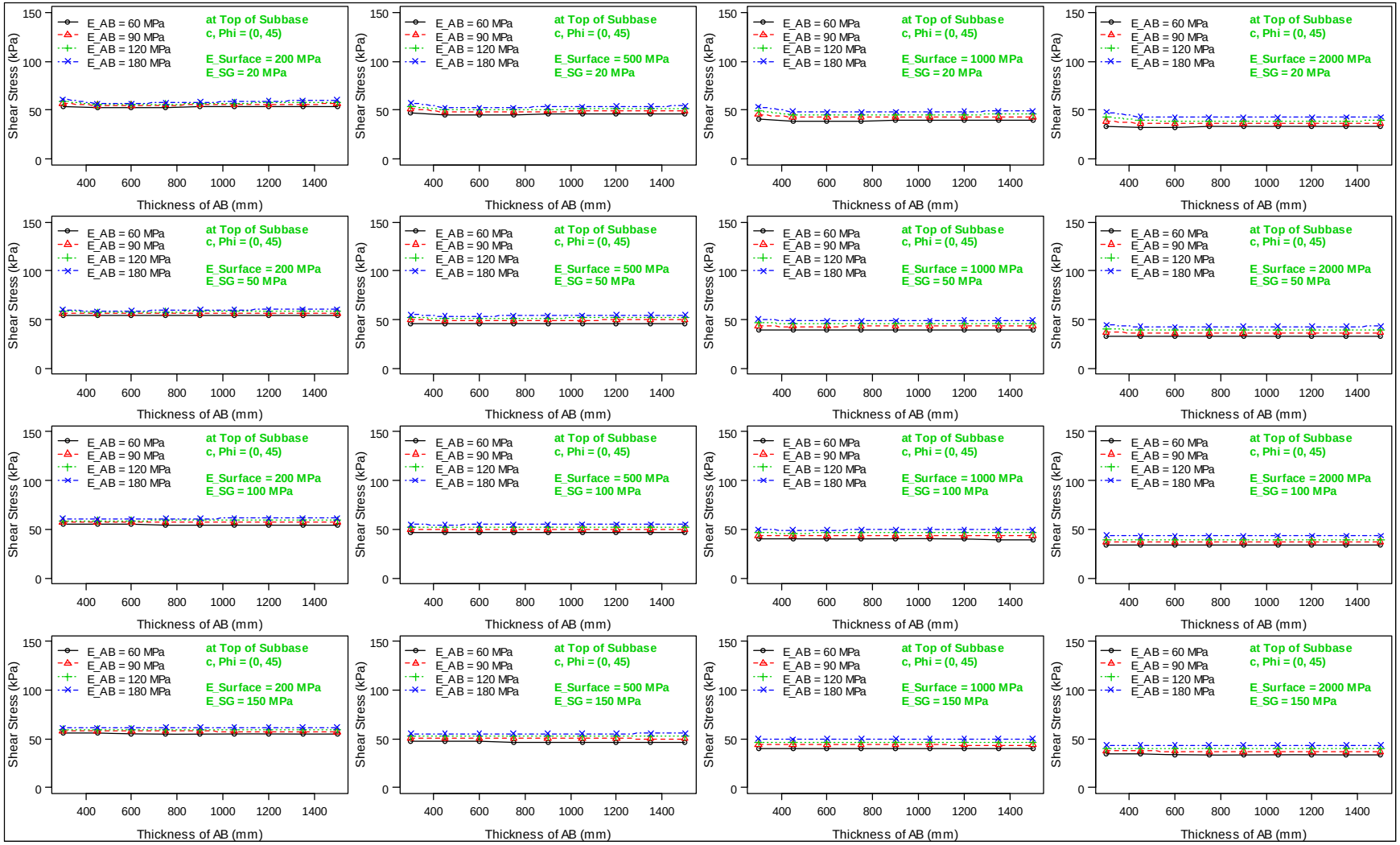

Figure A.5: Shear stress at the failure plane τ_f.

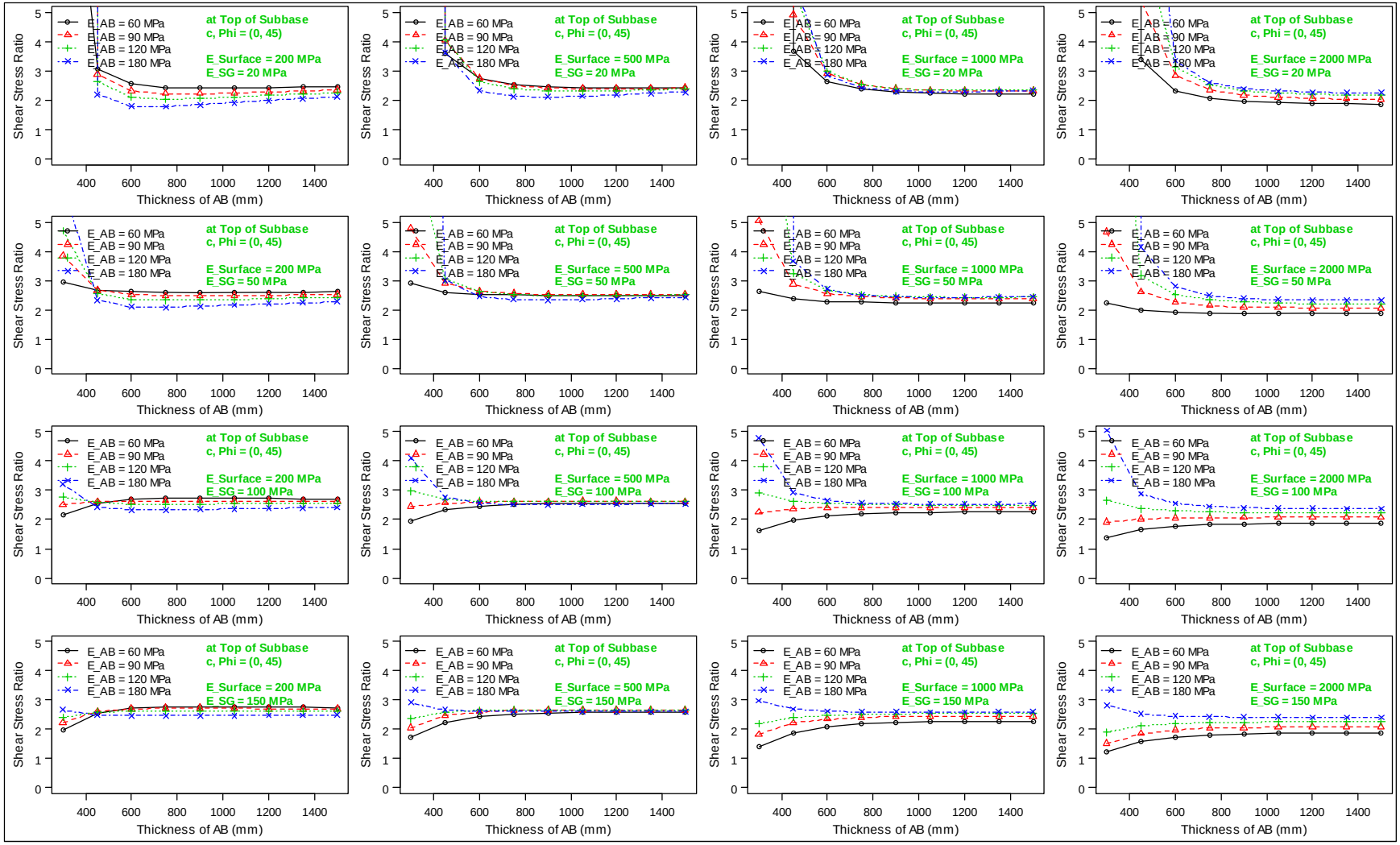

Figure A.6: Shear stress/strength ratio at the failure plane SSR.

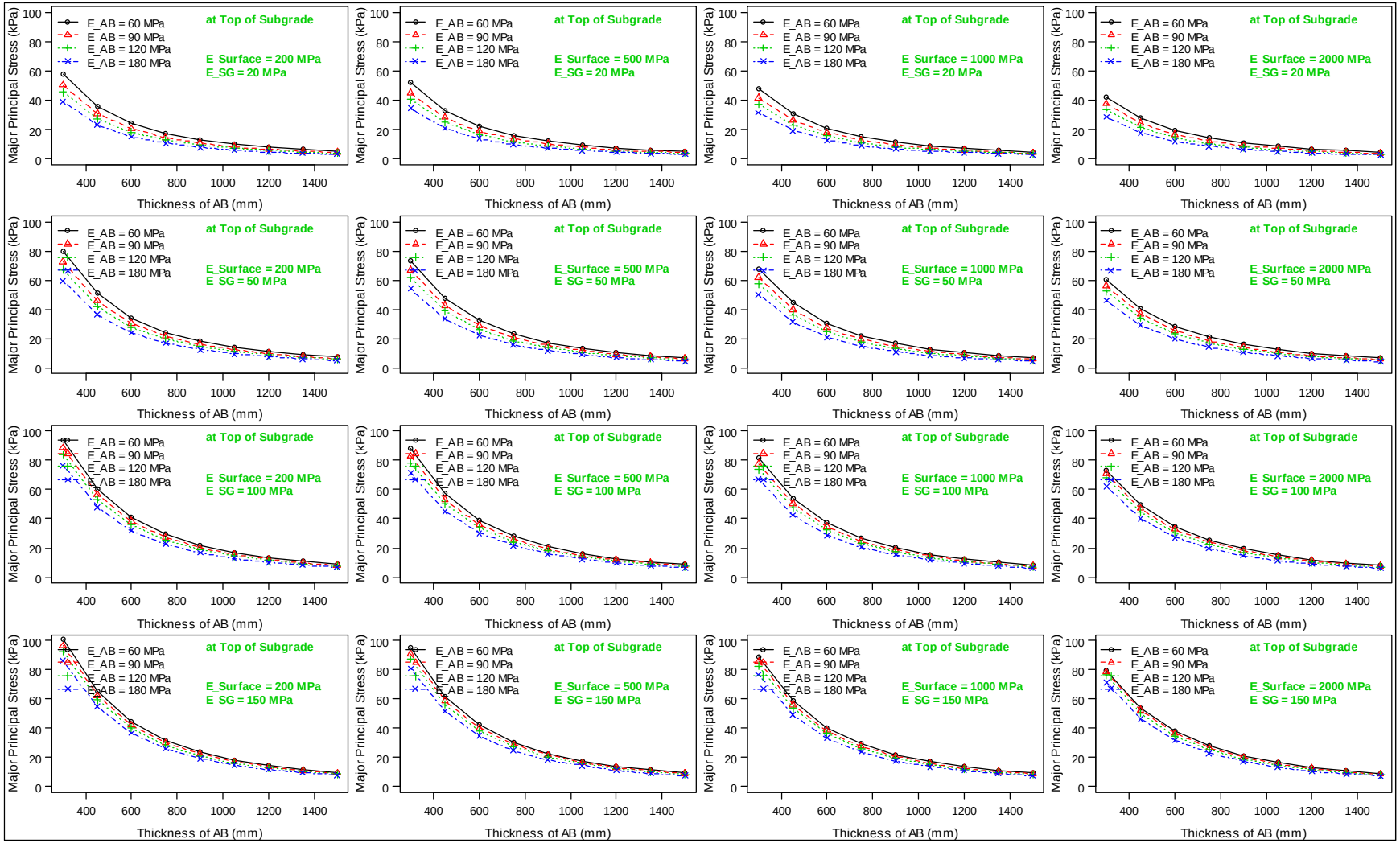

Figure A.7: Major principal stress σ_1.

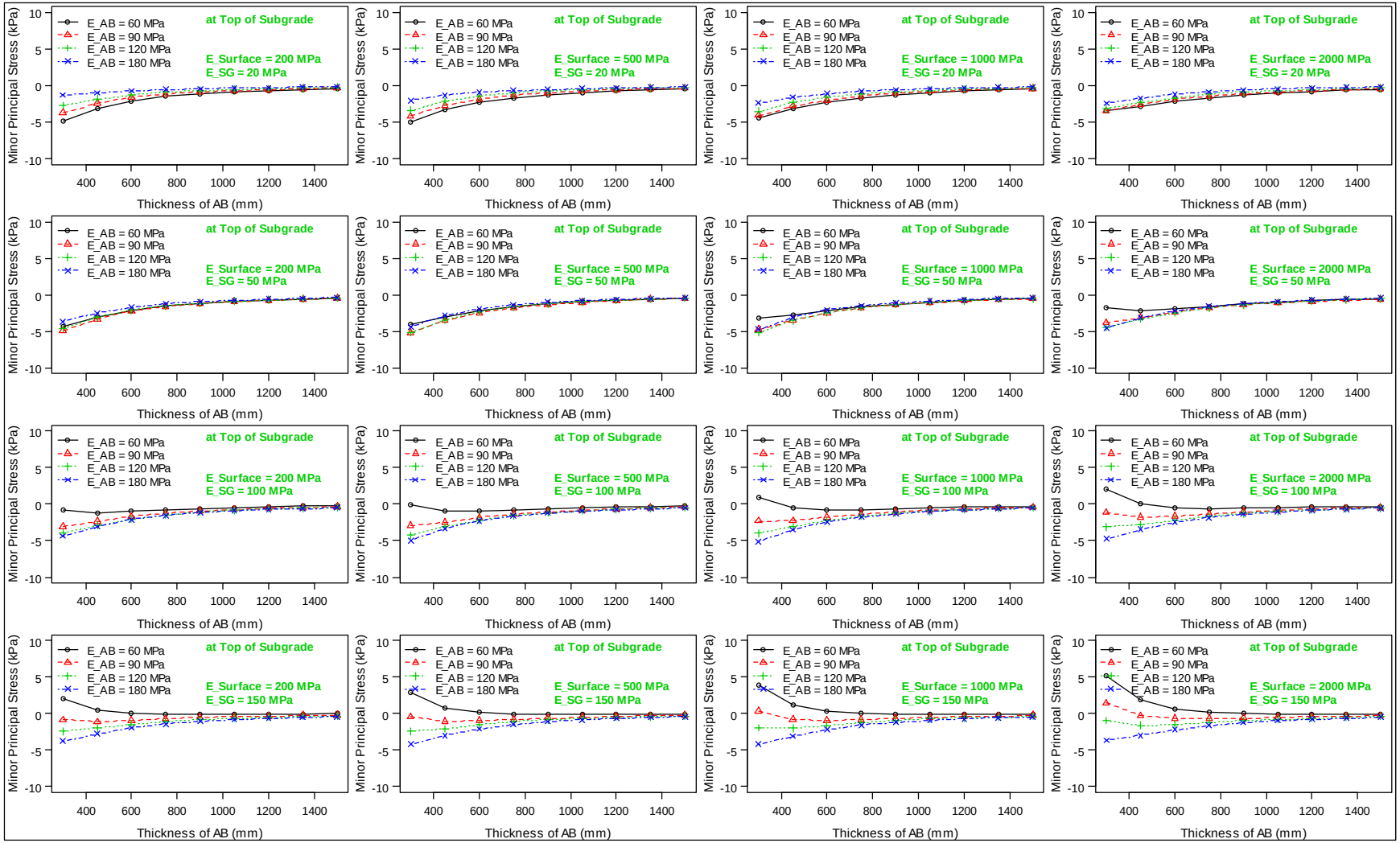

Figure A.8: Minor principal stress σ_3.

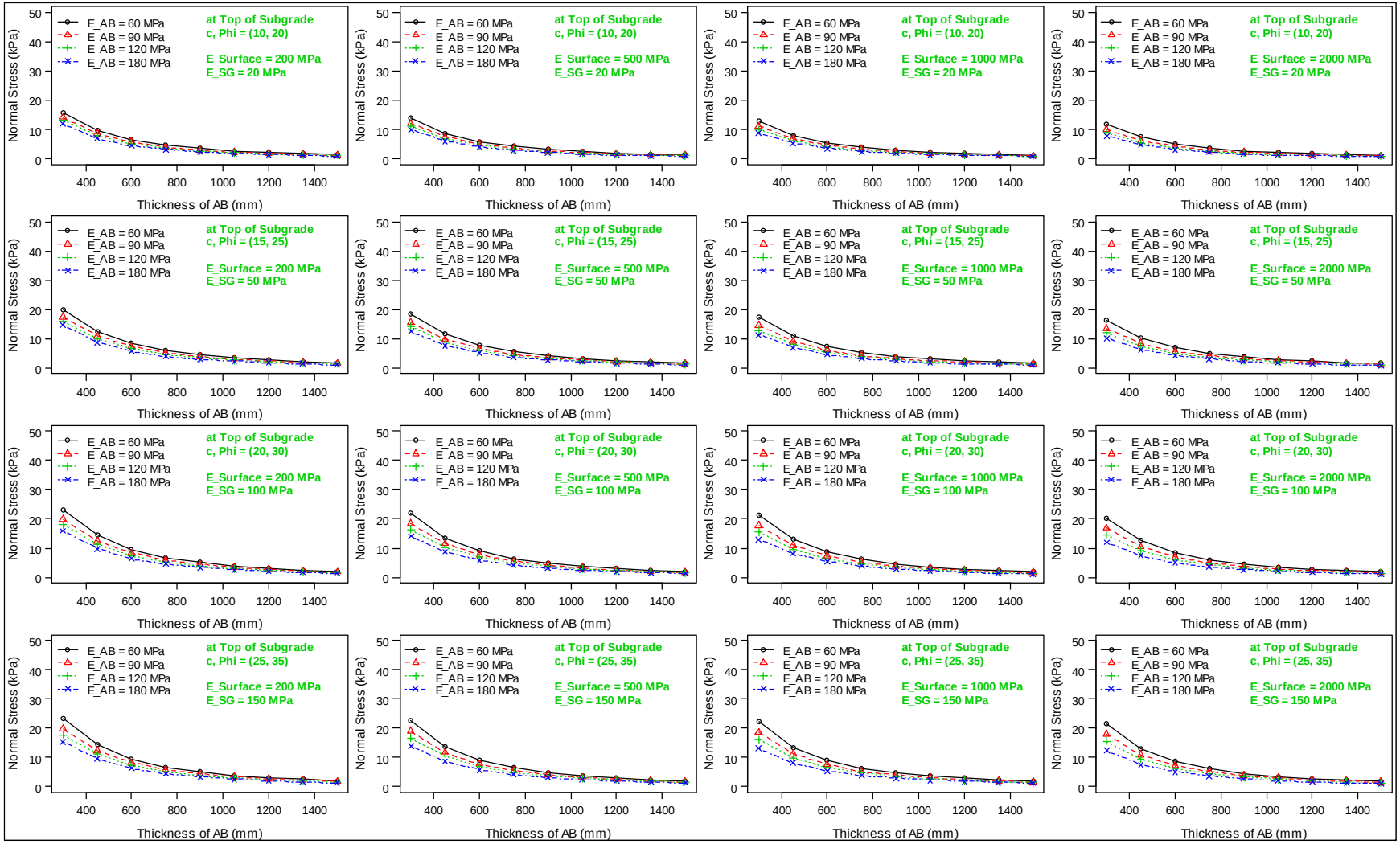

Figure A.9: Normal stress at the failure plane σ_f ($\phi \neq 0$).

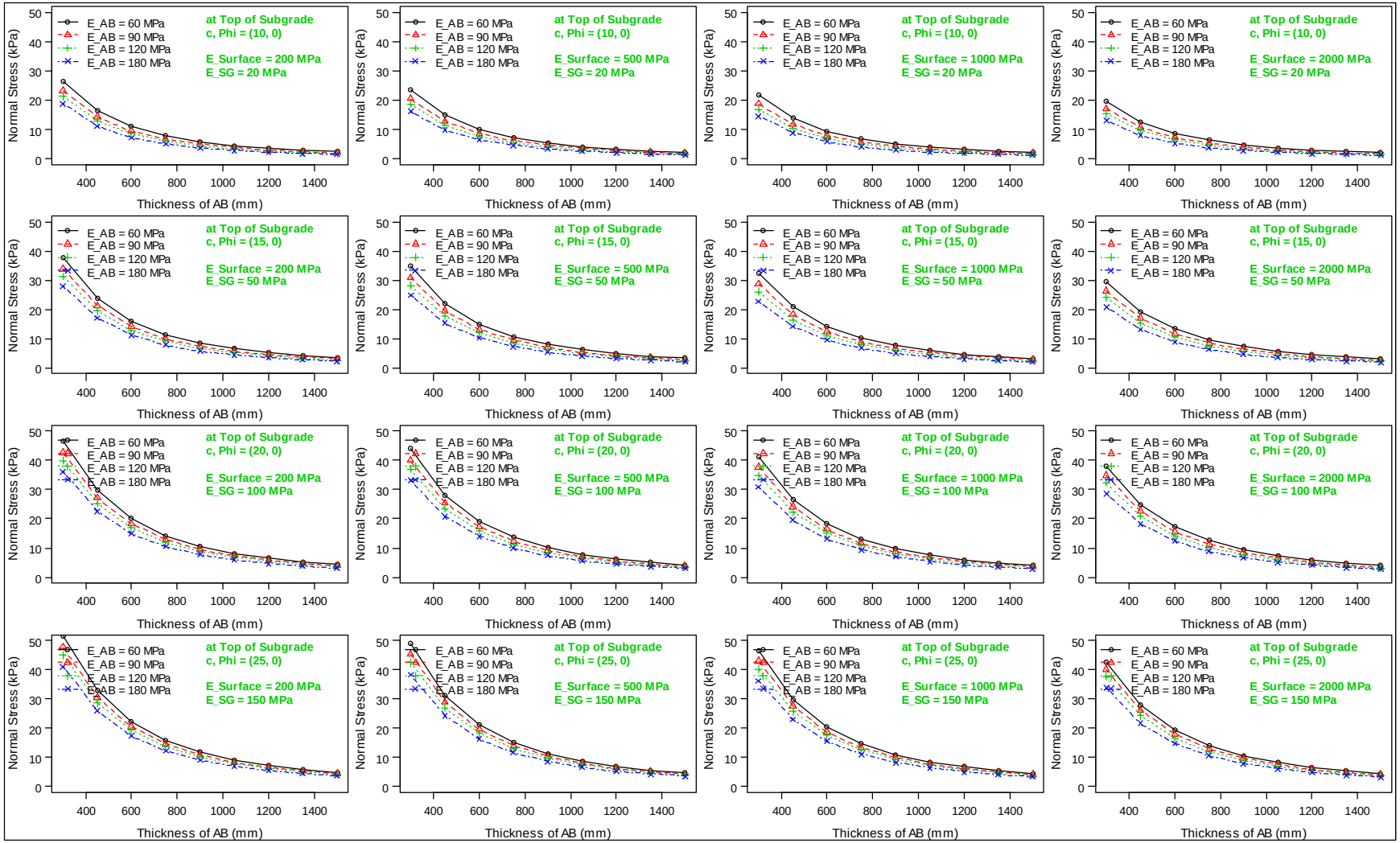

Figure A.10: Normal stress at the failure plane σ_f ($\phi = 0$).

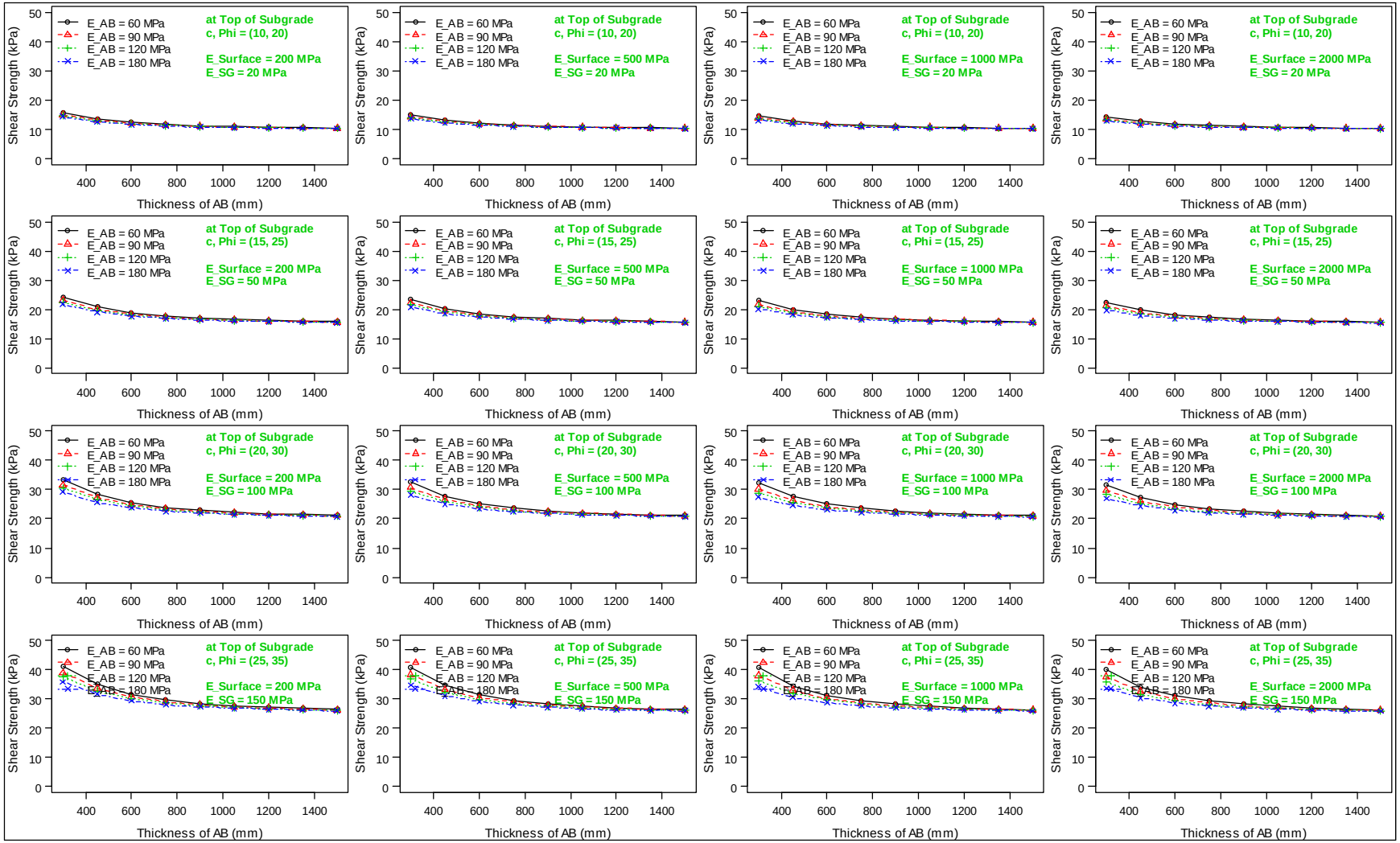

Figure A.11: Shear strength τ_{max} ($\phi \neq 0$).

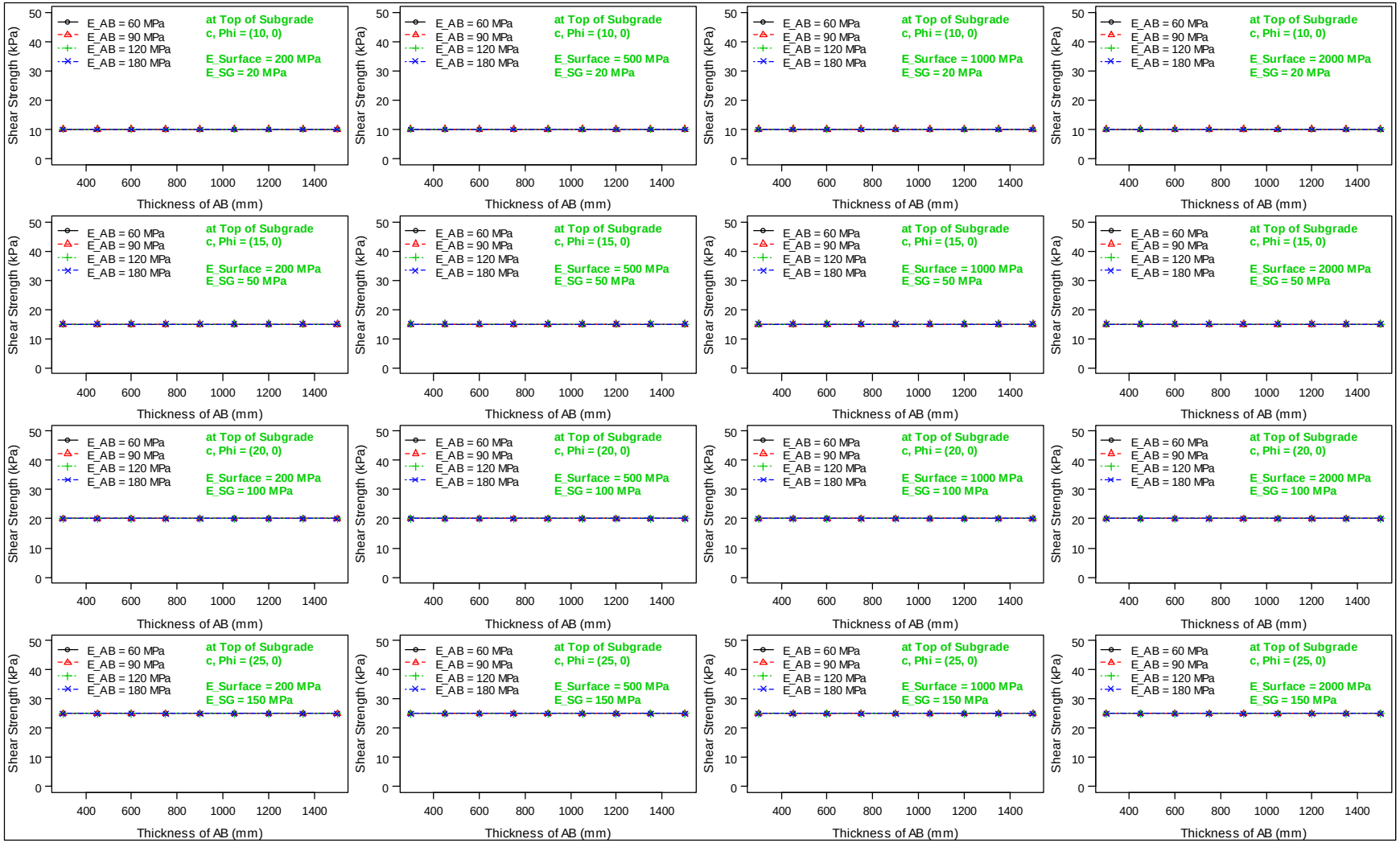

Figure A.12: Shear strength τ_{max} ($\phi = 0$).

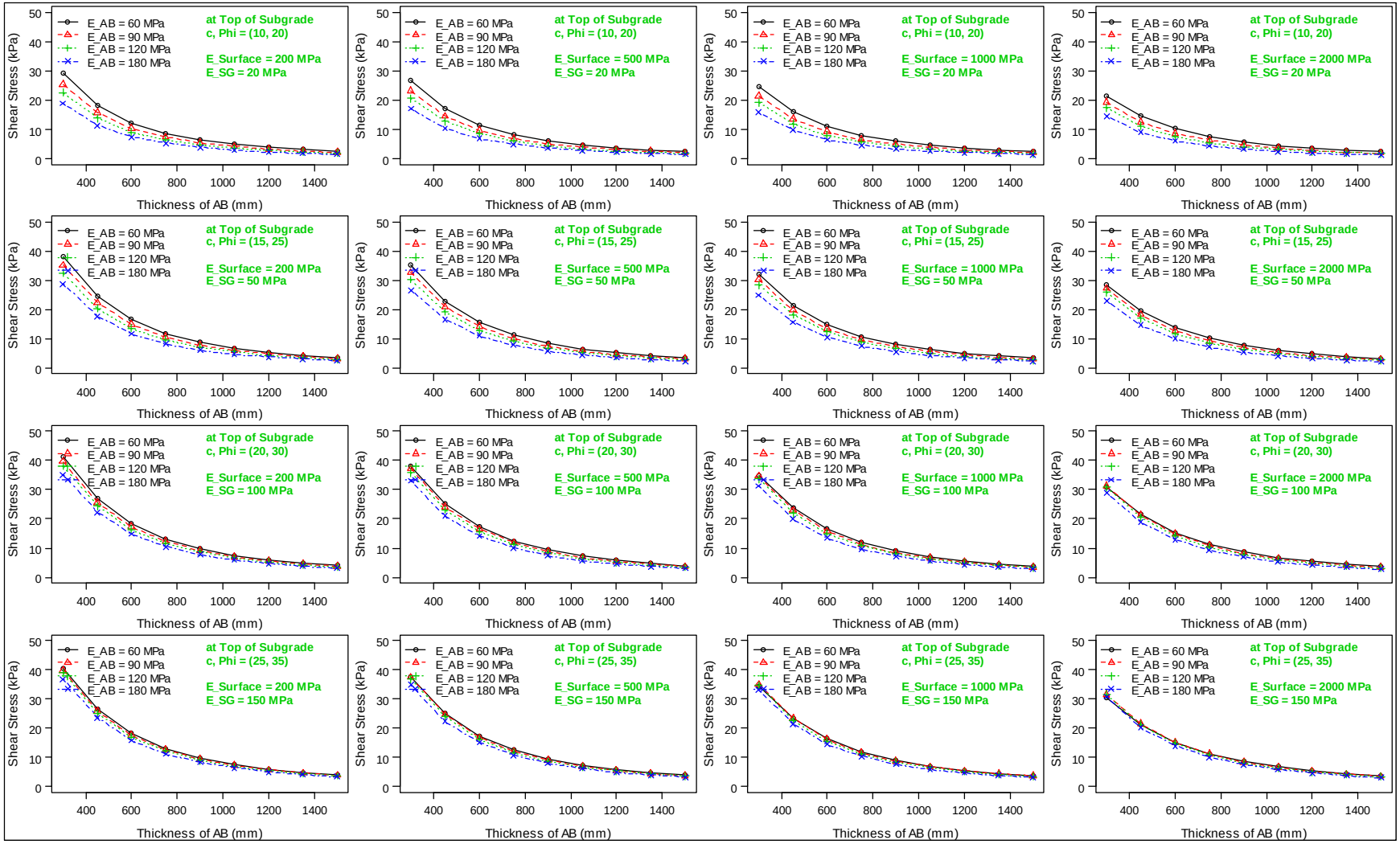

Figure A.13: Shear stress at the failure plane τ_f ($\phi \neq 0$).

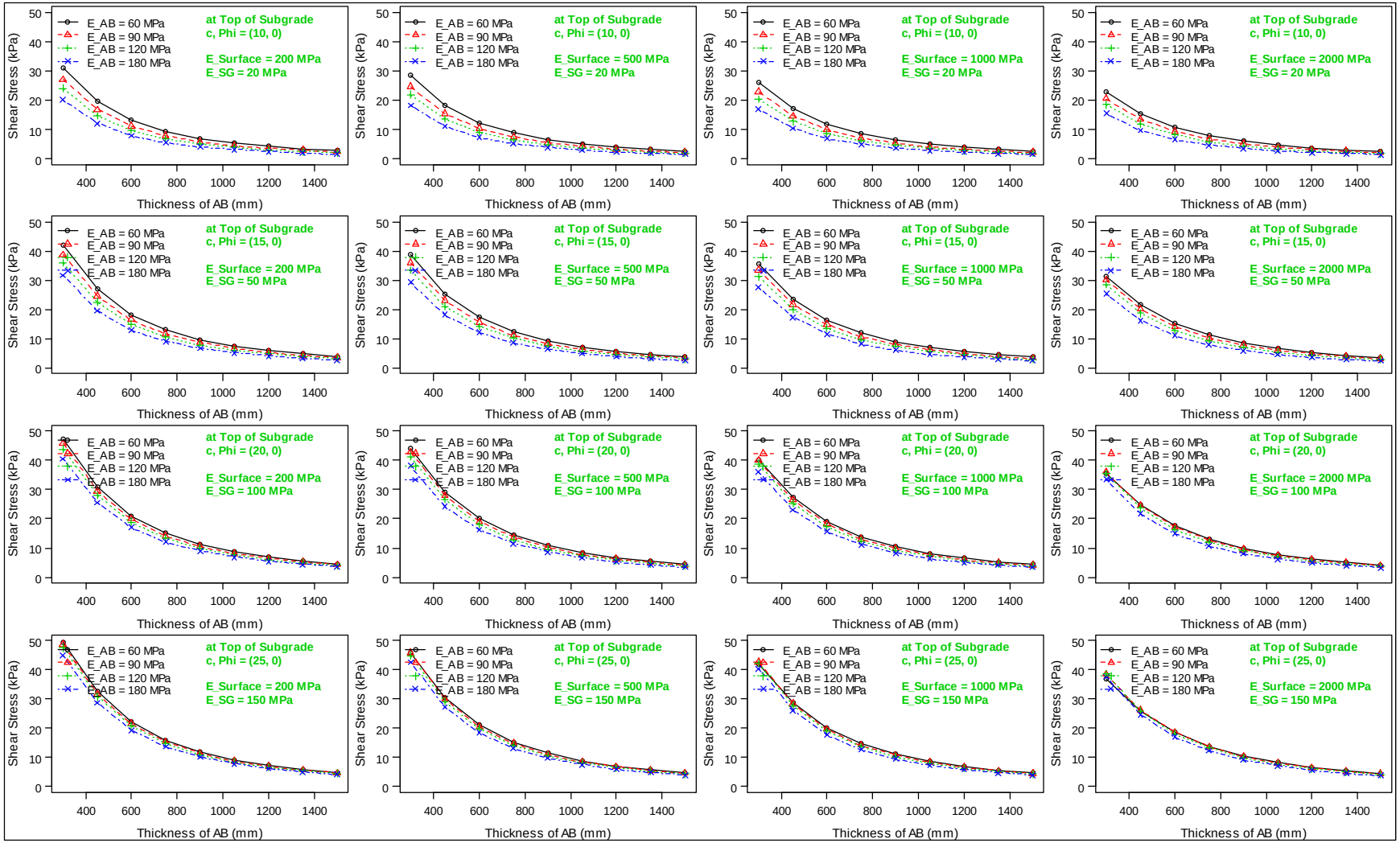

Figure A.14: Shear stress at the failure plane τ_f ($\phi = 0$).

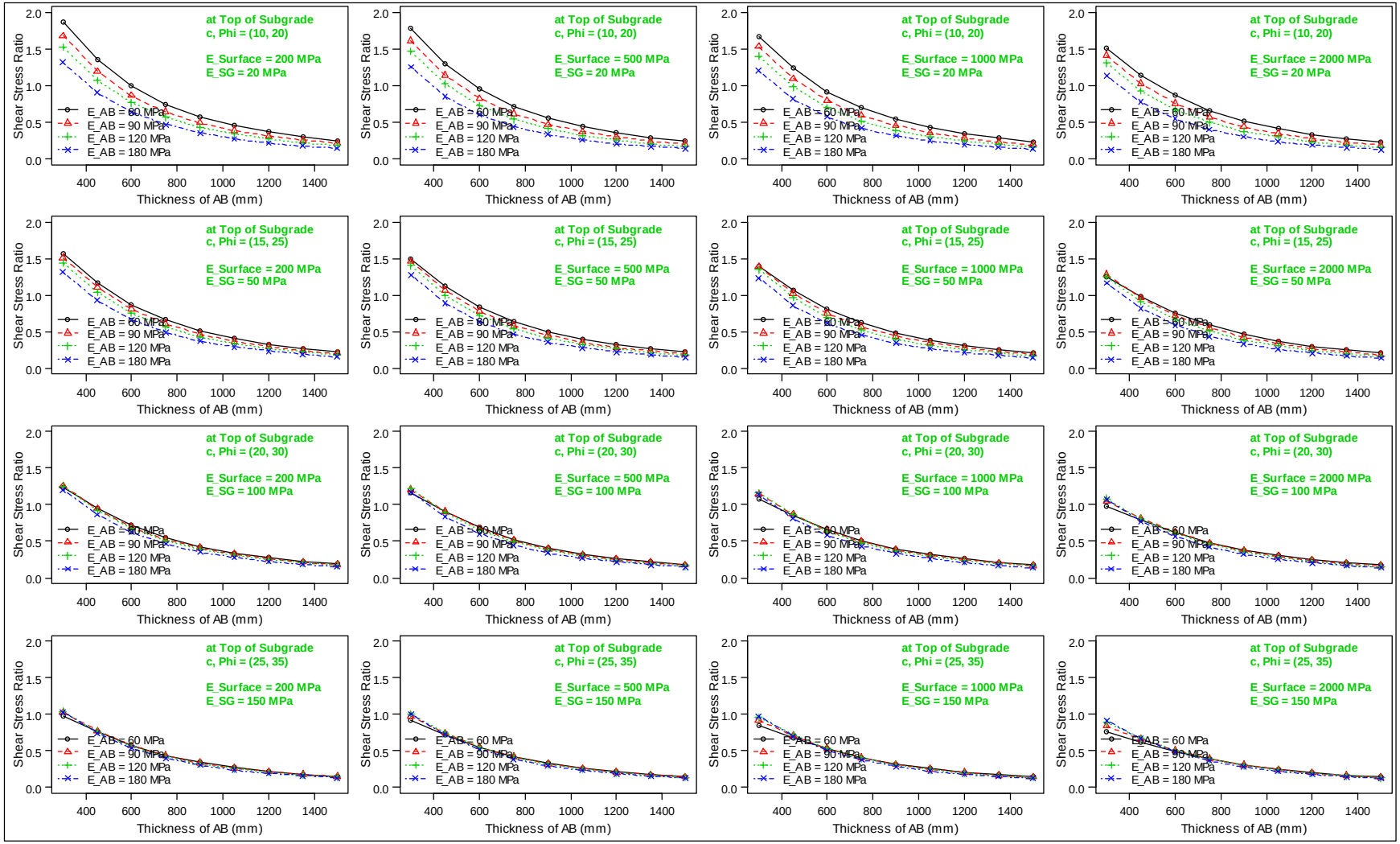

Figure A.15: Shear stress/strength ratio at the failure plane SSR ($\phi \neq 0$).

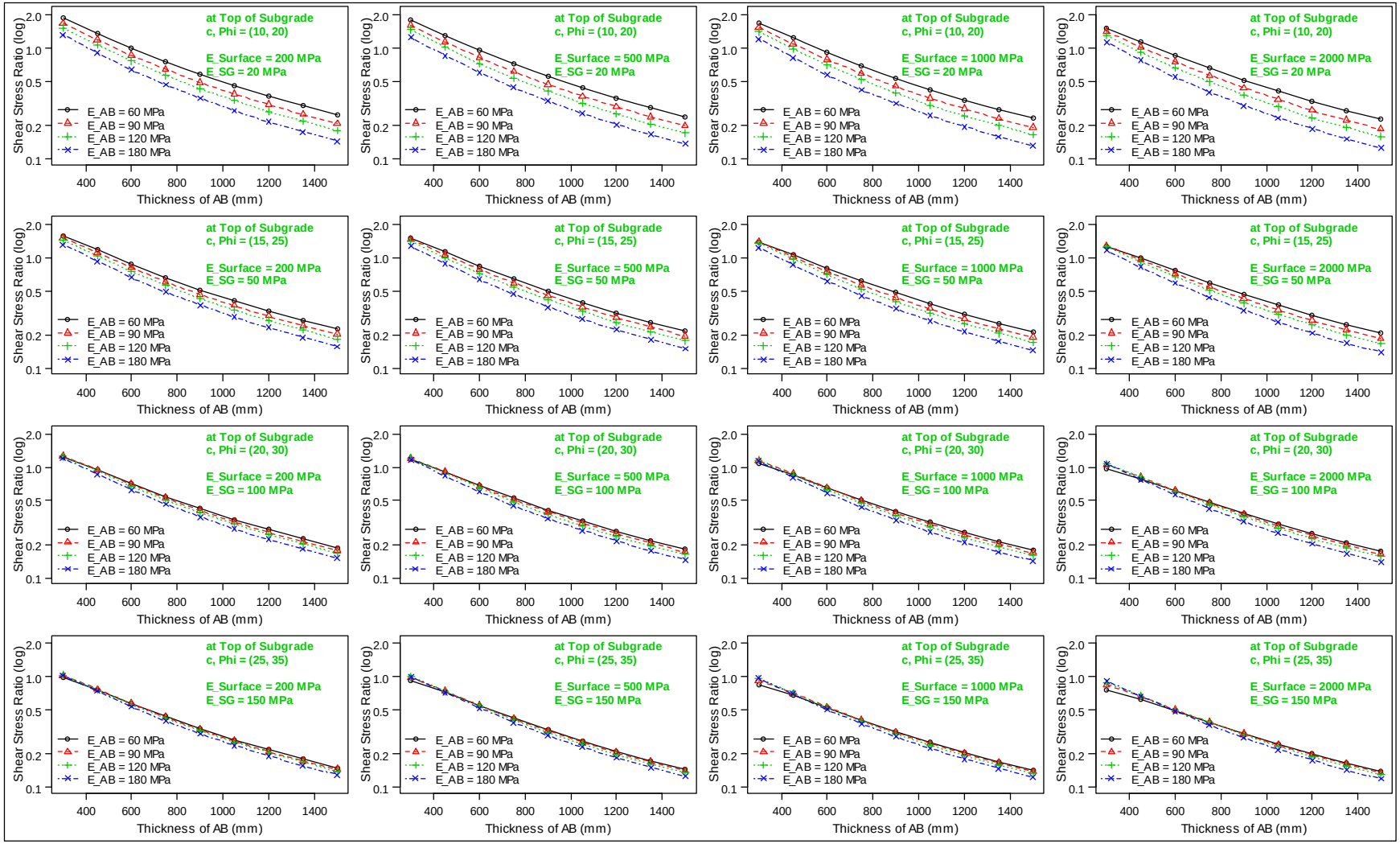

Figure A.16: Shear stress/strength ratio at the failure plane SSR ($\phi \neq 0$, log scale for SSR).

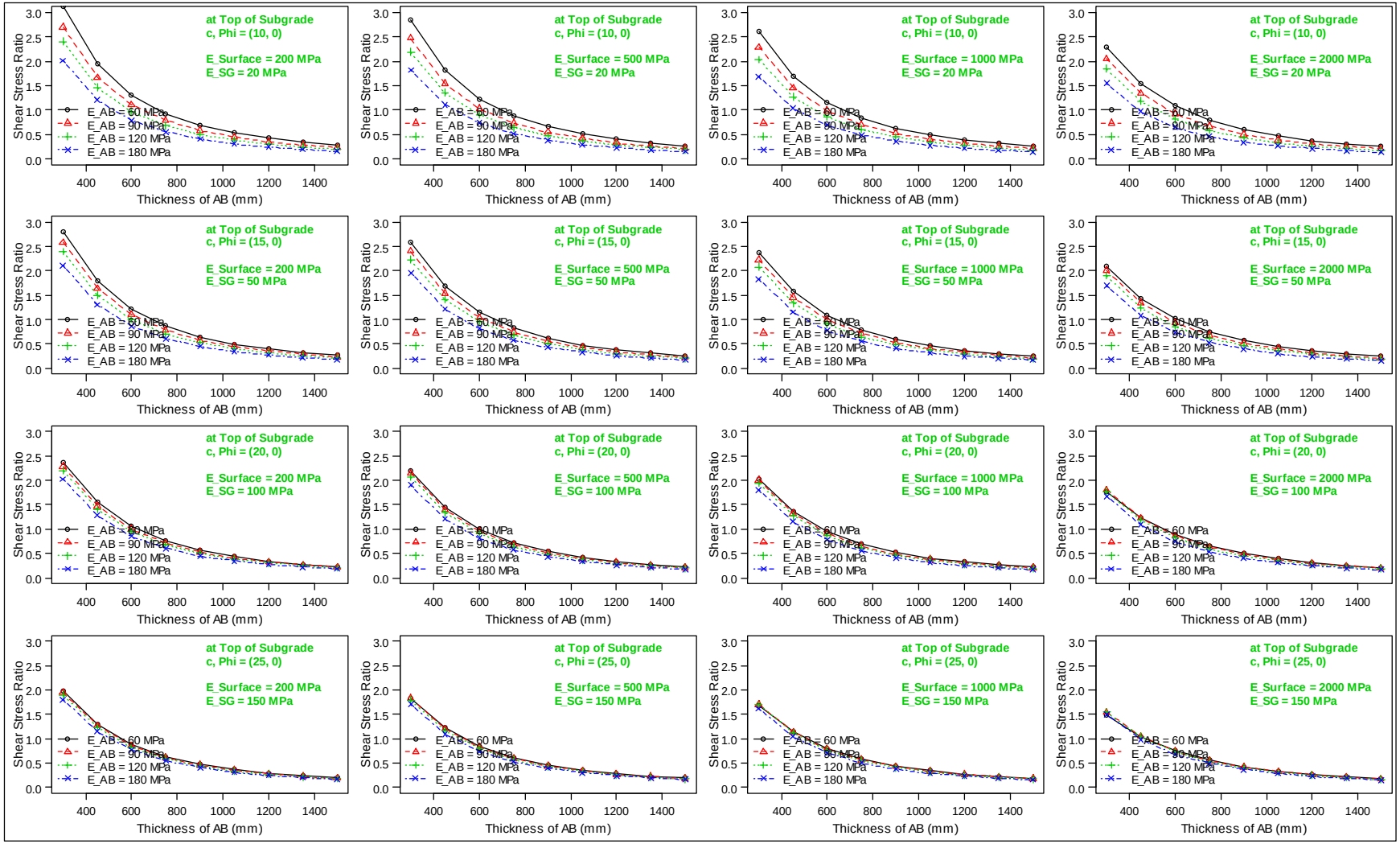

Figure A.17: Shear stress/strength ratio at the failure plane SSR ($\phi = 0$).

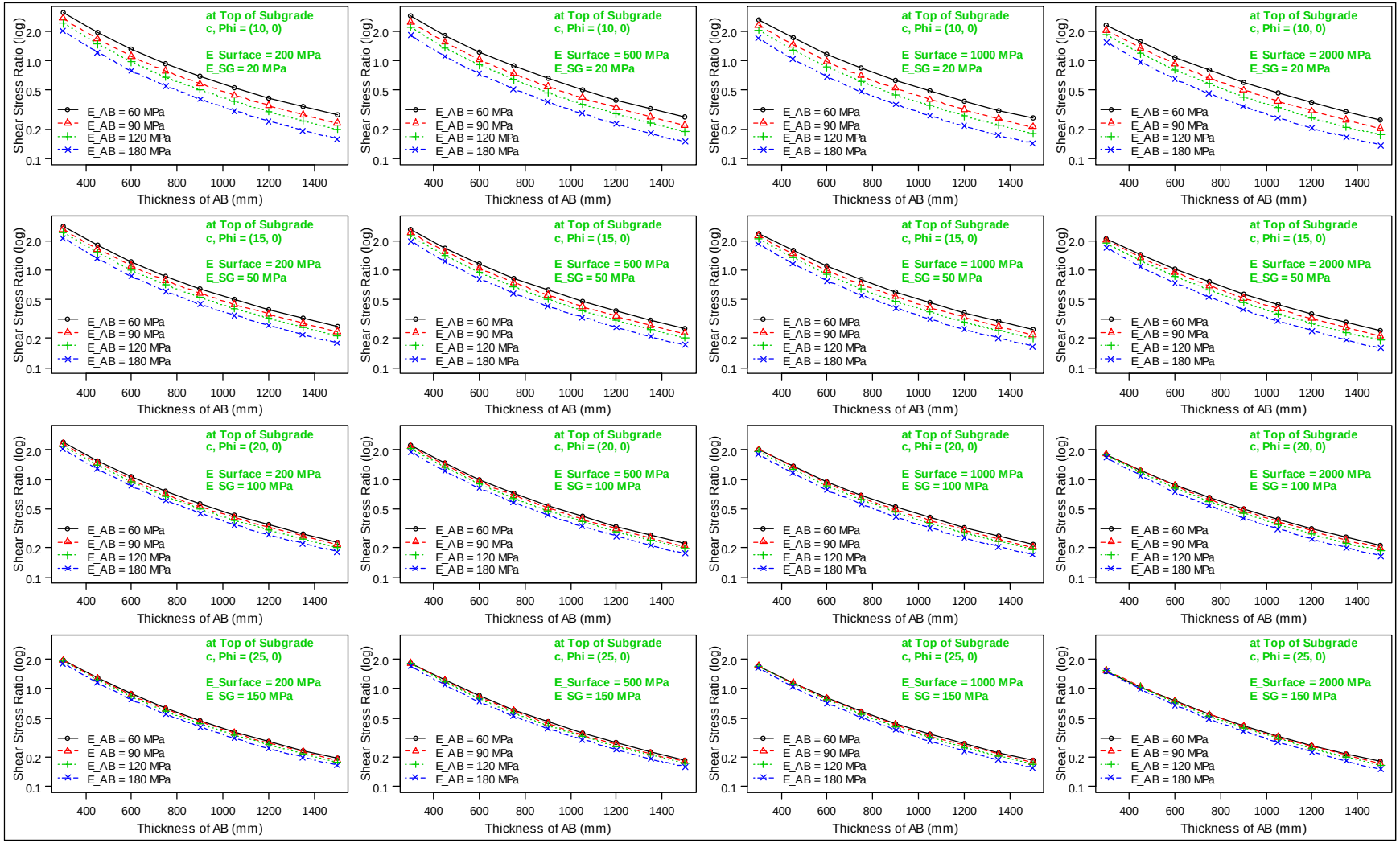

Figure A.18: Shear stress/strength ratio at the failure plane SSR (ϕ = 0, log scale for SSR).